Thermodynamic Studies on CO_2 Capture through Gas Hydrate Formation Technology

Poorandokht Ilani-Kashkouli

MSc. Analytical Chemistry (Shiraz University, Shiraz, Iran, (Sept2009-Jan2012))

This dissertation (ENNO8RPH1) is submitted for the degree of doctorate of philosophy in Engineering (Ph.D. Eng) in the School of Chemical Engineering at the University of KwaZulu-Natal.

Supervisor: Prof. Deresh Ramjugernath

Co-supervisor(s): Prof. Amir H. Mohammadi, Dr. Paramespri Naidoo

April 2015

Declaration

I, Poorandokht Ilani-Kashkouli, declare that:

i. The research reported in this dissertation, except where otherwise indicated is my original work.

ii. This dissertation has not been submitted for any degree or examination at any university.

iii. This dissertation does not contain other person's data, pictures, graphs or other information, unless specifically acknowledged as being sourced from other persons.

iv. This dissertation does not contain other person's writing, unless specifically acknowledged as being sourced from other researchers. Where other written sources have been quoted then:

    a) Their words have been re-written but the general information attributed to them has been referenced;

    b) Where their exact words have been used, their writing has been placed inside quotation marks, and referenced.

v. Where I have reproduced a publication of which I am an author or co-author I have indicated in detail which part of the publication was actually written by myself alone and have fully referenced such publications.

vi. This dissertation does not contain text, graphics or tables copied and pasted from the internet, unless specifically acknowledged, and the source are detailed in the dissertation and in the References sections.

_____

P. Ilani-Kashkouli (candidate)

As the candidate's supervisor/co-supervisor I agree/ do not agree to the submission of this dissertation.

_____

Prof. D Ramjugernath (supervisor)

_____   _____

Dr. P Naidoo (co-supervisor)   Prof. A.H Mohammadi (co-supervisor)

Abstract

CO_2 capture and sequestration or storage (CCS) is one of the important area of research mainly due to the increased public and governmental awareness of carbon dioxide's drastic green-house effects. The use of gas hydrate technology for the capture of CO_2 from flue gas is generating much attention in the literature. Gas hydrates are non-stoichiometric, ice-like crystalline compounds formed from water and suitably sized guest molecule(s) generally under low-temperatures and elevated pressures. As the pressure required for gas hydrate formation is generally high, aqueous solutions of particular chemicals are added to the system as gas hydrate promoters. These promoters generally reduce the required hydrate formation pressure and increase the formation temperature leading to the possibility of modifying the selectivity of hydrates cages to capture various gas molecules. Some ionic liquids (ILs) such as tetra butyl ammonium bromide (TBAB), tetra butyl ammonium nitrate (TBANO$_3$), tetra butyl phosphonium bromide (TBPB), etc. can be applied as hydrate formation promoters, in which the anion portion participates in the hydrogen-bonded cages formed by networks of water molecules and the cation part can be trapped in the hydrate cavities. Such compounds are called "semi-clathrate" hydrates.

In the present work, the thermodynamic knowledge of semi-clathrate hydrates of various gases including different hydrate types, and their properties were studied. New efficient gas hydrate promoters (TBPB, TBANO$_3$ and TBAF) were used to reduce the system pressure required for hydrate formation. Thereafter, new phase equilibrium data of semi-clathrate hydrates for (CO_2/CH_4/N_2/Ar) in the presence of (TBPB / TBANO$_3$ / TBAF) at varying concentrations (0.05, 0.075, 0.10, 0.15, 0.20 and 0.30 mass fraction TBPB), (0.05, 0.10, 0.15, 0.20 mass fraction TBANO3) and (0.041, 0.067 mass fraction TBAF) were generated. Measurements were undertaken in the temperature range of (275.1 to 293.3) K and in the pressure range of (1.07 to 9.90) MPa. All the measurements were performed using a static high pressure cell using the isochoric pressure search technique. The results indicate that the addition of the quaternary ammonium salts moderate the hydrate dissociation conditions.

Increasing the TBPB concentration increases its promotion effect on CO_2/CH_4/N_2/Ar semi-clathrate hydrate, i.e. the formation conditions were shifted to low pressures and high temperatures in comparison with the clathrate hydrates of corresponding gases in the presence of water.

TBANO$_3$ shows both hydrate inhibition and promotion effect. TBANO$_3$ acts as a hydrate promoter at low concentrations (e.g. 0.05 mass fraction) and low pressure and as well as an inhibitor at higher pressure.

A comparison of hydrate phase equilibrium data in the presence or absence of TBAF shows drastic promotion effect of TBAF on CO_2 hydrate formation.

These effects may lead to separation of CO_2 from gas mixtures using hydrate crystallization and for economic studies, the optimum value of salts concentration are required.

A thermodynamic model was presented to calculate/predict the dissociation conditions of semi-clathrate hydrate of CO_2/CH_4/N_2/Ar in the presence of TBPB/TBANO$_3$/TBAF. The solid solution theory of the vdW-P (J.H. van der Waals, 1959) with modification of the expressions to determine the vapour pressure of water in empty hydrate lattice and the Langmuir constants was used to develop the model.

Additionally the PR-EoS along with the Mathias-Copeman alpha function (Mathias and Copeman, 1983) including re-tuned parameters were used for calculation of the fugacity of the gaseous hydrate formers in the gas phase. The Nelder-Mead optimization algorithm (Nelder and Mead, 1965) was used to determine the optimal value of the model parameters. The model used for the CO_2 + promoters system to obtain the optimal value and the tuned parameters was later used to estimate the semi-clathrate hydrate dissociation conditions of CH_4/N_2/Ar in the presence of promoters.

Determination of accurate experimental phase equilibrium data is essential for industrial applications in order to design efficient processes and estimation of the optimal parameters of the thermodynamic models for prediction of the phase equilibria of the systems of interest at various operational conditions. In order to assess the reliability of experimental phase equilibrium data, the Leverage approach was used. This method consists of numerical and graphical algorithms to detect the outliers in different phase equilibrium data of the systems containing gas hydrates.

تقدیم به

همسر مهربانم وپدرم و مادرعزیزمکه دراین همکلمه دراین کتاب حضوردارند ، چه ، هرکلمه اي

در این کتاب ، نه لفظي ،که پاره اي از "بودن " من بوده است.

Acknowledgements

I would like to express my gratitude to the many people who supported me for the successful achievement of this research project. My deepest gratitude goes to God for everything that happens for me and for what I have.

I would like to express greatest thank to my thesis supervisors, Prof. Deresh Ramjugernath, Prof Amir H. Mohammadi and Dr. Paramespri Naidoo who gave me the golden opportunity to do this wonderful project. Without their guidance and help this dissertation would not have been possible.

I also would like to thank the staff members of the thermodynamic research unit including the head, technicians, and secretaries.

I must express my profound gratitude to my parents for their supports in all aspects of my life.

My husband, Farhad Gharagheizi, deserves to be highly acknowledged. He makes me familiar with important scientific aspects. This accomplishment would not have been possible without him.

List of Publications

1. **P. Ilani-Kashkouli,** Hashemi, H., F. Gharagheizi, Babaee, S., A. H. Mohammadi, D. Ramjugernath, *Gas Hydrate phase Equilibrium in Porous Media: An Assessment Test for Experimental Data. Fluid Phase Equilibria*. 360, 161–168, 2013.

2. **P. Ilani-Kashkouli,** Babaee, S., F. Gharagheizi, Hashemi, H., A. H. Mohammadi, D. Ramjugernath, *Assessment Test of Phase Equilibrium Data of Water Soluble and Insoluble Clathrate Hydrate Formers. Fluid Phase Equilibria.* 360, 68-76, 2013.

3. **P. Ilani-Kashkouli, Babaee,** S., F. Gharagheizi, Hashemi, H., A. H. Mohammadi, D. Ramjugernath, *Evaluation of Experimental Data for Gas Solubility in Liquid Water in Equilibrium with Gas Hydrates*, In book: *Advances in Chemistry Research* (Volume 24)., Publisher: Nova Science Publishers, Inc., NY, USA, Editors: James C. Taylor.

4. **P. Ilani-Kashkouli,** A. H. Mohammadi, P. Naidoo, D. Ramjugernath, *Hydrate dissociation data for CO_2, CH_4 or N_2 in the presence of Tetrabutylphosphonium Bromide (TBPB). Submitted to The Journal of Chemical Thermodynamics*.

5. **P. Ilani-Kashkouli,** A. H. Mohammadi, P. Naidoo, D. Ramjugernath, *Experimental phase equilibrium data for semi-clathrate hydrates of CO_2, CH_4, or N_2 in the presence of Tetrabutyl Ammonium Nitrate (TBANO3). Submitted to Fluid Phase Equilibria.*

6. **P. Ilani-Kashkouli,** A. H. Mohammadi, P. Naidoo, D. Ramjugernath, *Experimental phase equilibrium data for semi-clathrate hydrates of Ar in the presence of Tetrabutyl Ammonium Nitrate ($TBANO_3$) and Tetrabutylphosphonium Bromide (TBPB). Submitted.*

7. **P. Ilani-Kashkouli,** F. Gharagheizi, A. H. Mohammadi, P. Naidoo, D. Ramjugernath, *CO2 Capture by Hydrate Formation: State of the Art*. (Review). *Submitted.*

8. F. Gharagheizi, **P. Ilani-Kashkouli,** A. H. Mohammadi, D. Ramjugernath, *A Group Contribution Method for Determination of the Standard Molar Chemical Exergy of Organic Compounds, Energy* 70, 288-297, **2014**.

9. F. Gharagheizi, **P. Ilani-Kashkouli**, M. Sattari, A. H. Mohammadi, D. Ramjugernath, D. Richon, *Development of a General Model for Determination of Thermal Conductivity of Liquid Chemical Compounds at Atmospheric Pressure*, *AIChE Journal*. 59, 1702-1708, 2013.

10. F. Gharagheizi, **P. Ilani-Kashkouli,** M. Sattari, A. H. *Mohammadi, D. Ramjugernath, D. Richon, Quantitative Structure - Liquid Thermal Conductivity Relationship for Chemical Compounds, Fluid Phase Equilibria*. 355, 52-80, 2013.

11. F. Gharagheizi, **P. Ilani-Kashkouli,** M. Sattari, *A. H. Mohammadi, D. Ramjugernath. D. Richon, A Group Contribution Method for Determination of Thermal Conductivity of Liquid Chemicals at Atmospheric Pressure, Journal of Molecular Liquids,* 190, 223–230, 2013.

12. F. Gharagheizi, P. Ilani-Kashkouli, A. H. Mohammadi, D. Ramjugernath. D. Richon, *Development of a Group Contribution Method for Determination of Viscosity of Ionic Liquids at Atmospheric Pressure, Chemical Engineering Science*. 80, 326-333, 2012.

13. F. Gharagheizi, M. Sattari, **P. Ilani-Kashkouli**, A. H. Mohammadi, D. Ramjugernath. D. Richon, *Quantitative Structure-Property Relationship for Thermal Decomposition Temperature of Ionic Liquids, Chemical Engineering Science*. 84, 557-563, 2012.

14. F. Gharagheizi, **P. Ilani-Kashkouli**, M. Sattari, A. H. Mohammadi, D. Ramjugernath, *Development of a Group Contribution Method for Estimating the Thermal Decomposition Temperature of Ionic Liquids, Fluid Phase Equilibria*. 355, 81-86, 2013.

15. F. Gharagheizi, M. Sattari, P. Ilani-Kashkouli, A. H. Mohammadi, D. Ramjugernath. D. Richon, *A "Non-Linear" Quantitative Structure - Property Relationship for the Prediction of Electrical Conductivity of Ionic Liquids, Chemical Engineering Science*. 101, 478-485, 2013.

16. F. Gharagheizi, S.A. Mirkhani, **P. Ilani-Kashkouli,** A. H. Mohammadi, D. Ramjugernath, D. Richon, *Determination of the Normal Boiling Point of Chemical Compounds Using a Quantitative Structure–Property Relationship Strategy: Application to a very Large Dataset, Fluid Phase Equilibria*. 354, 250-258, 2013.

17. F. Gharagheizi, **P. Ilani-Kashkouli,** W.E. Acree, A. H. Mohammadi, D. Ramjugernath, *A Group Contribution Model for Determining the Sublimation Enthalpy of Organic Compounds at the Standard Reference Temperature of 298 K, Fluid Phase Equilibria*. 354, 265-285, 2013.

18. F. Gharagheizi**, P. Ilani-Kashkouli**, W.E. Acree, A. H. Mohammadi, D. Ramjugernath, *A Group Contribution Model for Determining the Vaporization Enthalpy of Organic*

Compounds at the Standard Reference Temperature of 298 K, Fluid Phase Equilibria. 360, 279–292, 2013.

19. F. Gharagheizi, **P. Ilani-Kashkouli,** A. H. Mohammadi, D. Ramjugernath, *Toward a Group Contribution Method for Determination of Speed of Sound in Saturated Liquids, Journal of Molecular Liquids*, 194, 159-165, 2014.

20. M. Sattari, F. Gharagheizi, **P. Ilani-Kashkouli,** A. H. Mohammadi, D. Ramjugernath. D. Richon, *Toward a Group Contribution Method for Estimation of Heat Capacity of Ionic Liquids. Journal of Thermal Analysis and Calorimetry*, 363, 27–31, 2013.

21. M. Sattari, F. Gharagheizi, **P. Ilani-Kashkouli,** A. H. Mohammadi, D. Ramjugernath. D. Richon, *Estimation of Heat Capacity of Ionic Liquids: A QSPR Approach. Industrial & Engineering Chemistry Research.* 52, 13217–13221, 2013.

22. M. Sattari, F. Gharagheizi, **P. Ilani-Kashkouli,** A. H. Mohammadi, D. Ramjugernath, *Toward a Group Contribution Method for Determination of Speed of Sound in Saturated Liquids, Journal of Molecular Liquids*, 196, 7-13, 2014.

23. F. Gharagheizi, **P. Ilani-Kashkouli,** A. Kamari, A. H. Mohammadi, D. Ramjugernath, *A Group Contribution Model for the Prediction of Refractive Indices of Organic Compounds, Journal of Chemical and Engineering Data*, 59, 1930-1943, 2014.

24. F. Gharagheizi, **P. Ilani-Kashkouli**, A. Kamari, A. H. Mohammadi, D. Ramjugernath, *A Chemical Structure based Model for the Estimation of Refractive Indices of Organic Compounds, Fluid Phase Equilibria,* 384, 1-13, 2014.

25. F. Gharagheizi, P. Ilani-Kashkouli, A. Kamari, A. H. Mohammadi, D. Ramjugernath*, A Group Contribution Model for the Prediction of Freezing Point of Organic Compounds, Fluid Phase Equilibria,* 382, 21-30, 2014.

Congresses and Seminars

1. **P. Ilani-Kashkouli,** A. H. Mohammadi, D. Ramjugernath, *Phase equilibria of semi-clathrate hydrates of carbon dioxide + TBPB or TBANO₃,* International Conference on Chemical Thermodynamics, 29 July-2 August, Durban, South Africa, 2014.

2. **P. Ilani-Kashkouli,** F. Gharagheizi, A. H. Mohammadi, D. Ramjugernath, *A Quantitative Structure-Property Relationship for the Prediction of the Enthalpy of Vaporization of the Pure Organic Fluorochemicals,* South African Chemical Institute (SACI) Convention, 1st -6th December, East London, South Africa, 2013.

3. F. Gharagheizi, **P.Ilani-Kashkouli**, A.H. Mohammadi, D. Ramjugernath, *A Group Contribution Model for Determining the Vaporization Enthalpy of Organic Compounds at the Standard Reference Temperature of 298 K*, South African Chemical Institute (SACI) Convention, 1st -6th December, East London, South Africa, 2013.

Award and honor

IACT Junior Travel Awards from the IACT (International Association of Chemical Thermodynamics) to outstanding PhD student, 2014.

Table of Contents

List of Figures

XIII

List of Tables

1 Introduction

The increasing accumulation of carbon dioxide in the atmosphere leads to global warming which is one of the most important environmental challenges. Increases in CO_2 concentrations in the atmosphere are substantially attributed to the combustion of coal, petroleum, and natural gas for electricity generation, transportation, industrial and domestic uses. According to the literature the majority of CO_2 emissions originates from just 20 countries (http://edgar.jrc.ec.europe.eu, 2011). The countries with the highest CO_2 emissions are presented in the Figure 1.1.
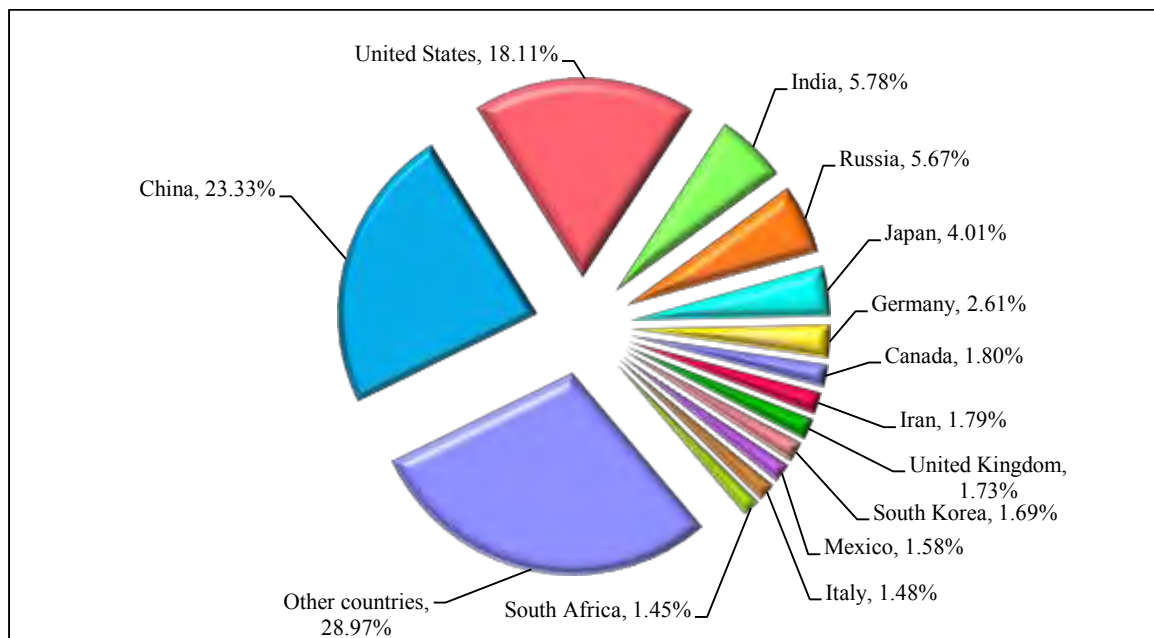
Figure 1.1: CO_2 emissions by countries (http://edgar.jrc.ec.europe.eu, 2011).

According to the National Oceanic and Atmospheric Administration (NOAA), the annual concentration of CO_2 in the atmosphere, has increased by 2.07 ppm in the past ten years. Figure 1.2 shows the average monthly and annual concentrations of CO_2 from 2000 to 2013.

1
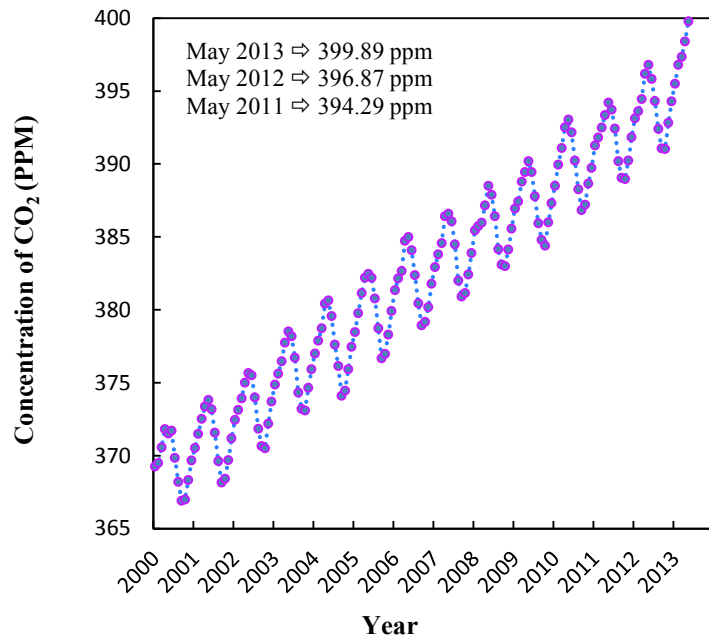
Figure 1.2: Atmospheric CO$_2$ concentration measured at Mauna Loa Observatory, Hawaii from 2000 to 2013. (Source: National Oceanic and Atmospheric Administration (NOAA)).

Figure 1.3 shows the variation of CO$_2$ emissions per capita in 2011 compared to 1990 and 2000.
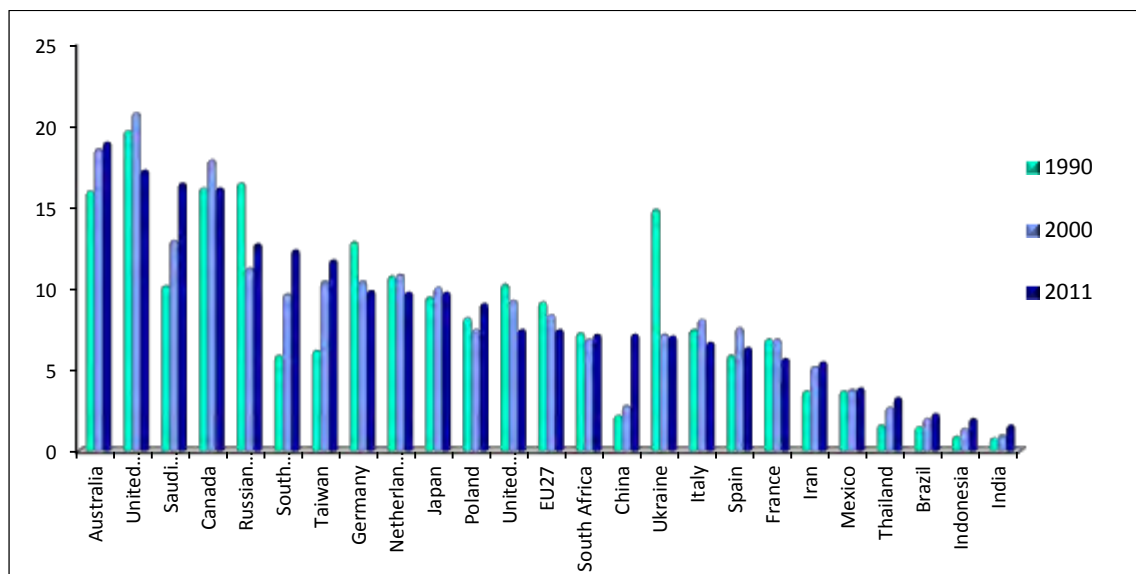
Figure 1.3: CO$_2$ emissions per capita in 1990, 2000 and 2011, in the top 25 CO$_2$ emitting countries (http://edgar.jrc.ec.europe.eu, 2011).

The capture and sequestration (storage) of carbon dioxide (CCS) is one of the interesting research fields of energy and environmental science because it is a suitable method to combat climate change (Yang et al., 2008). The separation and capture of CO_2 is typically the most expensive part of CCS and it represents approximately two thirds of the total cost of CCS (D'Alessandro et al., 2010). There are a variety of technologies for CO_2 capture such as absorption, adsorption, membrane, cryogenic separation, *etc*. Refer to Appendix A for the detail of each technology.

CCS is a three step process consisting: carbon dioxide capture and separation, transporting the carbon dioxide, and storing the carbon dioxide (Hester and Harrision, 2010). There are three different routes for separation of carbon dioxide from large sources: pre-combustion capture, post-combustion capture and oxy-fuel combustion (Haszeldine, 2009). These three options are illustrated in Figure 1.4. After the CO_2 is captured, it must be compressed and dehydrated, then transported by pipeline for safe storage sites. The carbon dioxide is then stored in the storage sites that are typically placed several kilometers under the earth's surface.
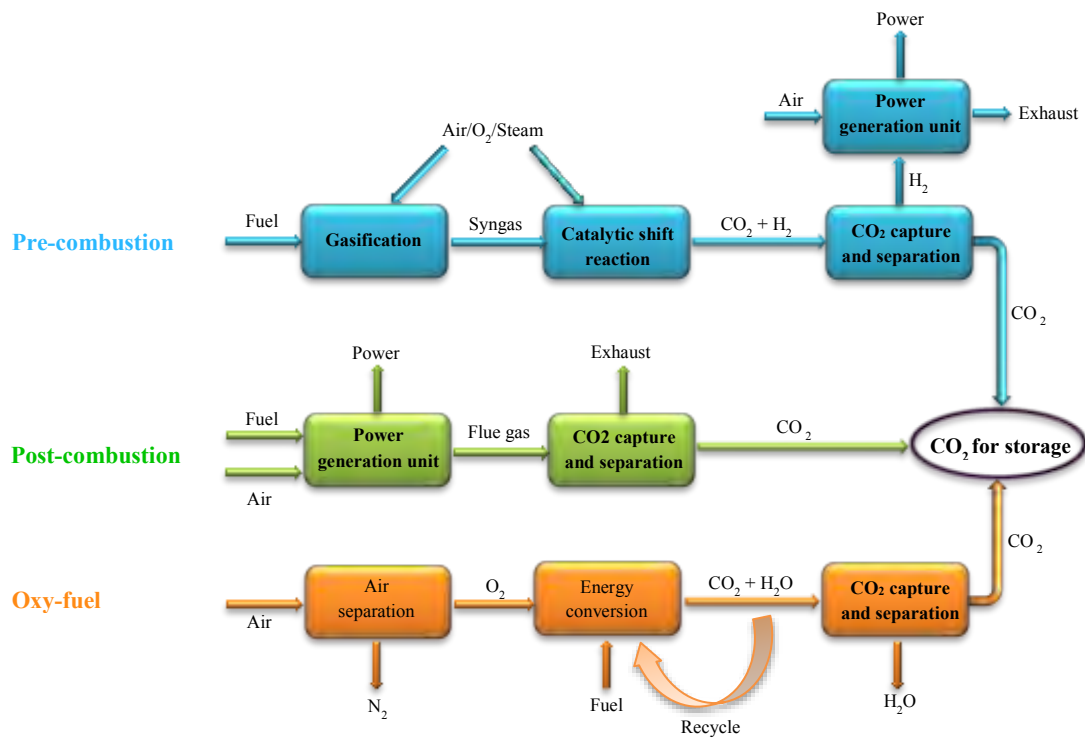
Figure 1.4: Diagrams illustrating pre-combustion, post-combustion and oxy-combustion.

In this chapter, CO_2 capture technologies and the advantages and limitations of each technology are examined.

1.1 CO$_2$ capture routes

Pre-combustion techniques: Removing CO$_2$ prior to combustion is the main goal of these methods. A primary fossil fuel is reacted with air or oxygen, to produce a syngas (hydrogen and carbon monoxide). This operation is called partial oxidation, or gasification. The syngas is transmitted through a catalytic reactor and catalytic shift reaction in which the CO reacts with water to produce a mixture of H$_2$ and CO$_2$. The CO$_2$ is then separated, captured and sent to the compression unit while the hydrogen produced is used as an energy carrier and an input to generate electricity. The most important advantages of the process compared with other similar processes may be the high concentration of carbon dioxide in the final syngas, its high pressure, the smaller equipment required, and the diversity of the solvents that can be used (Orr, 2009, Mondal et al., 2012, Thiruvenkatachari et al., 2009, Haszeldine, 2009).

Post-combustion processes: This process involves the removal of CO$_2$ from flue gas emitted from fossil fuels burning. One of the most widely used methods for post-combustion carbon dioxide removal is the chemical MEA (monoethanolamine) absorption process. Estimations indicate that an economical MEA process is supposed to capture more than 2000 ton CO$_2$ per year. This technique is normally suitable for flue gases containing CO$_2$ and N$_2$. Another approach is the PSA (pressure swing absorption) process, in which CO$_2$ can be removed from a flue gas containing CO$_2$ + H$_2$. This method seems to be less energy intensive compared with the MEA process accompanied by H$_2$ production; however, with less selectivity for CO$_2$ absorption (Haszeldine, 2009, Orr, 2009).

Oxy-combustion process: This technique involves burning a fuel using an oxygen rich gas. The resultant flue gas consists mainly of CO$_2$ and water vapour that can be easily separated. Compared with the conventional burning process in the presence of air, the oxy-combustion method requires less fuel and produces a smaller volume of flue gas due to the absence of nitrogen. In this process, the oxygen-rich stream is first fed to a combustion chamber to produce an exhaust gas stream containing a higher concentration of CO$_2$. This process needs an air separation process which makes it costly (Haszeldine, 2009, Orr, 2009). A summary of the advantages and drawbacks of each of these routes is provided in Table 1.1.

Table 1.1: Advantages and disadvantages of different CO₂ capture routes.

Pre-combustion	Post-combustion	Oxy-fuel combustion
Advantages: ➢ High concentration of CO_2 in the final syngas ➢ High CO_2 partial pressure ➢ high pressure ➢ The lower volume of gas to be handled ➢ The CO_2 capture equipment is much smaller ➢ Less expensive ➢ More technologies available for separation	*Advantages:* ➢ If the CO_2 capture unit is shut down for an emergency, one can still generate electricity, which is not possible with the other more integrated capture methods ➢ Chemical absorption processes are well known (Markewitz et al., 2012) ➢ High optimization potential to reduce energy losses (Markewitz et al., 2012) ➢ Retrofitting of existing power plants is possible (Figueroa et al., 2008a)	*Advantages:* ➢ High combustion efficiency (Kim et al., 2007) ➢ Low volume of exhaust gas (Kim et al., 2007) ➢ Low fuel consumption (Kim et al., 2007) ➢ Low NOx emission and reduced pollutant emissions (Kim et al., 2007) ➢ Environmental impacts are low ➢ Retrofit and repowering technology option (Figueroa et al., 2008b) ➢ Generates an exhaust stream that is almost exclusively CO_2 and H_2O. It is cheap and easy to separate CO_2 from this stream.
Disadvantages: ➢ It requires a chemical plant in front of the turbine (Mondal et al., 2012) ➢ Complicated chemical processes normally cause extra shut-downs of the plant, which can result in a lower power output (Mondal et al., 2012) ➢ It requires major modifications to existing plants for retrofit.	*Disadvantages:* ➢ High costs ➢ Comparably large environmental impact (Figueroa et al., 2008a) ➢ Flexible operation mode has yet to be demonstrated (Markewitz et al., 2012) ➢ Low CO_2 partial pressure ➢ Significantly higher performance or circulation volume required for high capture levels (Figueroa et al., 2008a)	*Disadvantages:* ➢ This process requires a large quantity of oxygen, which is expensive. ➢ Large electric power requirement inherent in conventional cryogenic air separation units required to produce oxygen (Figueroa et al., 2008b) ➢ Modification of burners and boiler design are necessary ➢ A costly air separation step is required.

1.2 CO_2 capture technologies

A variety of existing technologies for CO_2 capture from pre-combustion, post-combustion, and oxy-fuel processes are presented in Figure 1.5. The advantages and drawbacks of these separation methods are summarized in Table 1.2. Refer to Appendix A for further details on each technology.
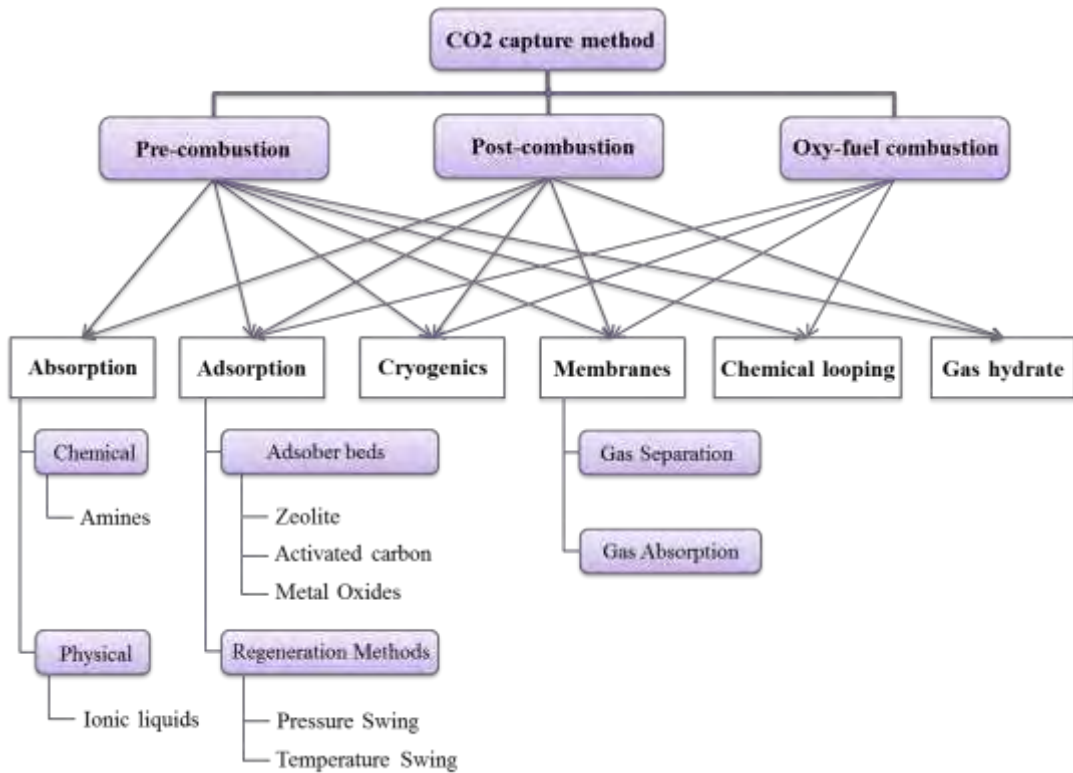
Figure 1.5: Overview of CO_2 capture technologies in the context of pre-combustion, post-combustion, and oxy-fuel processes (D'Alessandro et al., 2010).

Table 1.2: Advantages and disadvantages of different CO_2 capture technologies (refer to Appendix A.1 to A.5 .

Capture technology	Advantages	Drawbacks
Absorption	- Purity of CO_2 > 95% - Low utility consumption - Requires less energy for regeneration	- High regeneration costs - High energy requirements for CO_2 release - Requires a high partial pressure of CO_2 in the feed
Adsorption	- Relatively simple - Commercially available - Sorbent can be reused - Low concentrations of CO_2 yield and optimum performance	- Capacity and CO_2 selectivity of available adsorbents is low - Cannot handle easily large concentrations of CO_2 - Adsorption time is not practical - Low degree of CO_2 separation - Poor selectivity of sorbents to CO_2
Cryogenics	- No chemical absorbents are required - The process can be operated at atmospheric pressures - Smaller size of equipment since only O_2 is supplied for combustion	- Some components, such as water, have to be removed before the gas stream is cooled - Very expensive process - Requires high energy consumption - Corrosion might be caused by SO_2
Membranes	- Relatively simple to operate - No regeneration energy is required - Simple modular system. - No waste streams - Commercially available. - Require low maintenance. - Less energy intensive than PSA.	- Can be plugged by impurities in the gas stream - Low selectivity of membrane materials to CO_2. - Preventing membrane wetting is a major challenge - Purity of the CO_2 in the permeate stream is low
Chemical looping	CO_2 is inherently separated from the other flue gas components - No extra energy is needed for CO_2 separation. - No need of special CO_2 separation equipment - No thermal formation of NO_x - Less operational cost	- No large-scale demonstration has been performed - Mn-based oxygen carriers have lower oxygen transfer capability and thermodynamic limitations of purifying the CO_2 stream. - Fe-based oxygen carriers have a larger endothermic reduction enthalpy and lower reactivity.

To aid in the reduction of CO_2 levels in the atmosphere, hence negating the greenhouse effect, the implementation of gas hydrate formation for the capture of carbon dioxide has been studied extensively in recent years (Linga et al., 2007b, Kumar et al., 2009a, Babu et al., 2013b, Linga et al., 2007a, Kim et al., 2011, Park et al., 2013a).

This study focuses on gas hydrate technology as an environmental friendly technology for capturing of CO_2. Relative to the other gas separation technologies, the gas hydrate separation technology has the following advantages: (1) simple process, (2) low investment, (3) low material and energy loss.

The principle for separation through gas hydrates is the selective partition of the CO_2 component of a gas mixture between the gas phase and the hydrate phase upon hydrate formation. The experimental results demonstrate that the CO_2 selectivity in the hydrate phase is at least four times higher than in the gas phase (Duc et al., 2007a). CO_2 can be recovered after capturing in the hydrate phase by either heating or depressurization.

1.3   Research aims and objectives

Carbon dioxide capture from the flue gas of a power plant and fuel gas contains many chemical components such as carbon dioxide, nitrogen, oxygen, argon, methane, etc. The main objective of this study is to examine hydrate formation condition of flue gas and fuel gas components for CO_2 capture. It should be noted that, the knowledge gained from the obtained data is general and it may be useful in other applications.

The specific objectives of this study are as follows:

- Enhance the thermodynamic knowledge of semi-clathrate hydrates of various gases including different hydrate types, properties etc.
- Search for new efficient gas hydrate promoters to reduce the required pressure of hydrate formation phenomenon in separation processes.
- Generation of new phase equilibrium data of semi-clathrate hydrates especially for the systems containing CO_2.
- Providing predictive tools to calculate/estimate the phase equilibria of the systems of interest able to predict the structural changes of semi-catharses during the relevant industrial operations.
- Economic studies of the corresponding CO_2 capture processes.
- Examination of a mathematical model to assess the phase equilibrium data.

This thesis includes the following chapters:

- The current chapter provided a comprehensive overview on CO_2 capture technologies, their advantages and drawbacks. Also, it is explained that why gas hydrate have attracted more attention in recent years.

- Chapter 2 provides the basic information about gas hydrates, description of their chemical structures of hydrate and experimental studies that have been undertaken to date on the separation of CO_2 from different gas mixtures via clathrate/semi-clathrate hydrates in the absence and/or presence of additives.
- Chapter 3 and 4 present a complete overview on thermodynamic model to correlate/predict the phase equilibrium and a review on existing experimental methods and equipment which are available in the open literature.
- Chapter 5 describes the experimental method and equipment used in this study.
- Chapter 6 presents all research results which include:
  a. Phase equilibrium data of semi-clathrate hydrates of $CO_2/N_2/CH_4$ and Ar in the presence of TBPB and $TBANO_3$.
  b. Phase equilibrium data of semi-clathrate hydrates of CO_2 in the presence of TBAF.
  c. Explanation of the effect of TBPB/ $TBANO_3$ and TBAF on the equilibrium condition of $CO_2/N_2/CH_4$ and Ar semi-clathrate hydrates.
  d. Presentation a thermodynamic model for calculation/prediction of the clathrate hydrates dissociation conditions. This model may show the promotion and inhibition effect of the applied salts as well.
  e. Description of separation process and economic estimation of carbon dioxide capture.
  f. Presentation of the mathematical model to assess the phase equilibrium data. This model may determine the quality of experimental phase equilibrium data for the systems containing clathrate hydrates.

- In the 7th and final chapter of this study, conclusion are highlighted and some recommendations for further study of the thermodynamics of semi-clathrates are presented.

2   Clathrate hydrate (gas hydrate) for CO_2 capture

Inclusion compounds composed of water and small guest molecules are called clathrate hydrates. The water molecules are arranged in hydrogen bonded networks (host) with defined cavities to encage guest molecules. Clathrate hydrates were first discovered by Sir Humphry Davy (Davy, 1811) who found that a solid is formed when an aqueous solution of chlorine is cooled below 9.0 °C.

Faraday confirmed the existence of the chlorine hydrate and proposed that its composition was nearly 1 part of chlorine and 10 parts of water (Faraday and Davy, 1823). More than 100 guest compounds are known to form hydrates with water molecules. Typical hydrate-forming substances consist of methane, ethane, propane, and carbon dioxide (Sloan, 2008a, Faraday and Davy, 1823). The terms "gas hydrate" and "clathrate hydrates" have been applied for these solids. The formation of clathrate hydrate requires relatively low temperature and high pressure conditions. The crystal structure and composition of clathrate hydrates was discovered by X-ray diffraction (XRD) studies in the 1950s (Mak and McMullan, 1965).

The hydrate crystal structure determines by the guest molecule trapped in the lattice. In general, gas hydrates may form in the presence of adequate amounts of water and gas under high pressures and low temperatures. The temperature and pressure conditions for hydrate formation strongly depend on the nature of the incorporated gas molecule.

2.1   The structure of gas hydrates

Hydrates are crystalline solid compounds with well-defined crystal structures. Hydrogen bonds among water molecules form cage-like networks (host) that trap the small gas molecules (guest), which stabilize the crystal lattice. Three different structures for natural gas hydrates are known so far: cubic structure I (sI), cubic structure II (sII), or hexagonal structure H (sH) (Ripmeester et al., 1987, Pauling and Marsh, 1952). These structures distinguished by the size of the cavities and number of large cavities per small cavities.

A unit cell of structure I is composed of two pentagonal dodecahedron and six tetrakaidecahedron cages. Dodecahedron cages can be explained as twelve-sided polyhedron with a pentagon for each face (5^{12}). This cavity is the simplest and smallest type with an average diameter of about 0.79 nm. It is found in all three structures while tetrakaidecahedron cages are fourteen-sided polyhedron with twelve pentagonal faces and two hexagonal faces (6^2). This cavity type is slightly larger with a diameter of 0.87 nm (Schicks, 2010, Sloan and Koh, 2008). Hydrate formers such as methane, ethane, carbon dioxide, and hydrogen sulfide can form Structure I.

A unit cell of structure II is composed of 16 pentagonal dodecahedrons (5^{12}) and 8 hexakaidecahedrons ($5^{12}6^4$). The sII small cage is the same as that in sI. The sII large cage is a hexakaidecahedron and called the $5^{12}6^4$ cage due to its twelve 5-sided faces and four 6-sided faces. The sII $5^{12}6^4$ cage is larger than the sI large cage and has a diameter of about 0.95 nm. Formers such as nitrogen, propane and iso-butane form structure II.

Structure H has a hexagonal lattice containing three types of cavities: three pentagonal dodecahedron, two irregular dodecahedron, and one irregular icosahedron. Larger hydrocarbons, such as pentane or hexane can form structure H. (Lu et al., 2007). The numbers and types of cavities for the different structures are listed in Table 2.1.

Table 2.1: Numbers of cavities per unit cell for three different gases hydrate structures (Pelckmans et al., 2002, Falenty, 2009).

	Cavities	sI	sII	sH
Pentagonal dodecahedron (5^{12})		2	16	3
Tetrakaidecahedron ($5^{12}6^2$),		6	-	-
Hexakaidecahedron ($5^{12}6^4$),		-	8	-
Irregular dodecahedron ($4^35^66^3$)		-	-	2
Icosahedron ($5^{12}6^8$).		-	-	1

2.2 Characteristics of guest molecules

Chemical nature of guest molecules: A guest molecule (gas molecule) must be small to form hydrates. The gas molecule should not be soluble in water; if it dissolves in water, it cannot form hydrates (Carroll, 2009b). Hydrogen chloride and ammonia are highly soluble in water hence cannot form hydrates. A guest molecule must not interfere with hydrogen bonding among the water molecules. Methanol is a small molecule but does not form a hydrate because it forms hydrogen bonding and hence interferes with the hydrogen bonding among the water molecules (Carroll, 2009b). Methanol is also soluble in water.

Size and shape: Von Stackelberg (Von Stackelberg, 1949) documented the relationship between the guest molecule size and the type of hydrate formed as shown in

Figure *2.1.* It can be observed that molecules with diameters less than 3.8 Å do not form hydrates. All molecules between the sizes of argon (3.8 Å) and cyclobutanone (6.5 Å) can form sI and sII hydrates (Carroll, 2009b, Sloan, 2008a).

Molecules with sizes in the range of 3.8 to 4.2 Å form Type II hydrates and molecules with sizes in the range of 4.4 to 5.4 Å form Type I hydrates. These compounds are small enough to occupy both the small and larger cages (Carroll, 2009b, Sloan, 2008a).

Compounds with sizes in the range of 5.6 to 6 Å can form Type I hydrates, but only occupy the large cages. These substances are too large to occupy the small cages of a Type I hydrate which includes ethane (Carroll, 2009b, Sloan, 2008a).

The next region, contains larger molecules (ranging from about 6.0 to 6.9 Å) such as propane and isobutene. These molecules can form Type II hydrates but only occupy the large cages of the Type II structure. They are too large to enter the smaller cages of a Type II hydrate (Carroll, 2009b).

Molecules with diameter larger than 7 Å, such as pentane, hexane, and larger paraffin hydrocarbons do not form Type I or Type II hydrates (Carroll, 2009b). These compounds form type H structure and the maximum size for structure H is about 9 Å (Carroll, 2009b).

Size	Hydrate former	Cavities occupied
3 Å		No hydrate
	Ar	$5^{12} + 5^{12}6^4$
4 Å	Kr	**Structure II**
	N_2	
	O_2	
	CH_4	
	Xe H$_2$S	$5^{12} + 5^{12}6^2$
5 Å		**Structure I**
	CO_2	
	C_2H_6	$5^{12}6^2$
	$C-C_3H_6$	**Structure I**
6 Å		
	C_3H_8	
	iso-C_4H_{10}	$5^{12}6^4$
		Structure II
7 Å	n-C_4H_{10}	
		No SI or SII hydrates
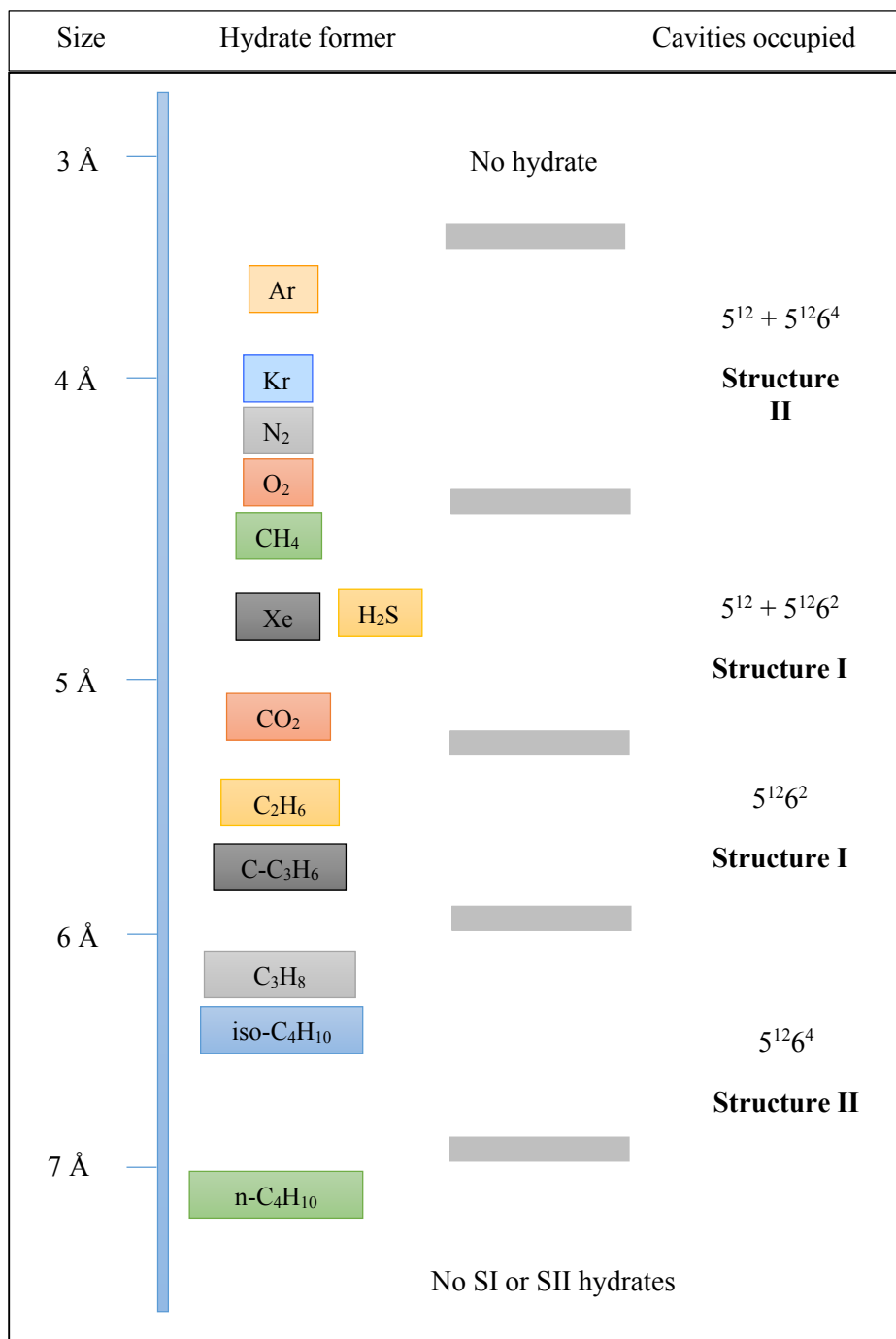
Figure 2.1: Relationship between guest molecule sizes and cavities occupied for various hydrate formers (Carroll, 2009b).

2.3 Formation conditions

The formation of a hydrate requires three conditions (Carroll, 2009b):

a) Suitable temperature and pressure conditions. Hydrate formation is favoured by low temperature and elevated pressure. The composition of the gas assigns the exact temperature and pressure.

b) A hydrate former such as methane, ethane, and carbon dioxide must be present. The size of hydrate cages determine what kind of hydrate formers can enter into the hydrate. The gas molecule must be small enough to fit into a specific hydrate structure.

c) A sufficient amount of water.

To prevent hydrate formation, only one of the three conditions explained has to be eliminated (Carroll, 2009b). Other conditions that increase the formation of hydrates include:

Turbulence: This can be either due to agitation or high velocity of the process fluid. Agitation is necessary to transform liquid water into the hydrate form. Mixing in the process vessel and pipeline increases the hydrate formation (Carroll, 2009b). According the Joule-Thomson effect a large pressure drop across the choke valve causes the temperature to drop in gas flow.

Nucleation Sites: A nucleation site determines the formation of solid from a fluid phase. A damage in the pipeline, a weld spot, or a pipeline fitting (elbow, tee, valve, etc.) are the good nucleation sites for hydrate formation.(Carroll, 2009b).

Free-Water: The presence of free-water increases hydrate formation but it is not necessary.

2.4 Semi-clathrate hydrates

As a mentioned previously, high pressure and low temperature operating conditions are required for hydrate technology. To overcome this problem, semi-clathrate hydrates formed with ionic guest substances have been applied.

Crystallographic studies and X-ray structure analysis have shown that alkyl amines can form special type of clathrates with some broken bonds in the hydrogen-bonded water framework (Jeffrey, 1984, McMullan et al., 1967). These groups of compounds are described as "semi-clathrate" hydrates. The structure of semi-clathrate hydrates are related to those of the clathrate hydrates with a water cavity. In fact, the functional group (amine group) forms a part of the hydrogen-bonded water network while the alkyl chain function may occupy the voids for stabilization of the hydrate.

The quaternary ammonium salts (TBAX) and phosphonium salts (TBPX) can form semi-clathrate hydrates in the presence of water (Jeffrey, 1984). TBAX (with X being bromide,

chloride, fluoride, nitrate, etc.) includes tetrabutyl ammonium bromide (TBAB) (Ye et al., 2014), tetrabutyl ammonium chloride (TBACl) (Sun and Liu, 2012), tetrabutyl ammonium fluoride (TBAF) (Mohammadi et al., 2013a), tetrabutyl ammonium hydroxide (TBAOH) (Karimi et al., 2014), tetrabutyl ammonium nitrate (TBANO$_3$) (Du et al., 2011a). TBPX includes tetrabutyl phosphonium bromide (TBPB) (Mayoufi et al., 2011) and tetrabutyl phosphonium chloride (TBPC). A typical structure of a TBAB semi-clathrate hydrate is shown in Figure 2.2.
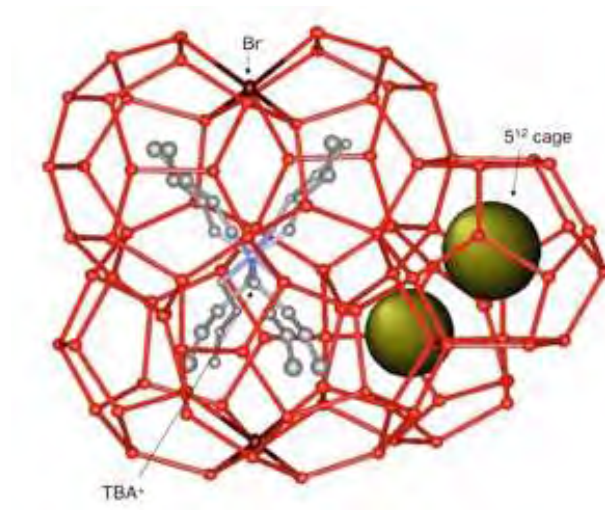
Figure 2.2: TBAB semi-clathrate structure (Shimada et al., 2005).

Recently, clathrate or gas hydrate crystallization as a novel technology for CO$_2$ capture and separation has been of interest to both both science and technology. Table 2.2 lists reviews and books on the subject of clathrate hydrates (Sloan and Koh, 2008). Also, a short report on the publications with the subject of "gas hydrate" is shown in Figure 2.3.

Table 2.2: Books and reviews on clathrate hydrates.

Title	Ref
Clathrate hydrates	(Englezos, 1993)
Gas hydrates to world margin stability and climatic change (Geological Society Special Publication No.137)	(Henriet and Mienert, 1998)
Natural gas hydrate in oceanic and permafrost environments	(Max, 2003)
Benefits and drawbacks of clathrate hydrates: a review of their areas of interest	(Chatti et al., 2005)
Economic geology of natural gas hydrate	(Max et al., 2006)
Clathrate hydrates of natural gases	(Sloan, 2008a)
Clathrate hydrates: from laboratory science to engineering practice	(Strobel et al., 2009a)
Clathrate hydrates in nature	(Hester and Brewer, 2009)
Natural gas hydrates a guide for engineers	(Carroll, 2009a)
Sediment-hosted gas hydrates: new insights on natural and synthetic systems (Geological Society Special Publication No. 319)	(Long et al., 2009)
Advances in the studies of gas hydrates	(Taylor and Kwan, 2010)
Methane gas hydrate (green energy and technology)	(Demirbas, 2010)
Natural gas hydrates in flow assurance	(Koh et al., 2010)
Physicochemical properties of ionic clathrate hydrates	(Shin et al., 2010)
Gas hydrates: immense energy potential and environmental challenges (green energy and technology)	(Giavarini and Hester, 2011)
Exploration of gas hydrates : geophysical techniques	(Thakur and Rajput, 2011)
Natural gas hydrates: experimental techniques and their applications	(Ye and Liu, 2013)
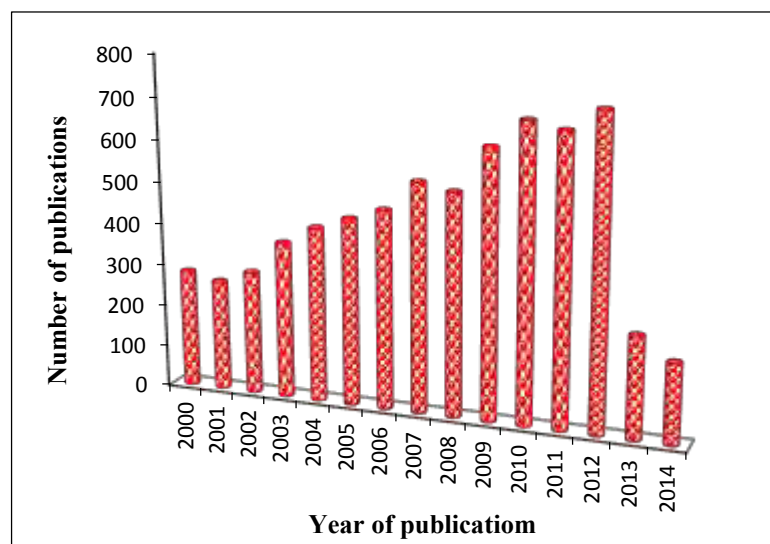
Figure 2.3: Number of publications on CO₂ capture by gas hydrate (with words 'gas hydrate' and 'CO₂' in titles). Data from ISI Web of Knowledge, Thomson Reuters.

2.5   Additives for forming CO$_2$ hydrates as promoters

Formation of gas hydrates typically needs a high pressure/low temperature condition which makes the process costly. In order to moderate and speed up the pressure conditions for hydrate phase formation, gas hydrate promoters are developed in crystallization processes.

Gas hydrate promoters can be classified according to their effect on the structure into two categories (Eslamimanesh et al., 2012f):

a) Additives that doesn't change the structures of the water hydrogen-bonded networks e.g. tetrahydrofuran (THF), anionic/non-ionic surfactants, cyclopentane, propane, SO$_2$, acetone etc.

b) Additives that take part in the structures of the ordinary water cages in the traditional clathrates networks such as quaternary ammonium salts particularly tetra-n-butylammonium salts (e.g. TBAB and tetra-n-butylammonium borohydride).

2.5.1   Water soluble organic promoters

Tetrahydrofuran is a cyclic ether which is one of the most studied thermodynamic promoters for capturing and recovering CO$_2$ from flue gas (Delahaye et al., 2005, Seo et al., 2008a). THF can be used to reduce the hydrate formation pressures of CO$_2$ hydrates. In particular, THF can form sII hydrate structures with water in which THF molecules fills only the large cavities ($5^{12}6^4$) in the hydrate lattice (Lee et al., 2012c). A number of publications that present THF as a promoter

17

in gas hydrate are available in the literature (Figure 2.4). Table 2.3 summarizes a list of all experimental studies on CO_2 hydrates in the presence of THF that has been reported in the literature.
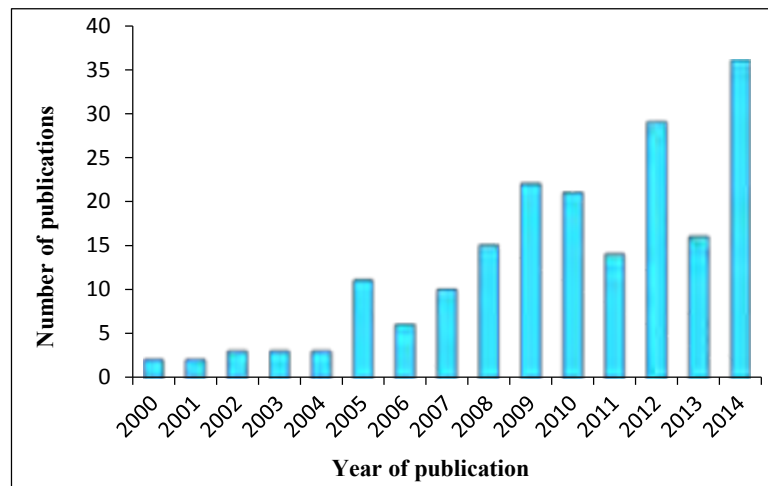
Figure 2.4: Publications presenting THF as a promoter of gas hydrate formation.

Table 2.3: Experimental studies on gas hydrates of carbon dioxide in the presence of THF.

Author(s)	Systems	Study
(Kang and Lee, 2000)	$CO_2+N_2+H_2O+THF$	Development of a new hydrate-based process for separating CO_2 from flue gas
(Kang et al., 2001)	$CO_2+N_2+H_2O+THF$	Thermodynamic studies of CO_2/N_2 hydrates and investigation of the hydrate stability region
(Delahaye et al., 2006)	CO_2+H_2O+THF	Investigation of the formation conditions and the latent heat of dissociation of hydrates
(Hashimoto et al., 2006a)	$CO_2+H_2+H_2O+THF$	Phase equilibria studies and investigation of the cage occupancy of H_2 by Raman spectroscopy
(Lee et al., 2008)	$CO_2+H_2+H2O+THF$	Pre-combustion CO_2 capture from fuel gas by gas hydrate technology
(Linga et al., 2008)	$CO_2+N_2+H_2O+THF$	Thermodynamic and kinetic studies for post-combustion capture of CO_2 through three hydrate stages coupled with a membrane
(Joon Shin et al., 2009)	CO_2+H_2O+THF	Measurement of hydrate dissociation conditions and Raman spectroscopy and X-ray diffraction analysis for the hydrate systems
(Liu et al., 2009)	$CO_2+H_2O+THF+SDS$	Investigation of the effect of water soluble additives and characterization of CO_2 hydrate formation in a high-pressure reactor
(Lu et al., 2009)	$CO_2+N_2+H2O+THF$	PVT studies on dissociation conditions of gas hydrates
(Adeyemo et al., 2010)	CO_2+H_2/N_2+THF+ silica gel	Investigation of the effect of the silica gel bed on CO_2 capture through gas hydrate crystallization from flue gas or fuel gas
(Lee et al., 2010)	CO_2+H_2+THF	Thermodynamic and kinetic studies on pre-combustion CO_2 capture
(Sabil et al., 2010b)	$CO_2+H_2O+THF+NaCl/MgCl_2/CaCl_2$	Investigation of the promotion effect of THF to prevent inhibition effect of electrolytes

(Sabil et al., 2010a)	CO_2+H_2O+THF	Estimations of enthalpies of dissociation of simple and mixed CO_2 hydrates through direct measurements
(Sabil et al., 2010b)	CO_2+H_2O+THF	Phase equilibria measurement of CO_2 hydrate in the presence of THF
(Torré et al., 2011)	$CO_2+H_2O+THF+SDS$	Thermodynamic and kinetic studies of CO_2 hydrate formation in quiescent hydrate-forming conditions
(Lee et al., 2012c)	CO_2+CH_4+THF	Studies of the thermodynamic stability of systems containing CO_2 and characterization of structures by X-ray diffraction (XRD) and Raman spectroscopy
(Lirio et al., 2013a)	$CO_2+THF+SDS$	Measurements of the formation conditions, storage capacity and induction time of CO_2 hydrates
(Park et al., 2013b)	$CO_2+H_2+H_2O+THF$	Thermodynamic, kinetic, and structural characterization study on the CO_2 hydrate
(Ricaurte et al., 2013b)	$CO_2+CH_4+THF+SDS$	Investigation of the effect of water soluble additives on CO_2 separation and capture from CO_2-CH_4 gas mixture
(Yang et al., 2013b)	$CO_2+H_2+H2O+THF+SDS$	Influences of the different concentrations of THF/SDS in porous media on the gas mixture separation
(Tang et al., 2013)	$CO_2+CH_4/N_2+THF/SDS$	Hydrate phase equilibrium measurement for hydrate-based gas separation
(Yang et al., 2013b)	$CO_2+H_2+H_2O+THF+SDS$	Thermodynamics and dynamics study of CO_2 hydrate to develop hydrate-based CO_2 capture technology in porous media
(Zhang et al., 2014)	$CO_2+N_2+H_2O+THF+SDS$	Hydrate phase equilibrium measurement for hydrate-based gas separation in porous media
(Sfaxi et al., 2014)	$CO_2+N_2+H_2O+THF+TBAB+$ $TBAF$	Thermodynamic equilibrium measurements to determine the hydrate stability conditions of CO_2/N_2
(Zhong et al., 2014)	$CO_2+CH_4+H_2O+THF$	Hydrate-based separation process to separate CO_2 from the shale gas

It was presumed that hydrogen cannot form clathrate hydrates because of its small molecular diameter. However, the formation of hydrogen sII hydrate at low temperatures and extremely high pressures was reported in 2004 and 1999 (Lokshin et al., 2004, Dyadin et al., 1999a). It has been shown that aqueous solutions of THF can decrease the hydrogen hydrate formation pressure (Mohammadi and Richon, 2010b, Anderson et al., 2007, Lee et al., 2005, Florusse et al., 2004, Sugahara et al., 2009, Mohammadi and Richon, 2009e, Strobel et al., 2009b, Ogata et al., 2008, Nagai et al., 2008, Hashimoto et al., 2007, Hashimoto et al., 2006b, Zhang et al., 2004). Also, methane which is one of the main components in petroleum and natural gas can form clathrate hydrates at high pressures. It has been reported that aqueous solutions of THF can significantly moderate the clathrate hydrate formation pressure of methane (Sun et al., 2010, Wang et al., 2008b, Ma et al., 2009, Giavarini et al., 2008, Zhang et al., 2005).

1, 4-Dioxane, propylene oxide, and furan are classified as cyclic ethers. 1, 4-Dioxane and propylene are water-soluble and furan is a water insoluble hydrate former (Manteghian et al., 2013, Jager et al., 1999, Cheng et al., 2013, Illbeigi et al., 2011, Seo et al., 2001a, Maekawa, 2013). By the addition of low concentration of these ethers, gas hydrate can be stabilized (Saito et al., 1996a).

Kamran-Pirzaman et al. (Kamran-Pirzaman et al., 2013) reported experimental hydrate phase equilibria for CO_2 + 1,4-Dioxane/furan + water. They showed that the promotion effect of 1, 4-Dioxane on CO_2 hydrates is negligible. Furthermore, they observed that furan has a noticeable promotion effect on CO_2 hydrates.

Seo and Kang (Seo et al., 2008a) measured the CO_2 hydrate dissociation pressure in the presence of THF, propylene oxide, and 1,4-dioxane. They found that, among these cyclic ethers, THF shows the highest stabilization effect.

Acetone is a water soluble hydrate promoter. Acetone can form structure II hydrates with water as a single guest (Du et al., 2010, Seo et al., 2001a). To the best of our knowledge, very limited experimental data for the systems including clathrate hydrates of CO_2 + acetone + water systems are available. Maekawa (Maekawa, 2011) and Kamran-Pirzaman (Kamran-Pirzaman et al., 2013) measured equilibrium conditions of the clathrate hydrates formed from CO_2 and different concentrations of acetone aqueous solutions.

2.5.2 Surfactants and kinetic promoters

Surfactants are another class of hydrate formation promoters which exist as non-ionic, anionic, and cationic types. Surfactant molecules can form micelles which encompass the gas and water molecules and enhance the water-gas interface (Zhong and Rogers, 2000, Karaaslan et al., 2002b, Kumar et al., 2013b, Okutani et al., 2008, Lee et al., 2007). Surfactant promoters have been

studied traditionally with methane (Sloan and Koh, 2008). The information for other gases like CO_2, H_2S and H_2 is limited as described below:

Kalogerakis et al. (Kalogerakis, 1993) investigated the effects of surfactants on the hydrate formation kinetics. Zhong and Rogers (Zhong and Rogers, 2000) and Sun et al. (Sun et al., 2003b, Sun et al., 2003a) concluded that surfactants increase the formation rates of gas hydrates. They showed that surfactants can also increase the hydrate storage capacity. Karaaslan and Parlaktuna (Karaaslan and Parlaktuna, 2000, Karaaslan et al., 2002a) experimentally investigated the formation kinetics of several surfactant promoted-gas hydrates. They found that the effect of a nonionic surfactant is less observable compared with anionic and cationic ones. Also, they showed that anionic surfactants increase the hydrate information rate more than cationic ones. Link et al. (Link et al., 2003) studied the formation/dissociation characteristics and the storage capability of methane hydrates promoted by a variety of surfactants. They concluded that SDS could speed up the process of methane hydrate formation.

According to Lin et al. (Lin et al., 2004) SDS affects the storage capacity and the formation/dissociation kinetic behavior (particularly below ice point) of methane hydrate. Ganji et al. (Ganji et al., 2007) investigated the effects of different surfactants (anionic, cationic and non-ionic) on methane hydrate formation rate, stability and storage capacity. They concluded that SDS has the best performance when using methane hydrates for storage and transportation of gas. They also found that SDS increases the hydrate formation rate and enhances the hydrate storage capacity as well.

Verrett et al. (Verrett et al., 2012) studied surfactant effects on methane solubility during hydrate growth in a semi-batch stirred crystallizer. The results demonstrated that SDS has no influence on methane solubility; however it has a positive effect on the methane mole fraction in the bulk liquid during hydrate growth. Ando et al. (Ando et al., 2012) described an experimental study of clathrate hydrate formation from a mixture of methane, ethane, and propane in an unstirred surfactant-containing system.

Mandal and Laik (Mandal and Laik, 2008) studied the effects of the surfactants on the hydrates formation rate and the hydrate storage capacity in a quiescent system. Torre et al. (Torre et al., 2012) presented experimental CO_2 hydrate equilibrium curves with/without the SDS and/or THF as additives.

The influence of Tween-80 (T-80), dodecyl trimethyl ammonium chloride (DTACl) and SDS as kinetic promoters was investigated by Kumar et al. (Kumar et al., 2013a). They found that SDS is most effective in enhancing the hydrate formation rate as well as reducing the induction time. Figure 2.5 shows the number of publications on gas hydrates in the presence of a surfactant.
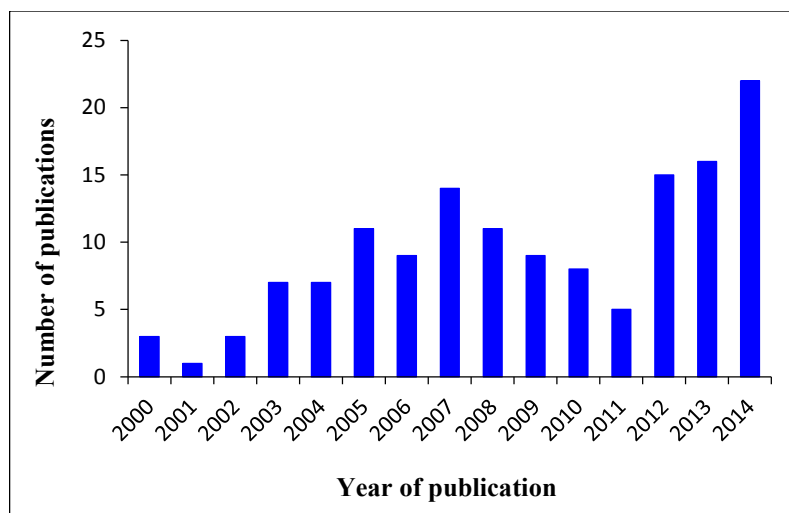
Figure 2.5: Publications presenting surfactants as a possible promoter.

Hydrotropes are small amphiphilic molecules with hydrophilic feature, having the ability to enhance aqueous solubility of organic compounds. Hydrotropes are considered as kinetic hydrate promoters which reduce the hydrate nucleation time and increase the hydrate growth rate. They can improve the solubility of the natural gas components in water. Gnanendran and Amin (Gnanendran and Amin, 2004) showed that hydrotrope para-toluene sulfonic acid (p-TSA) can promote natural gas-hydrate formation. According to Gnanendran and Amin, unlike surfactants, hydrotropes promote clathrate hydrate thermodynamics by formation of aggregate entities (Gnanendran and Amin, 2003). As a consequence, the stability conditions shift to higher temoeratures. Rovetto et al. (Rovetto et al., 2006) studied the influence of para-toluene sulfonic acid (p-TSA) on the phase equilibria of gas hydrate. They concluded that p–TSA does not have any effect on the stability conditions of gas hydrates storage/transportation.

2.5.3 Water insoluble promoters

Heavy hydrocarbons like cyclopentane (CP), cyclohexane (CH), methyl cyclohexane (MCH), etc. are known as thermodynamic promoters (Lv et al., 2013, Zhong et al., 2012, Mohammadi and Richon, 2011). They are water-insoluble hydrate formers which may form structure II or structure H (Khokhar et al., 1998, Illbeigi et al., 2011). They occupy only the large cavities. Small gas molecules such as nitrogen and methane can be trapped in the small cavities. Water insoluble promoters have been studied traditionally with methane as a help gas (Sloan and Koh, 2008). Information for other gases like CO_2, H_2S, H_2, N_2, etc. is limited as explained below:

Mehta and Sloan (Mehta and Sloan, 1994) studied the phase equilibrium data for structure H hydrates using heavier liquid hydrocarbons including 2-methylbutane, 2,2-dimethylbutane, and methylcyclohexane, with methane as the small help gas molecule.

Tohidi et al. have published several article on hydrate equilibrium data in the presence of heavy hydrocarbon compounds (Tohidi et al., 1997c, Tohidi et al., 1997a, Østergaard et al., 2001). They measured hydrate dissociation conditions for binary and ternary systems with methane or/and nitrogen in the presence of cyclopentane and neopentane hydrates (Tohidi et al., 1997c). In addition, they studied three structure-II and three structure-H heavy hydrate formers including cyclopentane, cyclohexane, neopentane, isopentane, methyl cyclopentane (MCP), and methyl cyclohexane (Tohidi et al., 1997a). They investigated the effect of heavy hydrate formers on the stability of hydrate structures.

Sun et al. (Sun et al., 2002) reported the dissociation conditions for methane + cyclohexane or cyclopentane systems. The results reveal that this system forms a structure sII hydrate whereas methane forms structure sI. Furthermore, the experimental results for this system show that the intermediate hydrocarbon compounds at lower temperatures act as a hydrate promoter whereas it behaves an inhibitor at higher temperatures.

Mohammadi and Richon (Mohammadi and Richon, 2009d) reported dissociation data for the ternary system of CO_2 + water-insoluble additives + water in various temperature ranges. These additives include methyl cyclopentane, methyl cyclohexane, cyclopentane and cyclohexane. Matsumoto et al. (Matsumoto et al., 2014) measured dissociation data for carbon dioxide and cyclopentane derivatives. They measured the phase equilibrium data for CO_2 + cyclopentane and confirmed data reported by Mohammadi and Richon (Mohammadi and Richon, 2009d). In another study (Mohammadi and Richon, 2010a), they showed that the existence of methyl cyclohexane can dramatically enhance the hydrate dissociation temperature or reduce the hydrate dissociation pressure of the CH_4 + water system. However, the promotion effect of methyl cyclohexane on the hydrogen sulfide (H_2S) + water system is not very remarkable (Mohammadi and Richon, 2010a). In a similar study, they reported the promotion effect of cyclopentane/cyclohexane in the presence of hydrogen sulfide and compared the data with the promotion effect of methyl cyclohexane promoter (Mohammadi and Richon, 2009a, Mohammadi and Richon, 2009c).

Zhang and Lee (Zhang and Lee, 2009b) studied the dissociation temperatures of H_2 + cyclopentane hydrates and CO_2 + cyclopentane hydrates. They found that the CO_2 hydrate formation rate is accelerated in the presence of a small amount of cyclopentane (Zhang and Lee, 2009a).

Li et al. (Li et al., 2010b) investigated CO_2 capture from simulated flue gas (CO_2/N_2 mixture) in the presence of cyclopentane. After that, the effect of cyclopentane or cyclopentane/water emulsion on hydrate formation kinetics was examined and reported.

Trueba et al. (Trueba et al., 2011) reported hydrate dissociation data for cyclopentane + water and H_2 + cyclopentane + water systems. They concluded that the hydrate dissociation temperature is independent of pressure because of the low compressibility of the phases. They compared the molecular geometry of various promoters and found that the compounds with the highest symmetry may produce the most stable clathrate hydrates.

Corak et al. (Corak et al., 2011) investigated cyclopentane hydrate formation at atmospheric pressure for sub-cooled temperature ranges between 3.6 K and 5.6 K. Karanjkar et al. (Karanjkar et al., 2012) studied the kinetics of cyclopentane hydrate formation in an emulsion. They concluded that the cyclopentane hydrate formation is an interfacial process depending on the availability of interfacial area between the water and the hydrate former phase.

Lim et al. (Lim et al., 2013) reported the influence of cyclopentane on the morphology of CO_2/H_2 clathrate in a non-stirred system. They also investigated the effect of SDS surfactant on the crystal growth and morphology. They proposed the mechanism for the kinetics of the CO_2 + H_2 + cyclopentane hydrate system which is in good agreement with their morphological observations.

Mooijer-van den Heuvel (Mooijer-van den Heuvel et al., 2001) studied phase behavior of CO_2 hydrates in the presence of water-insoluble additives (tetrahydropyran, cyclobutanone, cyclohexane and methyl cyclohexane). The result demonstrated that these additives can decrease the hydrate equilibrium pressure.

As mentioned previously, furan is another effective water-insoluble promoter. It can decrease the hydrate dissociation pressure of the CO_2 + water system (Kamran-Pirzaman et al., 2013).

2.5.4   Quaternary ammonium/ phosphonium salts

QAS/QAP, especially tetrabutyl ammonium/phosphonium salts (TBAX/TBPX) in which ''X'' represents halogen elements such as bromide, chloride, and fluoride are considered a kind of semi-clathrate. They are well known thermodynamic promoters that are able to decrease the hydrate formation pressure by breaking the water lattice and taking part in the structure of hydrogen-bonded networks (Eslamimanesh et al., 2012d, Mohammadi et al., 2011a, Mohammadi et al., 2013b, Koyanagi and Ohmura, 2013a, Kamran-Pirzaman et al., 2013, Li et al., 2010c, Sato et al., 2013, Trueba et al., 2012, Fan et al., 2009).

Aladko et al. (Aladko et al., 2002) studied clathrate formation in tetra-n-butyl ammonium (TBAX) and tetraisoamyl ammonium halides using thermal analysis (TA) and differential thermal analysis methods. They found that the stability of TBAX decreases with an increase in the size of halogen compounds (TBAX: F>Cl>Br).

Fan et al. (Fan et al., 2009) investigated the effects of TBAB and TBAF on the hydrate formation rate and CO_2 capture separation efficiency in flue gas samples. The results showed that TBAB and TBAF increases hydrate formation.

Li et al. (Li et al., 2010b) reported hydrate equilibrium data for CO_2 + TBAF/TBAB/TBAC. The comparison of the hydrate dissociation data for the stated systems with the CO_2 + water system illustrated that TBAB, TBAC, and TBAF can increase the hydrate stability region.

Lee et al. (Lee et al., 2012b) measured phase equilibria data for the CO_2 + TBAF + water and CH_4 + TBAF + water systems with various TBAF concentrations. NMR and Raman spectroscopy were used to analyze semi-clathrate hydrates. The gas uptake during the semi-clathrate formation was measured. The semi-clathrates formed were analyzed via NMR and Raman spectroscopy. A differential scanning calorimeter (DSC) was also used to verify the dissociation temperature and dissociation enthalpy of the pure TBAF semi-clathrates.

Trueba et al. (Trueba et al., 2013) investigated semi-clathrate hydrate formation kinetics of H_2 and CO_2 in presence of TBAF. The results show that CO_2-TBAF semi-hydrates may apply in separation technologies e.g., for removing CO_2 from flue gases. Furthermore, the CO_2 content in the hydrate phase is dramatically higher than the H_2 content at low pressures.

Sun et al. (Sun et al., 2011) measured semi-clathrate hydrate phase equilibrium data and latent heat for TBAC aqueous solutions at atmospheric pressure. According to their work, the phase equilibria temperature increases by enhancing the concentration of TBAC aqueous solution before the stoichiometric concentration (35 % mass fraction).

Arjmandi et al. (Arjmandi et al., 2007) measured phase equilibrium data of H_2, CH_4, N_2, CO_2 and natural gases in the presence of TBAB. They showed that hydrate stability is enhanced with an increase in the concentration of TBAB.

Duc et al. (Duc et al., 2007a) studied CO_2 separation from a CO_2 + N_2 mixture by hydrate crystallization using TBAB. They showed that six-stage hydrate crystallization working in the pressure range of 7.5 to 50 bar at 283 K can be optimal.

Kumar et al. (Kumar et al., 2009c) presented a hybrid process for pre-combustion capture of CO_2 and H_2 by using two hydrate crystallization stages operating at 273.7 K and 3.8 and 3.5 MPa, respectively.

Li et al. (Du et al., 2011b) focused on pre-combustion separation of CO_2 and H_2 with a one-stage hydrate/membrane process in the presence of TBAB. They reported that the separation efficiency increases with increasing TBAB concentration.

Kim et al. (Kim et al., 2011) studied the influence of TBAB on CO_2 capture from CO_2/H_2 gas mixtures through hydrate crystallization. They reported the thermodynamic and kinetic data for various TBAB concentrations.

Lee et al. (Lee et al., 2011) reported experimental phase equilibrium data and spectroscopic analyses of CH_4 and CO_2 hydrates in the presence of TBAB. Moreover, they used differential scanning calorimetry (DSC) to confirm the dissociation temperature and dissociation enthalpy of pure TBAB semi-clathrates.

Mohammadi et al. reported the phase equilibrium data of semi-clathrate hydrates for the CO_2 + N_2 + TBAB and CO_2+H_2/CH_4+TBAB (Mohammadi et al., 2011a, Mohammadi et al., 2013b) aqueous solution systems.

Koyanagi and Ohmura (Koyanagi and Ohmura, 2013b) studied the formation and growth of ionic semi-clathrate hydrate crystals in the system of aqueous solution of TBAB and CO_2 gas.

Park et al. (Park et al., 2013c) studied the capturing of CO_2 from simulated fuel gas mixtures using semi-clathrate hydrates formed in the presence of TBAB and TBAF. They demonstrated that TBAF is a better QAS in terms of thermodynamic stability.

Figure 2.6 shows the number of studies performed on semi-clathrate hydrates in presence of QAS to date.
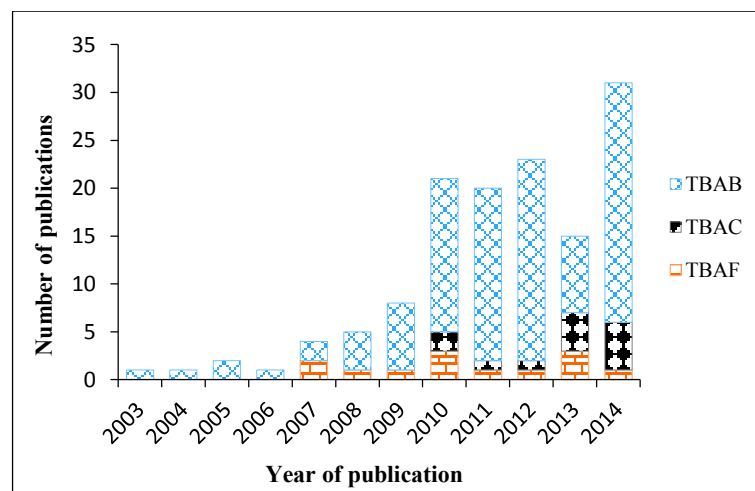
Figure 2.6: Publications presenting tetrabutyl ammonium salts as a promoter.

Tetrabutyl ammonium nitrate (TBANO$_3$) can form two different structures of semi-clathrate hydrates, TBANO$_3$·26H$_2$O and TBANO$_3$·32H$_2$O (Du et al., 2011b). Du et al. (Du et al., 2011b) studied the hydrogen + TBANO$_3$ semi-clathrate hydrate stability condition. The presence of TBANO$_3$ causes the dissociation conditions of hydrogen semi-clathrate hydrate shift to lower pressures and higher temperatures.

Li et al. (Li et al., 2012) studied the effect of TBAB, TBPB and TBANO$_3$ on hydrate formation and separation efficiency for CO$_2$ separation from CO$_2$/N$_2$ binary mixtures by a one-stage hydrate separation process. They concluded that the solubility of CO$_2$ in TBANO$_3$ is higher than TBAB and TBPB. For this reason, the higher solubility of CO$_2$ in TBANO$_3$ solution is more helpful for CO$_2$ capture in comparison with the other two solutions.

Suginaka et al. (Suginaka et al., 2012) measured thermodynamic properties including composition–temperature phase diagrams and the dissociation enthalpy of TBPB semi-clathrate hydrates. In other work (Suginaka et al., 2013) measured phase equilibrium data for CO$_2$, CH$_4$, or N$_2$ + TBPB. They presented that TBPB may be used as an additional guest for hydrate-based separation, and showed that CO$_2$ can be captured from CH$_4$ + CO$_2$ and N$_2$ + CO$_2$ mixtures.

Mayoufi et al. (Mayoufi et al., 2011, Mayoufi et al., 2009) investigated the phase behavior of simple and mixed semi-clathrate hydrates formed from CO$_2$ + TBPB + water mixtures by pressure-controlled differential scanning calorimetry (DSC).

2.5.5 Mixed promoter systems

2.5.5.1 Water- soluble and water-insoluble promoters

It is believed that the combination of water- soluble and water-insoluble promoters can improve gas separation performance. Li et al. (Li et al., 2011b) studied the capture of CO$_2$ from several fuel gas samples in the presence of TBAB and cyclopentane using hydrate formation technology. They investigated the effects of TBAB and cyclopentane on the gas uptake, the CO$_2$ separation efficiency, the induction time, and the hydrate formation rate at various conditions. The experimental results show that the presence of cyclopentane in pure water/gas systems does not significantly affect the gas uptake, whereas the presence of the cyclopentane in the TBAB solution dramatically increases the CO$_2$ separation and accelerates hydrate nucleation rate and reduces the induction time. A comparison between the studies of Li et al. (Li et al., 2011b) and Linga et al. (Linga et al., 2007c) shows that the presence of TBAB+ cyclopentane can increase the system gas uptake by 2 times that of THF. Moreover, TBAB+ cyclopentane decreases the induction time by 10 times compared to THF at a similar temperature–pressure condition with Linga et al. (Linga et al., 2007c).

Li et al. reported that a synergistic effect of cyclopentane and TBAB on hydrate-based CO_2 capture may occur (Li et al., 2011b). They demonstrated that the addition of cyclopentane into a TBAB solution causes greater gas uptake for the gas + cyclopentane + TBAB + H_2O system than the sum of uptakes for the gas + cyclopentane + H_2O and gas + TBAB + H_2O systems. Additionally, they found that cyclopentane and TBAB remarkably decreases the induction time for forming hydrates.

Herslund et al. (Herslund et al., 2013) used THF, cyclopentane and their mixtures for thermodynamically promoting carbon dioxide–clathrate hydrate formation. THF and cyclopentane are known as water-soluble and water-insoluble, respectively and both stabilize the sII hydrate structure. Therefore, they have a tendency for creation of large cavities of the hydrate structure. The results show that the addition of THF to water increases the solubility of cyclopentane and reduces the equilibrium pressure by 25–30% compared to the ternary system of H_2O/ cyclopentane /CO_2.

2.5.5.2 Kinetic and thermodynamic promoters

Application of both thermodynamic promoter (THF) and a kinetic promoter (SDS) may help to increase the separation of CO_2 by clathrate hydrate formation.

Studies by Liu et al. (Liu et al., 2009) showed that the combination of a SDS and THF can promote the hydrate formation rate considerably.

Torre et al. (Torré et al., 2011) studied the influence of THF and a SDS combination for enhancing CO_2 hydrate capture. They concluded that these two additives are very effective in promoting CO_2 capture.

Partoon and Javanmardi (Partoon and Javanmardi, 2013) presented the formation kinetics and stability of methane hydrates in the presence of propanone + SDS, as thermodynamic and kinetic hydrate promoters. The result illustrated that propanone and a mixture of propanone + SDS can enhance the formation rate and reduce induction time.

CO_2 separation from a CO_2 + CH_4 gas mixture by hydrate formation has been reported in the presence of THF and SDS by Ricaurate et al. (Ricaurte et al., 2013a). They investigated the effect of the concentration of additives, and the influence of the gas loading pressure and the hydrate formation temperature, on both the kinetics and the selectivity of CO_2 capture.

Lirio et al. (Lirio et al., 2013b) and Yang et al. (Yang et al., 2013a) investigated the influence of THF and SDS on the separation of CO_2. They concluded that the storage capacities of CO_2 hydrates can increase by using SDS. Also, an increase in THF concentration increased the driving

force for hydrate formation and reduced the hydrate induction time and hydrate phase equilibrium pressure.

Tang et al. (Tang et al., 2013) studied $CO_2 + N_2$ and $CO_2 + CH_4$ systems in the presence of SDS and THF to investigate the influence of hydrate additives on the gas separation process.

Joshi et al. (Joshi et al., 2013) measured phase equilibrium data for CO_2 in the presence of TBAB with a small amount of surfactant (SDS). It is observed that the addition of SDS may help to enhance clathrate hydrate formation while it does not influence phase equilibrium conditions.

2.5.6 CO_2 capture by gas hydrate formation in porous media

A porous medium (or a porous material) is a substance consisting of pores which can fill with a gas or liquid. One of the most common applications of porous media is in hydrate formation technology. Recently, several studies have been published on hydrate formation in porous media (Buffett and Zatsepina, 2000, Zatsepina and Buffett, 2001, Lee et al., 2002, Zatsepina and Buffett, 2002, Katsuki et al., 2006, Li et al., 2008, Kang et al., 2008, Baldwin et al., 2009, Seo et al., 2005). Yang and co-workers (Yang et al., 2013b) focused on analyzing the hydrate formation and dissociation process when CO_2 flows into porous media, which may be beneficial for CO_2 capture based on hydrate formation. They investigated the effects of flow rate, pressure, temperature, and flow direction on CO_2 hydrate formation and dissociation. Furthermore, they investigated the effects of THF/SDS on the thermodynamic and kinetic properties of the hydrate in porous media for separating of CO_2 from fuel gas (Yang et al., 2013a, Yang et al., 2013b). They also studied magnetic resonance imaging (MRI) measurements of CO_2 hydrate dissociation rate in a porous medium (Yang et al., 2011).

Dicharry et al. (Dicharry et al., 2013) focused on the formation behavior of CO_2 hydrates in porous silica gel and in the presence of a surfactant solution. They demonstrated that the combination a porous medium and a surfactant may have a positive influence on the kinetics of hydrate formation.

Kumar et al. (Kumar et al., 2013b) investigated CO_2 clathrate hydrate kinetics in porous media by using surfactants as a kinetic promoter. They used three different silica gels of diverse particle size and three different kinds of surfactants (SDS, DATCl and Tween-80) to investigate CO_2

gas hydrate formation. They found that, among the three surfactants, SDS is the most effective in increasing the hydrate formation rate and decreasing the induction time.

Song et al. (Song et al., 2013c) investigated the influence of several factors which affect CO_2 capture using hydrate formation in porous media. They found that the most important factor for hydrate phase equilibria is the porous property. The formation kinetics of CO_2 hydrates in porous

silica gels was studied by Kang and Lee (Kang and Lee, 2010) at different temperature and pressure conditions. They used SDS to investigate the influence of a kinetic promoter on the formation kinetics.

Babu et al. (Babu et al., 2013b) reported pre-combustion capture of carbon dioxide in silica sand and silica gel as a contact medium using the clathrate hydrate process.

2.5.7 CO_2 hydrate formation with nanoparticles

During the last decade, nanofluids have been employed to increase the hydrate formation rate, storage capacity, and to decrease the induction time. Li et al. (Li et al., 2006) investigated the formation and dissociation of HFC134a (CH_2FCF_3) hydrates in copper nanoparticles. They showed that adding copper nanoparticles increases the heat and mass transfer processes of HFC134a hydrate formation.

Park et al. (Park et al., 2010, Park et al., 2012) used multi-walled carbon nanotubes for promoting methane hydrate formation and increasing the hydrate formation rate. Arjang et al. (Arjang et al., 2013) showed that the presence of silver nanoparticles decreases the methane hydrate induction time. The effect of polymer nanocomposites on methane hydrate stability and storage capacity was reported by Ganji et al. (Ganji et al., 2013). Chari et al. (Chari et al., 2013) investigated methane hydrate formation and dissociation in nano silica. They claimed that the presence of nano silica improves the methane gas hydrate yield significantly.

Mohammadi et al. (Mohammadi et al., 2014) studied the influence of silver nanoparticles and SDS on CO_2 hydrate formation for the first time. The experimental results showed that these additives do not affect induction time, but the storage capacity does increase. Zhou Shi-dong et al. (ZHOU Shi-dongab, 2014) presented the effects of graphite nanoparticles on CO_2 hydrate formation processes. They reported that the graphite nanoparticles enhance the induction time of CO_2 hydrate formed by 80.762% on average. Furthermore, the amount of gas (CO_2) consumed is enhanced by 12.84% due to the presence of nanographite particles.

2.6 Summary of important studies on clathrate/semi-clathrate hydrates for CO_2 capture

Table 2.4 and Table 2.5 reports experimental studies that have been undertaken to date on the separation of CO_2 from different gas mixtures via clathrate/semi-clathrate hydrates in the absence and/or presence of hydrate promoters.

Table 2.4: Experimental studies for gas hydrates of carbon dioxide + gas/gas mixture systems in the presence of pure liquid water.

Author(s)	Gas system	Temperature range / K	Pressure range / MPa
(Unruh and Katz, 1949)	($CO_2 + CH_4$)	275.5 - 285.7	1.99 - 7.0
(Adisasmito et al., 1991)	($CO_2 + CH_4$)	273 -2 88	1.2 - 11
(Ohgaki et al., 1996)	($CO_2 + CH_4$)	280.3	3.04 - 5.46
(Seo et al., 2000)	($CO_2 + CH_4$)	272 - 284	1.5 - 5
(A. Hachikubo, 2002)	($CO_2 + CH_4$)	271.0	1.27 - 2.02
(Uchida et al., 2005)	($CO_2 + CH_4$)	258 - 274.1 and 190	0.5 - 3 and 0.1
(Belandria et al., 2010)	($CO_2 + CH_4$)	279.1 - 289.9	2.96 - 13.06
(Bruusgaard et al., 2010)	($CO_2 + CH_4$)	274 - 288	1.4 - 5
(Belandria et al., 2011c)	($CO_2 + CH_4$)	233 - 373	up to 60
(Lee et al., 2012a)	($CO_2 + CH_4 + N_2$)	273 - 282	up to 6
(Seo et al., 2000)	($CO_2 + N_2$)	271.7 - 284.25	1.2 - 23.5
(Kang et al., 2001)	($CO_2 + N_2$)	272 - 282	1.5 - 30
(Seo and Lee, 2004)	($CO_2 + N_2$)	272.1	3.2 - 14.05
(Park et al., 2006)	($CO_2 + N_2$)	-	-
(Bruusgaard et al., 2008)	($CO_2 + N_2$)	275 - 283	2 - 22.4
(Belandria et al., 2011a)	($CO_2 + N_2$)	273.6 - 281.7	up to 17.6
(Daraboina et al., 2013c)	($CO_2 + N_2$)	273.7	7.71
(Kim and Lee, 2005)	($CO_2 + H_2$)	273.15	-
(Sugahara et al., 2005)	($CO_2 + H_2$)	274.3 - 281.9	up to 10
(Rice, 2006)	($CO_2 + H_2$)	-	-
(Kumar et al., 2006)	($CO_2 + H_2$)	273.9 - 281.6	1.58 - 10.74
(Zhang et al., 2009)	($CO_2 + H_2 + CP$)	284 - 291	-
(Seo and Kang, 2010)	($CO_2 + H_2$)	274.15	6.5 and 8.9
(Belandria et al., 2011b)	($CO_2 + H_2$)	273.6–281.2	up to ~9
(Babu et al., 2013b)	($CO_2 + H_2$+Silica)	274.15	7.5, 8.5 and 9.0
(Kang et al., 2013)	($CO_2 + H_2$)	271.3 – 282.7	1.1 – 10.3
(Surovtseva et al., 2011)	($CO_2+H_2 +N_2+CH_4+Ar$)	-	-
(Babu et al., 2013a)	($CO_2 + H_2 + C_3H_8$)	274.15 -285.15 and 297.15	4.5 - 6

Table 2.5: Studies on clathrate/semi-clathrate hydrate for the carbon dioxide + gas/gases systems in the presence of hydrate promoters.

Author(s)	System
(Du and Wang, 2013)	($CO_2/N_2/CH_4$ + Tri-n-butylphosphine Oxide (TBPO))
(Mayoufi et al., 2011)	(CO_2 + TBPB aqueous solution)
(Li et al., 2012, Gharagheizi et al., 2012)	(CO_2 + Tetrabutyl-(ammonium/phosphonium) Salts)
(Zhang et al., 2013)	(CO_2 + Tetrabutyl-phosphonium Bromide (TBPB))
(Mayoufi et al., 2010)	(CO_2 + Peralkyl-(Ammonium/Phosphonium) Salts)
(Cha et al., 2013)	(CO_2 +CH_4+H_2+ Tri-n-butylphosphine Oxide)
(Shi et al., 2014)	(CO_2 +CH_4+ Tetrabutyl Ammonium Nitrate (TBANO$_3$))
(Du et al., 2011a)	(CO_2 + Tetrabutyl Ammonium Nitrate (TBANO$_3$))
(Ye and Zhang, 2014a, Ye and Zhang, 2014b)	(CO_2+ TBAC /TBPC)
(Li et al., 2010c)	(CO_2 + TBAF/TBAC/TBAB)
(Sun et al., 2011)	(CO_2 + TBAC aqueous solution)
(Kamran-Pirzaman et al., 2013)	(CO_2 + TBAF/TBAC/ furan/acetone/1,4-dioxane aqueous solution)
(Fan et al., 2009)	(CO_2 + TBAF/TBAB aqueous solution)
(Trueba et al., 2013)	(CO_2 + TBAF + aqueous solution)
(Linga et al., 2007a)	(CO_2 + N_2 + THF aqueous solution)
(Lu et al., 2009)	(CO_2 + N_2 + TBAB/THF aqueous solutions)
(Fan et al., 2009)	(CO_2 + N_2 + TBAB/TBAF aqueous solution)
(Deschamps and Dalmazzone, 2010)	(CO_2 + N_2 + TBAB aqueous solution)
(Li et al., 2010d)	(CO_2 + N_2 + TBAB aqueous solution in the presence of dodecyl trimethyl ammonium chloride (DTAC))
(Li et al., 2010b)	(CO_2 + N_2 + cyclopentane/water emulsion)
(Meysel et al., 2011)	(CO_2 + N_2 + TBAB aqueous solution)
(Mohammadi et al., 2012a)	(CO_2 + N_2 + TBAB aqueous solution)
(Belandria et al., 2012b)	(CO_2 + N_2 + TBAB aqueous solution)
(Tang et al.)	(CO_2 + N_2/CH4 + THF/SDS)
(Sun et al.)	(CO_2+N_2+THF)
(Fan et al., 2000)	(CO_2 + CH_4 + water/aqueous sodium chloride solution)
(Beltrá ́ and Servio, 2010)	(CO_2 + CH_4 + water/neohexane emulsion)
(Deschamps and Dalmazzone, 2010)	(CO_2 + CH_4 + TBAB aqueous solution)
(Lee et al., 2012c)	(CO_2 + CH_4 + THF)
(Ricaurte et al., 2013a)	(CO_2 + CH_4 + THF/SDS)
(Lirio et al., 2013b)	(CO_2 + THF + SDS)
(Fan et al., 2009)	(CO_2 + H_2 + TBAB aqueous solution)
(Kim et al., 2011)	(CO_2 + H_2 + TBAB aqueous solution)

(Lim et al., 2013) $(CO_2 + H_2 +$ cyclopentane + SDS)

(Park et al., 2013a) $(CO_2 + H_2 + THF)$

(Yang et al., 2013a) $(CO_2 + H_2 + THF/SDS)$

(Song et al., 2013a) $(CO_2 + H_2 + THF + SDS)$

(Trueba et al., 2013) $(CO_2 + TBAF$ aqueous solution)

(Koyanagi and Ohmura, 2013a) $(CO_2 + TBAB$ aqueous solution)

(Mohammadi et al., 2013b) $(CO_2 + H_2/CH_4 + TBAB$ aqueous solution)

(Komatsu et al.) $(CO_2 + THF/TBAB$ aqueous solution)

(Park et al., 2013c) $(CO_2 + H_2 + TBAF/TBAB$ aqueous solution)

(Dicharry et al., 2013) $(CO_2 + SDS + Tween-80)$

(Herslund et al., 2013) $(CO_2 + THF + cyclopentane)$

3 Review of the thermodynamic models to correlate/predict the phase equilibrium of gas hydrate

Recently, a considerable number of predictive methods have been formulated to represent/predict hydrate thermodynamic properties. These models can be later applied to predict the phase behaviors for other gas hydrate systems at conditions of interest.

The main aim of this chapter is to review the previously developed models for prediction of the phase equilibria of semi-clathrate hydrates.

3.1 Simple estimation techniques

Wilcox et al. (Wilcox et al., 1941) presented a model based on the vapour-solid distribution coefficient as follows:

$$K_i = \frac{y_i}{z_i} \tag{3.1}$$

where y_i and z_i denote the mole fractions of component i in the water-free vapour and water free solid hydrate, respectively. The values of the distribution coefficient are plotted as functions of temperature and pressure for conventional simple hydrate formers present in natural gas. These values are finally collapsed into a single 18-parameter correlation, which have been discussed in detail elsewhere (Sloan, 2008b).

The gas gravity charts of Katz (Katz, 1945b) is known as the simplest method to estimate the (L_w-H-V) equilibrium conditions. Gas gravity is defined as the ratio of molecular mass of the gas to that of air. The Katz chart is shown in Figure 3.1. When using this chart, the gas gravity should be calculated and either temperature or pressure is determined. The pressure or temperature at which hydrates will form is read directly from the chart.
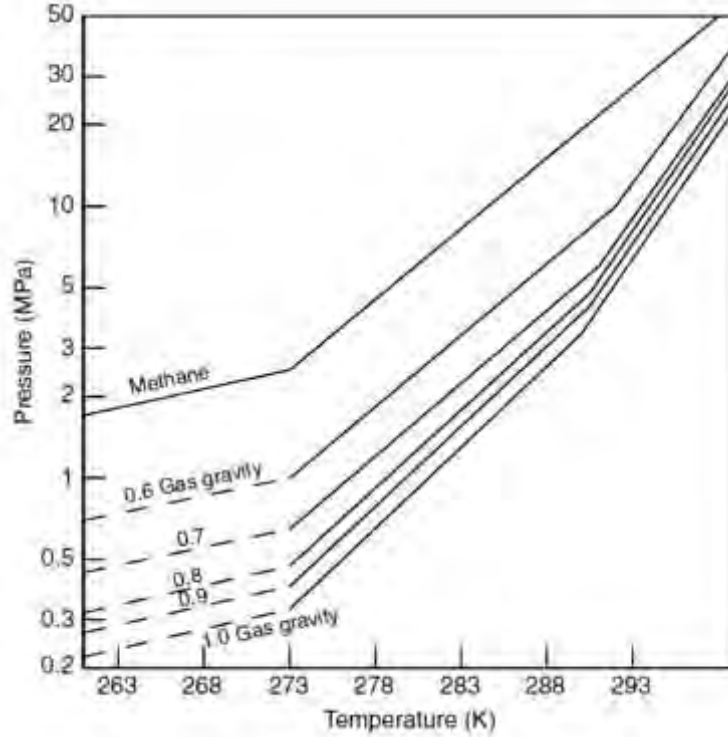
Figure 3.1: Gas gravity chart for prediction of three-phase (Lw–H–V) pressure and temperature (Reproduced from Sloan and Koh 2009).

3.2   Basic statistical thermodynamic model

3.2.1   Van Der Waals and Platteeuw (vdW-P) (1959) model

The first model for predicting hydrate phase equilibrium data of gas hydrate was presented by Van der Waals and Platteeuw (Waals and Platteeuw, 1959). This model is based on four important assumptions:

1. A single type of cavity consisting of only one guest molecule.
2. There is no guest-guest molecule interaction.
3. Classical statistics are valid.
4. The guest molecules do not distort the host lattice

In the final form of the vdW-P model, the difference between the chemical potential of water in the hydrate phase and empty lattice is expressed as:

$$\Delta\mu_w^{\beta-H} = RT \sum_i \nu_i \, ln(1 - y_i) \qquad (3.2)$$

Where R is the universal gas constant, v_i is the number of cavities and y_i is related to the Langmuir constant as follows:

$$y_i = \frac{C_i P}{1 + C_i P} \tag{3.3}$$

Where C_i stands for Langmuir constant and P is partial pressure.

3.2.2 Parrish and Prausnitz (1972) model

Parrish and Prausnitz (Parrish and Prausnitz, 1972) generalized the van der Waals and Platteeuw model. There are two differences between the van der Waals and Platteeuw (Waals and Platteeuw, 1959) model and that model developed by Parrish and Prausnitz (Parrish and Prausnitz, 1972).

Firstly, they extended the model to mixtures of hydrate formers:

$$\Delta\mu_w^{\beta-H} = RT \sum_i v_i \ln\left(1 - \sum_K y_{Ki}\right) \tag{3.4}$$

Secondly, they replaced the partial pressure in Equation (3.3) with the fugacity.

$$y_{Ki} = \frac{C_i f_k}{1 + \sum_j C_{ij} f_j} \tag{3.5}$$

where f_j is fugacity of component j.

3.2.3 Ng and Robinson (1977) model

One of the equation of state thermodynamic models which could be used to calculate the formation of hydrate with a hydrocarbon liquid former is that of Ng and Robinson (Ng and Robinson, 1977). This equation proposed as follows:

$$P = \frac{RT}{v - b} - \frac{\alpha(T)}{v(v + b) + b(v - b)} \tag{3.6}$$

where

$$\alpha = \alpha_c . \alpha(T_r, \omega) \tag{3.7}$$

$$\alpha_c = 0.45724 \frac{R^2 T_c^2}{P_c} \tag{3.8}$$

$$\alpha(T_r, \omega) = \left(1 + k\left(1 - T_r^{1/2}\right)\right)^2 \tag{3.9}$$

$$k = 0.37464 + 1.54226\omega - 0.26992\omega^2 \tag{3.10}$$

$$b = 0.07780 \frac{RT_c}{P_c} \tag{3.11}$$

In the Ng and Robinson model, the fugacities were calculated using the equation of state of Peng and Robinson (Peng and Robinson, 1976). This equation of state is applicable to both gases and the non-aqueous liquid.

3.3 Vapour-liquid equilibrium data regression (VLE)

Two common methods used to regress phase equilibrium data include the Gamma-Phi ($\gamma - \varphi$) and Phi-Phi ($\varphi - \varphi$).

3.3.1 Gamma-Phi ($\gamma - \varphi$) method

The calculation procedure for the Gamma-Phi method, specifically for an isothermal system is shown in Figure 3.2.
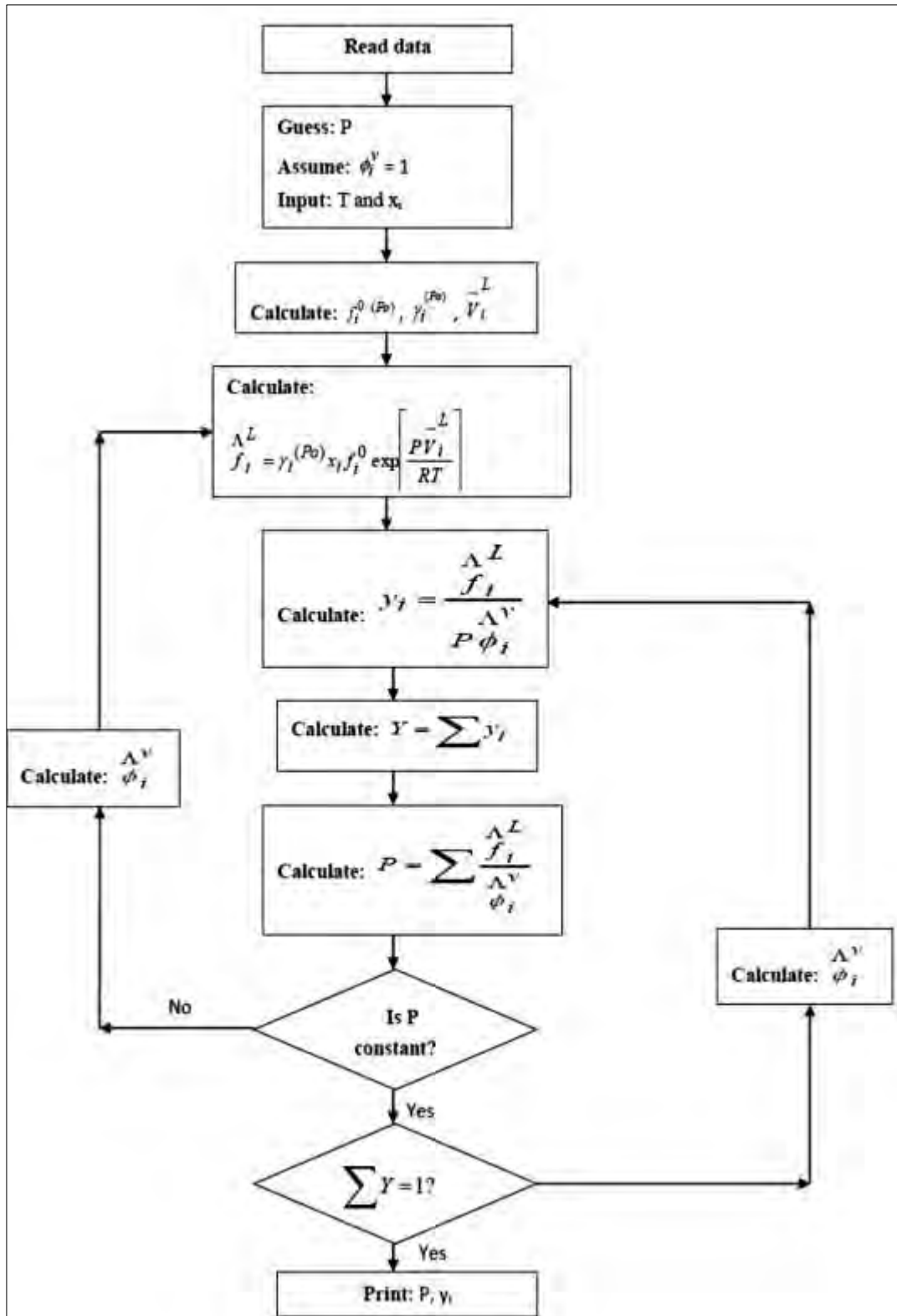
Figure 3.2: Flow diagram for the Gamma-Phi isothermal bubble-pressure method (Prausnitz and Chueh, 1968).

3.3.2   Phi-Phi (φ – φ) method

The calculation procedure for the Phi-Phi method is shown in Figure 3.3.
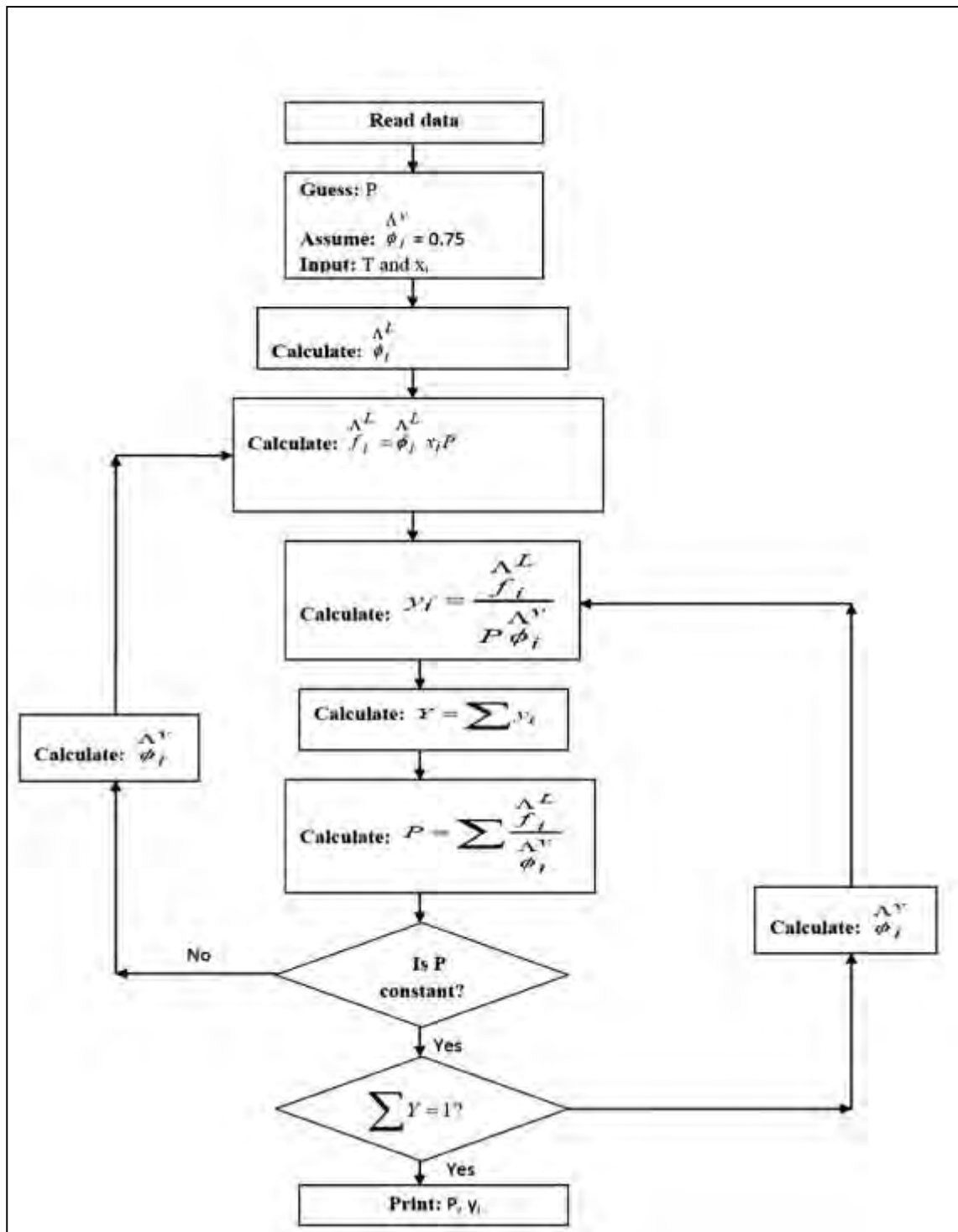
Figure 3.3: Flow diagram for the Phi-Phi isothermal bubble-pressure method (Prausnitz and Chueh, 1968).

3.4   Phase Equilibrium

The principles for phase equilibrium are:

a) Equality of the temperature and pressure of the phases
b) Equality of the chemical potentials of each of the components in each of the phases
c) Minimum global Gibbs free energy

Statistical thermodynamic modelling is based on the equality of the chemical potential between the hydrate phase, liquid phase and vapor phase. Most phase equilibrium calculations switch from chemical potentials to fugacities.

3.4.1   Equality of chemical potentials

Thermodynamic modelling of the liquid water- hydrate-vapour equilibrium (H-V-L) has been developed on the basis of the equality of the chemical potential of water in the hydrate phase with that in the water-rich liquid phase, ignoring the water content of the vapour phase:

$$\mu_w^{Lw}(T,P) = \mu_w^{H}(T,P)$$

(3.12)

where μ is the chemical potential, subscript w stands for water, and superscripts L_w and H are liquid water (or aqueous) and hydrate phases, respectively. If the chemical potential of an empty hydrate lattice is taken as a reference, Equation (3.12) becomes:

$$\Delta\mu_w^{Lw} = \Delta\mu_w^{H}$$

(3.13)

where

$$\Delta\mu_w^{Lw} = \mu_w^{MT} - \mu_w^{Lw}$$

(3.14)

$$\Delta\mu_w^{H} = \mu_w^{MT} - \mu_w^{H}$$

(3.15)

where superscript MT denotes the empty hydrate lattice. The chemical potential of water in the hydrate phase can be evaluated using the vdW-P theory:

$$\mu_w^{H} = \mu_w^{MT} - RT\sum_i v_i\,ln\left(1 + \sum_j C_{ij}f_j\right)$$

(3.16)

Fugacity (f_i) values are calculated using appropriate equations of state (EoS). Numerical values for the Langmuir constant (C_{ij}) can be calculated by choosing a model for the guest-host interaction:

$$C_{ij}(T) = \frac{4\pi}{KT} \int\limits_0^\infty exp\left(-\frac{w(r)}{KT}\right) r^2 \, dr \qquad (3.17)$$

where k is the Boltzmann's constant, w(r) is the spherically symmetric cell potential function in the cavity, with r measured from the centre and depends on the intermolecular potential function chosen for describing the encaged gas-water interaction. A potential function can be employed to determine the Langmuir constant. The following relation can be written in the case of application of the Kihara (Kihara, 1953) potential function:

$$w(r) = 2z\varepsilon \left[\frac{(\sigma^*)^{12}}{\bar{R}^{11}r} \left(\delta^{10} + \frac{\alpha}{\bar{R}}\delta^{11}\right) - \frac{(\sigma^*)^6}{\bar{R}^5 r} \left(\delta^4 + \frac{\alpha}{\bar{R}}\delta^5\right) \right] \qquad (3.18)$$

where,

$$\delta^{\bar{N}} = \frac{1}{\bar{N}} \left[\left(1 - \frac{r}{\bar{R}} - \frac{\alpha}{\bar{R}}\right)^{-\bar{N}} - \left(1 + \frac{r}{\bar{R}} - \frac{\alpha}{\bar{R}}\right)^{-\bar{N}} \right] \qquad (3.19)$$

z is the number of oxygen molecules in the sphere of each cavity (coordinate number), ε denotes the characteristic energy, a stands for the radius of the spherical molecular core, $\bar{R}$ represent the cavity radius, and $\bar{N}$ is an integer equal to 4, 5, 10 or 11. $\sigma^* = \sigma - 2\alpha$, where σ is the collision diameter.

Equation (3.20) is normally used for determining the chemical potential difference of water in the empty hydrate lattice and liquid water (Holder et al., 1980).

$$\frac{\Delta\mu_w^{MT-L_w}}{RT} = \frac{\mu_w^{MT}}{RT_0} - \frac{\mu_w^{L_w}}{RT_0} = \frac{\Delta\mu_w^0}{RT_0} - \int\limits_{T_0}^T \frac{\Delta h_w^{MT-L_w}}{RT^2} dT + \int\limits_0^P \frac{\Delta v_w^{MT-L_w}}{RT} dP - lna_w \qquad (3.20)$$

where superscripts 0 refers to reference property and MT- L_w stands for the difference property between empty hydrate lattice and water in liquid state. $\Delta\mu_w^0$ is the reference chemical potential difference between water in the empty hydrate lattice and pure water in the ice phase at standard condition (here it is 273.15 K) and a_w stands for the activity of water. In addition, Δv is the molar volume difference, and Δh stands for the enthalpy difference, which can be generally calculated by the following expression (Holder et al., 1980):

$$\Delta h_w^{\beta-L} = \Delta h_w^0 + \int_{T_0}^{T} \Delta C_{P_w} dT \qquad (3.21)$$

where C_{P_w} stands for the molar heat capacity, and Δh^0 is the enthalpy difference between the empty hydrate lattice and ice, at the ice point and zero pressure. Additionally, the difference between the heat capacity of the empty hydrate lattice and pure liquid water can be evaluated by the following equation (Holder et al., 1980):

$$\Delta C_{P_w} = -37.32 + 0.179(T - T_0) \qquad (3.22)$$

The heat capacity difference is assumed to be zero when T$\leq$ T$_0$. The values of the reference properties have been reported for the three different hydrate structures (sI, sII, and sH). Consequently, the following summarized equation can be written resulting from the equality of chemical potential of water in the phases present (ignoring water-content of the vapour phase, as already mentioned):

$$\frac{\Delta \mu_w^0}{RT_0} - \int_{T_0}^{T} \frac{\Delta h_w^{MT-L_w}}{RT^2} dT + \int_{0}^{P} \frac{\Delta v_w^{MT-L_w}}{RT} dP - \ln a_w - \sum_i v_i \ln\left(1 + \sum_j C_{ij} f_j\right) = 0 \qquad (3.23)$$

3.4.2 Equality of fugacities

These kinds of models have been developed on the basis of the equality of fugacity of water in the phases present (including hydrate phase), the final equilibrium criteria would be as follows:

$$f_i^v = f_i^{L_w} \qquad (3.24)$$

$$f_w^v = f_w^{L_w} = f_w^H \qquad (3.25)$$

where f is the fugacity, subscript i represent the ith component in the mixture (except water), and superscripts v stands for the vapour phase. An equation of state is normally used to calculate the fugacity of water in the vapour and aqueous phases. The equations required for pursuing this method are discussed in detail in the next section (Eslamimanesh 2012) (Eslamimanesh et al., 2012c) .

3.5   Eslamimanesh, Mohammadi and Richon model

The equality of fugacity of water in the aqueous ($f^L{}_w$) and in the hydrate ($f^H{}_w$) phases is used to calculate the liquid water- hydrate- gas/vapour (L_w-H-G/V) equilibrium conditions (Klauda and Sandler, 2000, Eslamimanesh et al., 2012c).

$$f_w^L = f_w^H \tag{3.26}$$

The fugacity of water in the hydrate phase depends on the difference in chemical potential of water in the filled and empty hydrate lattice ($\Delta\mu_w^{MT-H}$) by the following expression:

$$f_w^H = f_w^{MT} \exp\left(\frac{-\Delta\mu_w^{MT-H}}{RT}\right) \tag{3.27}$$

where the superscript MT denotes the empty hydrate lattice, R and T denote the universal gas constant and temperature, respectively, and μ represents the chemical potential. The fugacity of the hypothetical empty hydrate lattice (f_w^{MT}) is given by the following equation:

$$f_w^{MT} = P_w^{MT} \varphi_w^{MT} exp \int_{P_w^{MT}}^{P} \left(\frac{v_w^{MT} dP}{RT}\right) \tag{3.28}$$

where P_w^{MT} is the vapour pressure of water in the empty hydrate lattice, φ_w^{MT} is the fugacity coefficient of water in empty hydrate lattice. v_w^{MT} is the partial molar volume of water in the empty hydrate lattice in which the Poynting correction term of the above equation is assumed to be pressure independent (Eslamimanesh et al., 2012c). Therefore that equation can be written as follows:

$$f_w^{MT} = P_w^{MT} exp \left(\frac{v_w^{MT}(P - P_w^{MT})}{RT}\right) \tag{3.29}$$

By using the vdW-P model, $\Delta\mu_w^{MT-H}$ can be calculated (J.H. van der Waals, 1959):

$$\frac{\mu_w^H - \mu_w^{MT}}{RT} = \left[\sum_i v_i \, Ln\left(1 - \sum_k Y_{ki}\right)\right] \tag{3.30}$$

where v_i is the number of cavities of type i per water molecule in a unit hydrate cell and Y_{ki} is the fractional occupancy of the hydrate cavity i by guest molecule type k. Y_{ki} is calculated using the following equation (Eslamimanesh et al., 2012c):

$$Y_{ki} = \frac{C_{ki}f_k}{1 + \sum_k C_{ki}f_k} \tag{3.31}$$

where f_k and C_{ki} stand for the fugacity of the hydrate former and Langmuir constant, respectively. By replacing Equation(3.31) in Equation(3.31):

$$\frac{\mu_w^H - \mu_w^{MT}}{RT} = \sum_i Ln\left(1 + C_{ij}f_j\right)^{-\nu_i} \tag{3.32}$$

The fugacity of water in the aqueous phase (f_w^L) can be determined using the following equation:

$$f_w^L = x_W^L \, \gamma_w \, P_w^{sat} \exp\left(\frac{\nu_w^L(P - P_w^{sat})}{RT}\right) \tag{3.33}$$

where x_W^L, γ_w, P_w^{sat}, and ν_w^L represent the mole fraction of water in the aqueous phase, activity coefficient of water, vapour pressure of water, and molar volume of liquid water, respectively, and superscript *sat* represents the saturation condition. x_W^L can be calculated from the following equation:

$$x_W^L = \frac{1}{1 + 0.001 \times 2 \times m \times M_w} - x_g^L \tag{3.34}$$

where *m* is the molality of aqueous solution in (*mol. kg^{-1}*), M_w denotes the molecular weight of water in (*g. mol^{-1}*) and x_g^L is the solubility of the gaseous hydrate former in the aqueous phase, and subscript *g* represents the gaseous hydrate former. In Equation 6.1 dissociation of promoter in water is assumed. The molality of the solution (number of moles of promoter per kg mass of water) can be obtained by using the following relation:

$$m = \frac{18.0153 x_{cation}}{x_w} \tag{3.35}$$

The solubility of gases in the aqueous phase is obtained by the Krichevsky-Kasarnovsky equation (Krichevsky and Kasarnovsky, 1935):

$$x_g^L = \frac{f_g}{H_{g-w} exp\left(\frac{\nu_g^\infty}{RT}(P - P_w^{sat})\right)} \tag{3.36}$$

The Henry's constant of gas in water is denoted by H_{g-w}. Subscript g represents gas, and superscript ∞ indicates the infinite dilution condition.

As a result, the fugacity of the hydrate promoter in the aqueous phase should be determined as well by using the following equation:

$$f_p^L = x_p^L \, \gamma_p \, P_p^{sat} \exp\left(\frac{v_p^L\left(P - P_p^{sat}\right)}{RT}\right) \qquad (3.37)$$

where γ_p stands for the activity coefficient of the hydrate promoter in the aqueous solution, and subscript p denotes the hydrate promoter, respectively.

As a consequence, by substituting the previous equations into Equation (3.31) the following equation is achieved:

$$
\begin{aligned}
&\left[\frac{P_w^{MT} exp\left(\frac{v_w^{MT}(P - P_w^{MT})}{RT}\right)}{x_W^L \, \gamma_w \, P_w^{sat} \exp\left(\frac{v_w^L(P - P_w^{sat})}{RT}\right)}\right] \\
&\qquad \times \left[\left(1 + C^{small} f_g\right)^{-v_{smaLL\,typeA/B}}\right. \\
&\qquad \times \left(1 + C^{large_1} f_p^L\right)^{-v_{large_1\,typeA/B}} \\
&\qquad \left. \times \left(1 + C^{large_2} f_p^L\right)^{-v_{large_2\,typeA/B}}\right] = 1
\end{aligned}
\qquad (3.38)
$$

where superscripts/subscripts small and large stand for small and large cavities, respectively, and subscript type A/B represents the formation of types A or B semi-clathrate hydrates, respectively. Furthermore, subscripts 1 and 2 refer to occupation of large tetrakaidecahedra and pentakaidecahedra cages by cations.

3.6 Summary of important studies on predicting CO₂ hydrate phase equilibrium

Table 3.1 summarized previous studies on predicting CO_2 hydrate phase equilibrium (Xu and Li, 2014).

Table 3.1: List of equilibrium conditions predictions for hydrates containing CO₂ via computation models.

Authors	Temperature/ K	Pressure/ MPa	Study
Deaton & Frost (Deaton and Frost, 1946)	273-283	1.3-4.3	K-charts, giving the vapour-solid equilibria for natural gases
Carson & Katz (Carson and Katz, 1942)	277-283	2.0-4.5	Katz method, using vapour-solid equilibrium constants to predict the hydrate formation conditions.
Katz (Katz, 1945a)	273-322	0.2-42.0	Method of gas-gravity plots which relate the hydrate formation pressure and temperature to gas gravity.
Van der Waals & Platteeuw (Vanderwaals and Platteeuw, 1959)			Van der Waals-Platteeuw model which was based on a statistical thermodynamic approach
Larson (Larson, 1955)	257-283	0.5-4.5	Predicted the equilibrium hydrate formation conditions of CO_2 hydrates.
Miller & Smythe (Miller and Smythe, 1970)	151-193	0-0.000022	Dissociation pressure of CO_2 hydrate with equations for CO_2 hydrate dissociation pressures and vapour pressures.
Falabella (Falabella, 1975)	148.8-240.4	0.02-0.1	Van der Waals-Platteeuw model to predict the equilibria associated with experimental measurements.
Ng & Robinson (Ng and Robinson, 1976, Ng and Robinson, 1985b)	279-284	2.7-14.5	A modification of the Parrish and Prausnitz program, predicting hydrate forming conditions for pure gases in presence of methanol solutions.
Holder et al.(Holder et al., 1988)			Empirical correlations developed in different forms and with various numbers of parameters.
Adisasmito et al.(Adisasmito et al., 1991)	273-288	1.2-11.0	Verifying the work done by Unruh and Katz and by Berecz and Balla-Achs by experimental measurement.
Englezos (Englezos, 1992)	269-281	1.1-4.3	The CSMHYD in conjunction with Trebble-Bishnoi equation for prediction of the CO_2 hydrate formation pressure in NaCl solutions.
Dholabhai et al. (Dholabhai et al., 1993)	273-279	1.3-2.5	Combination of statistical thermodynamic model of van der Waals and Platteeuw with coefficient models for prediction of equilibrium conditions of CO_2 hydrate in pure water and single and mixed electrolytes.
Englezos & Hall (Englezos and Hall, 1994)	275-283	1.5-4.2	CSMHYD model for prediction of CO_2 hydrate formation pressure in electrolyte, water-soluble polymers and montmorillonite.
Tohidi et al.(Tohidi et al., 1997b)	268-284	1.0-5.0	Equation of state combination with a modified Debye-Huckel electrostatic term for the

			prediction of phase equilibrium conditions for CO_2 hydrates in presence of saline water.
Fan & Guo(Fan and Guo, 1999)	264-284	0.5-5.0	Hydrate phase equilibrium for CO_2/CH_4, CO_2/C_2H_6, CO_2/N_2, $CO_2/CH_4/C_2H_6/N_2$ in pure water and NaCl solution.
Seo & Lee (Seo and Lee, 2001, Seo et al., 2001b)	272-284	1.5-5.0	Prediction of the three phase equilibria of CO2 and CH4 aqueous solution
Duan & Sun (Sun and Duan, 2005, Duan and Sun, 2006)	253-293	0.5-200	Ab initio potential model for prediction of hydrate formation conditions for CH_4 and CO_2.
Li & Englezos (Li and Englezos, 2004)	298-313	5.0-11.0	SAFT equation of state for the correlation and prediction of vapour-liquid equilibrium of eighteen binary mixtures.
Bahadori & Vuthaluru (Bahadori and Vuthaluru, 2009)	265-298	1.2-40.0	A novel model based on the Katz gas-gravity charts to predict the hydrate formation conditions.
Zeng & Li (Zeng and Li, 2011)	270-282	0.8-4.0	PC-SAFT and van der Waals-Platteeuw model and capillary Kelvin model was employed to predict CH_4 and CO_2 hydrates formation equilibrium conditions in porous media.
Sloan(Sloan, 2008b)	277-283	Up to 400 MPa	Presenting an alternative set of K-values for Katz method which are dependent upon gas composition and hydrate structures
Karamoddin & Varaminian (Karamoddin and Varaminian, 2011)	260-330	0-5.0	A method using PR equation of state and different mixing rules for predicting hydrate formation conditions for binary mixtures of CH_4, C_2H_6, C_3H_8, $i-C_4H_{10}$, CO_2 and H_2S.
Elgibaly & Elkamel (Elgibaly and Elkamel, 1998)	250-320	0.001-1000	ANN models to predicting hydrate formation conditions based on *K*-value method and gas-gravity chart method.
Eslamimanesh et al. (Eslamimanesh et al., 2012e)	279-295	0-120	A thermodynamic model for prediction of phase equilibria of semi-clathrate hydrates of the CO_2, CH_4, or N_2+TBAB aqueous solution.
Eslamimanesh et al.(Eslamimanesh et al., 2011)	276-294	2-500	The model based on conventional Clapeyron model for predicting liquid water–hydrate–liquid hydrate former phase equilibria.
Shuker et al.(Shuker and Ismail, 2012)	270-295	0-2.5	ANN model for perdition of hydrate formation conditions for pure gases and gas mixtures.
Heydari et al.(Heydari et al., 2006)	273-296.5	0.3-29.0	ANN models for prediction of hydrate formation temperature.

4 A review of experimental methods and equipment

In order to measure reliable phase equilibrium data, appropriate thermodynamic facilities and techniques are required. The normal protocol in obtaining phase equilibria data includes observing the hydrate phase by indirect (non-visual) means, such as a pressure decrease or temperature increase in the fluid phase. The only direct evidence of the hydrate phase is visual observation.

4.1 Experimental methods

Three fundamental experimental methods for the measurement of hydrate-vapour-liquid equilibrium data have been presented: isothermal method, isobaric method, and isochoric method (Sloan, 2008a).

Isothermal method: In this method the temperature is constant. The pressure is set to a value above the hydrate formation region. The system is then maintained for a period of time to achieve the equilibrium condition and hydrate formation. After forming the hydrate, the temperature increases due to release of energy during crystallization of the gas and water molecules (Sloan and Koh, 2008). In addition, the pressure decreases due to encapsulation of the gas until three phase (L_w-H-V) and equilibrium point is reached (Figure 4.1). Hydrates are then dissociated through stepwise heating. This process may be time-consuming.

Isobaric method: In this method the pressure is kept constant. The system is gradually cooled to form hydrate. The formation of hydrate is detected by a significant increase in gas injected. After hydrate formation and once the system pressure has reached a steady state, the temperature is slowly increased to decompose the hydrate crystals (Figure 4.1). This point is achieved as the equilibrium temperature at a constant pressure and hydrate formation/dissociation may be determined by visual observation.

Isochoric method: The operation of this method is presented visually by using a pressure-temperature plot. After the pressure inside the cell is stabilized, the temperature is slowly decreased to form hydrate crystals. Thereafter, the temperature is slowly increased to dissociate the hydrate crystals. The intersection of the cooling trace and heating trace gives the hydrate dissociation point (equilibrium pressure and temperature). This method is independent of visual observation.
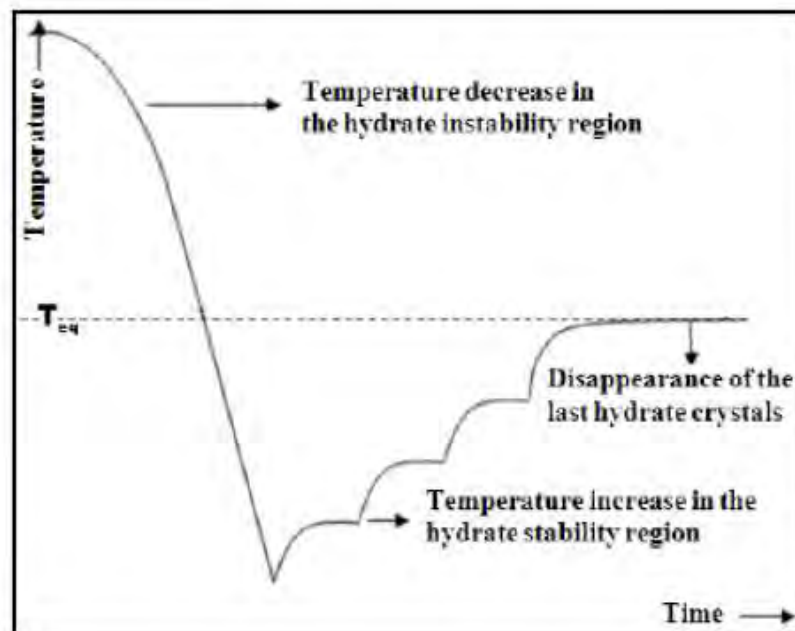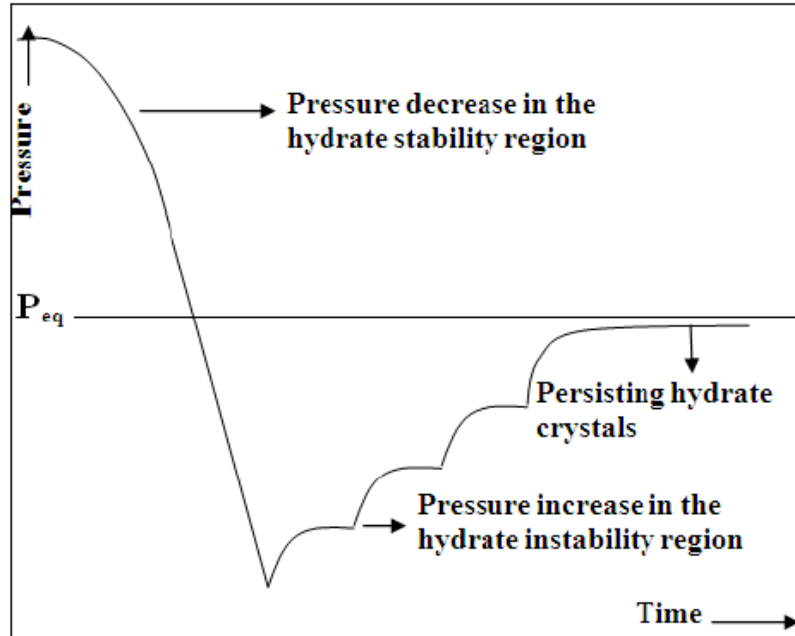
Figure 4.1: Typical diagram for isothermal (Top) and isobaric (bottom) method.

4.2 Experimental equipment

There are three important principles in developing apparatuses and methods for phase equilibria measurements (Sloan and Koh 2008):

1. Strong agitation is required to transform water to hydrate.
2. Hydrate dissociation is used to measure the hydrate equilibrium point.
3. A rapid reduction in pressure or an increase in temperature indicates hydrate formation in a constant volume apparatus.

The following subsections include a review on the apparatus used to measure hydrate phase equilibrium, which include the Volume variable cell, Quartz crystal microbalance, Cailletet, Rocking cell, High pressure differential scanning calorimetry and High pressure auto clave cell.

4.2.1 Volume variable cell

This equipment was designed by the Thermodynamics Research Unit (TRU) and housed in the TRU Laboratories in the School of Engineering (Ngema et al., 2014). A schematic diagram of the equipment is shown in Figure 4.2. This volume variable cell incorporates with a novel stirring device and consists of a hollow cylindrical sapphire tube which is compressed and sealed between two SS 316L metal flanges. The cell can withstand pressures up to approximately 20 MPa. Visual observations of gas hydrate formation and decomposition is possible because the sapphire tube is transparent. The inner volume of the cell is approximately 10 cm^3.

This equipment allows to measure hydrate dissociation point in the isothermal condition. In the isothermal technique, the equilibration times, is shorter than isochoric method. Consequently, this technique reduces the time requirement for hydrate formation and dissociation.
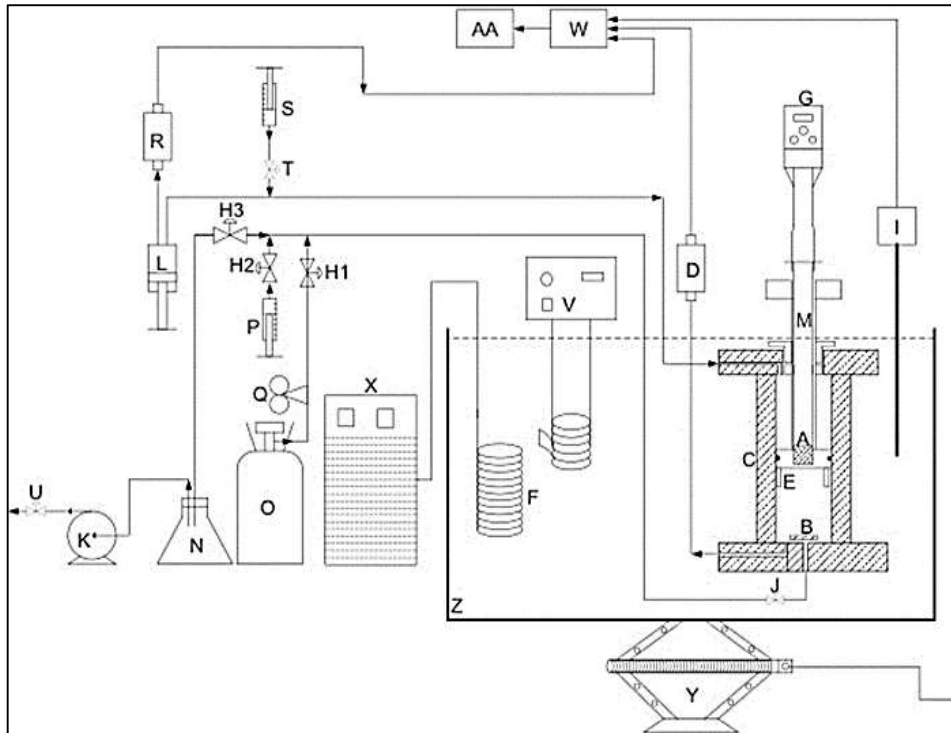
Figure 4.2: Schematic diagram for new variable volume equilibrium cell (Ngema et al., 2014).

4.2.2 Quartz crystal microbalance (QCM)

Tohidi et al. (Tohidi et al., 2002) presented a novel technique for measuring the hydrate stability zone based on the change in the resonant frequency of a quartz crystal microbalance (QCM). They showed that this new technique reduces the sample size and the time requirement significantly. Mohammadi et al. (Mohammadi et al., 2003) used QCM to present experimental data on methane, nitrogen, oxygen, and air hydrates.

A schematic of the QCM set up is given in Figure 4.3. The quartz crystal microbalance was initially developed for the measurement of small changes in mass, hence the term "microbalance" (Mohammadi et al., 2003). The QCM has a thin disk of quartz placed between two electrodes. When an electric currents is passed through the electrodes, crystal oscillation at a particular resonant frequency is activated. Hydrate formation is observed by a change in the resonance frequency and conductance at the resonant frequency of the quartz crystal. Pressure and temperature of the system are measured using a pressure transducer and a thermocouple in a high pressure cell (Sloan & Koh, 2008). The main advantages of this method are smaller amount of sample and shorter times are required for measuring hydrate phase equilibria. A requirement of hydrates adhere to the surface of the quartz crystal is a drawback for using this equipment.
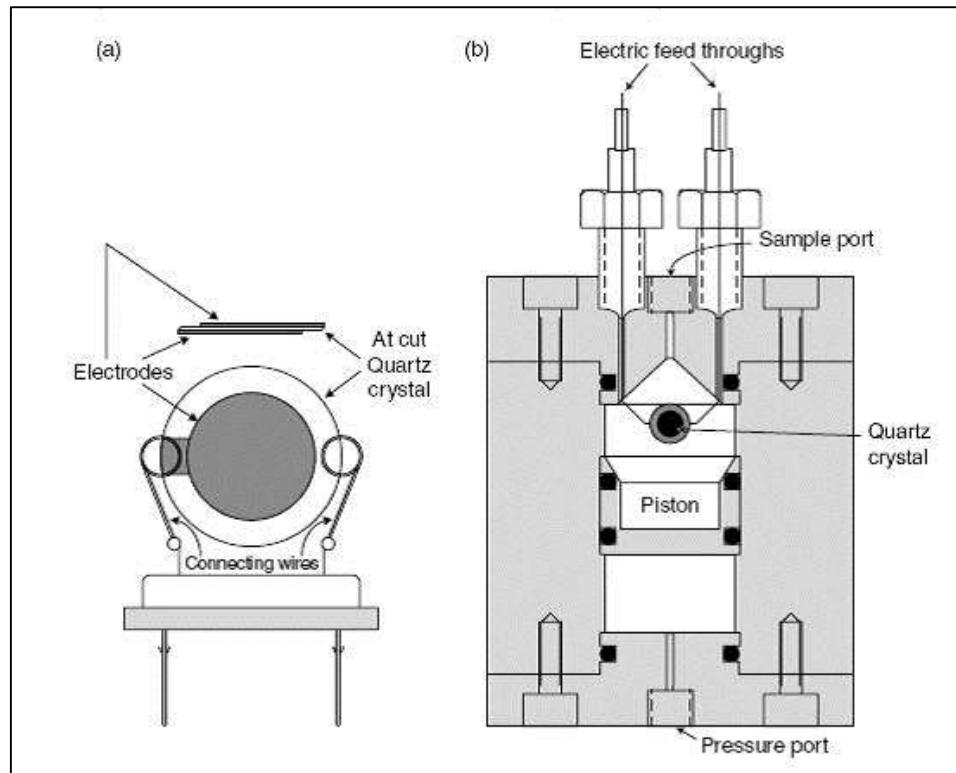
Figure 4.3: (a) Schematic of the Quartz Crystal Microbalance (QCM), and (b) the QCM mounted within a high pressure cell (Mohammadi et al., 2003).

4.2.3 Cailletet

Khalik et al. (2009) used a Cailletet apparatus for the measurement of H-L-V equilibria measurements. The schematic diagram of the Cailletet apparatus is shown in Figure 4.4. Once the sample is prepared, it is placed in the top of the Cailletet tube. The tube is then sealed by a mercury column which also acts as a part of the pressure transferring medium. The temperature is set to a specific value while the volume is adjusted until hydrate formation occurs. The pressure is measured and monitored until a constant pressure is obtained. A disadvantage for using this apparatus is regular volume adjustments. Mechanical movement may damage the equipment.
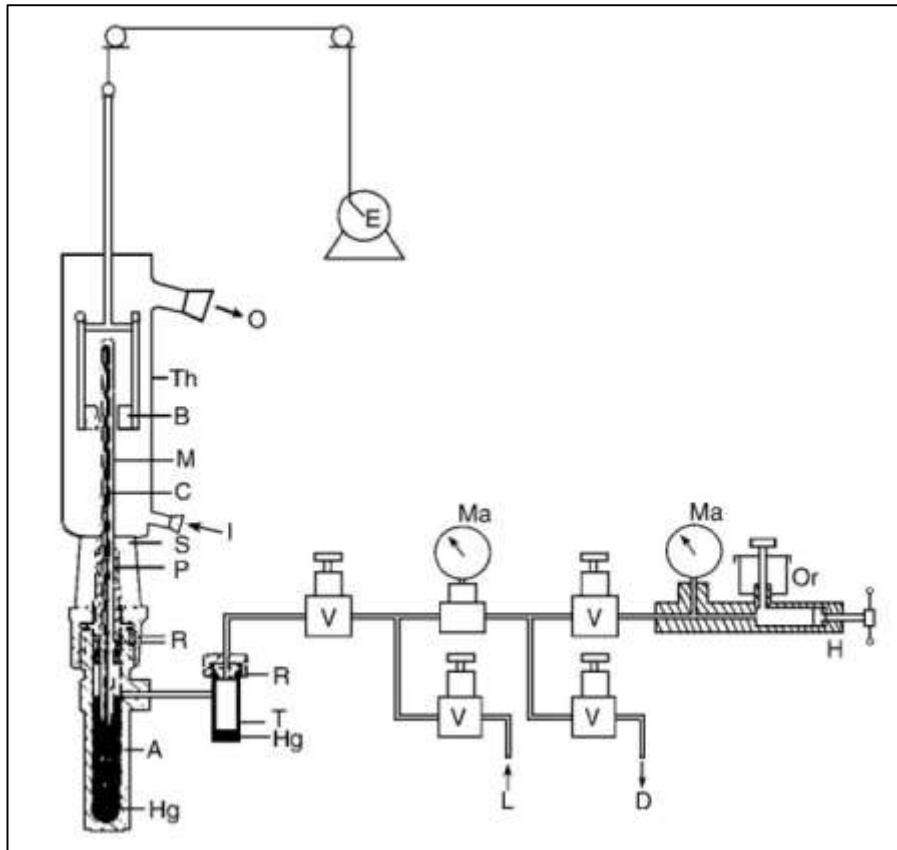
Figure 4.4: Schematic representation of a Cailletet apparatus (Bermejo et al., 2008).

4.2.4   Rocking cell

As shown in Figure 4.5, the apparatus consists of a high pressure cell and a sight-glass for visual observations. The high pressure cell is filled with the desired amount of water and the hydrate former may enter the cell. The cell is immersed in a thermostat bath. Agitation between gas and liquid phases is provided by rocking of the cell through a rocking motor. Direct observation of the hydrate formation is a promising aspect of this equipment, however the rocking motion may cause mechanical damage.
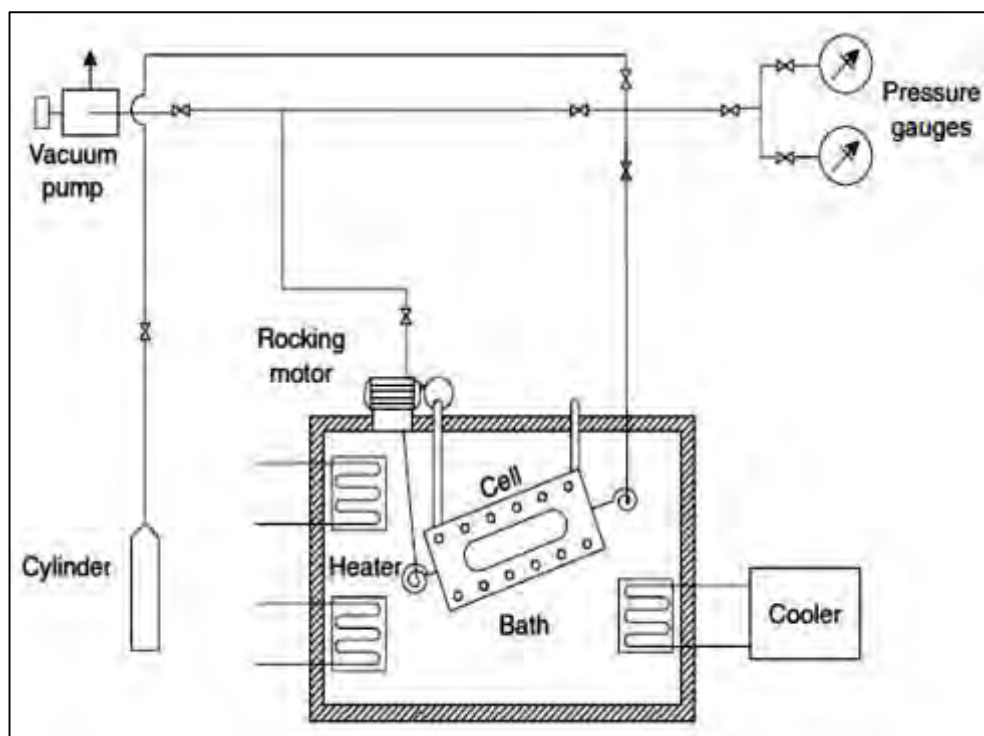
Figure 4.5: Typical rocking hydrate equilibrium apparatus (Sloan and Koh, 2008).

4.2.5   High pressure differential scanning calorimetry

Recently, calorimetric methods such as differential scanning calorimetry (DSC) has been developed for the determination of hydrate phase equilibria data and thermal property data for gas hydrates.

Dalmazzone et al. (Dalmazzone et al., 2002) introduced a micro-DSC analyzer coupled with special high-pressure vessels, namely High Pressure Differential Scanning Calorimetry (HP-DSC) technique. The same technique has been applied to investigate stability conditions and dissociation enthalpies of semi-clathrate hydrates of CO_2 + TBACl, TBANO$_3$, and TBPB (Mayoufi et al., 2009). Mayoufi et al. (Mayoufi et al., 2011) used DSC to investigate phase behavior of CO_2 + TBPB semi-clathrate hydrates. The experimental setup is shown in Figure 4.6. It is based on a high sensitivity DSC (micro DSC VII) fitted with two pressure-controlled cells. It can operate at temperatures between (228.15 and 393.15) K and up to 40 MPa coupled to a pressure multiplicator.

Moreover, Daraboina et al. (Daraboina et al., 2013a) investigated the performance of kinetic inhibitors for hydrate formation and decomposition by using high pressure micro differential scanning calorimeter (HP-μDSC). Lin et al. (Lin et al., 2014) studied phase equilibrium conditions and dissociation enthalpy of the semi-clathrate hydrates formed from mixed quaternary salts (TBAB + TBPB) with CO_2 by using DSC method for the first time.
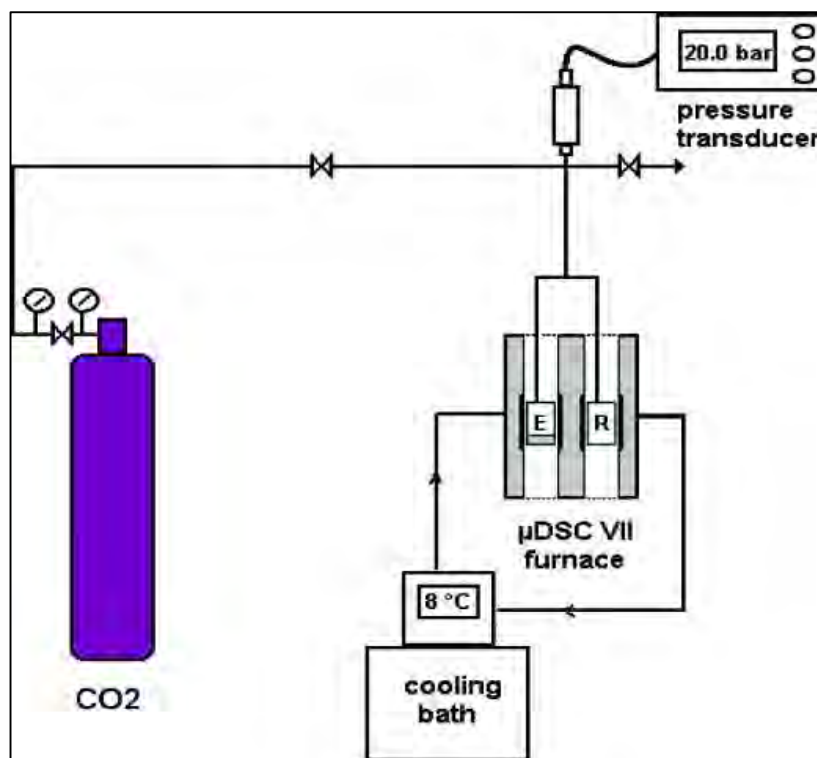
Figure 4.6: High pressure DSC measurement device (Mayoufi et al., 2009)

4.2.6 High pressure autoclave cell

The high pressure autoclave apparatus consists of a high-pressure cell submerged in a liquid bath for temperature control. The type of solution used in the bath can differ and depends on the temperature range required for experiment. The high pressure autoclave cell may be visual or non-visual. Magnetic stirrers are placed within the cell for agitation. Temperature probes are inserted into the cell to monitor the temperature inside the cell. Also, pressure transducer is installed into the cell to record the cell pressure. This type of setup was chosen as it is simple to construct and operate.

4.3 Diffraction and spectroscopic methods in gas hydrate research

During the last decade gas hydrate research has increasingly shifted to molecular-level methods including X-ray Diffraction (XRD) (Kumar et al., 2009a), Raman spectroscopy (Schicks and Luzi-Helbing, 2013, Joon Shin et al., 2009), Nuclear Magnetic Resonance (NMR) spectroscopy (Seo et al., 2005) and Infrared spectroscopy (Dartois and Schmitt, 2009, Fleyfel and Devlin, 1991). These methods can provide important information about hydrates (Sloan and Koh, 2008, Udachin et al., 1997, Udachin et al., 2001, Manakov et al., 2009) including: the hydration number, composition of hydrates, structure identification, the relative occupancy of molecules in each cage, identification of metastable phases, and the kinetics of formation of various structures.

Table 4.1 provides a summary of molecular-level techniques that have been used to CO_2 hydrate studies (Sloan and Koh, 2008).

Table 4.1 Molecular-level techniques applied to analyze CO_2 hydrate

Author	Study	Reference
Uchida et al.	**Analyzing of the growth process of CO_2 hydrates by Raman spectroscopic**	(Uchida et al., 1995)
Nakano et al.	**Raman Microprobe Spectroscopic Studies on the CO_2 Hydrate System**	(Nakano et al., 1998)
Takeya et al.	**In situ observation of CO_2 hydrate by XRD**	(Takeya et al., 2000)
Udachin et al.	**Determination of the structure and composition of CO_2 hydrate using X-ray diffraction**	(Udachin et al., 2001)
Seo and Lee	**Confirmation of the structure and guest distribution of the mixed $N_2 + CO_2$ hydrates by using X-ray diffraction and C^{13} NMR**	(Seo and Lee, 2003)
Kim and Lee	**Identification structure and guest distribution of the mixed $H_2 + CO_2$ hydrate by X-ray powder diffraction and NMR spectroscopy**	(Kim and Lee, 2005)
Lehmkühler et al.	**Analysis of CO_2-H_2O interface at conditions of gas hydrate formation by X-ray diffraction**	(Lehmkühler et al., 2008)
Lee et al.	**Identification the crystal structure and guest distribution of the $CO_2-CH_4-N_2$ mixture hydrate by synchrotron XRD, NMR, and Raman spectroscopy**	(Lee et al., 2012a)
Lee et al.	**Confirmation of the $CO_2/ CH_4 + THF$ hydrates structures by synchrotron XRD and Raman spectroscopy**	(Lee et al., 2012c)
Luzi et al.	**In situ investigation of hydrate formation and dissociation by means of Raman spectroscopy and powder X-ray diffraction (PXRD)**	(Luzi et al., 2012)
Xu et al.	**Analyzing of CO_2 separation from CO_2/H_2 gas mixtures with Raman spectroscopy**	(Xu et al., 2013b)
Lee et al.	**Examination of CH4–CO2 replacement in natural gas hydrates through thermodynamic and ^{13}C NMR spectroscopic**	(Lee et al., 2013)
Kumar et al.	**Investigation of CO2-containing clathrate hydrates by infrared spectroscopy**	(Kumar et al., 2009b)

5   Experimental methods and gas hydrates phase equilibrium measurements

The experimental technique and the apparatus used to perform the measurements is presented in this chapter. The isochoric pressure search method was used to measure the hydrate dissociation conditions (using both apparatus) (Tohidi et al., 2000, Mohammadi and Richon, 2009c).

An isochoric process called isovolumetric process because the volume of the measuring system remains constant and the temperature changes during the experiment. The reliability of the experimental method used has been demonstrated in the literature. A typical diagram of this experimental method is given in Figure 5.1. The intersection between the cooling curve and the hydrate dissociation curve was taken as dissociation point.
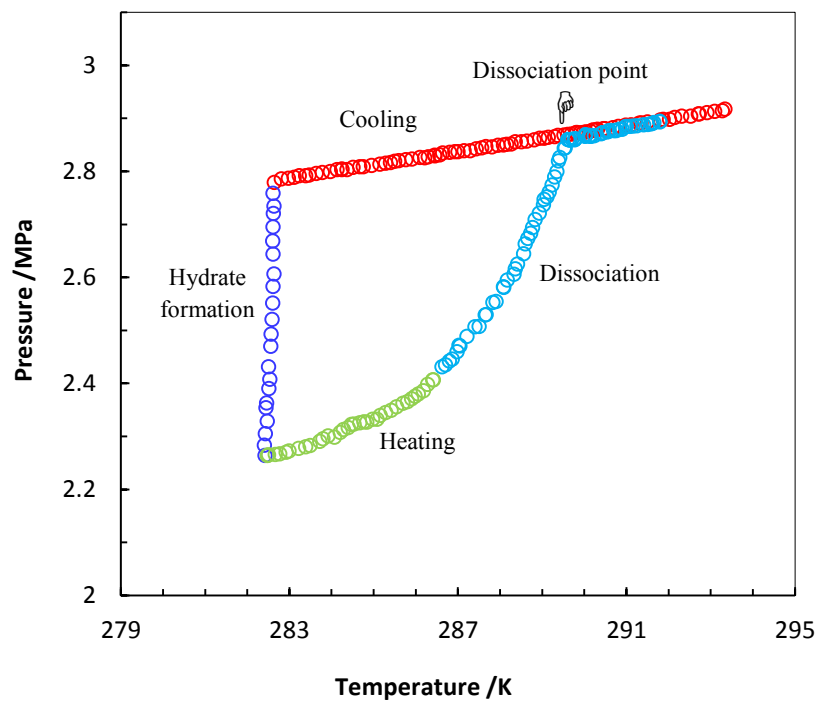
Figure 5.1: A representative diagram obtained using the isochoric pressure search method.

Important advantages of the isochoric pressure search method are:

a) No visual observation is required for determination of hydrate equilibrium data
b) No volume changes are required.

5.1 Materials

The chemicals used in the present study, their suppliers and purities are given in Table 5.1. The chemicals were used without additional purification. Aqueous solutions were prepared following the gravimetric method, using an accurate analytical balance (mass uncertainty: ± 0.0001 g). Distilled water was used to prepare all aqueous solutions.

Table 5.1: Purities and supplier details of the chemicals used in this study.

Chemical	Formula	Purity	Supplier
Carbon dioxide	CO_2	≥99.99 (vol %)	AFROX Ltd
Methane	CH_4	≥99.99 (vol %)	AFROX Ltd
Nitrogen	N_2	≥99.99 (vol %)	AFROX Ltd
Argon	Ar	≥99.99 (vol %)	Air Liquid
Tetrabutyl phosphonium bromide (TBPB)	$C_{16}H_{36}BrP$	98% (mass fraction)	Sigma-Aldrich
Tetrabutyl ammonium nitrate (TBANO₃)	$C_{16}H_{36}N_2O_3$	97% (mass fraction)	Sigma-Aldrich
Tetra butyl ammonium fluoride tri-hydrate (TBAF.3H₂O)	$C_{16}H_{36}FN$	≥97.0% (mass fraction)	DLD Scientific

5.2 Apparatus

Two different experimental apparatus were used for the hydrate dissociation measurements. The schematic diagram of apparatus 1 is shown in Figure 5.2. Figure 5.3 is shown a picture of experimental set up was used in this study.

The equipment was designed and commissioned by the Thermodynamics Research Unit (TRU) and housed in the TRU Laboratories in the School of Engineering.

The experimental apparatus consists of different parts: cylindrical equilibrium cell, agitation device, liquid bath, temperature controller, chilling unit, temperature and pressure sensors, vacuum pump, and data acquisition system.

Figure 5.2: Schematic diagram of the apparatus 1: GC, Gas Cylinder; LB, Liquid Bath; DAU, Data Acquisition Unit; EC, Equilibrium Cell; ER, External Refrigerator(chilling unit); TC, Temperature Controller; PT, Pressure Transducer; PP, Platinum Probes (PP1 - top probe, PP2 - bottom Probe); SD, Stirring Device; MS, Magnetic Stirrer; MG, Mechanical Gear; MJ, Mechanical Jack; VP, Vacuum Pump; V1, Vacuum valve; V2, Vent V3, Loading valve; V4, V5, Feeding valves; V6, Drain valve.
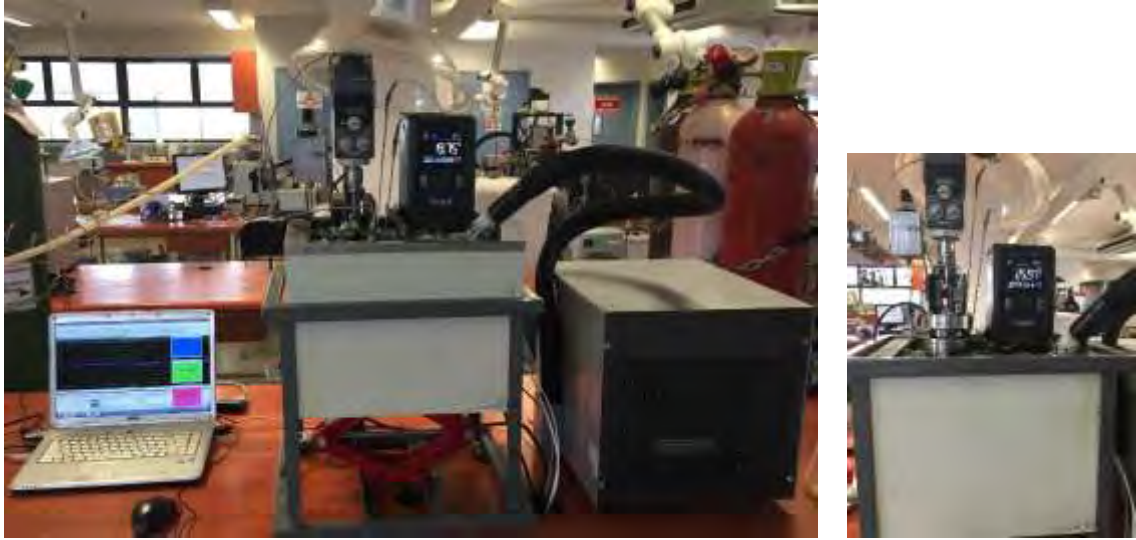
Figure 5.3: A picture of apparatus used in this study.

5.2.1 Cylindrical equilibrium cell

The main part of the apparatus is an equilibrium cell (EC) which has an inner volume of approximately 64 cm^3. The cell is made of 316 stainless steel and can withstand the high pressure required for hydrate measurements. The cell can perform well at both low and high temperature. Figure 5.4 shows the equilibrium cell which used in this study. It has a height of 40 mm and a diameter of 45 mm. Five inlet/outlet ports were drilled into the main body of the equilibrium cell with a diameter of 8 mm. The first port, was situated on the top of the cell for introducing the liquid into the cell and also for evacuation of the cell. The second port was located on the left top of the cell for pressure transducer. The third and fourth port on the right top and bottom of the cell were used for temperature probe sensors (Pt100s). The fifth port was located at the bottom of the cell for the draining of liquid.
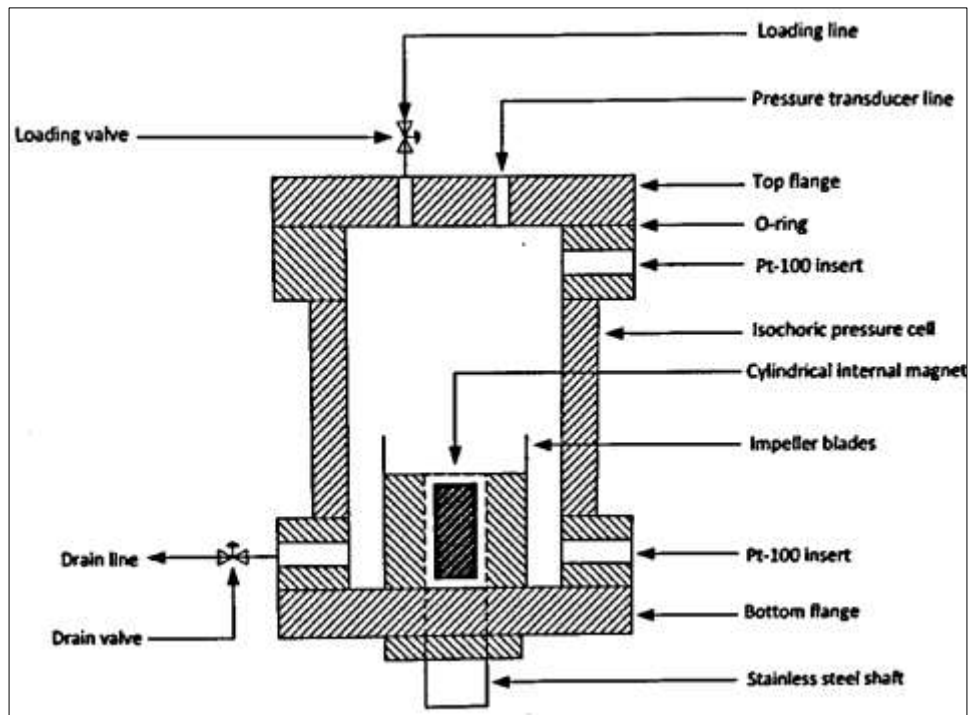
a) Schematic diagram
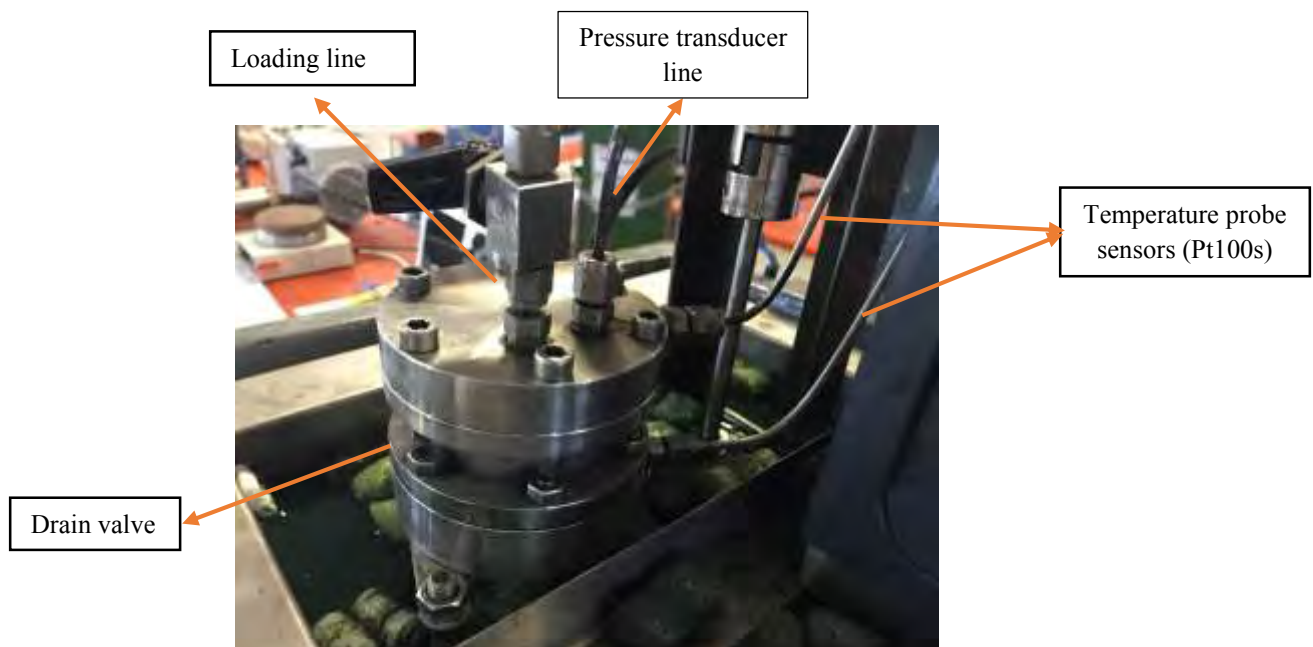
b) Real photograph

Figure 5.4: Hydrate equilibrium cell.

5.2.2 Liquid bath

The equilibrium cell was immersed in a bath filled with an ethylene glycol and water solution to ensure an isothermal environment is maintained. This allowed for an operating temperature between 228 K (melting point at atmospheric pressure) and 397 K (boiling point at atmospheric pressure). The bath is 43 cm × (length) ×35 cm (width) ×26 cm (height).

5.2.3 Agitation device

A magnetic stirrer was installed in the cell to agitate the fluids and hydrate crystals formed during the measurements. Stirring increases the rate of mass transfer between the vapour phase i.e gases and water. This new stirring device was designed by Richon (Ngema et al., 2014). The new design of the stirring device has two neodymium magnets as well as three blades each with a length of 5 mm, height of 33 mm and width 1 mm (Figure 5.5). A Teflon® covering was used to reduce friction caused by high magnetic field between the neodymium magnet and stainless steel shaft. Figure 5.6 shows the equilibrium cell without stirring device and with stirring device. The stirring device, located at the bottom of the cell, rotates by Heidolph RZR 2041 overhead stirrer which mounted outside the cell. The overhead stirrer drives a gear chain at the bottom of the cell, which drives the magnetic stirrer. Figure 5.7 shows the operation of magnetic stirrer. This stirring device with vigorous agitation improves the water transformation to hydrate and reduces hydrate dissociation time.

Figure 5.5: New magnetic stirrer device.
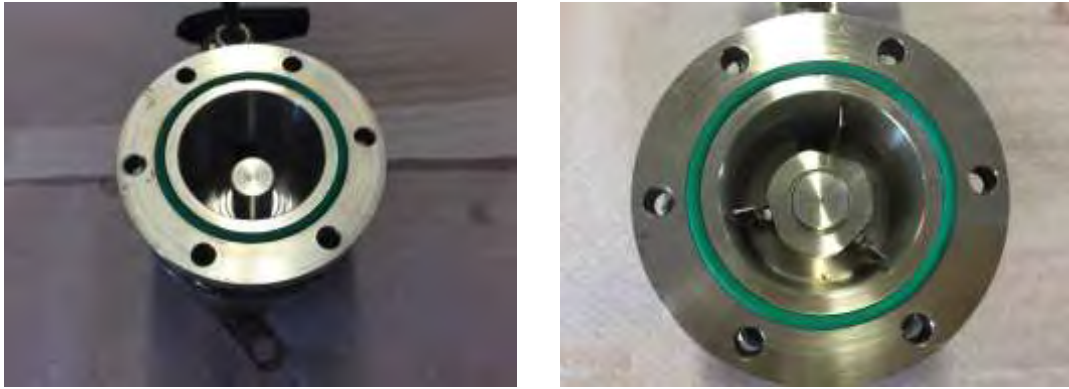
Figure 5.6: A partial picture of the equilibrium cell without magnetic device (left) and with magnetic device (right).

Figure 5.7: Schematic diagram for operating of magnetic stirrer device.

5.2.4 Temperature controller

The temperature of the bath was controlled at a prescribed value by the use of a programmable coolant circulator and a thermocouple in the bath (Grant Optima™ TX150). The controller temperature range is 243.15 K to 323.15. It has an immersion circulator pump with an internal

temperature probe. The temperature bath maintain a constant temperature of the equilibrium cell contents by heating or cooling of the ethylene glycol water mixture in the bath.

5.2.5 Chilling unit

An immersion cooler supplied by PolyScience® was used to cool the bath content. It operates at temperature as low as 173.15 K.

5.2.6 Temperature and pressure sensors

Two platinum temperature resistors, Pt100s, were inserted into the cell to monitor the temperature of the bulk and fluid phase. The Pt100s measure over a range of (73.15 to 1073.15) K and the uncertainty in the temperature measurement is estimated to be < 0.15 K. Each Pt100 was fixed to the top or bottom of the equilibrium cell and the measurement corresponded to the vapour and liquid phase respectively. The Pt100s were connected to Agilent data acquisition unit to record the temperature inside the cell.

A WIKA P-10 pressure transducer was used to measure the cell pressure. The transducer has a pressure range of 1-10 MPa and the uncertainty in the pressure measurement is estimated to be < 5 kPa. The pressure transducers are maintained at constant temperature (temperature higher than the highest temperature of the study). The transducer was connected to an Agilent data acquisition unit to record and display periodic pressure measurements of the system.

5.2.7 Data acquisition system

A 34972A LXI Agilent data acquisition unit was coupled with a personal computer to monitor the pressure and temperature and time data during the experiment. The Agilent Bench link Data Logger 3 software presents real-time data of pressure and temperature. Continuous recording of pressures and temperatures allows detection of any changes in the system and true equilibrium conditions.

The second apparatus (Apparatus 2) is similar to the one described earlier. However the inner volume of the equilibrium cell and the design of the mechanical stirrer were modified. The equilibrium cell, with a volume of 45 cm^3, was designed to operate at a pressure range of 1-20 MPa. A mechanical overhead stirrer with a speed range from 40 to 2000 rpm was utilized for this apparatus (RZR 2041, Heidolph). A Grant temperature bath controller (model TX-150) was used to provide the stable temperature profile. A detailed schematic of the apparatus is given in Figure 5.8.

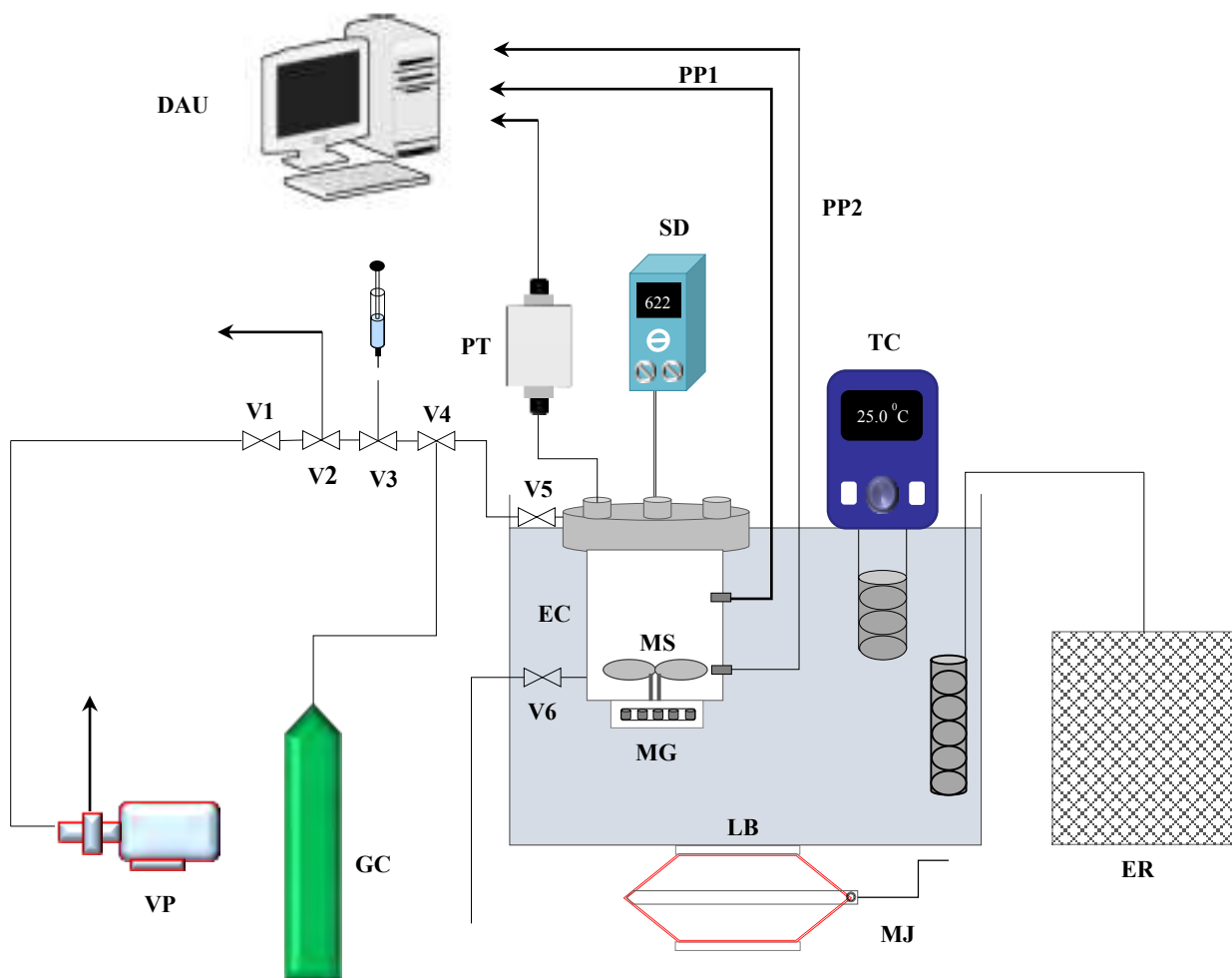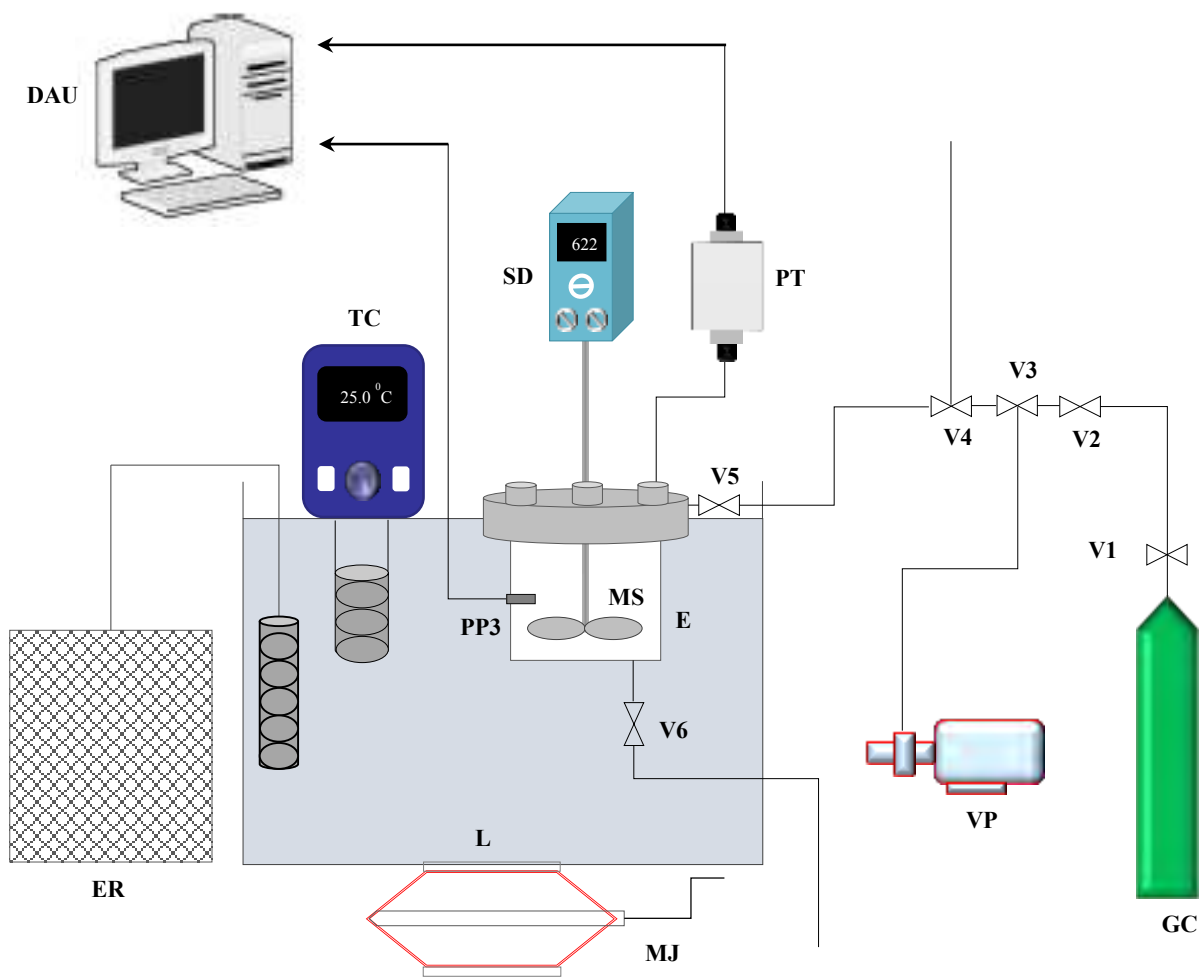**Figure 5.8: Schematic diagram of the apparatus 2: G, Gas Cylinder; LB, Liquid Bath; DAU, Data Acquisition Unit; EC, Equilibrium Cell; ER, External Refrigerator; TC, Temperature Controller; PT, Pressure Transducer; PP3, Platinum Probes; SD, Stirring Device; MS, Magnetic Stirrer; MJ, Mechanical Jack; VP , vacuum pump; V3, Vacuum valve; V1, V2, V5, Feeding valves; V6, Loading and Drain valve; V4, Vent valve.**

5.3   Calibration of measuring devices

The accuracy of the hydrate phase equilibrium data depends on the accuracy of measuring equipment. Calibration is the process of evaluating the accuracy of measurement equipment. In this way, careful calibration of all measuring devices, i.e., temperature probes, pressure transducers and etc. was accomplished against reference instruments previous to performing the experimental work. Calibration of the measured variables (temperature and pressure) were performed for both apparatus.

5.3.1   Calibration of the temperature probes

Two platinum (Pt) temperature resistors (Pt100s) were used for temperature measurement at the top and the bottom of the cell in order to check for temperature gradient along the equilibrium vessel. The probes were calibrated against a 100Ω reference probe (WIKA CTH 6500) with an accuracy of 0.03 K. The Pt100 probes and the reference probe were immersed in a calibration bath (WIKA CTB 9100) with silicon oil. The actual and set temperature were displayed simultaneously on a digital display. The temperature of the bath was increased and decreased at uniform intervals from (268.15 to 313.15) K, in order to detect any hysteresis within the probes. The temperature of the standard probe (standard temperature) was plotted against the recorded temperature of the two Pt100s (Figure 5.9 and Figure 5.10). The calibration equation of this line is subsequently used to determine actual temperature values. The maximum uncertainty on temperature measurement resulting from this calibration is within ± 0.026 K.

The calibration of the temperature probe for the second apparatus was performed as described above; the plot of the standard temperature against recorded temperature is provided in Figure 5.11.
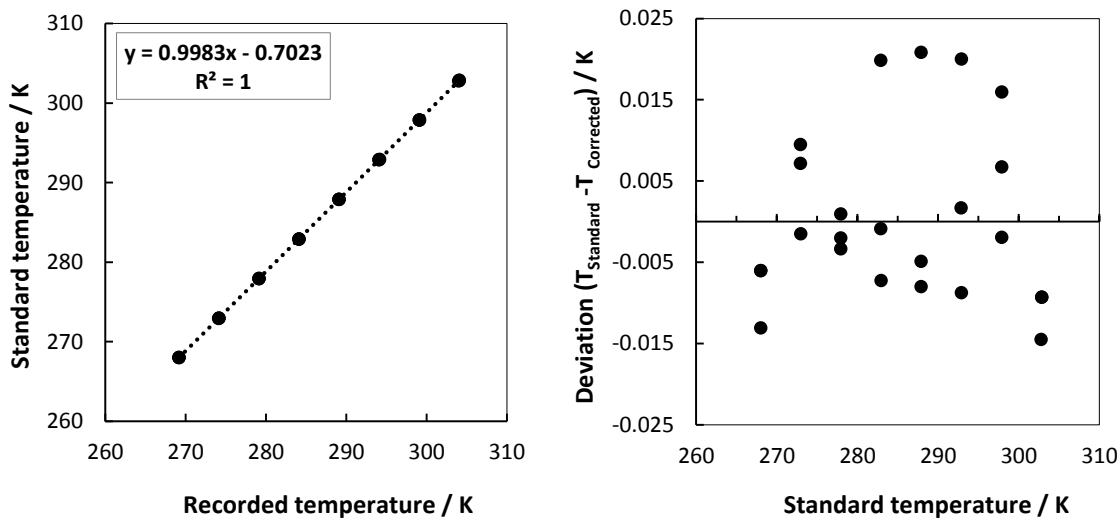
Figure 5.9: Calibration of the top platinum resistance thermometer probe (PP1) for apparatus 1.
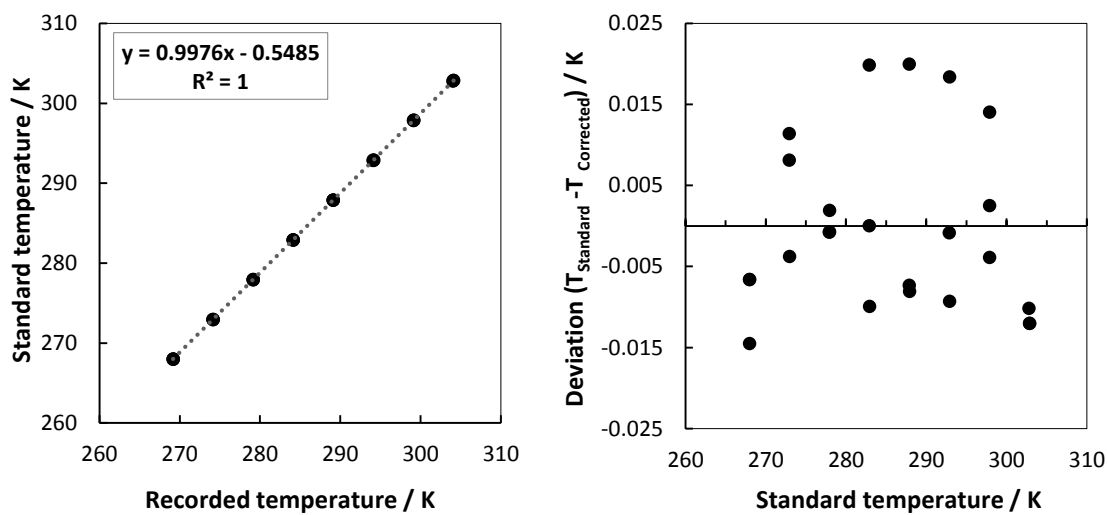
Figure 5.10: Calibration of the bottom platinum resistance thermometer probe (PP2) for apparatus 1
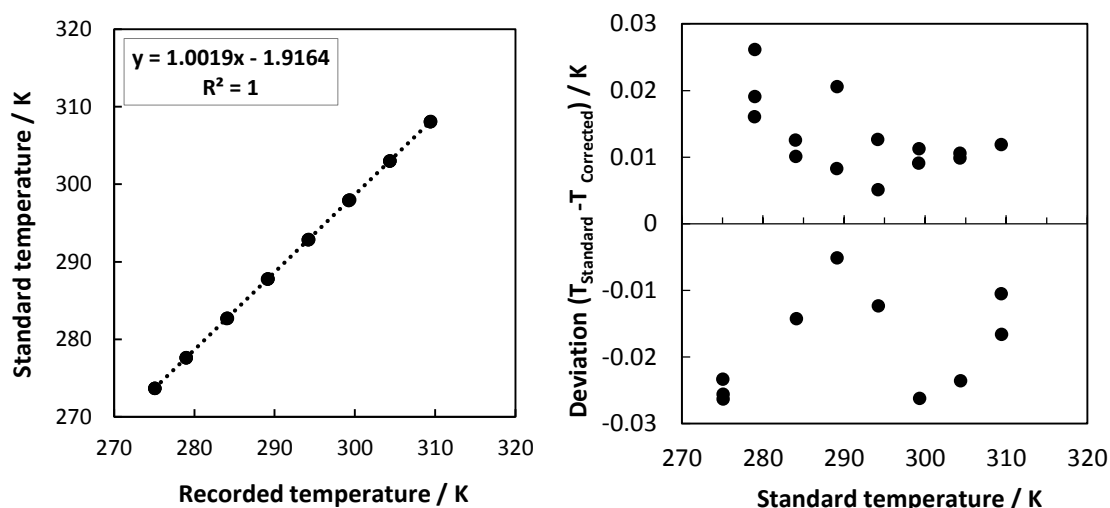
Figure 5.11: Calibration of the platinum resistance thermometer probe (PP3) for apparatus 2.

5.3.2 Pressure calibration

The pressure inside the equilibrium cell was measured using a calibrated pressure transducer. The calibration is performed against a standard pressure transducer (WIKA CPH6000). For calibrating the pressure transducer, the reference instrument was connected to a nitrogen cylinder as a pressure source and to the inlet of the equilibrium cell. In order to eliminate the effect of fluctuating temperature on the calibration, the equilibrium cell and the pressure transducer temperature are kept at a constant temperature. The equilibrium cell was controlled at 290.15 K and the pressure transducer was controlled at 313.15 K. The pressure of the cell was increased and decreased at uniform intervals from 1 to 10 MPa for detecting any hysteresis. Pressure readings from the cell pressure transducers are allowed to stabilize. The standard pressure was plotted against the recorded pressure (Figure 5.12). The maximum uncertainty is within 0.98 kPa.

The calibration of the pressure transducer for the second apparatus was performed as described above; the plot of the standard pressure against recorded pressure is provided in Figure 5.13.
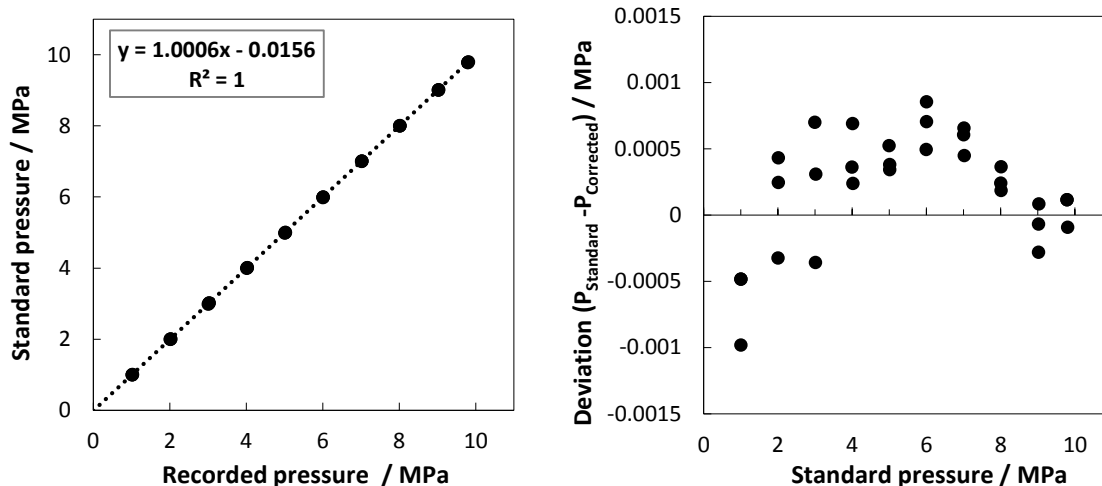
Figure 5.12: Calibration of the pressure transducer for apparatus 1.
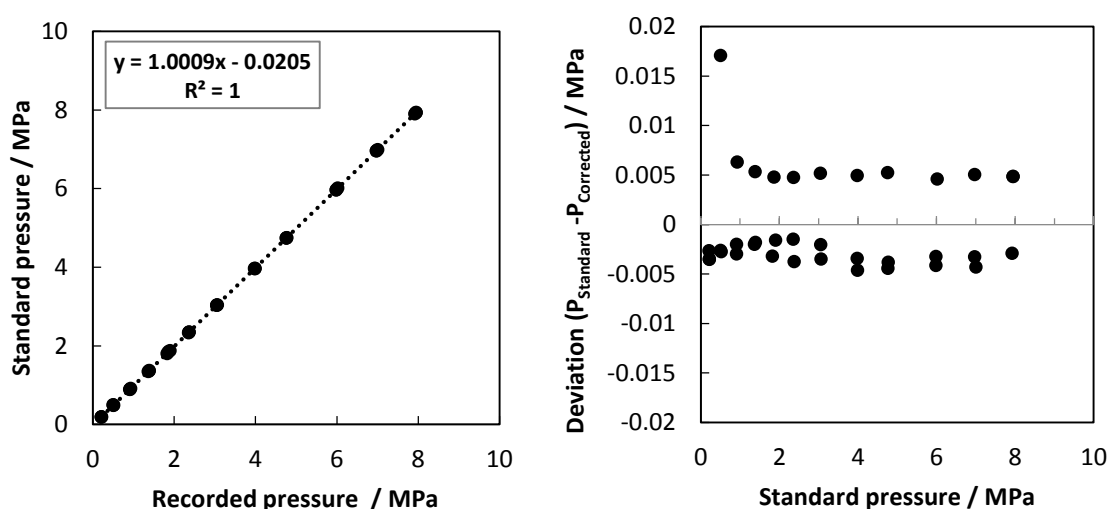
Figure 5.13: Calibration of the pressure transducer for apparatus 2.

5.4   Vapour pressure measurements

In order to verify the pressure and temperature calibration, the vapour pressure of carbon dioxide was measured. After evacuating the equilibrium cell to remove any trapped air or gas present in the lines, the equilibrium cell was pressurized with the experimental gas and the desired system temperature was set on the programmable thermostat. The system temperature was held for 1 hour until the system pressure stabilized. To eliminate the effects of hysteresis, the vapour pressure readings were repeated from a low system temperature to a high system temperature and vice versa. Vapour pressure measurements for carbon dioxide were recorded for temperatures

ranging from 270.4 to 274.0 K, respectively. Table 5.2 and Figure 5.14 shows the experimental vapour pressure data for carbon dioxide.

Table 5.2: The experimental vapour pressure data of carbon dioxide (CO_2).

Apparatus	T(K)	P(MPa)	ΔP^1 (MPa)	ΔP^2 (MPa)
1	274.0	3.54	± 0.02	± 0.04
	267.5	2.99	± 0.00	± 0.01
	287.2	4.90	± 0.07	± 0.10
	282.2	4.37	± 0.03	± 0.05
	278.1	3.95	± 0.02	± 0.03
2	292.1	5.56	± 0.03	± 0.05
	287.8	5.02	± 0.03	± 0.05
	283.1	4.48	± 0.02	± 0.04
	279.1	4.07	± 0.00	± 0.02
	274.8	3.63	± 0.01	± 0.02
	270.4	3.22	± 0.02	± 0.03

$\Delta P = | P_{exp} - P_{literature} |$
^{1} = lit (NIST- Wagner25);
^{2} = lit (DDBST- Antoine Equation (Thomson, 1946))
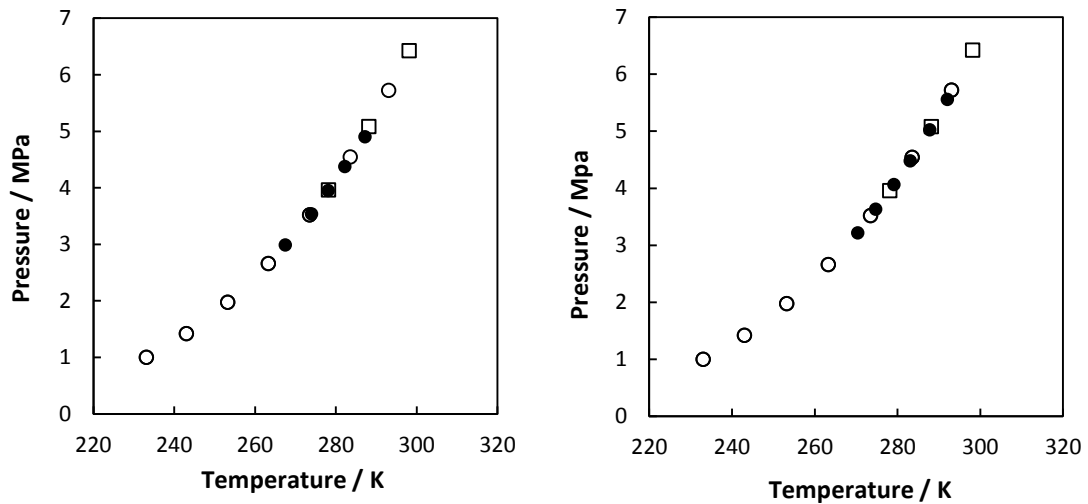
Figure 5.14: Vapour pressure data of carbon dioxide for apparatus 1 (left) and apparatus 2 (right). ●, this work; □, ref (Kim et al., 2010); ○, ref (Saleh and Wendland, 2005).

5.5   Experimental procedure for hydrate measurements

The following steps explain the experimental procedure for hydrate measurements in this study:

1. The equilibrium cell (EC) was washed with distilled water previous to every experimental run to remove any contamination (refer to Figure 5.2).

2. The cell was immersed in a temperature controlled bath (LB). Mechanical jack (MJ) was used to move the liquid bath.

3. The air inside the cell was evacuated for an hour using an Edwards vacuum pump (VP) to 0.01 kPa (all the valves were closed and V1 and V5 were opened).

4. After evacuating the cell, all the valves were closed and then the evacuated cell was initially charged with aqueous solution through V3. (Approximately 30 % by volume of the cell is filled with aqueous solution).

5. After loading the aqueous solution into the cell, the cell contents were once again degassed by applying a vacuum to the equilibrium cell for a few seconds, this aids in removing the air in the cell.

6. The temperature was set far from the hydrate zone through temperature controller (TC).

7. The gas was then supplied from a gas cylinder (G) through a pressure-regulating valve into the evacuated cell until the pressure inside the cell was increased to the desired level.

8. The stirrer device (SD) was turned on and adjusted desired stirring speed to mix the gas and aqueous solution inside the cell.

9. Once the temperature and pressure have stabilized, the valve on the line connecting the cell and the gas cylinder was closed.

10. Subsequently, temperature was slowly decreased at a rate of -10 K. h^{-1} until form hydrate. During cooling, a steady decrease of pressure was observed. Initial hydrate formation was detected by a rapid decrease in pressure due to encapsulation of hydrate former. Since hydrate formation is an exothermic process, an abrupt increase in pressure was also observed. Once crystallization stops, the temperature returns to the operative temperature. Throughout the process, pressure and temperature changes were monitored and recorded by an Agilent data acquisition system (DAU).

11. After the completion of hydrate formation, the system was slowly heated at a rate of 1 K.h $^{-1}$ to dissociate the hydrate. An abrupt increase in the pressure reading marks the start of the dissociation process. The system was then allowed to reach equilibrium (for 2 hours).

12. By starting hydrate dissociation, temperature of the equilibrium cell was then increased step-by-step to dissociate the hydrate. For accurate equilibrium data, the dissociation process should be performed at a slow heating rate $(0.1 K.h^{-1})$ to allow the system to reach equilibrium and prevent metastability. The complete decomposition of hydrates

(equilibrium point) was noted by a decrease in the pressure-temperature gradient. The procedure was repeated at different pressures for determination of the hydrate phase boundaries over a wide temperature range.

The hydrate dissociation point is considered as a point on the phase diagram of gas hydrates. It should be noted that the location of this point of the phase diagram of the corresponding gas hydrate is independent of measurement time.

6 Results and discussion

6.1 Experimental results

Tetrabutyl ammonium (TBA) or phosphonium (TBP) salts can form semi-clathrate hydrates because the cations (TBA^+ and TBP^+) fit into the hydrate cage easily. They have been proposed as good hydrate promoters, which effectively reduce the equilibrium pressure and affect the formation rate. The semi-clathrate structure consists empty cages which can be occupied by gas molecules.The clathrate/semi-clathrate hydrate dissociation conditions for the following systems have been measured and reported:

1. Carbon dioxide, methane, nitrogen and argon in presence of TBPB aqueous solutions
2. Carbon dioxide, methane, nitrogen and argon in presence of $TBANO_3$ aqueous solutions
3. Carbon dioxide in presence of TBAF aqueous solutions

Table 6.1 summarizes the hydrate phase equilibria measured in this study. The uncertainties in the measured variables were estimated according to the NIST guidelines as included in Appendix B. A summary of the uncertainties of these values are given in Table B. 1 and .

Table 6.1: Summary of the clathrate/semi-clathrate phase equilibria measured in this study.

System	Mass fraction of promoter	Temperature range/ K	Pressure range/ MPa
$CO_2 + H_2O$	0	281.9 - 283.3	3.69 - 4.45
$CO_2 + TBPB + H_2O$	0.05, 0.15	283.9 - 289.3	1.10 - 3.70
$CH_4 + TBPB + H_2O$	0.1, 0.15, 0.2	287.2 - 291.4	2.74 - 6.91
$N_2 + TBPB + H_2O$	0.075, 0.1, 0.2	281.5 - 288.0	2.43 - 7.79
$Ar + TBPB + H_2O^*$	0.10, 0.20, 0.30	283.4 - 293.1	1.07 - 9.90
$CO_2 + TBANO_3 + H_2O$	0.05, 0.1, 0.15	276.5 -284.3	1.21 - 4.30
$CH_4 + TBANO_3 + H_2O$	0.1, 0.15	281.8 - 285.1	2.74 - 5.05
$N_2 + TBANO_3 + H_2O$	0.1, 0.20	275.1 - 279.9	2.24 - 7.27
$Ar + TBANO_3 + H_2O^*$	0.05, 0.10, 0.20	277.7 - 286.3	1.22 - 9.56
$CO_2 + TBAF + H_2O$	0.041, 0.067	287.9 - 293.3	2.11 - 4.93

U (T) = 0.08 K, U (P) = 0.03 MPa (Apparatus 1)

U (T) = 0.21 K, U (P) = 0.05 MPa (Apparatus 2)

[*] These systems are novel which have not been yet studied in the literature.

6.1.1 CO₂/CH₄/N₂/Ar + TBPB aqueous solution system

It is known that TBPB forms semi-clathrate hydrates with 32 and 38 water molecules (TBPB·32H$_2$O and TBPB·38H$_2$O) (Muromachi et al., 2014). TBPB·32H$_2$O includes: ten 5^{12} small cages, sixteen $5^{12}6^2$ and four $5^{12}6^3$ cages per unit cell (Dyadin and Udachin, 1987, Dyadin and Udachin, 1984). Therefore, small gas molecules such as carbon dioxide and methane can be encaged within the semi-clathrate.

The experimental phase equilibrium data for clathrate/ semi-clathrate hydrate for systems with CO$_2$, CH$_4$, N$_2$ or Ar + TBPB are tabulated in Table 6.2 to Table 6.5 and plotted in Figure 6.1 to Figure 6.4. These data are compared to literature data which have been published.

Table 6.2: Hydrate equilibrium data of the (CO₂ + TBPB + H₂O) system

TBPB mass fraction	T/K	P/MPa
0	279.3	2.57
	281.0	3.21
	281.9	3.69
	283.3	4.45
0.05	283.9	2.38
	284.9	2.79
	285.8	3.23
	286.3	3.66
0.15	285.8	1.06
	287.1	1.54
	288.0	1.98
	288.7	2.45
	289.3	3.04
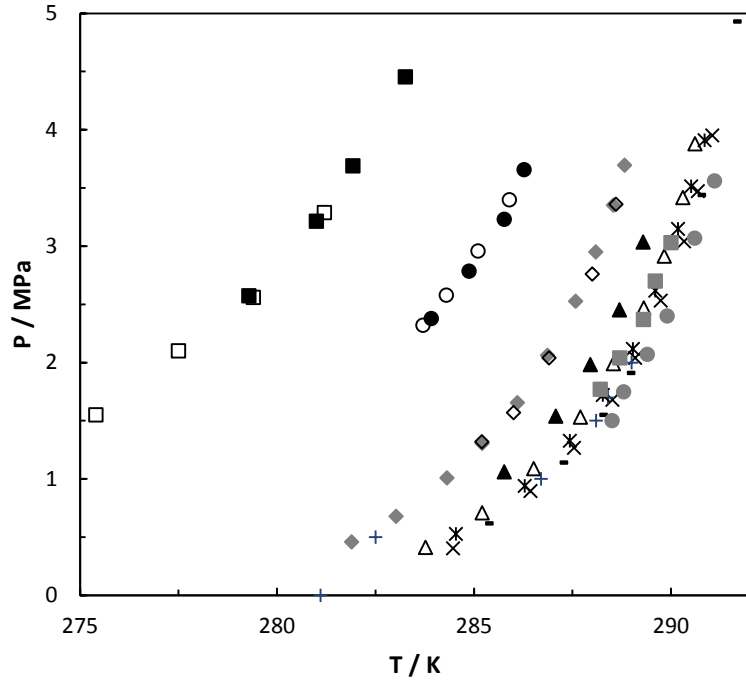
Figure 6.1: Hydrate equilibrium data of the (CO_2 + TBPB + H_2O) System, □, pure CO_2 hydrate, ref (Li et al., 2010c); ■, pure CO_2 hydrate, this work; ○, w_{TBPB}=0.05, ref (Li et al., 2010c); ●, w_{TBPB}=0.05, this work; ◆, w_{TBPB}=0.10, ref (Zhang et al., 2013); ◇, w_{TBPB}=0.10, ref (Shi et al., 2013); ▲, w_{TBPB}=0.15, this work; △, w_{TBPB}=0.20, ref (Zhang et al., 2013); ×, w_{TBPB}=0.35, ref (Zhang et al., 2013); −, w_{TBPB}=0.35, ref (Suginaka et al., 2013); +, w_{TBPB}=0.371, ref (Mayoufi et al., 2010); ●, w_{TBPB}=0.371, ref (Shi et al., 2013); ✱, w_{TBPB}=0.50, ref (Zhang et al., 2013); ■, w_{TBPB}=0.60, ref (Shi et al., 2013).

Table 6.3: Hydrate equilibrium data of the (CH_4 + TBPB + H_2O) system.

TBPB mass fraction	T/K	P/MPa
	287.2	3.00
0.10	288.7	4.29
	289.8	5.60
	290.5	6.91
	288.4	2.86
0.15	289.4	3.75
	290.1	4.65
	290.7	5.52
	288.9	2.74
0.20	290.0	3.71
	290.8	4.61
	291.4	5.46
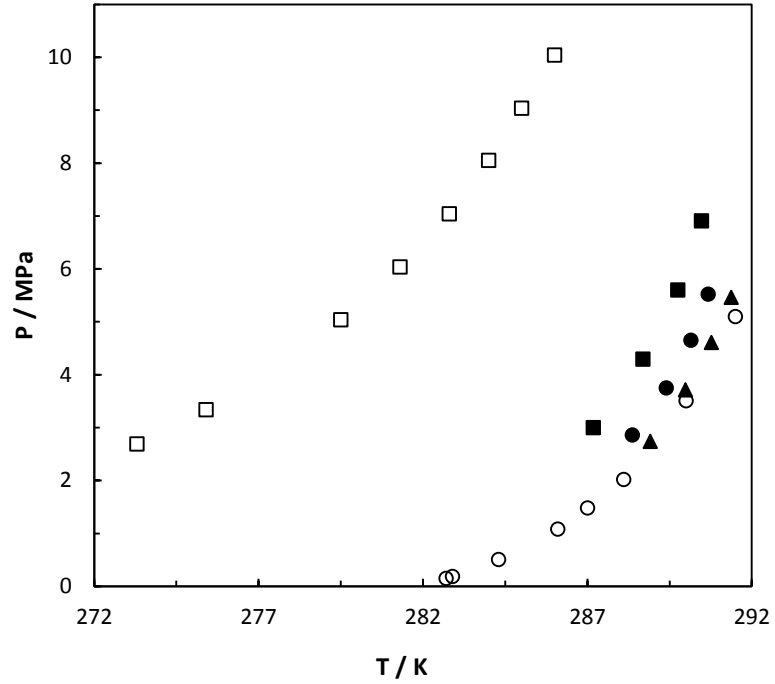
Figure 6.2: Hydrate equilibrium data of the (CH_4 + TBPB + H_2O) System:□, pure CH_4 hydrate, ref (Sloan, 2008a); ■, w_{TBPB}=0.1, this work; ●, w_{TBPB}=0.15, this work; ▲, 0.2, this work; ○, w_{TBPB}=0.35, ref (Suginaka et al., 2013).

Table 6.4: Hydrate equilibrium data of the (N_2 + TBPB + H_2O) system.

TBPB mass fraction	T/K	P/MPa
	281.5	3.08
0.075	282.4	4.26
	283.6	6.02
	284.4	7.56
	282.7	3.30
0.10	284.0	4.85
	284.9	6.24
	285.6	7.68
	284.4	2.43
0.20	285.8	4.22
	287.1	6.07
	288.0	7.79
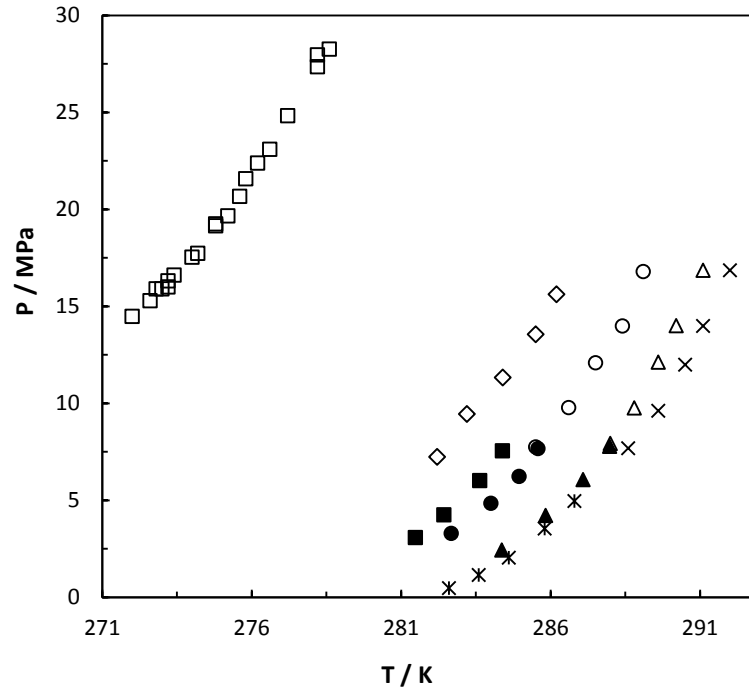
Figure 6.3: Hydrate equilibrium data of the (N_2 + TBPB + H_2O) System:□, pure CH_4 hydrate, ref (Sloan, 2008a); ◇, w_{TBPB}=0.05, ref (Shi et al., 2013); ■, w_{TBPB}=0.075, this work; ●, w_{TBPB}=0.1, this work; ○, w_{TBPB}=0.1, ref (Shi et al., 2013); ▲, w_{TBPB}=0.2, this work; ∗, w_{TBPB}=0.35, ref (Suginaka et al., 2013); ✕, w_{TBPB}=0.371, ref (Shi et al., 2013);△, w_{TBPB}=0.6, ref (Shi et al., 2013).

Table 6.5: Hydrate equilibrium data of the (Ar + TBPB + H₂O) system.

TBPB mass fraction	T/K	P/MPa
	290.2	9.26
	289.3	7.42
	288.1	5.71
0.1	286.8	4.04
	285.3	2.78
	283.4	1.64
	292.5	9.78
	291.8	8.42
	290.8	6.78
0.2	289.9	5.43
	288.7	3.98
	286.8	2.39
	284.6	1.07
	293.1	9.90
	292.5	8.27
	291.5	6.73
0.3	290.8	5.50
	289.3	3.96
	287.9	2.62
	285.8	1.30
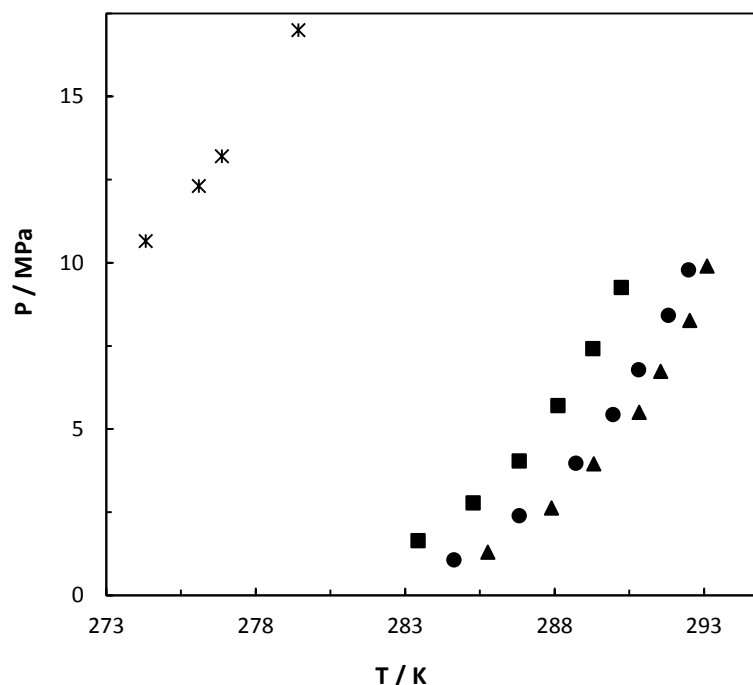
Figure 6.4: Hydrate equilibrium data of the (Ar + TBPB + H$_2$O) System: $*$, pure Ar hydrate, ref (Marshall et al., 1964); ■, w$_{TBPB}$=0.10, this work; ●, w$_{TBPB}$=0.20, this work; ▲, w$_{TBPB}$=0.30, this work.

It can be seen from the figures (6.1, 6.2, 6.3 and 6.4) that TBPB has a strong promotion effect on semi-clathrate hydrates formation for the systems under consideration. TBPB causes the formation conditions of CO$_2$/ CH$_4$ / N$_2$ and Ar hydrates to be shifted to moderate conditions (lower pressure and higher temperature) when compared with the clathrate hydrates of (CO$_2$/ CH$_4$/ N$_2$/ Ar) in the presence of water. It is clearly seen that the pressure equilibrium conditions of CO$_2$ + TBPB hydrate are lower than those of CH$_4$ + TBPB, N$_2$ + TBPB and Ar + TBPB hydrates. The difference between the equilibrium conditions may reveal the possibility of CO$_2$ capture from CO$_2$ + CH$_4$, CO$_2$ + N$_2$ and CO$_2$ + Ar mixtures.

By increasing the mass fraction of the TBPB solution (from w = 0.05 to w = 0.371), the phase equilibrium temperature increases and the equilibrium pressure decreases. Moreover, the stability of hydrate is enhanced. While, with the increases of mass fraction of the salt up to a mass fraction of 0.371, the stability of hydrate is lessened. It can be concluded that the maximum promotion effect of TBPB is in mass fraction of 0.371. To obtain a desired concentration of TBPB for a separation process based on semi-clathrate hydrates, some economic studies are required.

It is evident in Figure 6.1 that an increase in the concentration of TBPB from (0.05 to 0.15) mass fraction increases the promotion effect of TBPB on the CO$_2$ hydrate formation. Moreover,

depending on the salt concentration, the temperature stability of CO_2 hydrate increases by (4.8 to 9.0) K at a given pressure.

Figures (6.2, 6.3 and 6.4) shows that the influence of TBPB on N_2, CH_4 and Ar hydrates are similar to the effect of TBPB on CO_2 hydrate, which means that the phase equilibrium conditions shifted to the higher temperature and lower pressure due to the presence of TBPB as a promoter.

All the measured data have been checked with the equilibrium temperature-mass fraction diagram of TBPB hydrates to ensure that measured hydrate dissociation conditions in this study are outside of the dissociation conditions of semi-clathrate hydrates of the TBPB + water system (Figure 6.5). The measured experimental data for dissociation of TBPB semi-clathrate hydrate at atmosphere pressure are listed in Table 6.6.
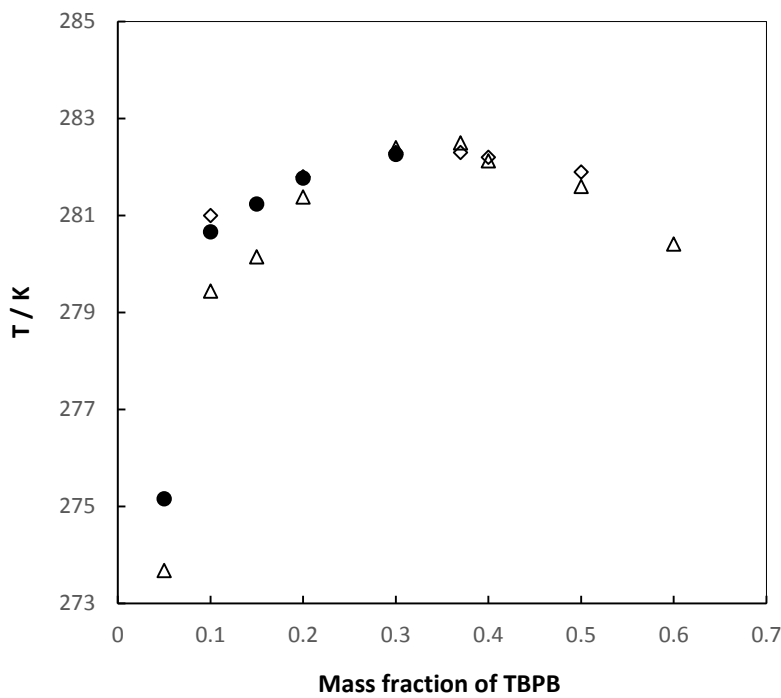
Figure 6.5: Phase diagram of TBPB semi-clathrate hydrate at atmospheric pressure: •, this work; △, ref (Zhang et al., 2013); ◇, ref (Suginaka et al., 2012).

Table 6.6: Measured Dissociation Temperature for TBPB Semiclathrate Hydrate at Atmospheric Pressure.

Mass fraction of TBPB	T_{diss} [a]/K
0.05	275.2
0.10	280.7
0.15	281.2
0.20	281.8
0.30	282.3

[a] $U (w_{TBPB}) = 0.0001$ mass fraction, $U (T) = 0.1$ K

6.1.2 CO₂/CH₄/N₂/Ar + TBANO₃ aqueous solution system

The tetrabutyl ammonium nitrate (TBANO₃) can form two different structures of semi-clathrate hydrates, $TBANO_3. 26H_2O$ and $TBANO_3. 32H_2O$. These structures are composed of 5^{12}, $5^{12}6^2$ and $5^{12}6^3$ cavities which gas molecules such as CO_2 can occupy.

The experimental phase equilibrium data for semi-clathrate hydrate for systems with CO_2, CH_4, N_2 + TBANO₃ or Ar + TBANO₃ are tabulated in Table 6.7 to Table 6.9 and plotted in Figure 6.6 to Figure 6.8. These data are compared to published literature data.

Table 6.7: Hydrate equilibrium data of the (CO₂ + TBANO₃+ H₂O) system.

TBANO₃ mass fraction	T/K	P/MPa
	276.5	1.21
	277.7	1.67
	278.9	2.25
0.05	279.6	2.60
	280.3	2.90
	280.9	3.20
	282.9	4.30
	279.8	1.73
	280.5	2.04
0.10	281.0	2.42
	281.3	2.67
	281.6	2.99
	281.5	1.42
	282.6	1.88
0.15	283.1	2.29
	283.5	2.72
	284.0	3.29
	284.3	3.90
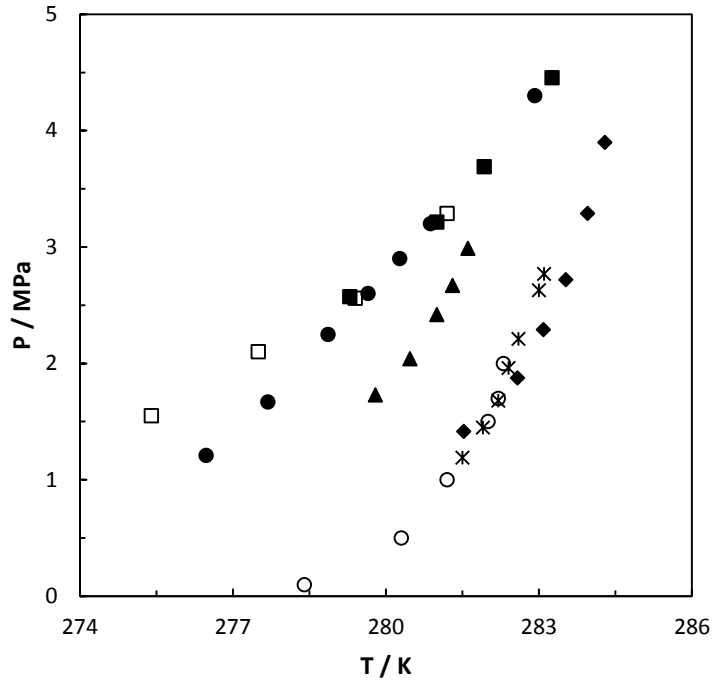
Figure 6.6: Hydrate equilibrium data of the (CO_2 + $TBANO_3$ + H_2O) System:□, pure CO_2 hydrate, ref (Li et al., 2010c); ■, pure CO_2 hydrate, this work; ●, w_{TBANO3}=0.05, this work; ▲, w_{TBANO3}=0.1, this work; ◆, w_{TBANO3}=0.15, this work; ○, w_{TBANO3}=0.394, ref (Mayoufi et al., 2010); ✳, w_{TBANO3}=0.394, ref (Du et al., 2011a).

Table 6.8: Hydrate equilibrium data of the (CH_4 + $TBANO_3$+ H_2O) system.

$TBANO_3$ mass fraction	T/K	P/MPa
0.10	281.8	3.03
	282.9	3.94
	283.7	4.64
	284.2	5.24
0.15	282.6	2.80
	283.7	3.64
	284.4	4.32
	285.1	5.05

83
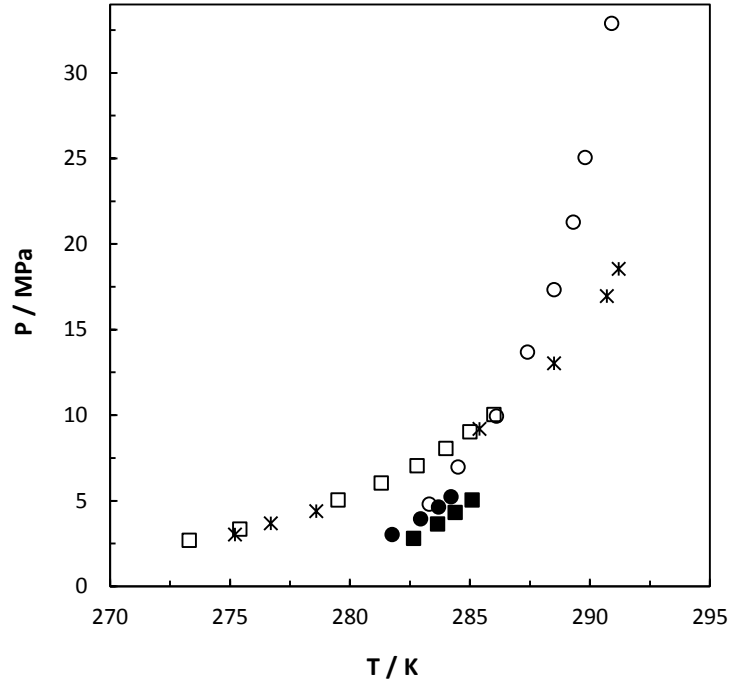
Figure 6.7: Hydrate equilibrium data of the (CH$_4$ + TBANO$_3$ + H$_2$O) System:□, pure CH$_4$ hydrate, ref (Sloan, 2008a); ∗, pure CH$_4$ hydrate, ref (Sloan, 2008a); ●, w$_{TBANO3}$=0.1, this work; ■, w$_{TBANO3}$=0.15, this work; ○, w$_{TBANO3}$=0.394, ref (Du et al., 2011a).

Table 6.9: Hydrate equilibrium data of the (N$_2$ + TBANO$_3$+ H$_2$O) system.

TBANO$_3$ mass fraction	T/K	P/MPa
	275.1	2.24
	276.5	3.70
0.10	277.6	5.01
	278.2	5.88
	279.0	7.27
	278.0	3.73
0.15	278.8	4.66
	279.5	5.56
	279.9	6.25
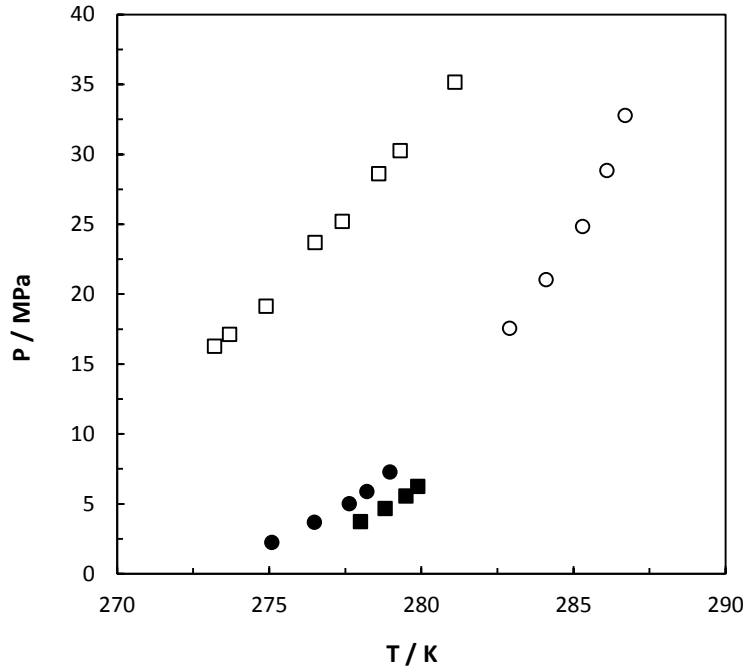
Figure 6.8: Hydrate equilibrium data of the (N_2 + TBANO$_3$ + H$_2$O) System:□, pure N$_2$ hydrate, (Sloan, 2008a); ●, w$_{TBANO3}$=0.1, this work; ■, w$_{TBANO3}$=0.15, this work; ○, w$_{TBANO3}$=0.394, (Du et al., 2011a).

Table 6.10: Hydrate equilibrium data of the (Ar + TBANO$_3$ + H$_2$O) system.

TBANO$_3$ mass fraction	T/K	P/MPa
	282.1	9.56
	281.2	8.10
0.05	280.1	6.56
	278.9	5.13
	277.6	3.75
	285.3	9.50
	283.9	7.34
0.1	282.0	5.16
	280.2	3.79
	283.3	6.77
	286.3	9.20
	285.3	7.74
	284.6	7.03
0.2	283.4	5.38
	282.0	3.89
	280.0	2.35
	278.4	1.22
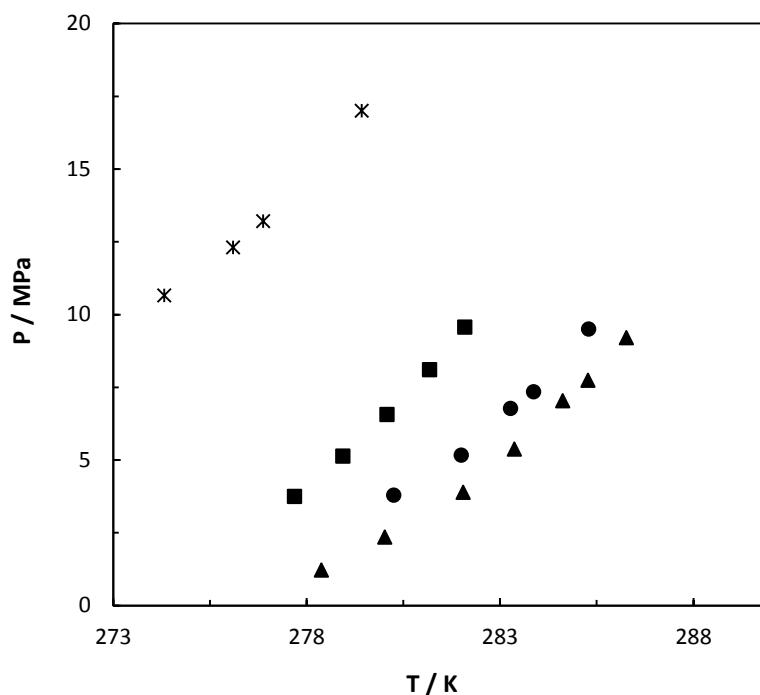
Figure 6.9: Hydrate equilibrium data of the (Ar + TBANO$_3$ + H$_2$O) System: ✳, pure Ar hydrate, ref (Marshall et al., 1964); ■, w$_{TBANO3}$=0.05, this work; ●, w$_{TBANO3}$=0.10, this work; ▲, w$_{TBANO3}$=0.20, this work.

It can be seen from Figure 6.6 and Figure 6.7, the influence of TBANO$_3$ is quite complicated among the system studied. Figure 6.6 shows that TBANO$_3$ forms semi-clathrate hydrates with CO$_2$. The presence of TBANO$_3$ with 0.1, 0.15 and 0.394 mass fraction, reduce the CO$_2$ semi-clathrate hydrate formation pressure. As also shown in Figure 6.6, the influence of TBANO$_3$ in solutions with 0.05 mass fraction, are entirely unlike to that in the solution with 0.15 and 0.394 mass fraction. When the mass fraction of TBANO$_3$ is 0.05, it shows both inhibition and promotion effects. TBANO$_3$ acts as a hydrate promoter at low pressure and as well as an inhibitor at higher pressure. At this concentration, the CO$_2$ + TBANO$_3$ semi-clathrate hydrate is stable at low pressures (below 2.57 MPa) and less stable at higher pressures (above 2.57 MPa) than pure CO$_2$ hydrate, respectively.

The experimental phase equilibrium data of CH$_4$ + TBANO$_3$ + water semi-clathrate hydrates are presented in Table 6.8 and are shown in Figure 6.7. The results demonstrate that TBANO$_3$ acts like an inhibitor at the pressure higher than 10 MPa. Furthermore, with increasing the concentration of TBANO$_3$ (w$_{TBANO3}$= 0.394) inhibition effect increases. In this study, the promotion effect of this salt were considered and experiments have been done at lower pressure to examine the promotion effect of TBANO$_3$ on CH$_4$ hydrate. TBANO$_3$ with 0.1 and 0.15 mass

fraction was acted as a good promoter and reduced the semi-clathrate hydrate formation pressure by half than pure CH_4 hydrate in the same temperature range.

From Table 6.9 and Figure 6.8, the presence of $TBANO_3$ causes the hydrate formation condition to shift to moderate conditions (lower pressure and higher temperature). The final phase equilibrium pressure for N_2+ $TBANO_3$ semi-clathrate hydrate was reduced by 17 MPa at 279.3 K.

The hydrate dissociation condition for the system of Ar + aqueous solutions of $TBANO_3$ were measured and results are given in Table 6.10 and Figure 6.9. It can be seen from Figure 6.9, $TBANO_3$ dramatically promote the argon hydrate formation condition. When the mass fraction of $TBANO_3$ increases from (0.05 to 0.2), the promotion effect of $TBANO_3$ increases significantly.

6.1.3 CO_2 + TBAF aqueous solutions

Experimental hydrate dissociation pressures for CO_2 in the presence of various aqueous solutions of TBAF are reported in Table 6.11 and the data plotted in Figure 6.10 against literature data.

Table 6.11: Hydrate equilibrium data of the (CO_2 + TBAF+ H_2O) system.

TBAF mass fraction	T/K	P/MPa
	287.9	2.11
	288.2	2.42
0.041	288.8	3.05
	289.3	3.53
	289.7	4.05
	291.6	2.48
	292.2	3.12
0.067	292.9	4.04
	293.3	4.93
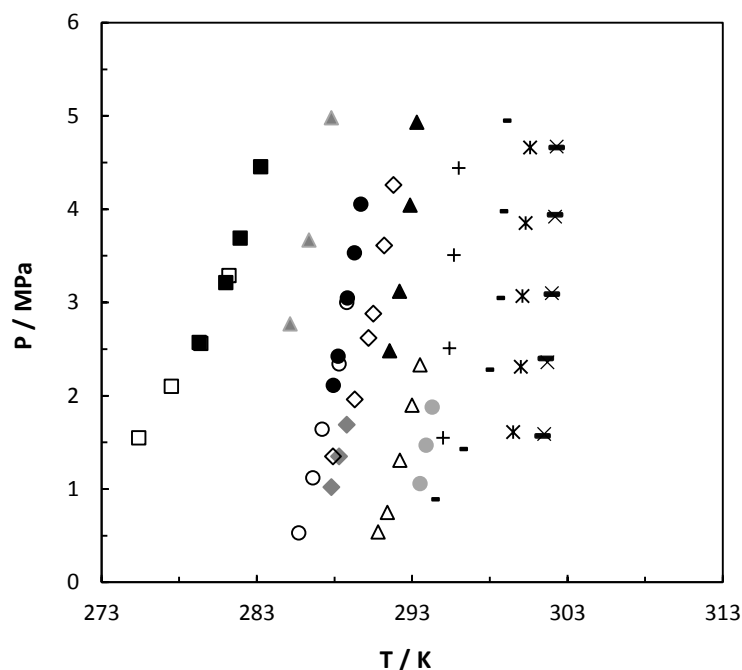
Figure 6.10: Hydrate equilibrium data of the (TBAF + CO₂ + H₂O) System:□, pure CO₂ hydrate, ref (Li et al., 2010c); ■, pure CO₂ hydrate, this work; ▲, w$_{TBANO3}$=0.02, ref (Mohammadi et al., 2013a); ●, w$_{TBANO3}$=0.041, this work; ○, w$_{TBANO3}$=0.041, ref (Li et al., 2010c); ◇, w$_{TBANO3}$=0.05, ref (Mohammadi et al., 2013a); ◆, w$_{TBANO3}$=0.05, ref (Kamran-Pirzaman et al., 2013); ▲, w$_{TBANO3}$=0.067, this work; △, w$_{TBANO3}$=0.083, ref (Li et al., 2010c); ●, w$_{TBANO3}$=0.05, ref (Kamran-Pirzaman et al., 2013); +, w$_{TBANO3}$=0.105, ref (Lee et al., 2012b);-, w$_{TBANO3}$=0.15, ref (Mohammadi et al., 2013a); –, w$_{TBANO3}$=0.31, ref (Lee et al., 2012b); ×, w$_{TBANO3}$=0.331, ref (Lee et al., 2012b); ✳, w$_{TBANO3}$=0.448, (Lee et al., 2012b).

TBAF acts as a semi-clathrate hydrate former which has a lower dissociation pressure than that of the pure CO₂ hydrate. The hydrate dissociation conditions of CO₂ are shifted to lower pressures or higher temperatures due to the presence of TBAF in the system (in the concentration ranges studied in the present work) when compared to the pure CO₂ hydrate. It can be seen in Figure 6.10 that the hydrate stability zone is increased with increasing TBAF concentrations.

All the measured data have been checked with the equilibrium temperature-mass fraction diagram of TBAF hydrates (Mohammadi et al., 2013a) to ensure that measured hydrate dissociation conditions in this study are outside of the dissociation conditions of semi-clathrate hydrates of the TBAF + water system.

The promotion effect of TBPB, TBANO₃ and TBAF on the hydrate formation is useful for application of hydrate formation technology in gas separation.

6.2   Model development and results

In this section, a thermodynamic approach is used to model the dissociation conditions of the CO_2, CH_4, N_2, or Ar semi-clathrate hydrates in the presence of TBPB, $TBANO_3$ and TBAF aqueous solution. In this study, the model proposed by Eslamimanesh (Eslamimanesh et al., 2012c) (explained in chapter 3) was used with major modifications in the optimization algorithm, used to obtain the optimal values of the adjustable model parameters.

In this approach, the van der Waals - Platteeuw solid solution theory (vdW-P 1959) (J.H. van der Waals, 1959) was used to model the gas hydrate phase. Then, the fugacity of water in the liquid phase was calculated using the Peng-Robinson equation of state with the Mathias-Copeman alpha-function (PR-EoS) (Peng and Robinson, 1976). The Non-Random Two-Liquid (NRTL) model (Renon and Prausnitz, 1968) was applied to determine the activity coefficient of the non-electrolyte species in the aqueous phase.

6.2.1   Model Parameters

Vapour pressure of empty hydrate (P_w^{MT}): Vapour pressure of empty hydrate, Eq. 6.1 shows that the presence of promoter has influence on the vapour pressure of water in empty hydrate lattice. Hence, the vapour pressure of the empty hydrate lattice is calculated using the method of Dharawardhana et al. (1980):

$$P_w^{MT} = 0.1 exp\left(17.44 - \frac{6003.9}{T} + h \times w_p\right)$$

(6.1)

where h is an adjustable parameter, and w_p denotes the weight fraction of the promoter in the aqueous solution.

Langmuir constants: In order to calculate the Langmuir constants, the method presented by Parrish and Prausnitz (Parrish and Prausnitz, 1972) was used with a modification to account for:

a. Disorders in the structures of cavities formed by anion (F^-, Br^-, NO_3^-) bonds to water molecules.
b. Interactions between large molecules of promoters with each other.

For dodecahedral cages:

$$C^{small} = \frac{aa}{T} + exp\left(\frac{bb}{T}\right)$$

(6.2)

For tetrakaidecahedra cages:

$$C^{large_1} = \left(\frac{c}{T} \times exp\left(\frac{d}{T}\right)\right) \times (1 + e \times w_p) \qquad (6.3)$$

For pentakaidecahedra cages:

$$C^{large_2} = \left(\frac{f'}{T} \times exp\left(\frac{g}{T}\right)\right) \times (1 + i \times w_p) \qquad (6.4)$$

where *aa* and *bb* are the parameters recommended by Parrish and Prausnitz (Parrish and Prausnitz, 1972) for each gaseous hydrate former encaged in small dodecahedral cages (Table 6.12) while *c*, *d*, *e*, *f'*, *g*, and *i* are adjustable parameters for tetrakaidecahedra and pentakaidecahedra cavities as shown in the Equations (6.2), (6.3) and (6.4).

Table 6.12: Parameters of Langmuir constants for a dodecahedral cage

Hydrate former	aa /(K.MPa^{-1})	bb / (K)
CO_2	0.0011978	2860.5
CH_4	0.0037237	2708.8
N_2	0.0038087	2205.5
Ar	0.0257791	2227.0

For determination of Langmuir constants, the following assumptions have been made about the structures of the semi-clathrate hydrates formed in the presence of the aqueous solutions of TBPB, TBANO$_3$ and TBAF:

- The hydration numbers for each promoter are listed in
-
- *Table 6.13*;

Table 6.13: Hydration numbers for TBPB, TBANO$_3$ and TBAF (Muromachi et al., 2014, Du et al., 2011b, Mohammadi et al., 2013a)

Promoter	Hydration number	
	Type A	Type B
TBPB	32	38

TBANO₃	26	32
TBAF	28	32

- Hydrate formers are located in the small dodecahedral cages;
- The TBP⁺ and TBA⁺ cations are engaged in two large tetrakaidecahedra and two large pentakaidecahedra cages;
- For each structure, the number of cages per water molecule in a unit hydrate cell are calculated as follows and summarized in Table 6.14:

$$\nu^{small} = \frac{6}{2 \times hydration\ number} \qquad (6.5)$$

$$\nu^{large} = \frac{4}{2 \times hydration\ number} \qquad (6.6)$$

Table 6.14: Number of cavities of per water molecules in a unit TBPB, TBANO₃ and TBAF

Promoter	TBPB		TBANO₃		TBAF	
	Type A	Type B	Type A	Type B	Type A	Type B
ν^{small}	3/32	3/38	3/26	3/32	3/28	3/32
ν^{large1}	1/16	1/19	1/13	1/16	1/14	1/16
ν^{large2}	1/16	1/19	1/13	1/16	1/14	1/16

The value of ν_w^{MT} is calculated by applying the following equation, assuming that the volume of the empty hydrate lattice and hydrate structure I is similar (as the gaseous hydrate former occupies only dodecahedral cages).

$$\nu_w^{MT} = (11.835 + 2.217 \times 10^{-5}T^2 + 2.242 \times 10^{-6}T^2)\frac{10^{-30}N_A}{N_w^{MT}}$$

$$- 8.006 \times 10^{-9}P + 5.448 \times 10^{-12}P^2 \qquad (6.7)$$

where N_A denotes Avogadro's number, N_w^{MT} is the number of water molecules per hydrate cell. The pressure and temperature units in the Equation (6.7)(6.7) are MPa and K, respectively.

Activity coefficient: For determination of the activity coefficient of water in the aqueous phase, the NRTL (Renon and Prausnitz, 1968) model with interaction parameters reported in Table 6.15 was used. It is assumed that the interaction parameters of the NRTL model used in this study are similar to interaction parameters for TBAB systems (Eslamimanesh 2012).

Table 6.15: The interaction parameters of the NRTL (Renon and Prausnitz, 1968) model used in this work.

Hydrate former	A_{12} (kJ.mol^{-1})	A_{21} (kJ.mol^{-1})	A
CO_2	5.82	6.81	0.3
CH_4	4.00	2.15	0.6
N_2	7.11	7.12	0.3
Ar	6.98	7.22	0.3

To the best of our knowledge, no experimental data of activity coefficient of TBPB, TBANO$_3$ and TBAF in aqueous solution at various temperature and pressure have been reported to date. This causes some limitations in obtaining the optimum values of the required parameters for modeling the electrolytic solution. Furthermore, the main aim of the model focused on examining the effect of the applied promoter on the hydrate cages (or hydrate structures). Therefore, Eslamimanesh (Eslamimanesh et al., 2012c) correlation has been utilized to calculate the activity coefficient of the hydrate promoters (TBPB, TBANO$_3$ and TBAF) in the following expression:

$$\gamma_p = -0.5057 w_p^3 + 1.1603 w_p^2 - 1.3689 w_p + 0.7655$$

(6.8)

Partial molar volume of water: The partial molar volume (cm^3.mol^{-1}) was estimated using a correlation recommended by Eslamimanesh (Eslamimanesh et al., 2012c):

$$v_w^L = \left(5.459/0.30452^{\left(1+(1-T/647.13)\right)^{0.081}}\right)^{-1}$$

(6.9)

Parameters for the Mathias–Copeman alpha function: The fugacity of the gaseous hydrate former calculated by the PR EoS (Peng and Robinson, 1976). The parameters of the Mathias–

Copeman alpha function (Mathias and Copeman, 1983) were re-tuned to accurately represent the vapour pressure of the pure compounds (CO_2, CH_4, and N_2) from the triple point to the critical point. The common global optimum values of these parameters (Eslamimanesh 2012) are indicated in Table 6.16 and the applied critical properties and acentric factors of the gases are shown in Table 6.17.

Table 6.16: The optimal values of the Mathias-Copeman alpha function (Mathias and Copeman, 1983) [*] used in this study.

Hydrate former	Optimal values of parameters				
	Temperature range / K	CC_1	CC_2	CC_3	AARD%
CO_2	217 - 304	0.709	-0.317	1.91	0.5
N_2	64 - 126	0.449	-0.158	0.469	0.6
CH_4	91 - 190	0.416	-0.173	0.348	0.4
Ar	86 -150	0.408	-0.115	0.503	0.4

[*] $\alpha(T) = \left[1 + CC_1 \left(1 - \sqrt{\frac{T}{T_c}} \right) + CC_2 \left(1 - \sqrt{\frac{T}{T_c}} \right)^2 + CC_3 \left(1 - \sqrt{\frac{T}{T_c}} \right)^3 \right]^2$ for $T < T_C$

Otherwise,

[*] $\alpha(T) = \left[1 + CC_1 \left(1 - \sqrt{\frac{T}{T_c}} \right) \right]^2$

Table 6.17: Critical properties and acentric factor of the pure compounds used in this study.

Hydrate former	P_c[1] / MPa	T_c[2] / K	Z_C[3]	ω[4]
CO_2	4.599	190.56	0.2862	0.0114
CH_4	7.377	304.13	0.2744	0.2239
N_2	3.399	126.20	0.2917	0.0377
Ar	4.898	150.86	0.2910	0.000
H_2O	22.055	647.13	0.2294	0.3449

[1] Critical pressure
[2] Critical temperature
[3] Critical compressibility factor
[4] Acentric factor

6.2.2   Optimization of model parameters

To determine the optimal values of the model parameters, the Nelder-Mead optimization algorithm (Nelder and Mead, 1965) was used. The algorithm is used for minimizing an objective function in a multi-dimensional space. The algorithm is appropriate for non-smooth functions because it does not need any derivatives objective function.

The Nelder-Mead algorithm is considered as a simplex optimization algorithm. In this study the algorithm used was described by Lagarias et al. (Lagarias et al., 1998). This algorithm uses a simplex of n + 1 points for n-dimensional vectors x. The algorithm first makes a simplex around the first guess x_0 by adding 5% of each component $x_0(i)$ to x_0, and using these n vectors as elements of the simplex in addition to x_0. (It uses 0.00025 as component i if $x_0(i) = 0$.) Then, the algorithm modifies the simplex repeatedly according to the procedure shown in Figure 6.11.

Figure 6.11: The Nelder-mead algorithm flow chart developed by Lagarias et al. (1998).
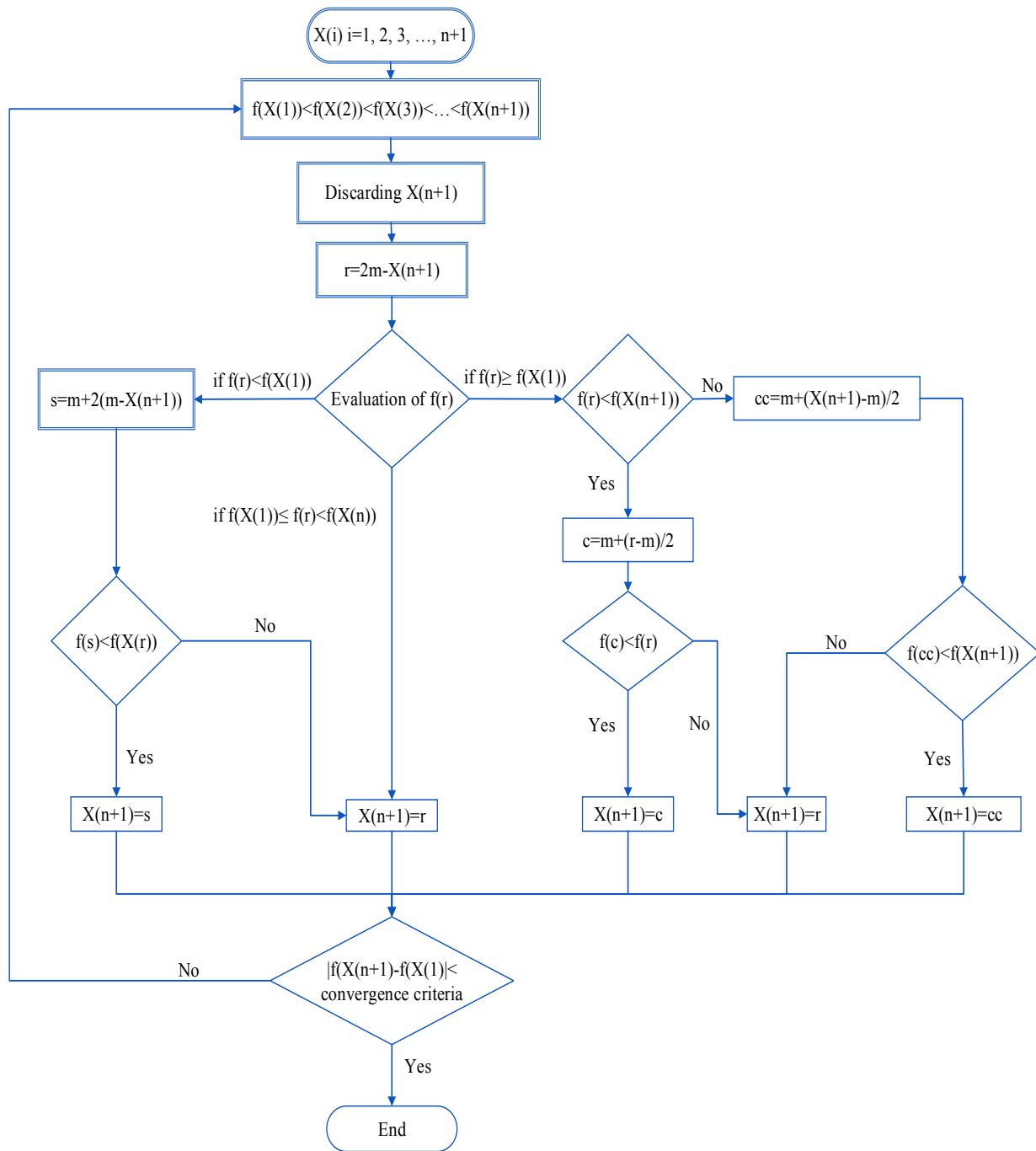
Pursing the above mentioned optimization steps, the optimal values of the adjustable parameters of the model were obtained and are reported in Table 6.18.

Table 6.18: Optimal values of the parameters in Equations. (6.1), (6.3) and (6.4).

Parameter	TBPB		TBANO3		TBAF	
	Type A[a]	Type B	Type A	Type B	Type A	Type B
h	0.2028	0.2070	0.2206	0.2109	0.2000	0.1979
c / (K.MPa⁻¹)	0.510165	0.463273	0.517354	0.513510	0.513723	0.530174
d/ (K)	4291.7	4424.7	4064.9	4330.0	4281.3	4462.4
e	-0.7276	-0.7313	-0.7292	-0.7413	-0.7345	-0.7248
f'/ (K.MPa⁻¹)	0.607010	0.641872	0.586940	0.588224	0.606561	0.575785
g/ (K)	6758.2	7317.6	5859.8	6281.5	6698.2	7146.1
i	-0.969571	-0.889876	-1.007787	-0.963322	-0.936270	-0.945130

[a] Calculations were performed assuming formation of semi-clathrate hydrate of type A or type B

6.2.3 Modeling results

It should be noted that the predictions of the phase behavior for the semi-clathrate hydrates systems studied were performed in two steps, assuming formation of type A or type B.

In modeling these semi-clathrate hydrates, only the experimental data of CO_2 semi-clathrate hydrate were used to obtain the optimal values of the model parameters. Thereafter, the parameters were used to predict the dissociation conditions of $CO_2/CH_4/N_2/Ar$ semi-clathrate hydrates in the presence of TBPB/TBANO$_3$/TBAF aqueous solutions. The performance of the model for prediction of the semi-clathrate hydrate dissociation conditions for aforementioned system are shown in Table 6.19.

The predicted phase equilibria of the $CO_2/CH_4/N_2/Ar$ + TBPB/TBANO$_3$/TBAF aqueous solution systems are shown in Figure 6.12 to Figure 6.20.

Table 6.19: Summary of the model results for the prediction of the dissociation conditions of semi-clathrate hydrates of $CO_2/CH_4/N_2$ + TBPB/TBANO$_3$/TBAF aqueous solution.

System	N_D	Temperature range/ K	Pressure range / MPa	Concentration of promoter	AARD [a]/ %	
					Type A	Type B
CO_2+TBPB aqueous solution	87	275.4 - 291.6	0.01-4.93	0.00, 0.05, 0.10, 0.15, 0.20, 0.35, 0.371, 0.50, 0.60	2.04	2.12
CH_4+TBPB aqueous solution	35	273.3 - 291.5	0.15-9.97	0.00, 0.10, 0.15, 0.20, 0.35	3.13	2.95
N_2+TBPB aqueous solution	65	272.0 – 292.0	0.48-35.16	0.00, 0.075, 0.1, 0.2, 0.35, 0.371, 0.60	8.78	7.41
CO_2+TBANO$_3$ aqueous solution	39	275.4 - 284.3	0.01 - 4.45	0.00, 0.05, 0.10, 0.15, 0.394	2.00	1.75
CH_4+TBANO$_3$ aqueous solution	29	273.3 - 290.9	2.69 - 32.89	0.00, 0.10, 0.15, 0.394	6.16	13.11
N_2+TBANO$_3$ aqueous solution	42	272 - 286.7	2.24 - 35.16	0.00, 0.10, 0.15, 0.394	7.57	7.11
CO_2+TBAF aqueous solution	67	275.4 - 302.3	0.53 - 4.98	0.00, 0.02, 0.041, 0.05, 0.067, 0.083, 0.10, 0.15, 0.31, 0.33, 0.448	3.61	3.71
Ar+TBPB aqueous solution	24	274.3 - 293.1	1.07 - 17.00	0.00, 0.10, 0.20, 0.30	2.87	2.05
Ar+TBANO$_3$ aqueous solution	21	274.3 - 286.3	1.22 - 17.00	0.00, 0.05, 0.10, 0.20	6.62	1.32

[a] $= \dfrac{100}{N_D} \sum_i^N \dfrac{\left| P_{i,pred.}^{diss.} - P_{i,exp.}^{diss.} \right|}{P_{i,exp.}^{diss.}}$, where N_D is the number of the experimental data points, and subscript pred.

stands for the predicted values.

In order to select which type of semi-clathrate hydrate is formed at the conditions of interest (i.e. pressure-temperature-concentration of promoter in aqueous solution), the lowest value of the average absolute relative deviation (AARD) of predicted hydrate dissociation pressures from the experimental value can be applied.

It can be concluded from Table 6.19, low difference between AARD value for type A and type B for $CO_2/CH_4/N_2/Ar$ + TBPB semi-clathrate hydrate. Hence at the given formation conditions, these semi-clathrate hydrates may form type A or type B and there are a few structural changes

from type A to type B or vice versa. Furthermore, in the presence of TBANO₃, carbon dioxide and nitrogen may form both type A and type B hydrate structures while methane prefers to form type A due to of low value of AARD and Ar prefers to form type B. The AARD value for the CO_2+TBAF aqueous solution of type A and type B are approximately the same thus the structural changes for this semi-clathrate hydrate at given conditions are low.
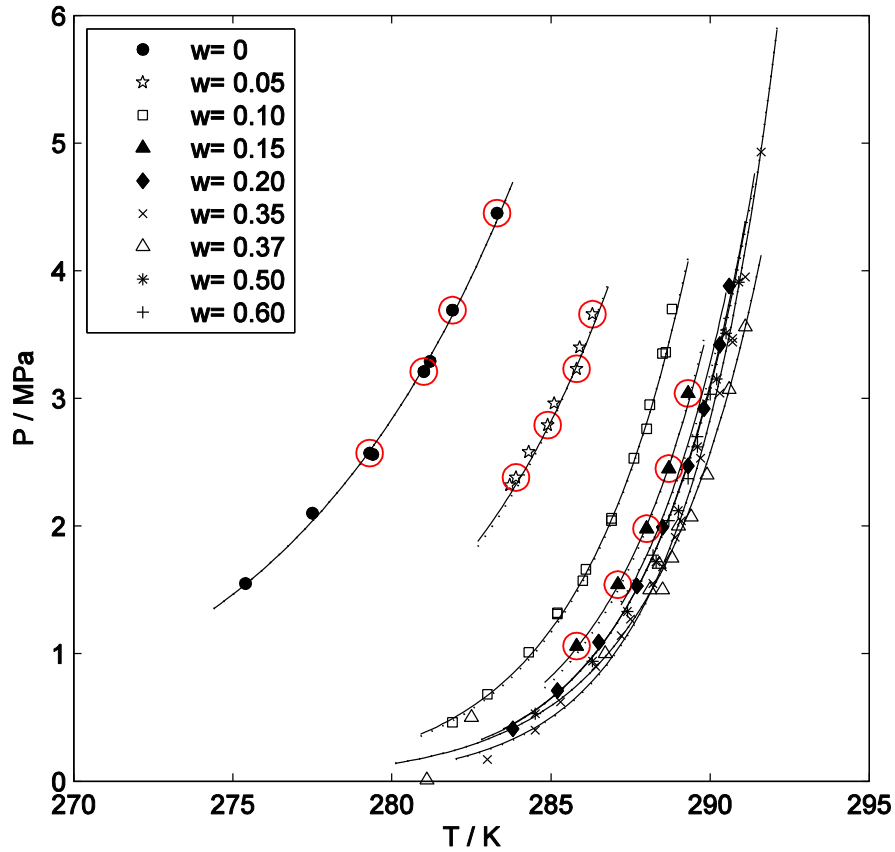
Figure 6.12: Experimental and predicted dissociation conditions of CO_2 + TBPB semi-clathrate hydrates. Symbols represent the experimental data and the lines represent the thermodynamic model predictions. The experimenal data measured in this study are distingushied by red circles and the solid and the dotted lines denote the model predictions assuming formation of Type A and Type B of clathrate hydrates, respectively.

Figure 6.13: Experimental and predicted dissociation conditions of CH₄ + TBPB semi-clathrate hydrates. Symbols represent the experimental data and the lines represent the thermodynamic model predictions. The experimental data measured in this study are distinguished by red circles and the solid and the dotted lines denote the model predictions assuming formation of Type A and Type B of clathrate hydrates, respectively.
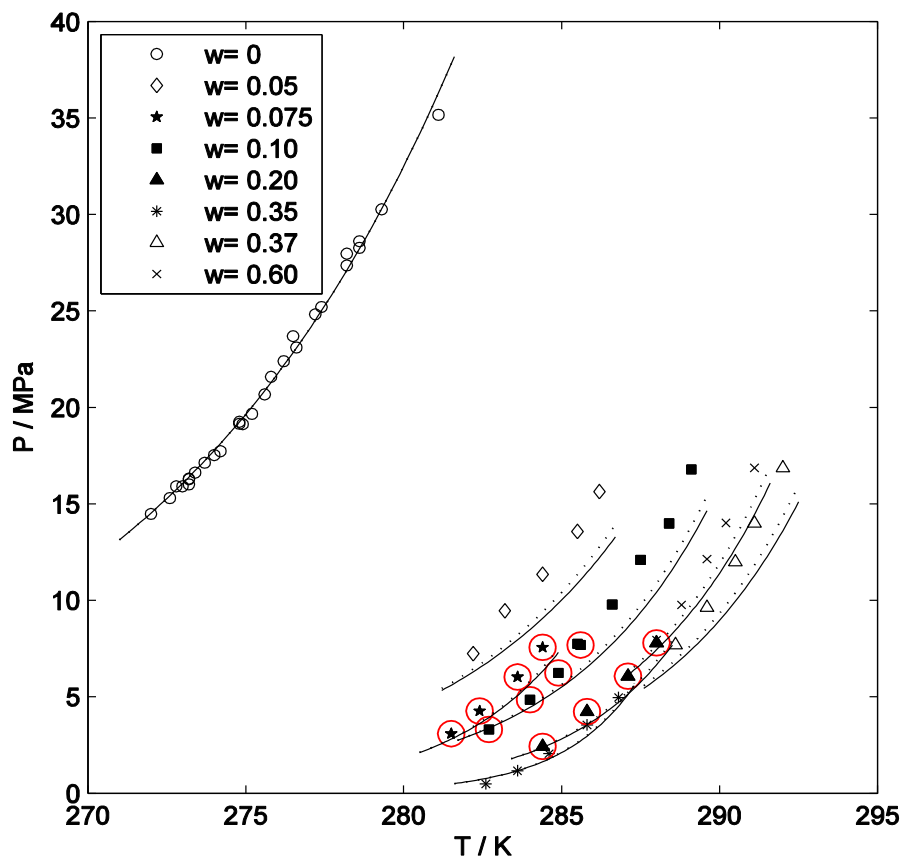
Figure 6.14: Experimental and predicted dissociation conditions of N₂ + TBPB semi-clathrate hydrates. Symbols represent the experimental data and the lines represent the thermodynamic model predictions. The experimenal data measured in this study are distingushied by red circles and the solid and the dotted lines denote the model predictions assuming formation of Type A and Type B of clathrate hydrates, respectively.
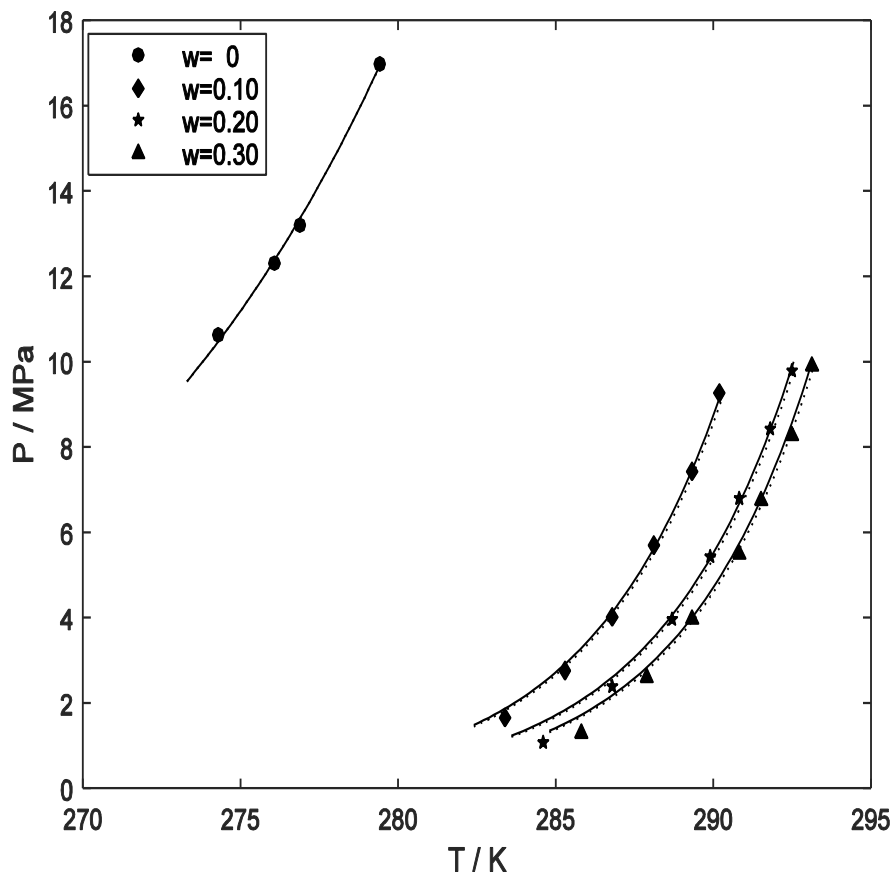
Figure 6.15: Experimental and predicted dissociation conditions of Ar + TBPB semi-clathrate hydrates. Symbols represent the experimental data and the lines represent the thermodynamic model predictions. The experimenal data measured in this study are distingushied by red circles and the solid and the dotted lines denote the model predictions assuming formation of Type A and Type B of clathrate hydrates, respectively.

Figure 6.16: Experimental and predicted dissociation conditions of CO_2 + TBANO$_3$ semi-clathrate hydrates. Symbols represent the experimental data and the lines represent the thermodynamic model predictions. The experimenal data measured in this study are distingushied by red circles and the solid and the dotted lines denote the model predictions assuming formation of Type A and Type B of clathrate hydrates, respectively.

Figure 6.17: Experimental and predicted dissociation conditions of CH$_4$ + TBANO$_3$ semi-clathrate hydrates. Symbols represent the experimental data and the lines represent the thermodynamic model predictions. The experimenal data measured in this study are distingushied by red circles and the solid and the dotted lines denote the model predictions assuming formation of Type A and Type B of clathrate hydrates, respectively.
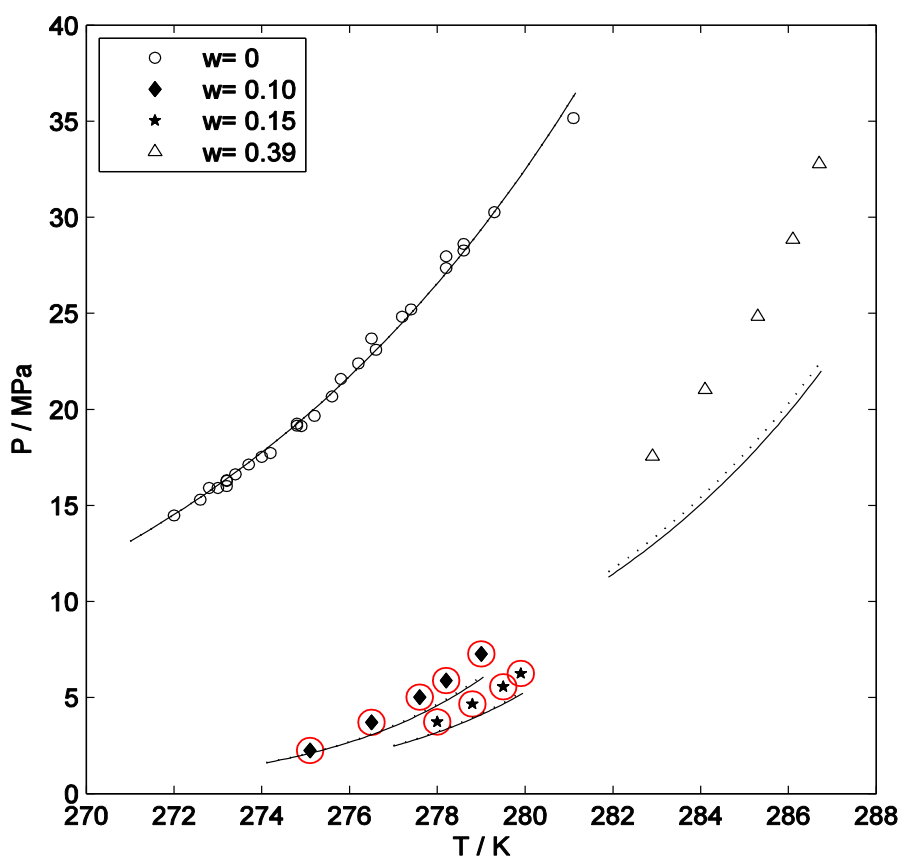
Figure 6.18: Experimental and predicted dissociation conditions of N_2 + TBANO$_3$ semi-clathrate hydrates. Symbols represent the experimental data and the lines represent the thermodynamic model predictions. The experimenal data measured in this study are distingushied by red circles and the solid and the dotted lines denote the model predictions assuming formation of Type A and Type B of clathrate hydrates, respectively.
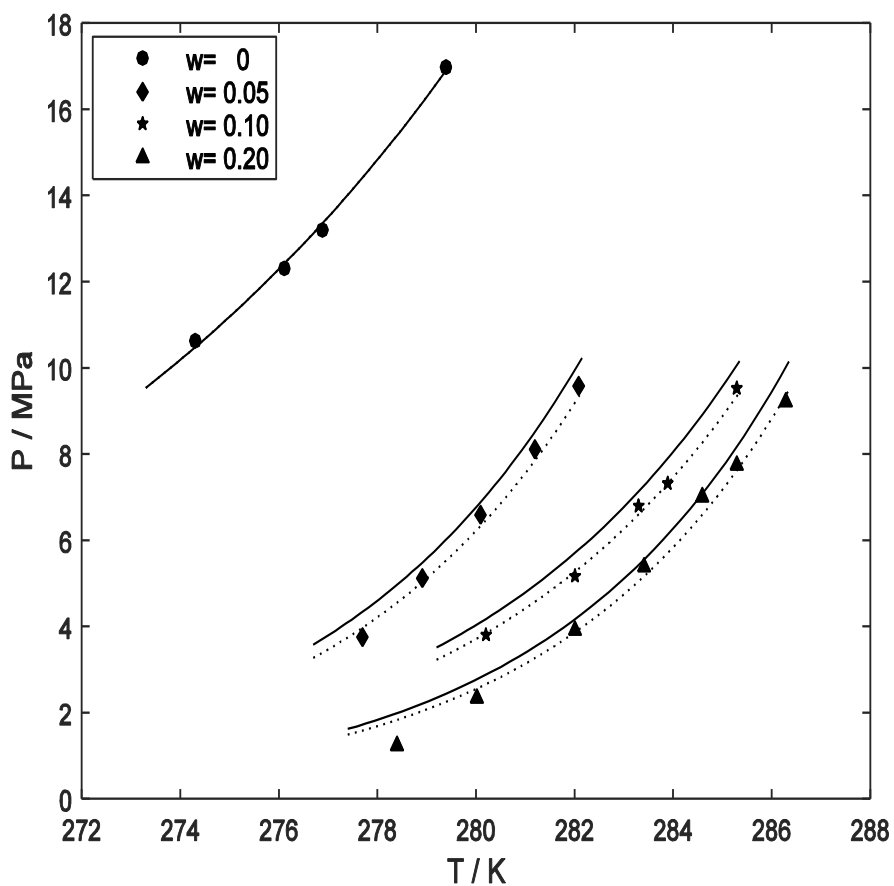
Figure 6.19: Experimental and predicted dissociation conditions of Ar + TBANO₃ semi-clathrate hydrates. Symbols represent the experimental data and the lines represent the thermodynamic model predictions. The experimenal data measured in this study are distingushied by red circles and the solid and the dotted lines denote the model predictions assuming formation of Type A and Type B of clathrate hydrates, respectively.

Figure 6.20: Experimental and predicted dissociation conditions of CO_2 + TBAF semi-clathrate hydrates. Symbols represent the experimental data and the lines represent the thermodynamic model predictions. The experimenal data measured in this study are distingushied by red circles and the solid and the dotted lines denote the model predictions assuming formation of Type A and Type B of clathrate hydrates, respectively.

6.3   Separation process: batch or continuous

Although gas hydrates have many applications, their industrial applications have not been widely reported so far. Gas hydrate potential for industrial applications encourages researchers to find more practical methods (Erfani et al., 2013). Therefore, several patents and papers on processes and apparatuses for the efficient continuous production, separation and pelletizing of gas hydrates have not presented recently (Balczewski, 2008, Balczewski, 2010, Lee et al., 2013, Xu et al., 2013a). Such methods and techniques have been proposed generally for gas storage processes using gas hydrate crystallization. However, they can also be applied or improved for gas separation purposes.

Since the energy demand is increasing in the world, it is needed to design more efficient hydrate formation, separation, and pelletizing processes as well as their transportation, storage, separation and gasification techniques.

6.3.1   Gas hydrate formation

The gas hydrate formation is considered as a crystallization of a solid in which a super-saturated solution undergoes temperature reduction at atmospheric pressure (Bishnoi and Natarajan, 1996). The crystallization process includes two main steps; the nucleation and the growth (Bishnoi et al., 1994, Fandiño and Ruffine, 2014, Walsh et al., 2009). An efficient hydrate formation process may be regarded as the formation of gas hydrate from a solution which is as saturated as possible. This way can help us to enhance the suitable nucleation sites in the solution. It should be mentioned that mass and heat transfer resistances may adversely affect the hydrate formation process.

Generally, gas hydrate formation in a simple system contains dissolution of gas in water, diffusion of gas molecules into the water-hydrate interface, and nucleation and growth of the crystals. As a result, to improve the efficiency of any process equipment, such steps should be optimized (Wu et al., 2013).

Autoclaves (agitated vessels) are thermal jacket-controlled devises working under high pressures. They can be used to hydrate formation in either batch-wise or continuous modes. The agitators are used to enhance the mass transfer and hydrate formation may result in increase in shaft work and power consumption (Townson et al., 2012, Daraboina et al., 2013b).

Sprayers are widely used to enhance the level of contact between liquid-gas phases. Various types of nozzles can be used to form gas hydrates (Karimi and Abdi, 2009, Li et al., 2010a). In such systems, water is sprayed through the nozzle into the gas phase. One of the main advantages of such systems is that most of the injected water is consumed and there is no need for excess

water which makes the separation process much easier (Matsuda et al., 2006, Lee et al., 2010, Ohmura et al., 2002). Rossi et al. (Rossi et al., 2012) designed and developed a new scaled-up spraying reactor to rapid hydrate formation. This method, increase the interfacial area between reactants and reduce mass transfer barriers.

Bubble columns are also used in gas hydrate formation in which the gas is bubbled to the column of water (Hashemi et al., 2009). In such equipment, the hydrates are formed at the bubbles surfaces which enhance the mass and heat transfer resistances. This point adversely affects the hydrate growth and should be solved somehow (Luo et al., 2007). Xu et al. (Xu et al., 2012) designed a visual bubble reactor for CO_2 capture. In this reactor, while the gas bubble move from the bottom to the top of the reactor, the gas hydrate forms around the bubble, then the hydrate gradually grows up.

6.3.2 Separation of gas hydrate

The separation of gas hydrates from unreacted water is considered as a solid-liquid separation process (Takeya et al., 2012). Since there is a density difference between hydrates and water, they can be separated using physical methods based on gravity and centrifugal force. However, the difference in their densities is very low therefore; the residence time of the separation process just using the gravity is high. In separation by gravity force, gas hydrate is formed in agitated vessel and accumulated on the water surface, and then water and gas hydrate transport to a settlement chamber (Kaehler and Hamann, 2012, Erfani et al., 2013).

6.3.3 Gas hydrate pelletizing systems

The pelletizing of gas hydrates increase their gas storages capacity, their fluidity and their stability. They can be pelletized using a cylinder-piston system in which the pellets are made by compressing the hydrate crystals. The most important drawback of such systems is the pressure drop at exit which reduces the quality of the produces pellets.

Twin-rolling is another system used to pelletize the gas hydrates. In such systems, the slurry of gas hydrate is poured on two side by side rollers and then the hydrate pellets are produced from the bottom of the rollers and discharge by means of a spiral (Erfani et al., 2013).

The schematic diagram of the proposed operating process for CO_2 separation is illustrated in Figure 6.21.
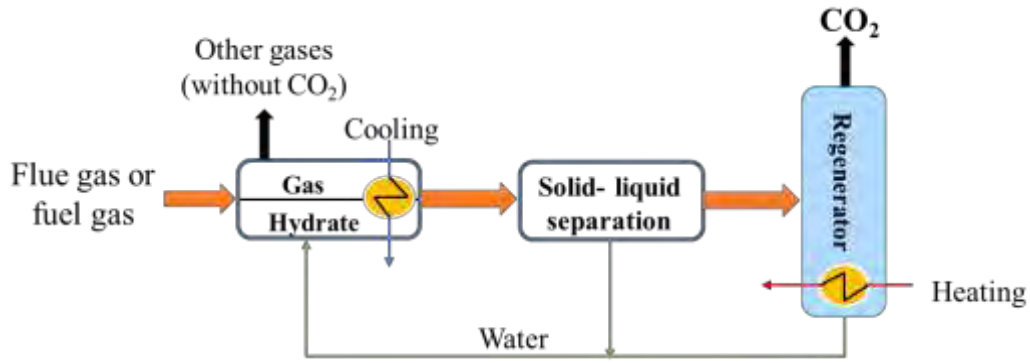
Figure 6.21: Schematic diagram for CO_2 capture and separation process.

6.4 Economic estimation of carbon dioxide capture

One of the main challenges of CCS technology is total cost. The first CCS step includes the capture process in which both the capital and operating costs significantly vary with the facilities configurations. This step is considered as most expensive step of CCS and needs approximately two third of total costs (D'Alessandro et al., 2010). The next steps of CCS include transport and storage of CO_2 from the capture facility to the storage location as well as injection and monitoring at the storage site.

There are several methods for CCS from which the amine process and the membrane technology (zeolite adsorption) have been more widely studied. In both methods, expensive chemicals are used that can be considered as the main drawback of such methods.

The hydrate technology in which the only chemical needed is water has recently attracted many attentions in CCS. It can also be considered as an environment friendly cheaper alternative for currently available methods if an appropriate process is developed. According to the economic studies recently performed, the capital cost for transportation of natural gas in gas hydrate form is less than that of liquefied natural gas (LNG) (Javanmardi et al., 2005). Furthermore, the energy cost of CO_2 capture by gas hydrates may be about 30 € per ton of CO_2 (Duc et al., 2007b). Therefore, the hydrate technology is comparable to other CO_2 capture methods such as absorption by amine, adsorption, membranes, etc.

Javanmardi et al. (Javanmardi et al., 2005) presented the installed costs of the natural gas hydrate production which is given in Table 6.20.

Table 6.20: The installed costs of different equipment of the natural gas hydrate production process.

Equipment	Installed cost, US $
Compressor	17.39×10^6
Condenser	2.41×10^6
Heat exchanger	3.98×10^5
Separator	1.09×10^6
Dryer	2.57×10^5
Reactor	1.49×10^6
Pump	4.5×10^4
Storage tank	1.98×10^6
Total capital investment for each train	59.12×10^6

More investigations reveals that other costs related to CO_2 capture (e.g. equipment, maintenance) using gas hydrates would be about 40.8 € per ton of CO_2 (Duc et al., 2007b). There are two important points regarding the aforementioned explanations;

1. It may be possible to design more economically efficient processes (i.e. pinch technology or exergy-based analyses can be used to re-design of the aforementioned process)

2. The hydrate formation techniques for gas separation may be considered more competitive in such cases in which there are high pressure feed gas streams.

6.5 Application of a mathematical model to assess the phase equilibrium data

Experimental phase equilibrium data for clathrate and semi-clathrate hydrate systems have been reported extensively in the literature. The quantities of these reported data and their accuracy seem to be adequate for industrial applications.

In this chapter, the reliability of phase equilibrium data of the systems containing gas hydrates is checked using a statistical method. The Leverage approach was used to detect doubtful data (outlier) and their quality, as well as the applicability domain of the model for prediction in following systems:

- Carbon dioxide, methane, and ethane hydrates dissociation data in the presence of pure water and different types of porous media (mesoporous silica gel, porous glass, and silica gel) (Ilani-Kashkouli et al., 2013b).

- The experimental dissociation data for structure II and H hydrate in the presence of water soluble/insoluble promoters (Ilani-Kashkouli et al., 2013a).

- The experimental data for methane, ethane, propane and carbon dioxide solubility in pure water which is in equilibrium with gas hydrates.

6.5.1   Leverage method

Outlier detection may be important in developing of a predictive mathematical model. Outliers are a group of data that may not be consistent with other data presented in the same dataset. In other words, data which are outliers in each experimental dataset must be detected (Rousseeuw and Leroy, 1987, Goodall, 1993, Eslamimanesh et al., 2012a). The proposed method typically consists of two algorithms which include a graphical and numerical method (Rousseeuw and Leroy, 1987, Goodall, 1993, Eslamimanesh et al., 2012a). The Leverage method uses the values of the residuals (i.e. the deviations of a model results from the experimental data) and a matrix known as the Hat matrix. The Hat matrix includes the experimental data and the represented/predicted values obtained from a correlation (or a model) (Gramatica, 2007). For employing the aforementioned strategy, appropriate suitable mathematical model is required.

For the Hat matrix applied in the Leverage method and the indices are defined as:

$$H = X(X^t X)^{-1} X^t$$

(6.11)

where X is a two-dimensional matrix consisting n chemicals or data (rows) and k parameters of the model (columns) and t stands for the transpose matrix. Diagonal elements of the H matrix are defined as the Hat values in the practicable region of the problem.

For a graphical presentation of the outliers or suspect experimental data, the Williams plot was plotted based on Equation (6.11). This plot demonstrates the correlation of the Hat values and standardized residuals (R), which are defined as the difference between the predicted values and the experimental data.

A warning leverage (H^*) is generally fixed at 3n/p, where n is number of training points and p is the number of model variables plus one. The cut-off value for the standardized residuals (R) is considered as 3 to accept the points that within the ±3 (two horizontal red lines in the figures) standard deviations from the mean. Presence of the greatest part of training and test data points in the range of $0 \le H \le H^*$ and $-3 \le R \le 3$, presents that both model development and its representations/predictions are done in applicability domain. "Good High Leverage" points are located in domain of $H > H^*$ and $-3 \le R \le 3$. These points fit the model well, and make it more stable and precise. "Bad high leverage" points are located in ranges $R < -3$ and $R > 3$ and $H > H^*$. They are outliers of the model. The points are located in domain of $H < H^*$ and $R < -3$ and $R > 3$,

are wrongly predicted but in this case they belong to the model applicability domain. This erroneous prediction could probably be attributed to wrong experimental data rather.

6.5.2   An assessment test for gas hydrate phase equilibrium data in porous

The least squares support vector machine (LSSVM) (Suykens and Vandewalle, 1999, Eslamimanesh et al., 2012a) algorithm has been used to predict the hydrate dissociation pressures in presence of porous media (Mohammadi et al., 2011b). The LSSVM algorithm is given in the Appendix C. The percentage absolute relative deviations (ARD %) of the proposed model are acceptable to be used for the Leverage statistical method.

Experimental hydrate dissociation data for various types of porous media compiled from different literature sources are listed in Table 6.21 (Ilani-Kashkouli et al., 2013b). The H values are calculated through Equation (6.11) and the Williams plots are sketched in Figure 6.22 to Figure 6.27. The warning Leverages (H^*) are fixed at 3n/p for the entire data set. In addition, the recommended cut-off value of 3 are applied.

All experimental data for ethane (C_2H_6) hydrates in silica gel, except for 3 points, have been recognized within the applicability domain of the correlation. The three points are in the "suspect data" region with $R \geq 3$ or $R \leq -3$. These data are also known as bad high leverage points. In the case of methane hydrates in silica gel, mesoporous silica, porous glass and carbon dioxide hydrates in silica gel and porous glass there are no experimental data in the suspected region. Good high Leverage data points which are in the range of $H^* < H$ and $-3 \leq R \leq 3$, are also depicted in figures and tables as well (one point for ethane). Although these data lie outside the applicability domain of the applied model and fit the model well, and make it more stable and precise.

Table 6.21: Experimental hydrate dissociation conditions for various type of porous media.

Hydrate former	Media	Pore diameter (nm)	T range /K	P range /MPa	Ref.
CH_4	Silica gel porous	7	263–276.2	2.64–5.25	(Handa and Stupin, 1992)
CH_4	Silica gel porous	6.8, 14.6, 30.5	275.3–284.53	4.01–10.28	(Seo et al., 2002)
CH_4	Mesoporous silica	9.2, 15.8, 30.6	271.8–287.5	3.69–14.06	(Anderson et al., 2003)
CH_4	Porous glass	10, 30, 50	277.2–283.7	4.8–8.5	(Uchida et al., 1999)
CH_4	Porous glass	9.2, 15.8, 30.6	271.8–287.5	3.69–14.06	(Zhang et al., 2002)

CO_2	Silica gel porous	6.8, 14.6, 30.5	271.8–281.35	1.13–3.918	(Seo et al., 2002)
CO_2	Porous glass	9.2, 15.8, 30.6	270.2–279.8	1.41–3.33	(Anderson et al., 2003)
C_2H_6	Silica gel pores	6, 10, 15	243.15–277.15	0.112–1.504	(Zhang et al., 2002)
C_2H_6	silica gel porous	6.8, 14.6, 30.5, 94.5	271.97–285.24	0.9–2.81	(Seo et al., 2009)
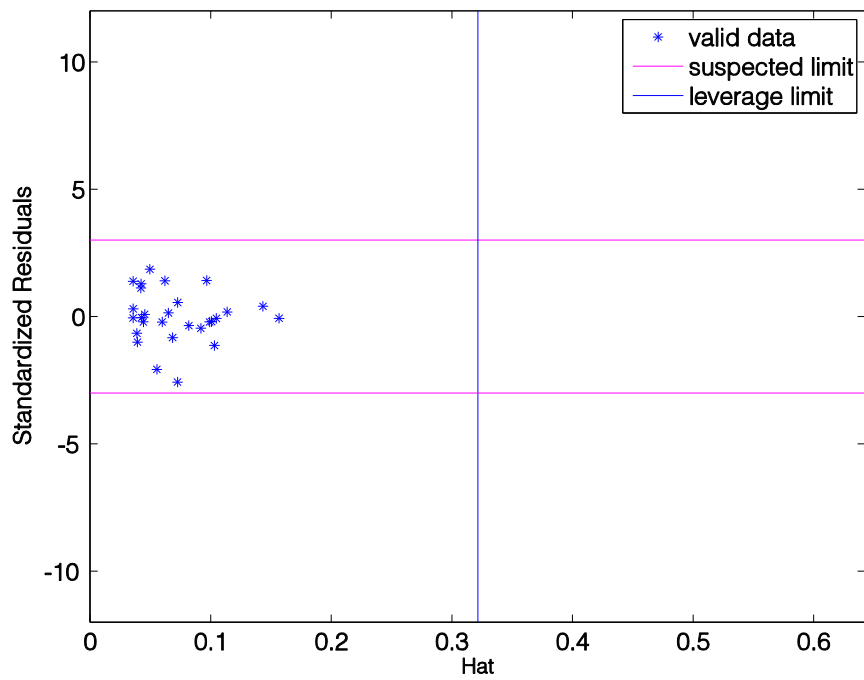
Figure 6.22: Williams Plot for a CH$_4$ gas hydrate system in silica gel. The H* value equals 0.321.
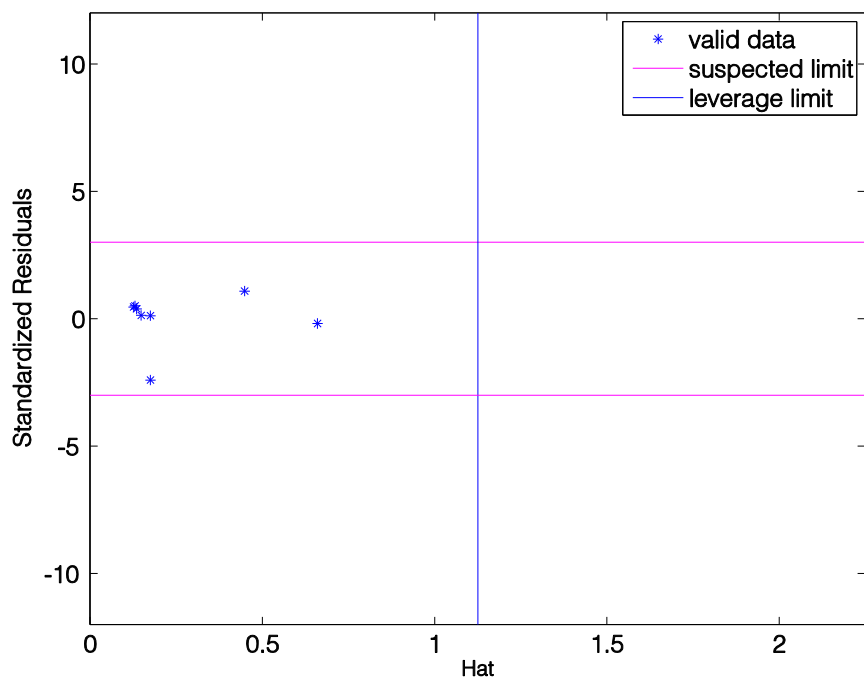
Figure 6.23: Williams Plot for a CH$_4$ gas hydrate system in porous glass. The H* value equals 1.125.
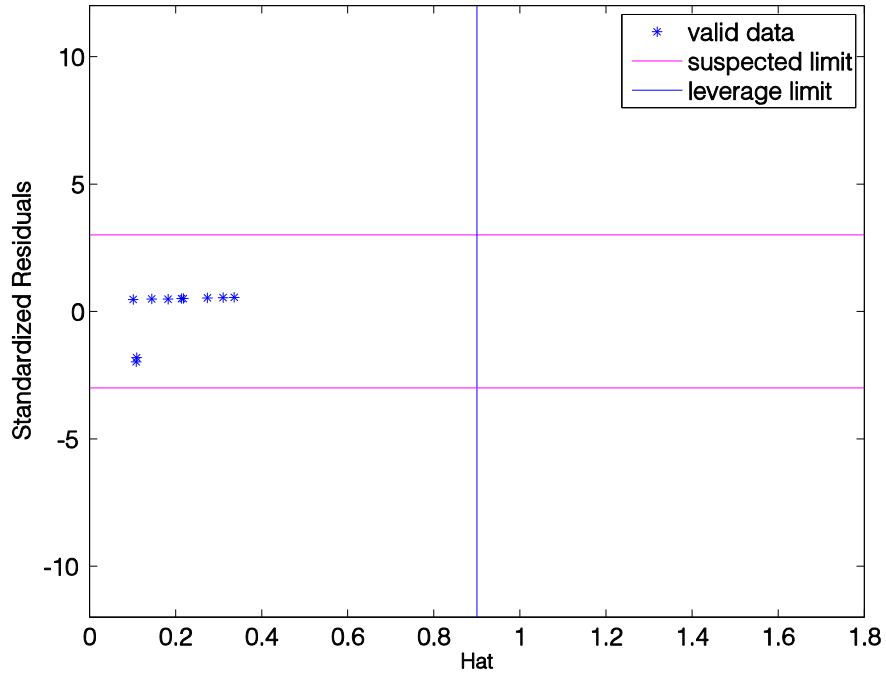
Figure 6.24: Williams Plot for a CH$_4$ gas hydrate system in mesoporous silica. The H* value equals 0.9.
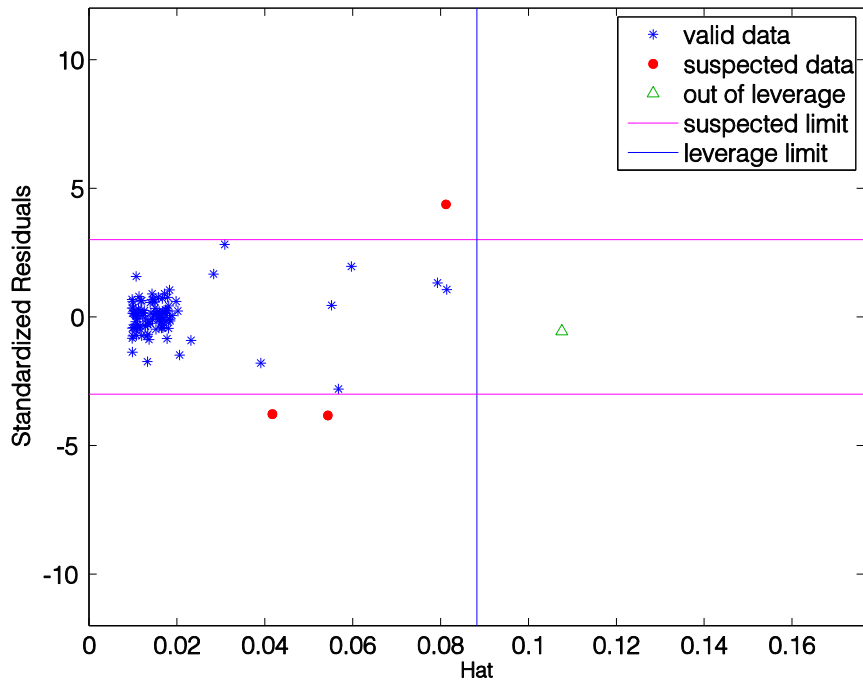
Figure 6.25: Williams Plot for a C$_2$H$_6$ hydrate system in silica gel porous. The H* value equals 0.088.
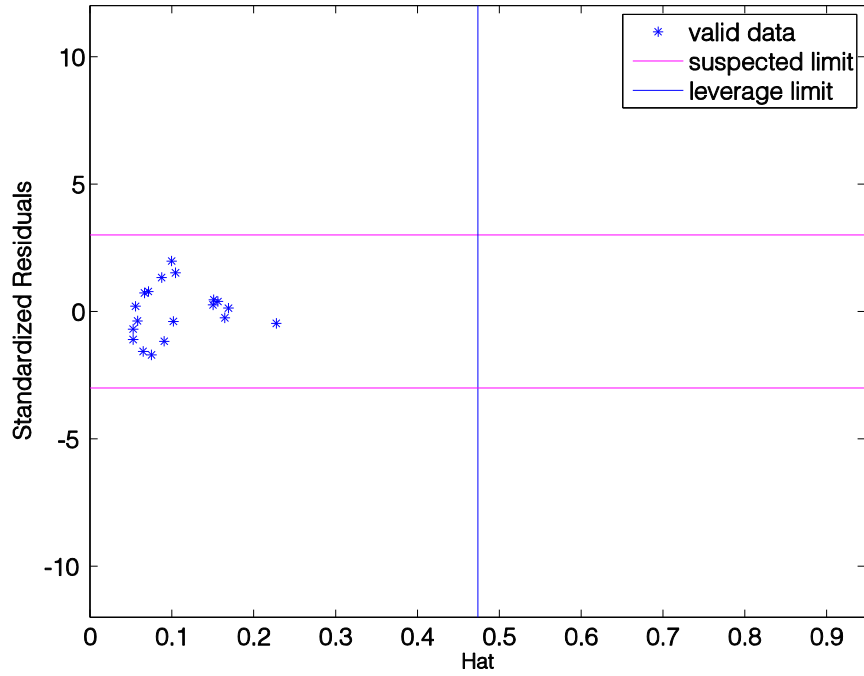
Figure 6.26: Williams Plot for a CO_2 gas hydrate system in silica gel. The H* value equals 0.47.
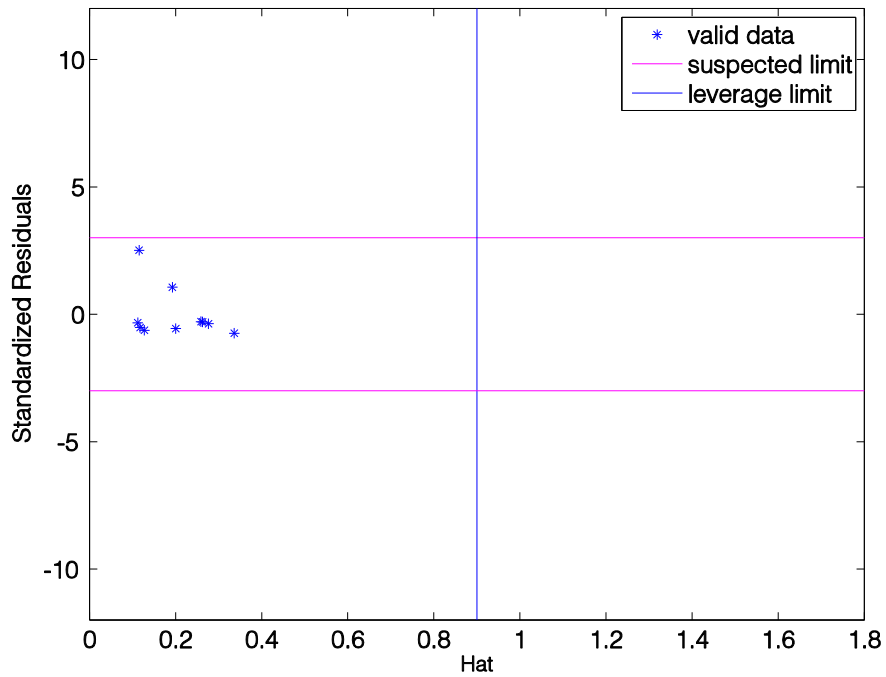
Figure 6.27: Williams Plot for a CO_2 gas hydrate system in porous glass. The H* value equals 0.9.

116

6.5.3 An assessment test for phase equilibrium data of water soluble and insoluble clathrate hydrate formers

LSSVM method has been used for the prediction of dissociation conditions of clathrate hydrates of methane, carbon dioxide, nitrogen, and hydrogen in the presence of water soluble organic promoters (tetrahydrofuran (THF), 1,4-dioxane, and acetone) and twenty-one water insoluble hydrocarbon promoters (Eslamimanesh et al., 2012a).

Available experimental gas hydrate dissociation data in the presence of water soluble and water insoluble promoters in liquid water–hydrate–vapour (L_W–H–V) and liquid water–liquid hydrocarbon–hydrate–vapour (L_W–L_{HC}–H–V) regions, respectively, are tested. Table 6.22 reports the ranges of the experimental data as well as their references.

As explained earlier, the H values and the absolute relative deviation percentage (ARD %) of the represented model results from the experimental hydrate dissociation pressure in the presence of water soluble and insoluble promoters are calculated. The Williams plots for structure H gas hydrate in the presence of water soluble and water insoluble promoters are shown in Figure 6.28 to Figure 6.39 using the LSSVM model. The warning Leverages (H*) have been fixed at 3n/p for all data series and have been presented in Figures. In addition, the recommended cut-off value of three has been applied.

The majority of the data, which is approximately around 98% of the 1014 gas hydrate experimental data points in the presence of water soluble/insoluble promoters are presented in $0 \leq H < H^*$ and $-3 \leq R \leq 3$. As previously mentioned, good high leverage points are gathered in the domains of $H^* < H$ and $-3 \leq R \leq 3$. However, these points may lie outside the applicability domain of the applied model such as the triangles point in Figure 6.31, Figure 6.33 and Figure 6.34. Another group of data points which include bad high leverage points are in the range of $R < -3$ or $3 < R$ (ignoring their H values). These erroneous predictions can be classified as suspect or doubtful data as can be considered in Figure 6.34 and Figure 6.39.

Table 6.22: The range of experimental hydrate dissociation pressure and temperature tested in this study.

System	Equilibrium region	T range / K	P range / MPa
Carbon dioxide+ 1,4 Dioxane	(Lw+H+V)	274.8-282.5	1.08-4.4
Carbon dioxide +Acetone	(Lw+H+V)	269.2-282.8	0.9-4.4
Carbon dioxide +THF	(Lw+H+V)	272.6-291.0	0.2-4.4
Hydrogen +Acetone	(Lw+H+V)	265.6-273.9	10.8-258.9
Hydrogen +THF	(Lw+H+V)	267.20-282.03	2.09-258.9
Methane+1,4 Dioxane	(Lw+H+V)	274.2-326.8	1.1-1000
Methane+ Acetone	(Lw+H+V)	274.2-326.8	1.2-1000
Methane+THF	(Lw+H+V)	274.2-326.8	0.3-1000
Nitrogen+1,4 dioxane	(Lw+H+V)	274.5-309.4	3.701-439.0
Nitrogen +Acetone	(Lw+H+V)	274.5-309.4	19.1-439.0
Nitrogen +THF	(Lw+H+V)	274.5-309.4	2.5-439.0
Methane+ Isopentane	(Lw+L_{HC}+H+V)	274.0-279.0	2.24-4.15
Methane+ Neopentane	(Lw+L_{HC}+H+V)	276.6-292.8	0.4-4.9
Methane+ Neohexane	(Lw+L_{HC}+H+V)	244.8-288.2	0.5-5.2
Methane+2,3 Dimethyl butane	(Lw+L_{HC}+H+V)	275.9-286.4	2.07-8.19
Methane+2,2,3-Trimethylbutane	(Lw+L_{HC}+H+V)	275.6-289.4	1.47-7.55
Methane+2,2-Dimethylpentane	(Lw+L_{HC}+H+V)	274.8-290.0	1.73-7.28
Methane+ Methylcyclopentane	(Lw+L_{HC}+H+V)	275.2-287.8	1.75-11.47
Methane+ Methylcyclohexane	(Lw+L_{HC}+H+V)	251.5-290.4	0.52-11.20
Methane+ cis-1,2-Dimethylcyclohexane	(Lw+L_{HC}+H+V)	274.2-290.0	1.57-11.32
Methane+2,3-Dimethyl-1-butene	(Lw+L_{HC}+H+V)	275.7-280.8	2.53-4.80
Methane+3,3-Dimethyl-1-butene	(Lw+L_{HC}+H+V	276.2-281.4	2.02-3.87
Methane+3,3-Dimethyl-1-butyne	(Lw+L_{HC}+H+V)	275.8-279.6	2.85-4.57
Methane+ Cycloheptene	(Lw+L_{HC}+H+V)	275.1-281.0	2.11-3.81
Methane+ cis-Cyclooctene	(Lw+L_{HC}+H+V)	276.9-281.3	2.08-3.56
Methane+ Adamantane	(Lw+L_{HC}+H+V)	275.1-280.2	1.78-3.00
Methane+ Ethylcyclopentane	(Lw+L_{HC}+H+V)	280.2-287.4	3.59-9.13
Methane+1,1-Dimethylcyclohexane	(Lw+L_{HC}+H+V)	274.7-293.2	1.07-11.53
Methane+cis-1,4-Dimethylcyclohexane	(Lw+L_{HC}+H+V)	274.1-287.9	1.62-9.13
Methane+ Ethylcyclohexane	(Lw+L_{HC}+H+V)	283.6-286.0	6.30-8.90
Methane+ Cycloheptane	(Lw+L_{HC}+H+V)	281.4-290.4	3.29-10.93
Methane+ Cyclooctane	(Lw+L_{HC}+H+V)	274.1-290.4	1.60-11.65

Among the entire data set, one point for hydrate dissociation pressure data of the CO_2 + THF system in the $L_W + V + H$ region, 4 points for $CH_4 + 1$, 4-dioxane hydrate dissociation pressure data in the $L_W + V + H$ region, three points related to CH_4 + acetone hydrate dissociation pressure data in the $L_W + V + H$ region, one point related to CH_4 + THF hydrate dissociation pressure data in $L_W + V + H$ region, one point for $N_2 + 1$,4-dioxane hydrate dissociation pressure data in the $L_W + V + H$ region, and finally 2 points for CH_4 + 2,2-dimethylpentane hydrate dissociation pressure data in $L_W + L_{HC} + V + H$ region are presented as suspect or doubtful data. These twelve suspect or doubtful data are depicted as red circular points in Figure 6.30, Figure 6.33, Figure 6.34, Figure 6.35, Figure 6.36 and Figure 6.39.There are two data points in the ranges $H^* < H$ and $R < -3$ or $3 < R$: one point for CH_4 + acetone hydrate dissociation pressure data in $L_W + V + H$ region and another point for $CH_4 + 2$, 2-dimethylpentane (insoluble promoter) hydrate dissociation pressure data in $L_W + L_{HC} + V + H$ region. The good high leverage points (green triangles) are accumulated in the domains of in the ranges $H^* < H$ and $-3 \leq R \leq 3$. These points may be declared to be outside of applicability domain of the applied correlation.
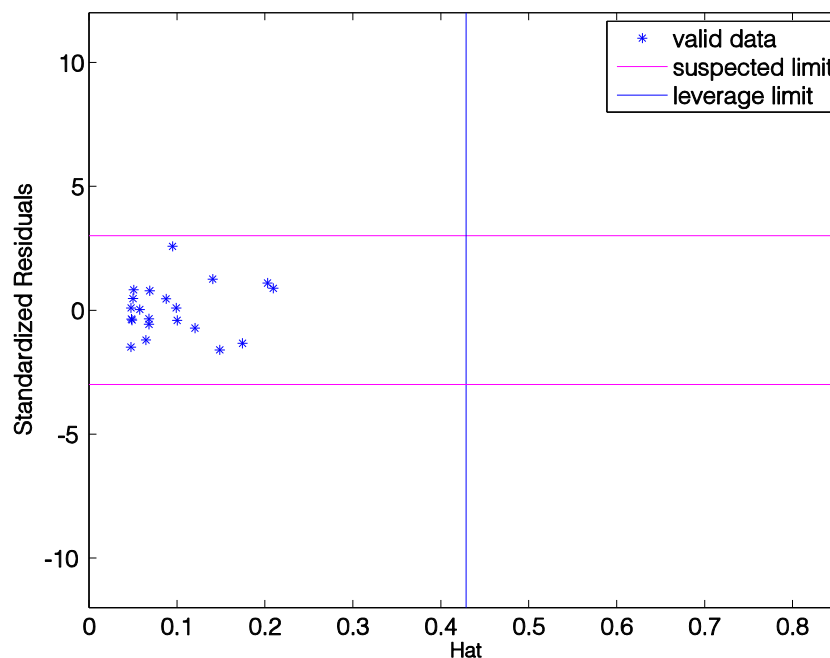
Figure 6.28: Williams plot for a CO_2 structure H hydrate in the presence of 1, 4 dioxane in the Lw–H–V region (Mohammadi et al., 2005, Fan et al., 2000, Ohgaki et al., 1993, Ng and Robinson, 1985a, Seo et al., 2008b). The H^* value is 0.428.
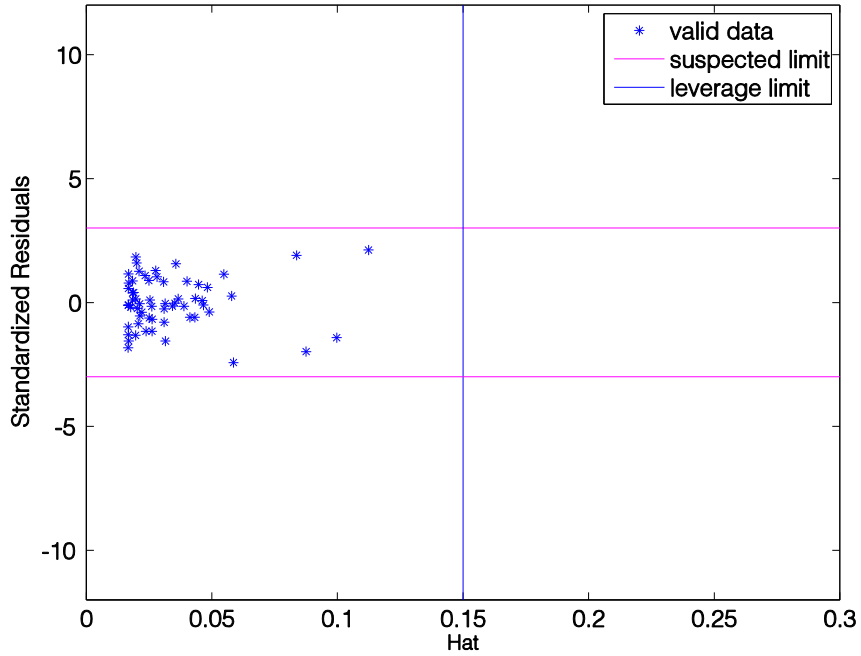
Figure 6.29: Williams plot for a CO_2 structure H hydrate in the presence of Acetone in the Lw–H–V region (Mohammadi et al., 2005, Fan et al., 2000, Ohgaki et al., 1993, Ng and Robinson, 1985a, Seo et al., 2008b). The H^* value is 0.15.
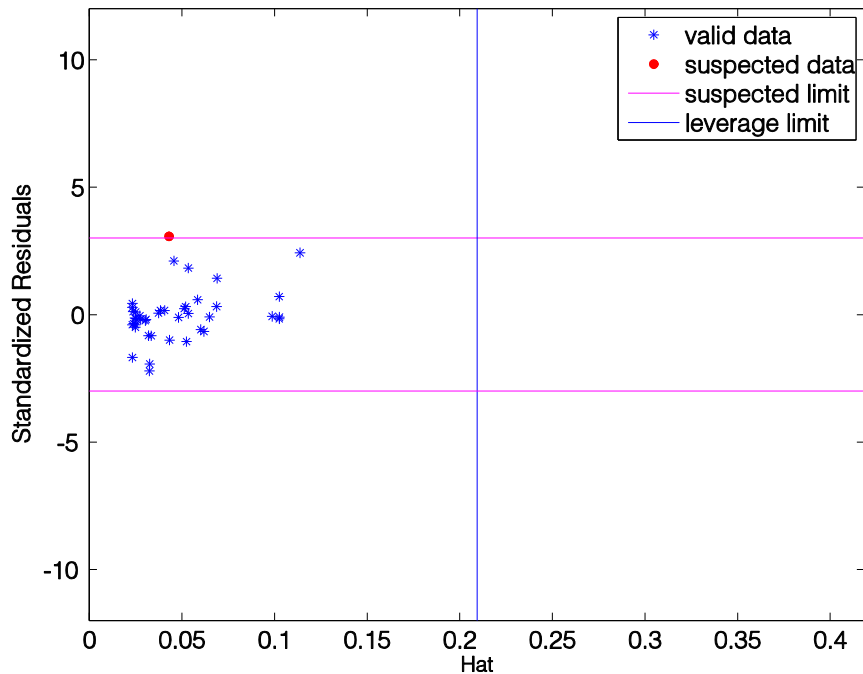
Figure 6.30: Williams plot for a CO_2 structure H hydrate in the presence of THF in the L_w–H–V region (Mohammadi et al., 2005, Fan et al., 2000, Ohgaki et al., 1993, Ng and Robinson, 1985a, Seo et al., 2008b). The H^* value is 0.209.
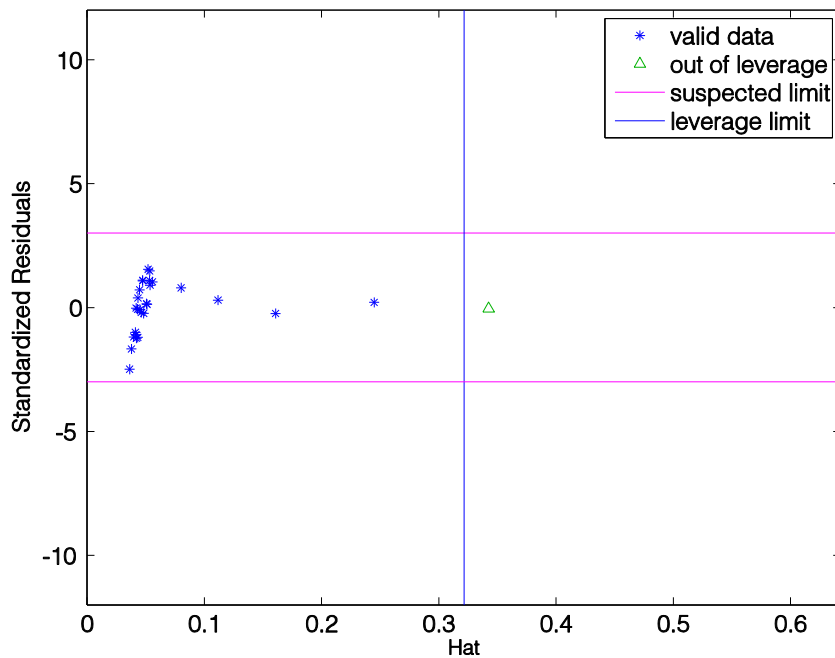
Figure 6.31: Williams plot for a H$_2$ structure H hydrate in the presence of Acetone in the L$_w$–H–V region (Dyadin et al., 1999b, Du et al., 2010). The H* value is 0.321.
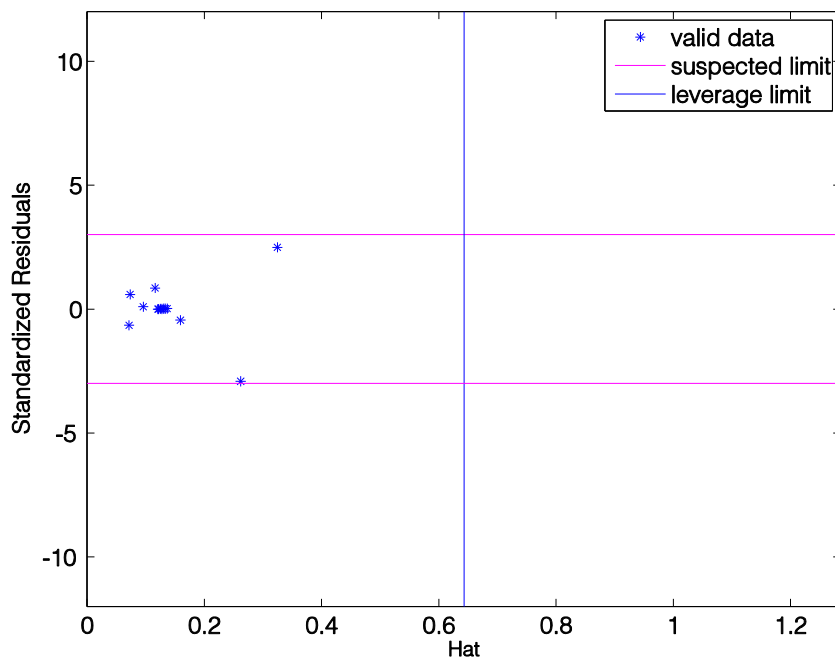
Figure 6.32: Williams plot for a H$_2$ structure H hydrate in the presence of THF in the Lw–H–V region (Dyadin et al., 1999b, Komatsu et al., 2010). The H* value is 0.643.
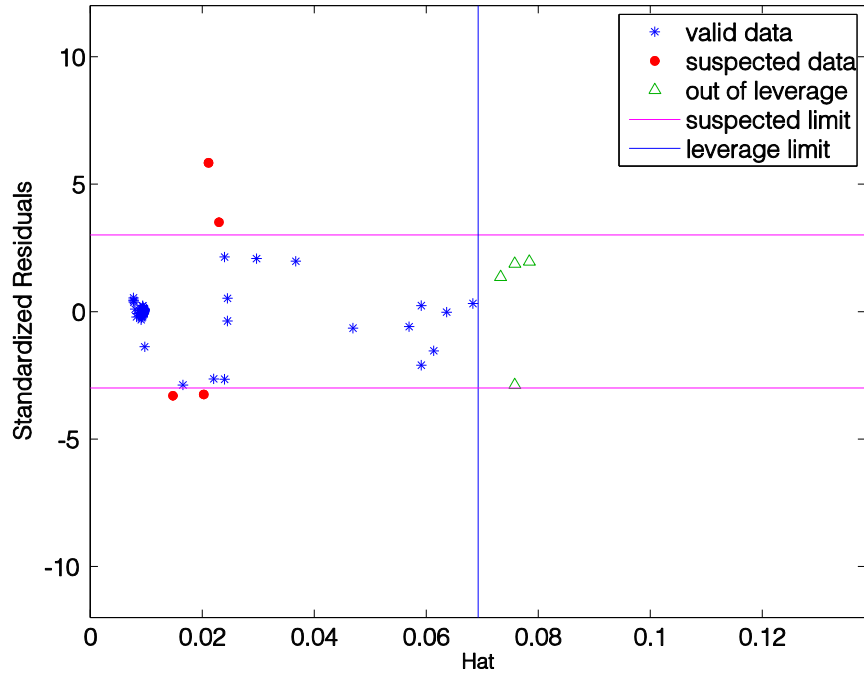
Figure 6.33: Williams plot for a CH₄ structure H hydrate in the presence of 1, 4 dioxane in the L$_w$–H–V region (Nakamura et al., Mohammadi et al., 2005, Dyadin and Aladko, 1996, Seo et al., 2001a, Jager et al., 1999). The H* value is 0.069.
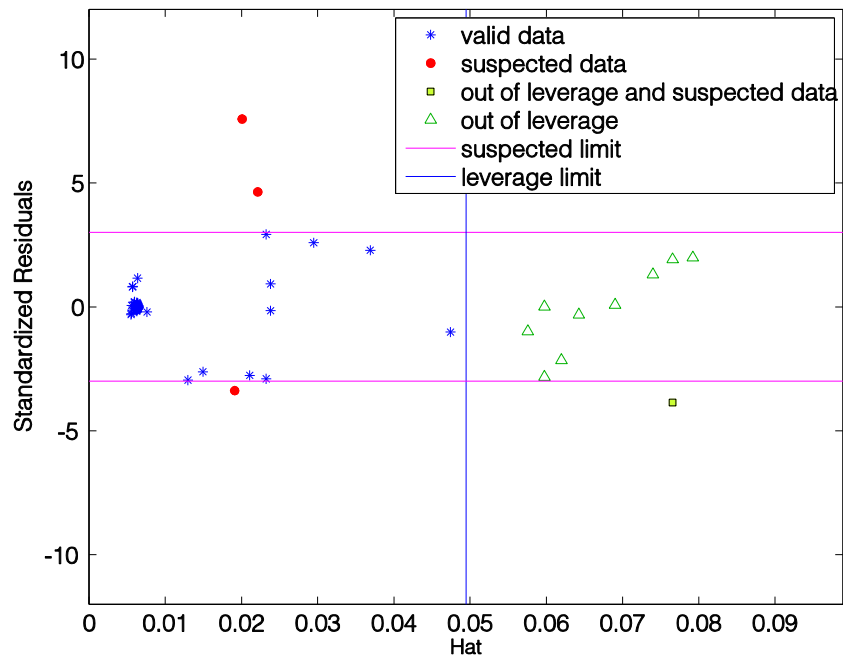
Figure 6.34: Williams plot for a CH₄ structure H hydrate in the presence of Acetone in the L$_w$–H–V region (Mohammadi et al., 2005, Nakamura et al., Dyadin and Aladko, 1996, Mainusch et al., 1997, Seo et al., 2001a, Saito et al., 1996b, Ng and Robinson, 1994, Du et al., 2010). The H* value is 0.049.
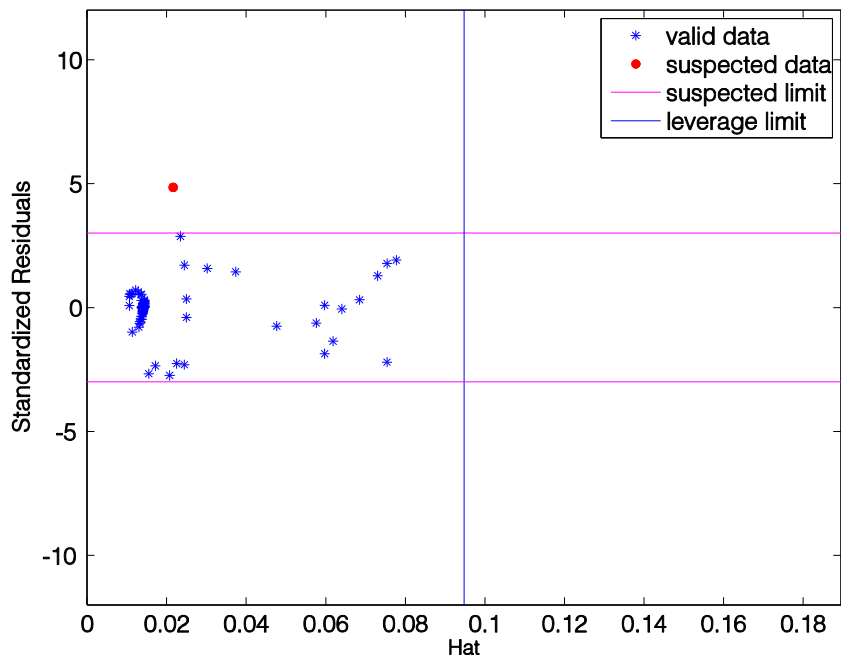
Figure 6.35: Williams plot for a CH₄ structure H hydrate in the presence of THF in the Lw–H–V region (Mohammadi et al., 2005, Nakamura et al., Dyadin and Aladko, 1996, Seo et al., 2001a, Saito et al., 1996b, de Deugd et al., 2001). The H* value is 0.094.
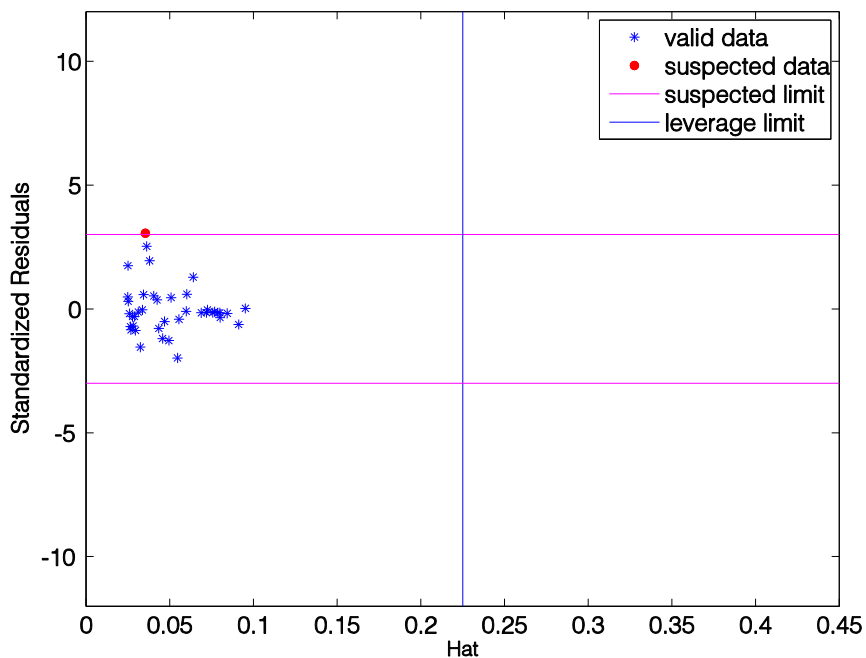
Figure 6.36: Williams plot for a N₂ structure H hydrate in the presence of 1, 4 Dioxane in the Lw–H–V region (Mohammadi et al., 2003, Sugahara et al., 2002, Seo et al., 2001a). The H* value is 0.225.
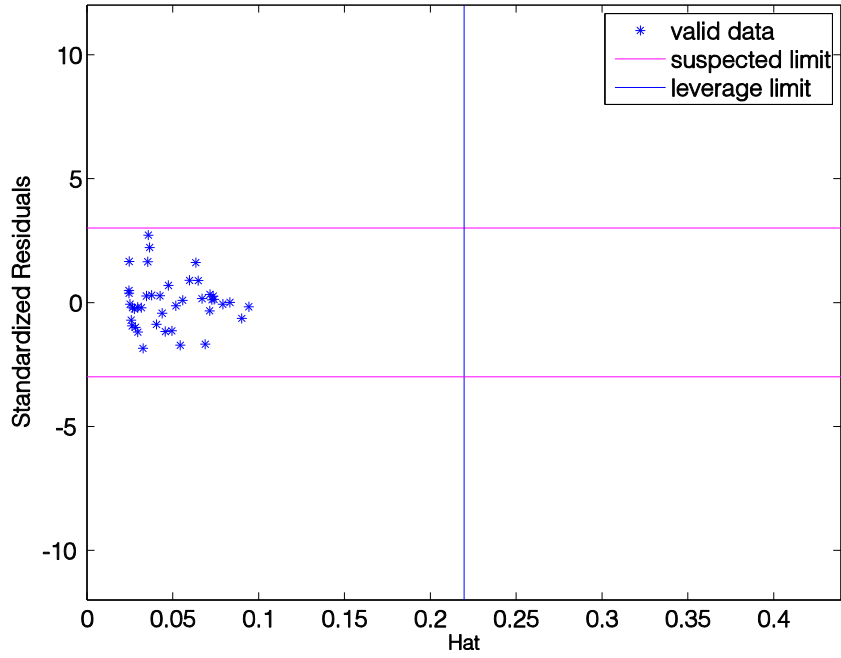
Figure 6.37: Williams plot (Mohammadi et al., 2003, Sugahara et al., 2002, Seo et al., 2001a) for the N_2 structure H hydrate in the presence of Acetone in the L_w–H–V region. The H^* value is 0.219.
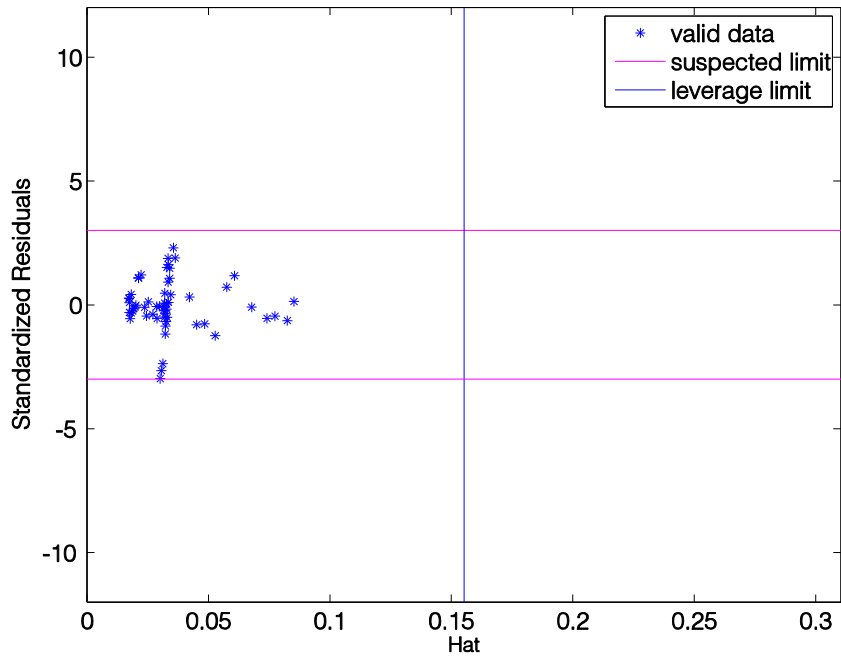
Figure 6.38: Williams plot for a N_2 structure H hydrate in the presence of THF in the L_w–H–V region (Mohammadi et al., 2003, Sugahara et al., 2002, Seo et al., 2001a). The H^* value is 0.155.
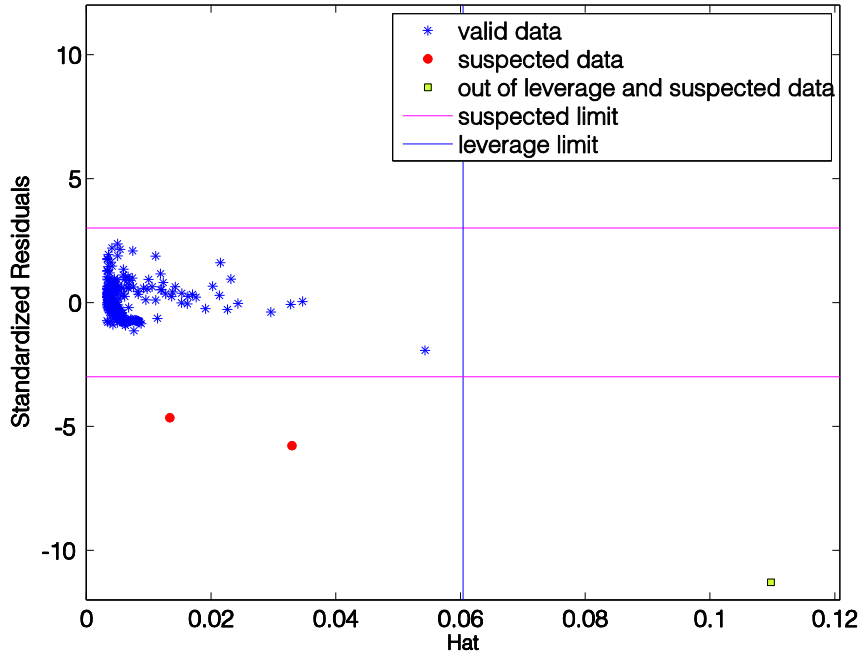
Figure 6.39: Williams plot for a CH$_4$ structure H hydrate in the presence of insoluble promoters in the L$_W$–L$_{HC}$-H–V region (Tohidi et al., 1997c, Nakamura et al., 2003, Danesh et al., 1994, Hütz and Englezos, 1995, Lederhos et al., 1992, Makino et al., 2004, Makogon et al., 1996, Mehta, 1996, Mehta and Sloan, 1994, Mehta and Sloan Jr, 1994, Mooijer-Van Den Heuvel et al., 2000, Ohmura et al., 2005, Thomas and Behar, 1995, Tohidi et al., 1996). The H* value is 0.064.

6.5.4 An assessment test for evaluation of experimental data for gas solubility in liquid water in equilibrium with gas hydrates

The Leverage statistical approach was used to assess the quality of the experimental solubility data of methane, ethane, propane and carbon dioxide in water in the equilibrium with gas hydrates (Mohammadi and Richon, 2009b). A thermodynamic model was used to predict the L$_w$-H equilibrium phase (Mohammadi and Richon, 2009b). The range of conditions of the experimental data in the collated dataset, as well as the sources references are reported in Table 6.23.

Table 6.23: Range of conditions for hydrate dissociation temperature and pressure experimental data.

Gas	T range (K)	P range (MPa)	ND	Ref
Methane	274.15-281.70	3.50-143.62	38	(Yang, 2000, Servio and Englezos, 2001, Kim et al., 2003)
Ethane	277.30-278.50	10.10-151	6	(Yang, 2000, Servio and Englezos, 2001, Kim et al., 2003)
Propane	274.16-276.16	0.25-0.36	6	(Gaudette and Servio, 2007)
Carbon dioxide	273.95-282.95	2-14.20	44	(Servio and Englezos, 2001, Yang et al., 2000)

Figure 6.40 to Figure 6.43 show the Williams plots for assessment of L_w- H equilibrium conditions for gas + water systems using the applied model. In these figures, H values are presented applying Equation (6.11). In addition, the warning Leverages (H*) values are calculated and shown in Figure 6.40 to Figure 6.43 as Leverage limits (blue or vertical line). As can be seen the recommended cut-off value of three (Eslamimanesh et al., 2012b, Mohammadi et al., 2012b, Mohammadi et al., 2012c) and the suspected data limits (red lines or horizontal lines) are presented in these plots.

As observed in Figure 6.40 to Figure 6.43, there is no experimental data in the H* < H and -3 $\leq$ R $\leq$ 3 region. As mentioned before, this region is related to the good high leverage points which are outside the applicability domain of the predicted model.

As seen in Figure 6.40, all of the experimental data for methane solubility in water in equilibrium with methane hydrate, lie in the acceptable range except one data point which is shown as a red point in Figure 6.40. This data point is considered as a suspect/doubtful or bad high leverage data point which is lies in R$\leq$ -3 and R $\geq$ 3 range regardless of corresponding H* value.

Figure 6.41 and Figure 6.42 show that all of the experimental data for ethane and propane solubility in water in equilibrium with gas hydrate are presented in an acceptable range: (0 $\leq$ H $\leq$ H* and -3 $\leq$ R $\leq$ 3) which further confirms the wide applicability of applied model and the accuracy of these experimental data.

Finally, as it can be observed in Figure 6.43, all of the experimental data for carbon dioxide solubility in L_w-H equilibrium conditions fall within the acceptable range, except two suspected/doubtful data points which are presented as the red points in Figure 6.43. These experimental data points are located in R $\leq$ -3 and R $\geq$ 3 ranges, regardless of the corresponding H* values. The possible reasons for these doubtful experimental data is probably due to

inaccuracies in experimental measurement methods and/or incorrect calibration of the instruments used in the experimental measurements.
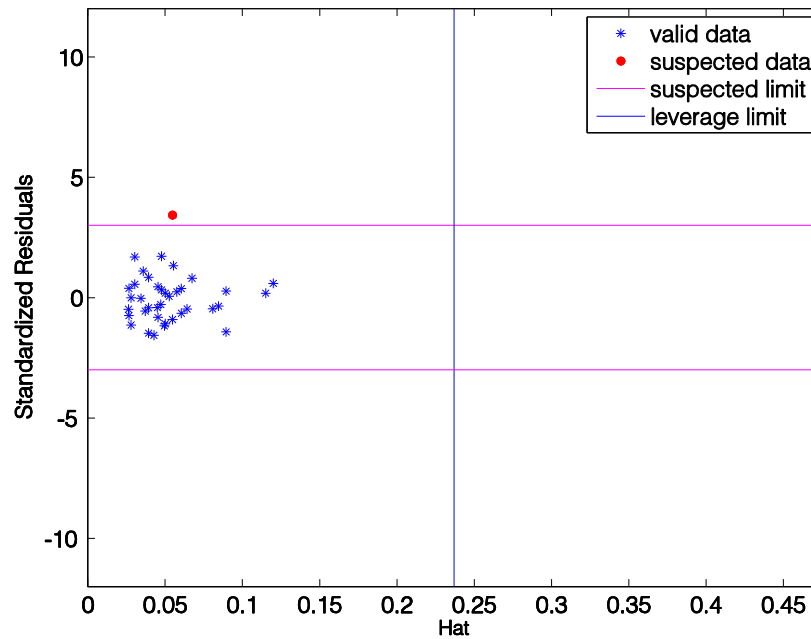
Figure 6.40: Williams plot for methane in pure water being in equilibrium with gas hydrate (liquid water-gas hydrate (L-H) equilibrium). The H* value is 0.237.
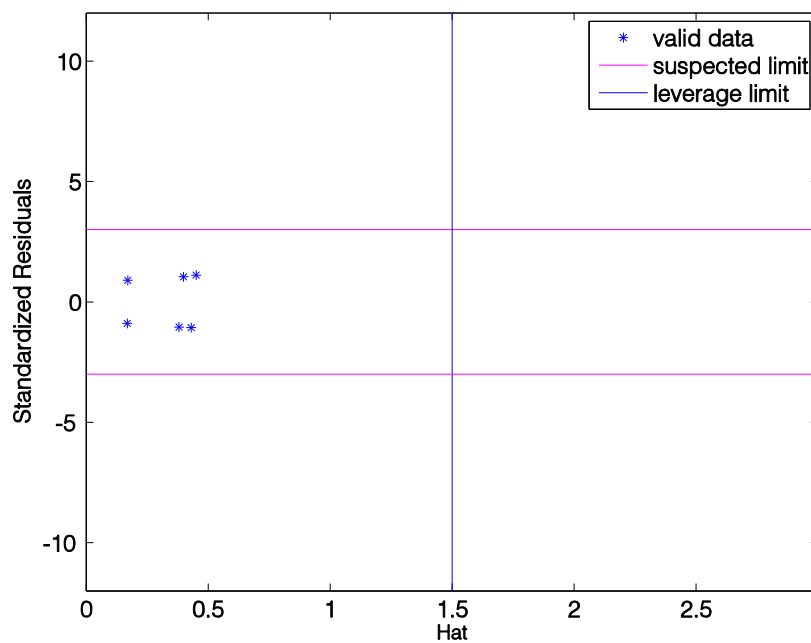
Figure 6.41: Williams plot for ethane in pure water being in equilibrium with gas hydrate (liquid water-gas hydrate (Lw-H) equilibrium). The H* value is 1.5.
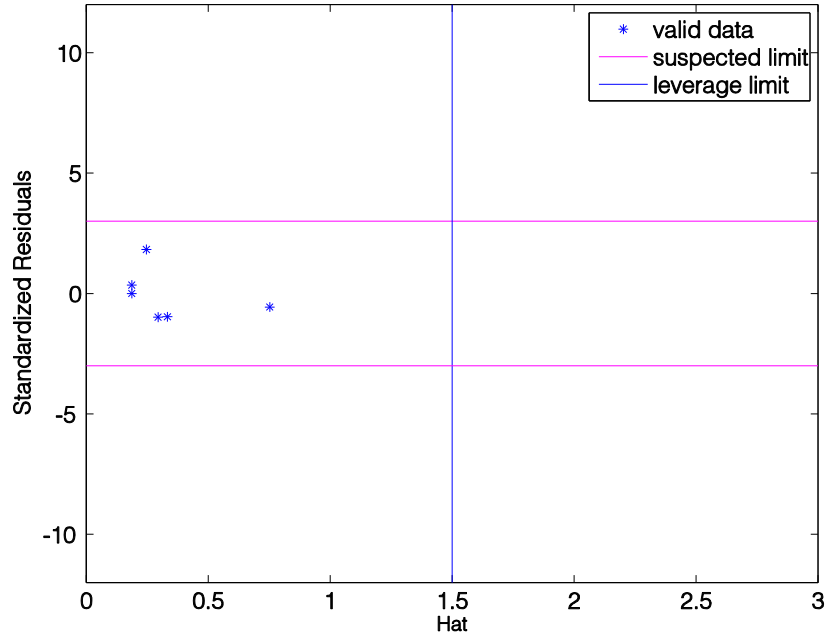
Figure 6.42: Williams plot for propane in pure water being in equilibrium with gas hydrate (liquid water-gas hydrate (Lw-H) equilibrium). The H* value is 1.5.
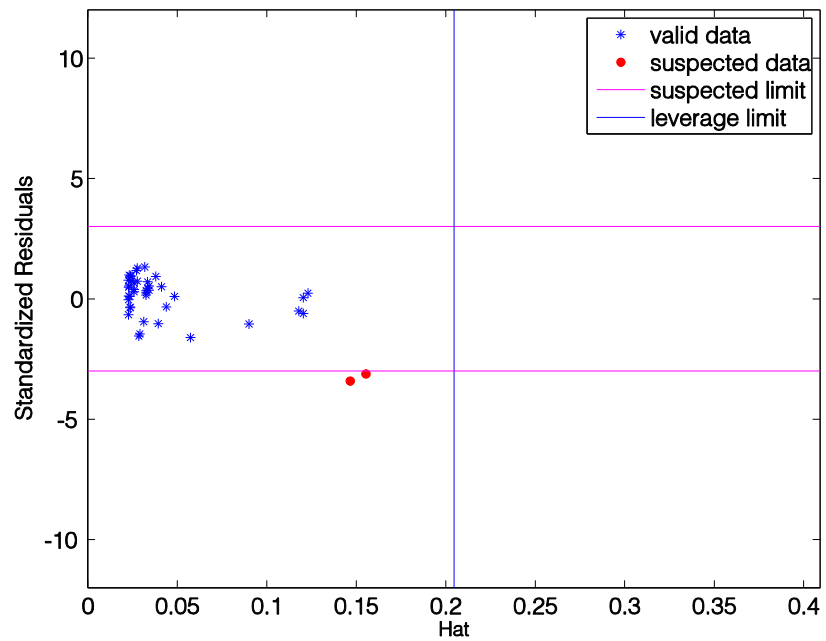
Figure 6.43: Williams plot carbon dioxide in pure water being in equilibrium with gas hydrate (liquid water-gas hydrate (Lw-H) equilibrium). The H* value is 0.204.

7 Conclusions

The main aim of this work was performed on thermodynamic studies on phase equilibria of clathrate/semi-clathrate hydrates with the final goal of their potential use in CO_2 capture and storage process.

An isochoric pressure search method was used to measure the phase equilibrium data because: i) no visual observation is required for determination of hydrate equilibrium data and ii) also no volume changes are required.

It is concluded that the presence of TBPB, $TBANO_3$ and TBAF can influence the hydrate dissociation condition. They have been proposed as hydrate promoters which can reduce the equilibrium pressure and increase the equilibrium temperature (below stoichiometric ratios of the clathrate hydrates of TBPB/$TBANO_3$ and TBAF + water).

The presence of TBPB causes the phase equilibrium conditions shift to the lower pressure and higher temperature area which represented as the stabilized area. By increasing the mass fraction of the TBPB solution (from w = 0.05 to w = 0.371), the phase equilibrium temperature increases and the equilibrium pressure decreases. While, with the increases of mass fraction of the salt up to a mass fraction of 0.371, the stability of hydrate is lessened. It can be concluded that the maximum promotion effect of TBPB is in mass fraction of 0.371.

TBAF has the same effect on semi-clathrate hydrate. By increasing the mass fraction of the TBAF from (0.02 to 0.31) the promotion effect of TBAF increases but when the mass fraction of TBAF goes up to 0.31 the equilibrium temperature and promotion effect of the TBAF decreases. It can be concluded that the maximum promotion effect of TBAF is in mass fraction of 0.31.

The result for CO_2 + $TBANO_3$, CH_4 + $TBANO_3$, N_2 + $TBANO_3$ and Ar + $TBANO_3$ semi-clathrate hydrates showed that $TBANO_3$ has a promotion effect on the N_2 and Ar semi-clathrate hydrates but in CO_2 and CH_4 semi-clathrate hydrates, $TBANO_3$ shows both promotion and inhibition effect. i.e in the CH_4 + $TBANO_3$ system, $TBANO_3$ at the mass fraction of 0.394 acts as promoter at the pressure lower than 10 MPa because $TBANO_3$ increases the equilibrium temperature and decreases the equilibrium pressure while it acts like an inhibitor at the pressure higher than 10 MPa because it decreases the equilibrium temperature.

It is found from experimental results that a small increase in the temperature causes a large increase in the hydrate equilibrium pressure. This fact shows that hydrate dissociation measurements must be done very carefully to avoid the generation of incorrect experimental data and high experimental errors during the measurements. Therefore, the dissociation process was performed at a slow heating rate (step-change of 0.1 K per hour) and an efficient interval time (about 4-5 h) at each temperature step.

The measured data may provide valuable information on the practical applications for CO_2 capture processes from flue gas and fuel gas streams.

A thermodynamic model was applied to calculate/predict the dissociation conditions of semi-clathrate hydrate of CO_2/CH_4/N_2/Ar in the presence of TBPB/TBANO$_3$/TBAF. There is an acceptable agreement between the predicted data and the experimental dissociation conditions for all the studied systems except for N_2 + TBPB/TBANO$_3$ aqueous solutions at higher pressures. The results showed that the prediction capability of model for semi-clathrate hydrates decreases at high pressure. By applying the aforementioned model, the promotion and inhibition effects of TBPB/TBANO$_3$/TBAF can be predicted. The model depicted the promotion and inhibition effect of TBANO$_3$ with very good accuracy.

The developed model cannot be used for prediction of the S-L equilibria of the salts + water system and in the wide ranges of temperature-pressure-composition of the salts in aqueous solution. Moreover, the model is not applicable for prediction of structural changes of the semi-clathrate.

The experimental data may have noticeable uncertainties due to the different source of errors during measurements. For this reason a statistical method for identification of the doubtful data was applied to discuss the quality of the experimental phase equilibrium data for the systems containing clathrate hydrates. This method was used to detect the outliers and to check the data reliability for the experimental dissociation data. The result showed that there are few data points from the total investigated hydrate dissociation data are specified as "suspect" data and known as outliers. This method can be used for checking the quality of the data points before developing thermodynamic models to predict the phase equilibrium of clathrate hydrates

8   Recommendations

- The phase equilibrium data available for gas mixtures containing CO_2 in the presence of ionic liquids are still limited. The isochoric pressure search method can be used to measure dissociation condition of these semi-clathrate hydrates in different concentrations. In addition, the combination of TPBP and $TBANO_3$ has not been applied for semi-clathrate hydrate formation. The information from phase equilibria data of these systems would be beneficial for the development of a novel CO_2 capture technology.

- Phase behaviour of semi-clathrate hydrates containing other mixed promoters including $TBANO_3$ + TBAB, $TBANO_3$+ TBAC, TBPB + TBAC, etc. can attract much attention.

- Measurements of the dissociation conditions of gas mixture such as (CO_2 + CH_4), (CO_2 + H_2) and (CO_2 + Ar) gas mixtures in the presence of TBPB and $TBANO_3$ would be useful for CO_2 capture.

- One of the important obstacle in hydrate-based technology for CO_2 capture is the slow formation rate of hydrates. To overcome this issue, the mixture of kinetic promoters such as THF, SDS and thermodynamic promoters such as TBPB and $TBANO_3$ can be used. Furthermore, kinetics of formation and dissociation of hydrate in the aforementioned systems can be carried out.

- In parallel with experimental studies, thermodynamic modeling can be developed to represent/predict the phase equilibria of semi-clathrate hydrates of mixed hydrate formers and mixed hydrate promoters.

- Various experimental efforts using RAMAN spectroscopy, NMR spectroscopy, X-ray diffraction, crystallography, calorimetry etc. can be undertaken at laboratory scale for a better understanding of the phase behavior of hydrates. These methods can provide important information about the hydration number, composition of hydrates, structure identification, the relative occupancy of molecules in each cage, identification of metastable phases, and the kinetics of formation of various structures.

- One of the main challenges of CCS technology is total cost of the process. The first CCS step includes the capture process in which both the capital and operating costs vary significantly with the configurations based on the facilities. Economic studies of a real

industrial gas separation process through semi-clathrate hydrate formation technology should be undertaken for this aim.

References

A. HACHIKUBO, A. M., K. HYAKUTAKE, K. ABE, H. SHOJI 2002. *Fourth International Conference on Gas Hydrates.* Japan.

ADANEZ, J., ABAD, A., GARCIA-LABIANO, F., GAYAN, P. & DE DIEGO, L. F. 2012. Progress in Chemical-Looping Combustion and Reforming technologies. *Progress in Energy and Combustion Science,* 38**,** 215-282.

ADEYEMO, A., KUMAR, R., LINGA, P., RIPMEESTER, J. & ENGLEZOS, P. 2010. Capture of carbon dioxide from flue or fuel gas mixtures by clathrate crystallization in a silica gel column. *International Journal of Greenhouse Gas Control,* 4**,** 478-485.

ADISASMITO, S., FRANK, R. J. & SLOAN, E. D. 1991. Hydrates of carbon dioxide and methane mixtures. *Journal of Chemical and Engineering Data,* 36**,** 68-71.

ALADKO, L. S., DYADIN, Y. A., RODIONOVA, T. V. & TEREKHOVA, I. S. 2002. Clathrate Hydrates of Tetrabutylammonium and Tetraisoamylammonium Halides. *Journal of Structural Chemistry,* 43**,** 990-994.

ANDERSON, R., CHAPOY, A. & TOHIDI, B. 2007. Phase Relations and Binary Clathrate Hydrate Formation in the System H2−THF−H2O. *Langmuir,* 23**,** 3440-3444.

ANDERSON, R., LLAMEDO, M., TOHIDI, B. & BURGASS, R. W. 2003. Experimental Measurement of Methane and Carbon Dioxide Clathrate Hydrate Equilibria in Mesoporous Silica. *The Journal of Physical Chemistry B,* 107**,** 3507-3514.

ANDO, N., KODAMA, T., KONDO, W. & MORI, Y. H. 2012. Clathrate Hydrate Formation from a Methane + Ethane + Propane Mixture in an Unstirred Surfactant-Containing System. *Energy & Fuels,* 26**,** 1798-1804.

ARJANG, S., MANTEGHIAN, M. & MOHAMMADI, A. 2013. Effect of synthesized silver nanoparticles in promoting methane hydrate formation at 4.7 MPa and 5.7 MPa. *Chemical Engineering Research and Design,* 91**,** 1050-1054.

ARJMANDI, M., CHAPOY, A. & TOHIDI, B. 2007. Equilibrium Data of Hydrogen, Methane, Nitrogen, Carbon Dioxide, and Natural Gas in Semi-Clathrate Hydrates of Tetrabutyl Ammonium Bromide. *Journal of Chemical & Engineering Data,* 52**,** 2153-2158.

BABU, P., KUMAR, R. & LINGA, P. 2013a. Medium pressure hydrate based gas separation (HBGS) process for pre-combustion capture of carbon dioxide employing a novel fixed bed reactor. *International Journal of Greenhouse Gas Control,* 17**,** 206-214.

BABU, P., KUMAR, R. & LINGA, P. 2013b. Pre-combustion capture of carbon dioxide in a fixed bed reactor using the clathrate hydrate process. *Energy,* 50**,** 364-373.

BAHADORI, A. & VUTHALURU, H. B. 2009. A novel correlation for estimation of hydrate forming condition of natural gases. *Journal of Natural Gas Chemistry,* 18**,** 453-457.

BAKER, R. W. 2002. Future Directions of Membrane Gas Separation Technology. *Industrial & Engineering Chemistry Research,* 41**,** 1393-1411.

BALCZEWSKI, J. T. 2008. Apparatus for continuous production of hydrates. Google Patents.

BALCZEWSKI, J. T. 2010. Process for continuous production of hydrates. Google Patents.

BALDWIN, B. A., STEVENS, J., HOWARD, J. J., GRAUE, A., KVAMME, B., ASPENES, E., ERSLAND, G., HUSEBØ, J. & ZORNES, D. R. 2009. Using magnetic resonance imaging to monitor CH4 hydrate formation and spontaneous conversion of CH4 hydrate to CO2 hydrate in porous media. *Magnetic Resonance Imaging,* 27**,** 720-726.

BELANDRIA, V., ESLAMIMANESH, A., MOHAMMADI, A. H. & RICHON, D. 2011a. Gas Hydrate Formation in Carbon Dioxide + Nitrogen + Water System: Compositional

Analysis of Equilibrium Phases. *Industrial & Engineering Chemistry Research,* 50**,** 4722-4730.

BELANDRIA, V., ESLAMIMANESH, A., MOHAMMADI, A. H. & RICHON, D. 2011b. Study of Gas Hydrate Formation in the Carbon Dioxide + Hydrogen + Water Systems: Compositional Analysis of the Gas Phase. *Industrial & Engineering Chemistry Research,* 50**,** 6455-6459.

BELANDRIA, V., ESLAMIMANESH, A., MOHAMMADI, A. H., THÉVENEAU, P., LEGENDRE, H. & RICHON, D. 2011c. Compositional Analysis and Hydrate Dissociation Conditions Measurements for Carbon Dioxide + Methane + Water System. *Industrial & Engineering Chemistry Research,* 50**,** 5783-5794.

BELANDRIA, V., MOHAMMADI, A. H., ESLAMIMANESH, A., RICHON, D., SÁNCHEZ-MORA, M. F. & GALICIA-LUNA, L. A. 2012a. Phase equilibrium measurements for semi-clathrate hydrates of the (CO2+N2+tetra-n-butylammonium bromide) aqueous solution systems: Part 2. *Fluid Phase Equilibria,* 322–323**,** 105-112.

BELANDRIA, V., MOHAMMADI, A. H. & RICHON, D. 2010. Phase equilibria of clathrate hydrates of methane + carbon dioxide: New experimental data and predictions. *Fluid Phase Equilibria,* 296**,** 60-65.

BELANDRIA, V., MOHAMMADI, A. H. & RICHON, D. 2012b. Compositional analysis of the gas phase for the CO2+N2+tetra-n-butylammonium bromide aqueous solution systems under hydrate stability conditions. *Chemical Engineering Science,* 84**,** 40-47.

BELTRÁN, J. G. & SERVIO, P. 2010. Morphological Investigations of Methane−Hydrate Films Formed on a Glass Surface. *Crystal Growth & Design,* 10**,** 4339-4347.

BERMEJO, M. D., KOTLEWSKA, A. J., FLORUSSE, L. J., COCERO, M. J., VAN RANTWIJK, F. & PETERS, C. J. 2008. Influence of the enzyme concentration on the phase behaviour for developing a homogeneous enzymatic reaction in ionic liquid-CO2 media. *Green Chemistry,* 10**,** 1049-1054.

BERNARDO, P., DRIOLI, E. & GOLEMME, G. 2009. Membrane Gas Separation: A Review/State of the Art. *Industrial & Engineering Chemistry Research,* 48**,** 4638-4663.

BERSTAD, D., ANANTHARAMAN, R. & NEKSÅ, P. Low-temperature CO2 capture technologies – Applications and potential. *International Journal of Refrigeration*.

BISHNOI, P. R. & NATARAJAN, V. 1996. Formation and decomposition of gas hydrates. *Fluid Phase Equilibria,* 117**,** 168-177.

BISHNOI, P. R., NATARAJAN, V. & KALOGERAKIS, N. 1994. A Unified Description of the Kinetics of Hydrate Nucleation, Growth, and Decompositiona. *Annals of the New York Academy of Sciences,* 715**,** 311-322.

BRUNETTI, A., SCURA, F., BARBIERI, G. & DRIOLI, E. 2010. Membrane technologies for CO2 separation. *Journal of Membrane Science,* 359**,** 115-125.

BRUUSGAARD, H., BELTRÁN, J. G. & SERVIO, P. 2010. Solubility measurements for the CH4 + CO2 + H2O system under hydrate–liquid–vapor equilibrium. *Fluid Phase Equilibria,* 296**,** 106-109.

BRUUSGAARD, H., BELTRÁN, J. G. & SERVIO, P. 2008. Vapor−Liquid Water−Hydrate Equilibrium Data for the System N2 + CO2 + H2O. *Journal of Chemical & Engineering Data,* 53**,** 2594-2597.

BUFFETT, B. A. & ZATSEPINA, O. Y. 2000. Formation of gas hydrate from dissolved gas in natural porous media. *Marine Geology,* 164**,** 69-77.

CARROLL, J. 2009a. *Natural Gas Hydrates A Guide for Engineers*, Elsevier.

CARROLL, J. J. 2009b. *Natural Gas Hydrates : A Guide for Engineers*, Elsevier.

CARSON, D. B. & KATZ, D. L. 1942. Natural gas hydrates. *Transactions of the American Institute of Mining and Metallurgical Engineers,* 146**,** 150-157.

CHA, J.-H., KIM, E. S., LEE, K. S., KANG, J. W., KANG, J. W. & KIM, K.-S. 2013. Phase Equilibria and Dissociation Enthalpies of Tri-n-butylphosphine Oxide Semiclathrate Hydrates Incorporated with CH4, CO2, and H2. *Journal of Chemical & Engineering Data.*

CHARI, V. D., SHARMA, D. V. S. G. K., PRASAD, P. S. R. & MURTHY, S. R. 2013. Methane hydrates formation and dissociation in nano silica suspension. *Journal of Natural Gas Science and Engineering,* 11**,** 7-11.

CHATTI, I., DELAHAYE, A., FOURNAISON, L. & PETITET, J.-P. 2005. Benefits and drawbacks of clathrate hydrates: a review of their areas of interest. *Energy Conversion and Management,* 46**,** 1333-1343.

CHEN, J., SUN, C. Y., PENG, B. Z., LIU, B., SI, S., JIA, M. L., MU, L., YAN, K. L. & CHEN, G. J. 2013. Screening and compounding of gas hydrate anti-agglomerants from commercial additives through morphology observation. *Energy and Fuels,* 27**,** 2488-2496.

CHEN, Z.-Y., LI, Q.-P., YAN, Z.-Y., YAN, K.-F., ZENG, Z.-Y. & LI, X.-S. 2010. Phase Equilibrium and Dissociation Enthalpies for Cyclopentane + Methane Hydrates in NaCl Aqueous Solutions†. *Journal of Chemical & Engineering Data,* 55**,** 4444-4449.

CHENG, C.-T., CHEN, L.-J., LIN, S.-T., TANG, M., CHEN, P.-C. & CHEN, Y.-P. 2013. Measurements for the dissociation conditions of methane hydrate in the presence of 2,5-dihydrofuran and 3,4-dihydro-2H-pyran. *Fluid Phase Equilibria,* 338**,** 114-118.

CHIU, P. C. & KU, Y. 2012. Chemical Looping Process - A Novel Technology for Inherent CO2 Capture. *Aerosol and Air Quality Research,* 12**,** 1421-1432.

CHOI, S., DRESE, J. H. & JONES, C. W. 2009. Adsorbent Materials for Carbon Dioxide Capture from Large Anthropogenic Point Sources. *ChemSusChem,* 2**,** 796-854.

CORAK, D., BARTH, T., HØILAND, S., SKODVIN, T., LARSEN, R. & SKJETNE, T. 2011. Effect of subcooling and amount of hydrate former on formation of cyclopentane hydrates in brine. *Desalination,* 278**,** 268-274.

D'ALESSANDRO, D. M., SMIT, B. & LONG, J. R. 2010. Carbon Dioxide Capture: Prospects for New Materials. *Angewandte Chemie International Edition,* 49**,** 6058-6082.

DALMAZZONE, D., KHARRAT, M., LACHET, V., FOUCONNIER, B. & CLAUSSE, D. 2002. DSC and PVT measurements. *Journal of Thermal Analysis and Calorimetry,* 70**,** 493-505.

DANESH, A., TOHIDI, B., BURGASS, R. W. & TODD, A. C. 1994. Hydrate equilibrium data of methyl cyclo-pentane with methane or nitrogen. *Chemical Engineering Research and Design,* 72**,** 197-200.

DARABOINA, N., MALMOS, C. & VON SOLMS, N. 2013a. Investigation of Kinetic Hydrate Inhibition Using a High Pressure Micro Differential Scanning Calorimeter. *Energy & Fuels,* 27**,** 5779-5786.

DARABOINA, N., MOUDRAKOVSKI, I. L., RIPMEESTER, J. A., WALKER, V. K. & ENGLEZOS, P. 2013b. Assessing the performance of commercial and biological gas hydrate inhibitors using nuclear magnetic resonance microscopy and a stirred autoclave. *Fuel,* 105**,** 630-635.

DARABOINA, N., RIPMEESTER, J. & ENGLEZOS, P. 2013c. The impact of SO2 on post combustion carbon dioxide capture in bed of silica sand through hydrate formation. *International Journal of Greenhouse Gas Control,* 15**,** 97-103.

DARTOIS, E. & SCHMITT, B. 2009. Carbon dioxide clathrate hydrate FTIR spectrum. *Astronomy and Astrophysics,* 504**,** 869-873.

DAVY, H. 1811. The Bakerian Lecture: On Some of the Combinations of Oxymuriatic Gas and Oxygene, and on the Chemical Relations of These Principles, to Inflammable Bodies. *Philosophical Transactions of the Royal Society of London,* 101**,** 1-35.

DE DEUGD, R. M., JAGER, M. D. & DE SWAAN ARONS, J. 2001. Mixed hydrates of methane and water-soluble hydrocarbons modeling of empirical results. *AIChE Journal,* 47**,** 693-704.

DEATON, W. M. & FROST, M. 1946. Gas hydrates and their relation to the operation of natural-gas pipeline. *U.S. Bureau of Mines Monograph.*

DELAHAYE, A., FOURNAISON, L., MARINHAS, S., CHATTI, I., PETITET, J.-P., DALMAZZONE, D. & FÜRST, W. 2005. Effect of THF on Equilibrium Pressure and Dissociation Enthalpy of CO2 Hydrates Applied to Secondary Refrigeration. *Industrial & Engineering Chemistry Research,* 45**,** 391-397.

DELAHAYE, A., FOURNAISON, L., MARINHAS, S., CHATTI, I., PETITET, J. P., DALMAZZONE, D. & FÜRST, W. 2006. Effect of THF on equilibrium pressure and dissociation enthalpy of CO 2 hydrates applied to secondary refrigeration. *Industrial and Engineering Chemistry Research,* 45**,** 391-397.

DEMIRBAS, A. 2010. *Methane Gas Hydrate (Green Energy and Technology),* Springer.

DENNIS, J. S. & SCOTT, S. A. 2010. In situ gasification of a lignite coal and CO2 separation using chemical looping with a Cu-based oxygen carrier. *Fuel,* 89**,** 1623-1640.

DESCHAMPS, J. & DALMAZZONE, D. 2010. Hydrogen Storage in Semiclathrate Hydrates of Tetrabutyl Ammonium Chloride and Tetrabutyl Phosphonium Bromide. *Journal of Chemical & Engineering Data,* 55**,** 3395-3399.

DHOLABHAI, P. D., KALOGERAKIS, N. & BISHNOI, P. R. 1993. Equilibrium Conditions for Carbon-Dioxide Hydrate Formation in Aqueous-Electrolyte Solutions. *Journal of Chemical and Engineering Data,* 38**,** 650-654.

DICHARRY, C., DUCHATEAU, C., ASBAÏ, H., BROSETA, D. & TORRÉ, J.-P. 2013. Carbon dioxide gas hydrate crystallization in porous silica gel particles partially saturated with a surfactant solution. *Chemical Engineering Science,* 98**,** 88-97.

DU, J.-W., LIANG, D.-Q., LI, D.-L., CHEN, Y.-F. & LI, X.-J. 2011a. Phase Equilibrium Conditions of Tetrabutyl Ammonium Nitrate + CO2, N2, or CH4 Semiclathrate Hydrate Systems. *Industrial & Engineering Chemistry Research,* 50**,** 11720-11723.

DU, J. & WANG, L. 2013. Equilibrium Conditions for Semi-Clathrate Hydrates Formed with CO2, N2 or CH4 in the Presence of Tri-n-butylphosphine Oxide. *Industrial & Engineering Chemistry Research.*

DU, J., WANG, L., LIANG, D. & LI, D. 2011b. Phase Equilibria and Dissociation Enthalpies of Hydrogen Semi-Clathrate Hydrate with Tetrabutyl Ammonium Nitrate. *Journal of Chemical & Engineering Data,* 57**,** 603-609.

DU, J. W., LIANG, D. Q., LI, D. L. & LI, X. J. 2010. Phase Equilibrium Data of Binary Hydrate in the System Hydrogen + Acetone + Water. *Journal of Chemical & Engineering Data,* 55**,** 4532-4535.

DUAN, Z. H. & SUN, R. 2006. A model to predict phase equilibrium of CH4 and CO2 clathrate hydrate in aqueous electrolyte solutions. *American Mineralogist,* 91**,** 1346-1354.

DUC, N. H., CHAUVY, F. & HERRI, J.-M. 2007a. CO2 capture by hydrate crystallization – A potential solution for gas emission of steelmaking industry. *Energy Conversion and Management,* 48**,** 1313-1322.

DUC, N. H., CHAUVY, F. & HERRI, J. M. 2007b. CO2 capture by hydrate crystallization – A potential solution for gas emission of steelmaking industry. *Energy Conversion and Management,* 48**,** 1313-1322.

DYADIN, Y. & ALADKO, E. 1996. *in Proc. Second International Conference on Natural Gas Hydrates (Monfort, J.P., ed.).* Toulouse.

DYADIN, Y. A., LARIONOV, É. G., ALADKO, E. Y., MANAKOV, A. Y., ZHURKO, F. V., MIKINA, T. V., KOMAROV, V. Y. & GRACHEV, E. V. 1999a. Clathrate formation in water-noble gas (Hydrogen) systems at high pressures. *Journal of Structural Chemistry,* 40**,** 790-795.

DYADIN, Y. A., LARIONOV, E. G., MANAKOV, A. Y., ZHURKO, F. V., ALADKO, E. Y., MIKINA, T. V. & KOMAROV, V. Y. 1999b. Clathrate hydrates of hydrogen and neon. *Mendeleev Communications,* 9**,** 209-210.

DYADIN, Y. A. & UDACHIN, K. A. 1984. Clathrate formation in water-peralkylonium salts systems. *Journal of inclusion phenomena,* 2**,** 61-72.

DYADIN, Y. A. & UDACHIN, K. A. 1987. Clathrate polyhydrates of peralkylonium salts and their analogs. *Journal of Structural Chemistry,* 28**,** 394-432.

ELGIBALY, A. A. & ELKAMEL, A. M. 1998. A new correlation for predicting hydrate formation conditions for various gas mixtures and inhibitors. *Fluid Phase Equilibria,* 152**,** 23-42.

ENGLEZOS, P. 1992. Computation of the Incipient Equilibrium Carbon-Dioxide Hydrate Formation Conditions in Aqueous-Electrolyte Solutions. *Industrial & Engineering Chemistry Research,* 31**,** 2232-2237.

ENGLEZOS, P. 1993. Clathrate hydrates. *Industrial & Engineering Chemistry Research,* 32**,** 1251-1274.

ENGLEZOS, P. & HALL, S. 1994. Phase-Equilibrium Data on Carbon-Dioxide Hydrate in the Presence of Electrolytes, Water-Soluble Polymers and Montmorillonite. *Canadian Journal of Chemical Engineering,* 72**,** 887-893.

ERFANI, A., MOHAMMDI, M., ASGARI NESHAT, S. & VARAMINIAN, F. Processes and apparatuses for formation, separation and pelletizing of gas hydrate. 2nd National Iranian Conference on Gas Hydrate (NICGH), 2013 Semnan University.

ESLAMIMANESH, A., GHARAGHEIZI, F., ILLBEIGI, M., MOHAMMADI, A. H., FAZLALI, A. & RICHON, D. 2012a. Phase equilibrium modeling of clathrate hydrates of methane, carbon dioxide, nitrogen, and hydrogen+water soluble organic promoters using Support Vector Machine algorithm. *Fluid Phase Equilibria,* 316**,** 34-45.

ESLAMIMANESH, A., GHARAGHEIZI, F., MOHAMMADI, A. H. & RICHON, D. 2012b. A statistical method for evaluation of the experimental phase equilibrium data of simple clathrate hydrates. *Chemical Engineering Science,* 80**,** 402-408.

ESLAMIMANESH, A., MOHAMMADI, A. H. & RICHON, D. 2011. An improved Clapeyron model for predicting liquid water-hydrate-liquid hydrate former phase equilibria. *Chemical Engineering Science,* 66**,** 1759-1764.

ESLAMIMANESH, A., MOHAMMADI, A. H. & RICHON, D. 2012c. Thermodynamic modeling of phase equilibria of semi-clathrate hydrates of CO2, CH4, or N2+tetra-n-butylammonium bromide aqueous solution. *Chemical Engineering Science,* 81**,** 319-328.

ESLAMIMANESH, A., MOHAMMADI, A. H. & RICHON, D. 2012d. Thermodynamic modeling of phase equilibria of semi-clathrate hydrates of CO2, CH4, or N-2+tetra-n-butylammonium bromide aqueous solution. *Chemical Engineering Science,* 81**,** 319-328.

ESLAMIMANESH, A., MOHAMMADI, A. H. & RICHON, D. 2012e. Thermodynamic modeling of phase equilibria of semi-clathrate hydrates of CO2, CH4, or N-2+tetra-n-

butylammonium bromide aqueous solution (vol 81, pg 319, 2012). *Chemical Engineering Science,* 84**,** 381-381.

ESLAMIMANESH, A., MOHAMMADI, A. H., RICHON, D., NAIDOO, P. & RAMJUGERNATH, D. 2012f. Application of gas hydrate formation in separation processes: A review of experimental studies. *Journal of Chemical Thermodynamics,* 46**,** 62-71.

FALABELLA, B. J. 1975. *A Study of Natural Gas Hydrate.* Ph.D., University of Massachusetts.

FALENTY, A. 2009. *http://commons.wikimedia.org/wiki/File:Clathrate_hydrate_cages.jpg* [Online].

FAN, S., LI, S., WANG, J., LANG, X. & WANG, Y. 2009. Efficient Capture of CO2 from Simulated Flue Gas by Formation of TBAB or TBAF Semiclathrate Hydrates. *Energy & Fuels,* 23**,** 4202-4208.

FAN, S. S., CHEN, G. J., MA, Q. L. & GUO, T. M. 2000. Experimental and modeling studies on the hydrate formation of CO2 and CO2-rich gas mixtures. *Chemical Engineering Journal,* 78**,** 173-178.

FAN, S. S. & GUO, T. M. 1999. Hydrate formation of CO2-rich binary and quaternary gas mixtures in aqueous sodium chloride solutions. *Journal of Chemical and Engineering Data,* 44**,** 829-832.

FANDIÑO, O. & RUFFINE, L. 2014. Methane hydrate nucleation and growth from the bulk phase: Further insights into their mechanisms. *Fuel,* 117, Part A**,** 442-449.

FARADAY, M. & DAVY, H. 1823. On Fluid Chlorine. *Philosophical Transactions of the Royal Society of London,* 113**,** 160-165.

FIGUEROA, J. D., FOUT, T., PLASYNSKI, S., MCILVRIED, H. & SRIVASTAVA, R. D. 2008a. Advances in CO2 capture technology-The U.S. Department of Energy's Carbon Sequestration Program. *International Journal of Greenhouse Gas Control,* 2**,** 9-20.

FIGUEROA, J. D., FOUT, T., PLASYNSKI, S., MCILVRIED, H. & SRIVASTAVA, R. D. 2008b. Advances in CO2 capture technology—The U.S. Department of Energy's Carbon Sequestration Program. *International Journal of Greenhouse Gas Control,* 2**,** 9-20.

FLEYFEL, F. & DEVLIN, J. P. 1991. Carbon dioxide clathrate hydrate epitaxial growth: spectroscopic evidence for formation of the simple type-II carbon dioxide hydrate. *The Journal of Physical Chemistry,* 95**,** 3811-3815.

FLORUSSE, L. J., PETERS, C. J., SCHOONMAN, J., HESTER, K. C., KOH, C. A., DEC, S. F., MARSH, K. N. & SLOAN, E. D. 2004. Stable Low-Pressure Hydrogen Clusters Stored in a Binary Clathrate Hydrate. *Science,* 306**,** 469-471.

GANJI, H., AALAIE, J., BOROOJERDI, S. H. & ROD, A. R. 2013. Effect of polymer nanocomposites on methane hydrate stability and storage capacity. *Journal of Petroleum Science and Engineering,* 112**,** 32-35.

GANJI, H., MANTEGHIAN, M., SADAGHIANI ZADEH, K., OMIDKHAH, M. R. & RAHIMI MOFRAD, H. 2007. Effect of different surfactants on methane hydrate formation rate, stability and storage capacity. *Fuel,* 86**,** 434-441.

GAO, W., BUTLER, D. & TOMASKO, D. L. 2004. High-Pressure Adsorption of CO2 on NaY Zeolite and Model Prediction of Adsorption Isotherms. *Langmuir,* 20**,** 8083-8089.

GARCÍA-LABIANO, F., ADÁNEZ, J., DE DIEGO, L. F., GAYÁN, P. & ABAD, A. 2005. Effect of Pressure on the Behavior of Copper-, Iron-, and Nickel-Based Oxygen Carriers for Chemical-Looping Combustion. *Energy & Fuels,* 20**,** 26-33.

GAUDETTE, J. & SERVIO, P. 2007. Measurement of Dissolved Propane in Water in the Presence of Gas Hydrate. *Journal of Chemical & Engineering Data,* 52**,** 1449-1451.

GHARAGHEIZI, F., ILANI-KASHKOULI, P. & MOHAMMADI, A. H. 2012. Group contribution model for estimation of surface tension of ionic liquids. *Chemical Engineering Science,* 78**,** 204-208.

GIAVARINI, C. & HESTER, K. 2011. *Gas Hydrates: Immense Energy Potential and Environmental Challenges (Green Energy and Technology)*, Springer.

GIAVARINI, C., MACCIONI, F. & SANTARELLI, M. L. 2008. Dissociation Rate of THF-methane Hydrates. *Petroleum Science and Technology,* 26**,** 2147-2158.

GNANENDRAN, N. & AMIN, R. 2003. The effect of hydrotropes on gas hydrate formation. *Journal of Petroleum Science and Engineering,* 40**,** 37-46.

GNANENDRAN, N. & AMIN, R. 2004. Equilibrium hydrate formation conditions for hydrotrope–water–natural gas systems. *Fluid Phase Equilibria,* 221**,** 175-187.

GOODALL, C. R. 1993. *Computation Using the QR Decomposition.*

GRAMATICA, P. 2007. Principles of QSAR models validation: Internal and external. *QSAR and Combinatorial Science,* 26**,** 694-701.

GUI, M. M., YAP, Y. X., CHAI, S.-P. & MOHAMED, A. R. 2013. Amine-functionalization of multi-walled carbon nanotubes for adsorption of carbon dioxide. *Asia-Pacific Journal of Chemical Engineering,* 8**,** 262-270.

HANDA, Y. P. & STUPIN, D. Y. 1992. Thermodynamic properties and dissociation characteristics of methane and propane hydrates in 70-.ANG.-radius silica gel pores. *The Journal of Physical Chemistry,* 96**,** 8599-8603.

HART, A. & GNANENDRAN, N. 2009. Cryogenic CO2 capture in natural gas. *Energy Procedia,* 1**,** 697-706.

HASHEMI, S., MACCHI, A. & SERVIO, P. 2009. Gas–liquid mass transfer in a slurry bubble column operated at gas hydrate forming conditions. *Chemical Engineering Science,* 64**,** 3709-3716.

HASHIMOTO, S., MURAYAMA, S., SUGAHARA, T. & OHGAKI, K. 2006a. Phase equilibria for H2 + CO2 + tetrahydrofuran + water mixtures containing gas hydrates. *Journal of Chemical and Engineering Data,* 51**,** 1884-1886.

HASHIMOTO, S., MURAYAMA, S., SUGAHARA, T., SATO, H. & OHGAKI, K. 2006b. Thermodynamic and Raman spectroscopic studies on and tetra-n-butyl ammonium mixtures containing gas hydrates. *Chemical Engineering Science,* 61**,** 7884-7888.

HASHIMOTO, S., SUGAHARA, T., SATO, H. & OHGAKI, K. 2007. Thermodynamic Stability of H2 + Tetrahydrofuran Mixed Gas Hydrate in Nonstoichiometric Aqueous Solutions. *Journal of Chemical & Engineering Data,* 52**,** 517-520.

HASIB-UR-RAHMAN, M., SIAJ, M. & LARACHI, F. 2010. Ionic liquids for CO2 capture—Development and progress. *Chemical Engineering and Processing: Process Intensification,* 49**,** 313-322.

HASZELDINE, R. S. 2009. Carbon Capture and Storage: How Green Can Black Be? *Science,* 325**,** 1647-1652.

HENRIET, P. & MIENERT, J. 1998. *Gas Hydrates: Relevance to World Margin Stability and Climatic Change (Geological Society Special Publication No.137).*

HERSLUND, P. J., THOMSEN, K., ABILDSKOV, J., VON SOLMS, N., GALFRÉ, A., BRÂNTUAS, P., KWATERSKI, M. & HERRI, J.-M. 2013. Thermodynamic promotion of carbon dioxide–clathrate hydrate formation by tetrahydrofuran, cyclopentane and their mixtures. *International Journal of Greenhouse Gas Control,* 17**,** 397-410.

HESTER, K. C. & BREWER, P. G. 2009. Clathrate hydrates in nature. *Annual Review of Marine Science,* 1**,** 303-327.

HESTER, R. E. & HARRISION, R. M. 2010. *Carbon capture : sequestration and storage*, The Royal Society of Chemistry, Cambridge, UK.

HEYDARI, A., SHAYESTEH, K. & KAMALZADEH, L. 2006. Prediction of Hydrate Formation Temperature for Natural Gas Using Atificial Neural Network. *Oil & Gas Business***, 10.

HOLDER, G. D., CORBIN, G. & PAPADOPOULOS, K. D. 1980. Thermodynamic and Molecular Properties of Gas Hydrates from Mixtures Containing Methane, Argon, and Krypton. *Industrial & Engineering Chemistry Fundamentals,* 19**, 282-286.

HOLDER, G. D., ZETTS, S. P. & PRADHAN, N. 1988. Phase-Behavior in Systems Containing Clathrate Hydrates - a Review. *Reviews in Chemical Engineering,* 5**, 1-70.

HOSSAIN, M. M. & DE LASA, H. I. 2008. Chemical-looping combustion (CLC) for inherent separations—a review. *Chemical Engineering Science,* 63**, 4433-4451.

HTTP://EDGAR.JRC.EC.EUROPE.EU. 2011. *Emissions Database for Global Atmospheric Research (EDGAR)* [Online]. Available: http://edgar.jrc.ec.europa.eu/whats_new.php?p=1.

HÜTZ, U. & ENGLEZOS, P. 1995. Measurement of structure H hydrate phase equilibrium and effect of electrolytes. *Proc. 7th International Conference on Fluid Properties and Phase Equilibria for Chemical Process Design*.

ILANI-KASHKOULI, P., BABAEE, S., GHARAGHEIZI, F., HASHEMI, H., MOHAMMADI, A. H. & RAMJUGERNATH, D. 2013a. An assessment test for phase equilibrium data of water soluble and insoluble clathrate hydrate formers. *Fluid Phase Equilibria,* 360**, 68-76.

ILANI-KASHKOULI, P., HASHEMI, H., GHARAGHEIZI, F., BABAEE, S., MOHAMMADI, A. H. & RAMJUGERNATH, D. 2013b. Gas hydrate phase equilibrium in porous media: An assessment test for experimental data. *Fluid Phase Equilibria,* 360**, 161-168.

ILLBEIGI, M., FAZLALI, A. & MOHAMMADI, A. H. 2011. Thermodynamic Model for the Prediction of Equilibrium Conditions of Clathrate Hydrates of Methane + Water-Soluble or -Insoluble Hydrate Former. *Industrial & Engineering Chemistry Research,* 50**, 9437-9450.

J.H. VAN DER WAALS, J. C. P. 1959. Clathrate solutions. *Advances in Chemical Physics***, 1-57.

JAGER, M. D., DE DEUGD, R. M., PETERS, C. J., DE SWAAN ARONS, J. & SLOAN, E. D. 1999. Experimental determination and modeling of structure II hydrates in mixtures of methane+water+1,4-dioxane. *Fluid Phase Equilibria,* 165**, 209-223.

JAVANMARDI, J., NASRIFAR, K., NAJIBI, S. H. & MOSHFEGHIAN, M. 2005. Economic evaluation of natural gas hydrate as an alternative for natural gas transportation. *Applied Thermal Engineering,* 25**, 1708-1723.

JEFFREY, G. A. 1984. Hydrate inclusion compounds. *Journal of Inclusion Phenomena,* 1**, 211-222.

JOON SHIN, H., LEE, Y. J., IM, J. H., WON HAN, K., LEE, J. W., LEE, Y., DONG LEE, J., JANG, W. Y. & YOON, J. H. 2009. Thermodynamic stability, spectroscopic identification and cage occupation of binary CO2 clathrate hydrates. *Chemical Engineering Science,* 64**, 5125-5130.

JOSHI, A., SANGWAI, J. S., DAS, K. & SAMI, N. A. 2013. Experimental investigations on the phase equilibrium of semiclathrate hydrates of carbon dioxide in TBAB with small amount of surfactant. *International Journal of Energy and Environmental Engineering,* 4**, 1-8.

KAEHLER, N. & HAMANN, R. Safety and risk analysis of a natural gas hydrate pellet carrier. 2012. 35-40.

KALOGERAKIS, N. J., A. K. M.; DHOLABHAI, P. D.; BISHNOI, P. R.; 1993. Effect of Surfactants on Hydrate Formation Kinetics. *SPE International Symposium on Oilfield Chemistry*, 8.

KAMRAN-PIRZAMAN, A., PAHLAVANZADEH, H. & MOHAMMADI, A. H. 2013. Hydrate phase equilibria of furan, acetone, 1,4-dioxane, TBAC and TBAF. *The Journal of Chemical Thermodynamics,* 64**,** 151-158.

KANG, S.-P. & LEE, J.-W. 2010. Kinetic behaviors of CO2 hydrates in porous media and effect of kinetic promoter on the formation kinetics. *Chemical Engineering Science,* 65**,** 1840-1845.

KANG, S.-P., LEE, J.-W. & RYU, H.-J. 2008. Phase behavior of methane and carbon dioxide hydrates in meso- and macro-sized porous media. *Fluid Phase Equilibria,* 274**,** 68-72.

KANG, S.-P., LEE, J. & SEO, Y. 2013. Pre-combustion capture of CO2 by gas hydrate formation in silica gel pore structure. *Chemical Engineering Journal,* 218**,** 126-132.

KANG, S. P. & LEE, H. 2000. Recovery of CO2 from flue gas using gas hydrate: Thermodynamic verification through phase equilibrium measurements. *Environmental Science and Technology,* 34**,** 4397-4400.

KANG, S. P., LEE, H., LEE, C. S. & SUNG, W. M. 2001. Hydrate phase equilibria of the guest mixtures containing CO2, N2 and tetrahydrofuran. *Fluid Phase Equilibria,* 185**,** 101-109.

KARAASLAN, U. & PARLAKTUNA, M. 2000. Surfactants as hydrate promoters? *Energy and Fuels,* 14**,** 1103-1107.

KARAASLAN, U., ULUNEYE, E. & PARLAKTUNA, M. 2002a. Effect of an anionic surfactant on different type of hydrate structures. *Journal of Petroleum Science and Engineering,* 35**,** 49-57.

KARAASLAN, U., ULUNEYE, E. & PARLAKTUNA, M. 2002b. Effect of an anionic surfactant on different type of hydrate structures. *Journal of Petroleum Science and Engineering,* 35**,** 49-57.

KARAMODDIN, M. & VARAMINIAN, F. 2011. Prediction of Gas Hydrate Forming Pressures by Using PR Equation of State and Different Mixing Rules. *Iranian Journal of Chemical Engineering,* 8**,** 10.

KARANJKAR, P. U., LEE, J. W. & MORRIS, J. F. 2012. Calorimetric investigation of cyclopentane hydrate formation in an emulsion. *Chemical Engineering Science,* 68**,** 481-491.

KARIMI, A. & ABDI, M. A. 2009. Selective dehydration of high-pressure natural gas using supersonic nozzles. *Chemical Engineering and Processing: Process Intensification,* 48**,** 560-568.

KARIMI, A. A., DOLOTKO, O. & DALMAZZONE, D. 2014. Hydrate phase equilibria data and hydrogen storage capacity measurement of the system H2 + tetrabutylammonium hydroxide + H2O. *Fluid Phase Equilibria,* 361**,** 175-180.

KATSUKI, D., OHMURA, R., EBINUMA, T. & NARITA, H. 2006. Formation, growth and ageing of clathrate hydrate crystals in a porous medium. *Philosophical Magazine,* 86**,** 1753-1761.

KATZ, D. L. 1945a. Prediction of Conditions for Hydrate Formation in Natural Gases. *Transactions of the American Institute of Mining and Metallurgical Engineers,* 160**,** 140-149.

KATZ, D. L. 1945b. Prediction of conditions for hydrate formation in natural gases. *Trans. AIME,* 160**,** 140-149.

KHOKHAR, A. A., GUDMUNDSSON, J. S. & SLOAN, E. D. 1998. Gas storage in structure H hydrates. *Fluid Phase Equilibria,* 150–151**,** 383-392.

KIHARA, T. 1953. Virial Coefficients and Models of Molecules in Gases. *Reviews of Modern Physics,* 25**,** 831-843.

KIM, D.-Y. & LEE, H. 2005. Spectroscopic Identification of the Mixed Hydrogen and Carbon Dioxide Clathrate Hydrate. *Journal of the American Chemical Society,* 127**,** 9996-9997.

KIM, H. K., KIM, Y., LEE, S. M. & AHN, K. Y. 2007. NO reduction in 0.03–0.2 MW oxy-fuel combustor using flue gas recirculation technology. *Proceedings of the Combustion Institute,* 31**,** 3377-3384.

KIM, J., LIN, L.-C., SWISHER, J. A., HARANCZYK, M. & SMIT, B. 2012. Predicting Large CO2 Adsorption in Aluminosilicate Zeolites for Postcombustion Carbon Dioxide Capture. *Journal of the American Chemical Society,* 134**,** 18940-18943.

KIM, S. A., LIM, J. S. & KANG, J. W. 2010. Isothermal Vapor−Liquid Equilibria for the Binary System of Carbon Dioxide (CO2) + 1,1,1,2,3,3,3-Heptafluoropropane (R-227ea). *Journal of Chemical & Engineering Data,* 55**,** 4999-5003.

KIM, S. M., LEE, J. D., LEE, H. J., LEE, E. K. & KIM, Y. 2011. Gas hydrate formation method to capture the carbon dioxide for pre-combustion process in IGCC plant. *International Journal of Hydrogen Energy,* 36**,** 1115-1121.

KIM, Y. S., RYU, S. K., YANG, S. O. & LEE, C. S. 2003. Liquid Water−Hydrate Equilibrium Measurements and Unified Predictions of Hydrate-Containing Phase Equilibria for Methane, Ethane, Propane, and Their Mixtures. *Industrial & Engineering Chemistry Research,* 42**,** 2409-2414.

KLAUDA, J. B. & SANDLER, S. I. 2000. A Fugacity Model for Gas Hydrate Phase Equilibria. *Industrial & Engineering Chemistry Research,* 39**,** 3377-3386.

KOH, C., SUM, A. & SLOAN, E. D. 2010. *Natural Gas Hydrates in Flow Assurance*, Gulf Professional Publishing.

KOMATSU, H., HAYASAKA, A., OTA, M., SATO, Y., WATANABE, M. & SMITH JR, R. L. Measurement of pure hydrogen and pure carbon dioxide adsorption equilibria for THF clathrate hydrate and tetra-n-butyl ammonium bromide semi-clathrate hydrate. *Fluid Phase Equilibria.*

KOMATSU, H., YOSHIOKA, H., OTA, M., SATO, Y., WATANABE, M., SMITH, R. L. & PETERS, C. J. 2010. Phase Equilibrium Measurements of Hydrogen−Tetrahydrofuran and Hydrogen−Cyclopentane Binary Clathrate Hydrate Systems. *Journal of Chemical & Engineering Data,* 55**,** 2214-2218.

KONDURU, N., LINDNER, P. & ASSAF-ANID, N. M. 2007. Curbing the greenhouse effect by carbon dioxide adsorption with Zeolite 13X. *AIChE Journal,* 53**,** 3137-3143.

KOYANAGI, S. & OHMURA, R. 2013a. Crystal Growth of Ionic Semiclathrate Hydrate Formed in CO2 Gas + Tetrabutylammonium Bromide Aqueous Solution System. *Crystal Growth & Design,* 13**,** 2087-2093.

KOYANAGI, S. & OHMURA, R. 2013b. Crystal growth of ionic semiclathrate hydrate formed in CO2 gas + tetrabutylammonium bromide aqueous solution system. *Crystal Growth and Design,* 13**,** 2087-2093.

KRICHEVSKY, I. R. & KASARNOVSKY, J. S. 1935. Thermodynamical Calculations of Solubilities of Nitrogen and Hydrogen in Water at High Pressures. *Journal of the American Chemical Society,* 57**,** 2168-2171.

KUMAR, A., SAKPAL, T., LINGA, P. & KUMAR, R. 2013a. Influence of contact medium and surfactants on carbon dioxide clathrate hydrate kinetics. *Fuel,* 105**,** 664-671.

KUMAR, A., SAKPAL, T., LINGA, P. & KUMAR, R. 2013b. Influence of contact medium and surfactants on carbon dioxide clathrate hydrate kinetics. *Fuel,* 105**,** 664-671.

KUMAR, R., ENGLEZOS, P., MOUDRAKOVSKI, I. & RIPMEESTER, J. A. 2009a. Structure and composition of CO2/H2 and CO2/H2/C3H8 hydrate in relation to simultaneous CO2 capture and H2 production. *AIChE Journal,* 55**,** 1584-1594.

KUMAR, R., LANG, S., ENGLEZOS, P. & RIPMEESTER, J. 2009b. Application of the ATR-IR Spectroscopic Technique to the Characterization of Hydrates Formed by CO2, CO2/H2 and CO2/H2/C3H8. *The Journal of Physical Chemistry A,* 113**,** 6308-6313.

KUMAR, R., LINGA, P., RIPMEESTER, J. & ENGLEZOS, P. 2009c. Two-Stage Clathrate Hydrate/Membrane Process for Precombustion Capture of Carbon Dioxide and Hydrogen. *Journal of Environmental Engineering,* 135**,** 411-417.

KUMAR, R., WU, H.-J. & ENGLEZOS, P. 2006. Incipient hydrate phase equilibrium for gas mixtures containing hydrogen, carbon dioxide and propane. *Fluid Phase Equilibria,* 244**,** 167-171.

LAGARIAS, J. C., REEDS, J. A., WRIGHT, M. H. & WRIGHT, P. E. 1998. Convergence Properties of the Nelder--Mead Simplex Method in Low Dimensions. *SIAM Journal on Optimization,* 9**,** 112-147.

LARSON, S. D. 1955. *Phase Studies of the Two-Component Carbon Dioxide-Water System Involving the Carbon Dioxide Hydrate.* Ph.D., University of Michigan.

LEDERHOS, J. P., MEHTA, A. P., NYBERG, G. B., WARN, K. J. & SLOAN, E. D. 1992. Structure H clathrate hydrate equilibria of methane and adamantane. *AIChE Journal,* 38**,** 1045-1048.

LEE, H.-H., AHN, S.-H., NAM, B.-U., KIM, B.-S., LEE, G.-W., MOON, D., SHIN, H. J., HAN, K. W. & YOON, J.-H. 2012a. Thermodynamic Stability, Spectroscopic Identification, and Gas Storage Capacity of CO2–CH4–N2 Mixture Gas Hydrates: Implications for Landfill Gas Hydrates. *Environmental Science & Technology,* 46**,** 4184-4190.

LEE, H., LEE, J. W., KIM, D. Y., PARK, J., SEO, Y. T., ZENG, H., MOUDRAKOVSKR, I. L., RATCLIFFE, C. I. & RIPMEESTER, J. A. 2005. Tuning clathrate hydrates for hydrogen storage. *Nature,* 434**,** 743-746.

LEE, H. J., LEE, J. D. & KIM, Y. D. 2008. Pre-combustion capture of carbon dioxide using principles of gas hydrate formation. *Korean Journal of Materials Research,* 18**,** 650-654.

LEE, H. J., LEE, J. D., LINGA, P., ENGLEZOS, P., KIM, Y. S., LEE, M. S. & KIM, Y. D. 2010. Gas hydrate formation process for pre-combustion capture of carbon dioxide. *Energy,* 35**,** 2729-2733.

LEE, J.-W., CHUN, M.-K., LEE, K.-M., KIM, Y.-J. & LEE, H. 2002. Phase equilibria and kinetic behavior of co2 hydrate in electrolyte and porous media solutions: application to ocean sequestration of CO2. *Korean Journal of Chemical Engineering,* 19**,** 673-678.

LEE, J. D., KIM, H. J., KIM, S. R., HONG, S. Y., PARK, H. O., HA, M. K., JEON, S. K., AHN, H. & WOO, T. K. 2013. Apparatus and method for continuously producing and pelletizing gas hydrates using dual cylinder. Google Patents.

LEE, S., LEE, Y., PARK, S., KIM, Y., LEE, J. D. & SEO, Y. 2012b. Thermodynamic and Spectroscopic Identification of Guest Gas Enclathration in the Double Tetra-n-butylammonium Fluoride Semiclathrates. *Journal of Physical Chemistry B,* 116**,** 9075-9081.

LEE, S., PARK, S., LEE, Y., LEE, J., LEE, H. & SEO, Y. 2011. Guest gas enclathration in semiclathrates of tetra-n-butylammonium Bromide: Stability condition and spectroscopic analysis. *Langmuir,* 27**,** 10597-10603.

LEE, S., ZHANG, J., MEHTA, R., WOO, T. K. & LEE, J. W. 2007. Methane Hydrate Equilibrium and Formation Kinetics in the Presence of an Anionic Surfactant. *The Journal of Physical Chemistry C,* 111**,** 4734-4739.

LEE, Y. J., KAWAMURA, T., YAMAMOTO, Y. & YOON, J. H. 2012c. Phase equilibrium studies of tetrahydrofuran (THF) + CH4, THF + CO2, CH4 + CO2, and THF + CO2 + CH4 hydrates. *Journal of Chemical and Engineering Data,* 57**,** 3543-3548.

LEHMKÜHLER, F., PAULUS, M., STERNEMANN, C., LIETZ, D., VENTURINI, F., GUTT, C. & TOLAN, M. 2008. The Carbon Dioxide−Water Interface at Conditions of Gas Hydrate Formation. *Journal of the American Chemical Society,* 131**,** 585-589.

LI, G., LIU, D., XIE, Y. & XIAO, Y. 2010a. Study on Effect Factors for CO2 Hydrate Rapid Formation in a Water-Spraying Apparatus. *Energy & Fuels,* 24**,** 4590-4597.

LI, J.-R., MA, Y., MCCARTHY, M. C., SCULLEY, J., YU, J., JEONG, H.-K., BALBUENA, P. B. & ZHOU, H.-C. 2011a. Carbon dioxide capture-related gas adsorption and separation in metal-organic frameworks. *Coordination Chemistry Reviews,* 255**,** 1791-1823.

LI, J., LIANG, D., GUO, K., WANG, R. & FAN, S. 2006. Formation and dissociation of HFC134a gas hydrate in nano-copper suspension. *Energy Conversion and Management,* 47**,** 201-210.

LI, S., FAN, S., WANG, J., LANG, X. & WANG, Y. 2010b. Clathrate Hydrate Capture of CO2 from Simulated Flue Gas with Cyclopentane/Water Emulsion. *Chinese Journal of Chemical Engineering,* 18**,** 202-206.

LI, S. F., FAN, S. S., WANG, J. Q., LANG, X. M. & WANG, Y. H. 2010c. Semiclathrate Hydrate Phase Equilibria for CO2 in the Presence of Tetra-n-butyl Ammonium Halide (Bromide, Chloride, or Fluoride). *Journal of Chemical and Engineering Data,* 55**,** 3212-3215.

LI, X.-S., XU, C.-G., CHEN, Z.-Y. & WU, H.-J. 2011b. Hydrate-based pre-combustion carbon dioxide capture process in the system with tetra-n-butyl ammonium bromide solution in the presence of cyclopentane. *Energy,* 36**,** 1394-1403.

LI, X.-S., ZHAN, H., XU, C.-G., ZENG, Z.-Y., LV, Q.-N. & YAN, K.-F. 2012. Effects of Tetrabutyl-(ammonium/phosphonium) Salts on Clathrate Hydrate Capture of CO2 from Simulated Flue Gas. *Energy & Fuels,* 26**,** 2518-2527.

LI, X.-S., ZHANG, Y., LI, G., CHEN, Z.-Y., YAN, K.-F. & LI, Q.-P. 2008. Gas hydrate equilibrium dissociation conditions in porous media using two thermodynamic approaches. *The Journal of Chemical Thermodynamics,* 40**,** 1464-1474.

LI, X. S. & ENGLEZOS, P. 2004. Vapor-liquid equilibrium of systems containing alcohols, water, carbon dioxide and hydrocarbons using SAFT. *Fluid Phase Equilibria,* 224**,** 111-118.

LI, X. S., XU, C. G., CHEN, Z. Y. & WU, H. J. 2010d. Tetra-n-butyl ammonium bromide semi-clathrate hydrate process for post-combustion capture of carbon dioxide in the presence of dodecyl trimethyl ammonium chloride. *Energy,* 35**,** 3902-3908.

LIM, Y.-A., BABU, P., KUMAR, R. & LINGA, P. 2013. Morphology of Carbon Dioxide–Hydrogen–Cyclopentane Hydrates with or without Sodium Dodecyl Sulfate. *Crystal Growth & Design,* 13**,** 2047-2059.

LIN, W., CHEN, G. J., SUN, C. Y., GUO, X. Q., WU, Z. K., LIANG, M. Y., CHEN, L. T. & YANG, L. Y. 2004. Effect of surfactant on the formation and dissociation kinetic behavior of methane hydrate. *Chemical Engineering Science,* 59**,** 4449-4455.

LIN, W., DALMAZZONE, D., FÜRST, W., DELAHAYE, A., FOURNAISON, L. & CLAIN, P. 2014. Thermodynamic properties of semiclathrate hydrates formed from the TBAB + TBPB + water and CO2 + TBAB + TBPB + water systems. *Fluid Phase Equilibria,* 372**,** 63-68.

LINGA, P., ADEYEMO, A. & ENGLEZOS, P. 2007a. Medium-Pressure Clathrate Hydrate/Membrane Hybrid Process for Postcombustion Capture of Carbon Dioxide. *Environmental Science & Technology,* 42**,** 315-320.

LINGA, P., ADEYEMO, A. & ENGLEZOS, P. 2008. Medium-pressure clathrate hydrate/membrane hybrid process for postcombustion capture of carbon dioxide. *Environmental Science and Technology,* 42**,** 315-320.

LINGA, P., KUMAR, R. & ENGLEZOS, P. 2007b. The clathrate hydrate process for post and pre-combustion capture of carbon dioxide. *Journal of Hazardous Materials,* 149**,** 625-629.

LINGA, P., KUMAR, R. & ENGLEZOS, P. 2007c. Gas hydrate formation from hydrogen/carbon dioxide and nitrogen/carbon dioxide gas mixtures. *Chemical Engineering Science,* 62**,** 4268-4276.

LINK, D. D., LADNER, E. P., ELSEN, H. A. & TAYLOR, C. E. 2003. Formation and dissociation studies for optimizing the uptake of methane by methane hydrates. *Fluid Phase Equilibria,* 211**,** 1-10.

LIRIO, C. F. D. S., PESSOA, F. L. P. & ULLER, A. M. C. 2013a. Storage capacity of carbon dioxide hydrates in the presence of sodium dodecyl sulfate (SDS) and tetrahydrofuran (THF). *Chemical Engineering Science,* 96**,** 118-123.

LIRIO, C. F. D. S., PESSOA, F. L. P. & ULLER, A. M. C. 2013b. Storage capacity of carbon dioxide hydrates in the presence of sodium dodecyl sulfate (SDS) and tetrahydrofuran (THF). *Chemical Engineering Science,* 96**,** 118-123.

LIU, N., LIU, D. P. & XIE, Y. M. 2009. Experimental study on CO2 storage by hydrate crystallization. *Zhongguo Dianji Gongcheng Xuebao/Proceedings of the Chinese Society of Electrical Engineering,* 29**,** 36-40.

LOKSHIN, K. A., ZHAO, Y., HE, D., MAO, W. L., MAO, H.-K., HEMLEY, R. J., LOBANOV, M. V. & GREENBLATT, M. 2004. Structure and Dynamics of Hydrogen Molecules in the Novel Clathrate Hydrate by High Pressure Neutron Diffraction. *Physical Review Letters,* 93**,** 125503.

LONG, D., LOVELL, M. A., REES, J. G. & ROCHELLE, C. A. 2009. *Sediment-Hosted Gas Hydrates: New Insights on Natural and Synthetic Systems (Geological Society Special Publication No. 319)*, Geological Society Special Publication.

LU, C., BAI, H., WU, B., SU, F. & HWANG, J. F. 2008. Comparative Study of CO2 Capture by Carbon Nanotubes, Activated Carbons, and Zeolites. *Energy & Fuels,* 22**,** 3050-3056.

LU, H., SEO, Y. T., LEE, J. W., MOUDRAKOVSKI, I., RIPMEESTER, J. A., CHAPMAN, N. R., COFFIN, R. B., GARDNER, G. & POHLMAN, J. 2007. Complex gas hydrate from the Cascadia margin. *Nature,* 445**,** 303-306.

LU, T., ZHANG, Y., LI, X. S., CHEN, Z. Y. & YAN, K. F. 2009. Equilibrium conditions of hydrate formation in the systems of CO2-N2-TBAB and CO2-N2-THF. *Guocheng Gongcheng Xuebao/The Chinese Journal of Process Engineering,* 9**,** 541-544.

LUO, Y. T., ZHU, J. H., FAN, S. S. & CHEN, G. J. 2007. Study on the kinetics of hydrate formation in a bubble column. *Chemical Engineering Science,* 62**,** 1000-1009.

LUZI, M., SCHICKS, J. M., NAUMANN, R. & ERZINGER, J. 2012. Systematic kinetic studies on mixed gas hydrates by Raman spectroscopy and powder X-ray diffraction. *The Journal of Chemical Thermodynamics,* 48**,** 28-35.

LV, Q.-N., LI, X.-S., CHEN, Z.-Y. & FENG, J.-C. 2013. Phase Equilibrium and Dissociation Enthalpies for Hydrates of Various Water-Insoluble Organic Promoters with Methane. *Journal of Chemical & Engineering Data,* 58**,** 3249-3253.

LV, Y. X., YAN, G. H., XU, C. Q. & MIN XU, L. S. 2012. Review on Membrane Technologies for Carbon Dioxide Capture from Power Plant Flue Gas. *Advanced Materials Research,* 602-604**,** 1140-1144.

MA, Q.-L., CHEN, G.-J. & ZHANG, L.-W. 2009. Experimental and Modeling Study on Gas Hydrate Formation Kinetics of (Methane + Ethylene + Tetrahydrofuran + H2O)†. *Journal of Chemical & Engineering Data,* 54**,** 2474-2478.

MAEKAWA, T. 2011. Equilibrium conditions of clathrate hydrates formed from carbon dioxide and aqueous acetone solutions. *Fluid Phase Equilibria,* 303**,** 76-79.

MAEKAWA, T. 2013. Equilibrium conditions of clathrate hydrates formed from xenon and aqueous solutions of acetone, 1,4-dioxane and 1,3-dioxolane. *Fluid Phase Equilibria,* 339**,** 15-19.

MAINUSCH, S., PETERS, C. J., DE SWAAN ARONS, J., JAVANMARDI, J. & MOSHFEGHIAN, M. 1997. Experimental Determination and Modeling of Methane Hydrates in Mixtures of Acetone and Water. *Journal of Chemical & Engineering Data,* 42**,** 948-950.

MAK, T. C. W. & MCMULLAN, R. K. 1965. Polyhedral Clathrate Hydrates. X. Structure of the Double Hydrate of Tetrahydrofuran and Hydrogen Sulfide. *The Journal of Chemical Physics,* 42**,** 2732-2737.

MAKINO, T., NAKAMURA, T., SUGAHARA, T. & OHGAKI, K. 2004. Thermodynamic stability of structure-H hydrates of methylcyclopentane and cyclooctane helped by methane. *Fluid Phase Equilibria,* 218**,** 235-238.

MAKOGON, T. Y., MEHTA, A. P. & SLOAN JR, E. D. 1996. Structure H and structure I hydrate equilibrium data for 2,2-dimethylbutane with methane and xenon. *Journal of Chemical and Engineering Data,* 41**,** 315-318.

MANAKOV, A. Y., DYADIN, Y. A., OGIENKO, A. G., KURNOSOV, A. V., ALADKO, E. Y., LARIONOV, E. G., ZHURKO, F. V., VORONIN, V. I., BERGER, I. F., GORYAINOV, S. V., LIHACHEVA, A. Y. & ANCHAROV, A. I. 2009. Phase Diagram and High-Pressure Boundary of Hydrate Formation in the Carbon Dioxide−Water System. *The Journal of Physical Chemistry B,* 113**,** 7257-7262.

MANDAL, A. & LAIK, S. 2008. Effect of the promoter on gas hydrate formation and dissociation. *Energy and Fuels,* 22**,** 2527-2532.

MANTEGHIAN, M., MOUSAVI SAFAVI, S. M. & MOHAMMADI, A. 2013. The equilibrium conditions, hydrate formation and dissociation rate and storage capacity of ethylene hydrate in presence of 1,4-dioxane. *Chemical Engineering Journal,* 217**,** 379-384.

MARKEWITZ, P., KUCKSHINRICHS, W., LEITNER, W., LINSSEN, J., ZAPP, P., BONGARTZ, R., SCHREIBER, A. & MULLER, T. E. 2012. Worldwide innovations in the development of carbon capture technologies and the utilization of CO2. *Energy & Environmental Science,* 5**,** 7281-7305.

MARSHALL, D. R., SAITO, S. & KOBAYASHI, R. 1964. Hydrates at high pressures: Part I. Methane-water, argon-water, and nitrogen-water systems. *AIChE Journal,* 10**,** 202-205.

MATHIAS, P. M. & COPEMAN, T. W. 1983. Extension of the Peng-Robinson equation of state to complex mixtures: Evaluation of the various forms of the local composition concept. *Fluid Phase Equilibria,* 13**,** 91-108.

MATSUDA, S., TSUDA, H. & MORI, Y. H. 2006. Hydrate formation using water spraying onto a cooled solid surface in a guest gas. *AIChE Journal,* 52**,** 2978-2987.

MATSUMOTO, Y., MAKINO, T., SUGAHARA, T. & OHGAKI, K. 2014. Phase equilibrium relations for binary mixed hydrate systems composed of carbon dioxide and cyclopentane derivatives. *Fluid Phase Equilibria,* 362**,** 379-382.

MATTISSON, T., JOHANSSON, M. & LYNGFELT, A. 2004. Multicycle Reduction and Oxidation of Different Types of Iron Oxide ParticlesApplication to Chemical-Looping Combustion. *Energy & Fuels,* 18**,** 628-637.

MAX, M. D. 2003. *Natural Gas Hydrate in Oceanic and Permafrost Environments*, Springer.

MAX, M. D., JOHNSON, A. H. & DILLON, W. P. 2006. *Economic Geology of Natural Gas Hydrate*, Springer.

MAYOUFI, N., DALMAZZONE, D., DELAHAYE, A., CLAIN, P., FOURNAISON, L. & FÜRST, W. 2011. Experimental Data on Phase Behavior of Simple Tetrabutylphosphonium Bromide (TBPB) and Mixed CO2 + TBPB Semiclathrate Hydrates. *Journal of Chemical & Engineering Data,* 56**,** 2987-2993.

MAYOUFI, N., DALMAZZONE, D., FÜRST, W., DELAHAYE, A. & FOURNAISON, L. 2009. CO2 Enclathration in Hydrates of Peralkyl-(Ammonium/Phosphonium) Salts: Stability Conditions and Dissociation Enthalpies. *Journal of Chemical & Engineering Data,* 55**,** 1271-1275.

MAYOUFI, N., DALMAZZONE, D., FÜRST, W., DELAHAYE, A. & FOURNAISON, L. 2010. CO2 Enclathration in Hydrates of Peralkyl-(Ammonium/Phosphonium) Salts: Stability Conditions and Dissociation Enthalpies. *Journal of Chemical & Engineering Data,* 55**,** 1271-1275.

MCMULLAN, R. K., JORDAN, T. H. & JEFFREY, G. A. 1967. Polyhedral clathrate hydrates. XII. The crystallographic data on hydrates of ethylamine, dimethylamine, trimethylamine, n-propylamine (two forms), iso-propylamine, diethylamine (two forms), and tert-butylamine. *The Journal of Chemical Physics,* 47**,** 1218-1222.

MEHTA, A. P. 1996. *A Thermodynamic Investigation of Structure H Clathrate Hydrates*.

MEHTA, A. P. & SLOAN, E. D. 1994. Thermodynamic model for structure-H hydrates. *AIChE Journal,* 40**,** 312-320.

MEHTA, A. P. & SLOAN JR, E. D. 1994. Structure H hydrate phase equilibria of paraffins, naphthenes, and olefins with methane. *Journal of Chemical and Engineering Data,* 39**,** 887-890.

MEYSEL, P., OELLRICH, L., RAJ BISHNOI, P. & CLARKE, M. A. 2011. Experimental investigation of incipient equilibrium conditions for the formation of semi-clathrate hydrates from quaternary mixtures of (CO2 + N2 + TBAB + H2O). *The Journal of Chemical Thermodynamics,* 43**,** 1475-1479.

MILLER, S. L. & SMYTHE, W. D. 1970. Carbon Dioxide Clathrate in Martian Ice Cap. *Science,* 170**,** 531-&.

MOHAMMADI, A., MANTEGHIAN, M., HAGHTALAB, A., MOHAMMADI, A. H. & RAHMATI-ABKENAR, M. 2014. Kinetic study of carbon dioxide hydrate formation in presence of silver nanoparticles and SDS. *Chemical Engineering Journal,* 237**,** 387-395.

MOHAMMADI, A., MANTEGHIAN, M. & MOHAMMADI, A. H. 2013a. Dissociation Data of Semiclathrate Hydrates for the Systems of Tetra-n-butylammonium Fluoride (TBAF) + Methane + Water, TBAF + Carbon Dioxide + Water, and TBAF + Nitrogen + Water. *Journal of Chemical & Engineering Data,* 58**,** 3545-3550.

MOHAMMADI, A. H., ANDERSON, R. & TOHIDI, B. 2005. Carbon monoxide clathrate hydrates: Equilibrium data and thermodynamic modeling. *AIChE Journal,* 51**,** 2825-2833.

MOHAMMADI, A. H., ESLAMIMANESH, A., BELANDRIA, V. & RICHON, D. 2011a. Phase Equilibria of Semiclathrate Hydrates of CO2, N-2, CH4, or H-2 + Tetra-n-

butylammonium Bromide Aqueous Solution. *Journal of Chemical and Engineering Data,* 56**,** 3855-3865.

MOHAMMADI, A. H., ESLAMIMANESH, A., BELANDRIA, V., RICHON, D., NAIDOO, P. & RAMJUGERNATH, D. 2012a. Phase equilibrium measurements for semi-clathrate hydrates of the (CO2 + N2 + tetra-n-butylammonium bromide) aqueous solution system. *The Journal of Chemical Thermodynamics,* 46**,** 57-61.

MOHAMMADI, A. H., ESLAMIMANESH, A., GHARAGHEIZI, F. & RICHON, D. 2012b. A novel method for evaluation of asphaltene precipitation titration data. *Chemical Engineering Science,* 78**,** 181-185.

MOHAMMADI, A. H., ESLAMIMANESH, A. & RICHON, D. 2013b. Semi-clathrate hydrate phase equilibrium measurements for the CO2+H2/CH4+tetra-n-butylammonium bromide aqueous solution system. *Chemical Engineering Science,* 94**,** 284-290.

MOHAMMADI, A. H., ESLAMIMANESH, A., RICHON, D., GHARAGHEIZI, F., YAZDIZADEH, M., JAVANMARDI, J., HASHEMI, H., ZARIFI, M. & BABAEE, S. 2011b. Gas Hydrate Phase Equilibrium in Porous Media: Mathematical Modeling and Correlation. *Industrial & Engineering Chemistry Research,* 51**,** 1062-1072.

MOHAMMADI, A. H., GHARAGHEIZI, F., ESLAMIMANESH, A. & RICHON, D. 2012c. Evaluation of experimental data for wax and diamondoids solubility in gaseous systems. *Chemical Engineering Science,* 81**,** 1-7.

MOHAMMADI, A. H. & RICHON, D. 2009a. Clathrate Hydrates of Cyclohexane + Hydrogen Sulfide and Cyclohexane + Methane: Experimental Measurements of Dissociation Conditions. *Journal of Chemical & Engineering Data,* 55**,** 1053-1055.

MOHAMMADI, A. H. & RICHON, D. 2009b. Development of predictive techniques for estimating liquid water-hydrate equilibrium of water-hydrocarbon system. *Journal of Thermodynamics, Hindawi Publishing Corporation,* 2009**,** 1-12.

MOHAMMADI, A. H. & RICHON, D. 2009c. Phase Equilibria of Clathrate Hydrates of Cyclopentane + Hydrogen Sulfide and Cyclopentane + Methane. *Industrial & Engineering Chemistry Research,* 48**,** 9045-9048.

MOHAMMADI, A. H. & RICHON, D. 2009d. Phase equilibria of clathrate hydrates of methyl cyclopentane, methyl cyclohexane, cyclopentane or cyclohexane+carbon dioxide. *Chemical Engineering Science,* 64**,** 5319-5322.

MOHAMMADI, A. H. & RICHON, D. 2009e. Phase Equilibria of Clathrate Hydrates of Tetrahydrofuran + Hydrogen Sulfide and Tetrahydrofuran + Methane. *Industrial & Engineering Chemistry Research,* 48**,** 7838-7841.

MOHAMMADI, A. H. & RICHON, D. 2010a. Equilibrium Data of Methyl Cyclohexane + Hydrogen Sulfide and Methyl Cyclohexane + Methane Clathrate Hydrates. *Journal of Chemical & Engineering Data,* 55**,** 566-569.

MOHAMMADI, A. H. & RICHON, D. 2010b. Hydrate phase equilibria for hydrogen+water and hydrogen+tetrahydrofuran+water systems: Predictions of dissociation conditions using an artificial neural network algorithm. *Chemical Engineering Science,* 65**,** 3352-3355.

MOHAMMADI, A. H. & RICHON, D. 2011. Phase equilibria of binary clathrate hydrates of nitrogen+cyclopentane/cyclohexane/methyl cyclohexane and ethane+cyclopentane/cyclohexane/methyl cyclohexane. *Chemical Engineering Science,* 66**,** 4936-4940.

MOHAMMADI, A. H., TOHIDI, B. & BURGASS, R. W. 2003. Equilibrium Data and Thermodynamic Modeling of Nitrogen, Oxygen, and Air Clathrate Hydrates. *Journal of Chemical & Engineering Data,* 48**,** 612-616.

MOLDENHAUER, P., RYDEN, M., MATTISSON, T. & LYNGFELT, A. 2012. Chemical-looping combustion and chemical-looping with oxygen uncoupling of kerosene with Mn- and Cu-based oxygen carriers in a circulating fluidized-bed 300 W laboratory reactor. *Fuel Processing Technology,* 104**,** 378-389.

MONDAL, M. K., BALSORA, H. K. & VARSHNEY, P. 2012. Progress and trends in CO2 capture/separation technologies: A review. *Energy,* 46**,** 431-441.

MOOIJER-VAN DEN HEUVEL, M. M., PETERS, C. J. & DE SWAAN ARONS, J. 2000. Influence of water-insoluble organic components on the gas hydrate equilibrium conditions of methane. *Fluid Phase Equilibria,* 172**,** 73-91.

MOOIJER-VAN DEN HEUVEL, M. M., WITTEMAN, R. & PETERS, C. J. 2001. Phase behaviour of gas hydrates of carbon dioxide in the presence of tetrahydropyran, cyclobutanone, cyclohexane and methylcyclohexane. *Fluid Phase Equilibria,* 182**,** 97-110.

MUROMACHI, S., TAKEYA, S., YAMAMOTO, Y. & OHMURA, R. 2014. Characterization of tetra-n-butylphosphonium bromide semiclathrate hydrate by crystal structure analysis. *CrystEngComm,* 16**,** 2056-2060.

NAGAI, Y., YOSHIOKA, H., OTA, M., SATO, Y., INOMATA, H., SMITH, R. L. & PETERS, C. J. 2008. Binary hydrogen-tetrahydrofuran clathrate hydrate formation kinetics and models. *AIChE Journal,* 54**,** 3007-3016.

NAKAMURA, T., MAKINO, T., SUGAHARA, T. & OHGAKI, K. Stability boundaries of gas hydrates helped by methane-structure-H hydrates of methylcyclohexane and cis-1,2-dimethylcyclohexane. *Chem. Eng. Sci.,* 58**,** 269-273.

NAKAMURA, T., MAKINO, T., SUGAHARA, T. & OHGAKI, K. 2003. Stability boundaries of gas hydrates helped by methane - Structure-H hydrates of methylcyclohexane and cis-1,2-dimethylcyclohexane. *Chemical Engineering Science,* 58**,** 269-273.

NAKANO, S., MORITOKI, M. & OHGAKI, K. 1998. High-Pressure Phase Equilibrium and Raman Microprobe Spectroscopic Studies on the CO2 Hydrate System. *Journal of Chemical & Engineering Data,* 43**,** 807-810.

NELDER, J. A. & MEAD, R. 1965. A Simplex Method for Function Minimization. *The Computer Journal,* 7**,** 308-313.

NG, H.-J. & ROBINSON, D. B. 1977. The prediction of hydrate formation in condensed systems. *AIChE Journal,* 23**,** 477-482.

NG, H.-J. & ROBINSON, D. B. 1985a. Hydrate formation in systems containing methane, ethane, propane, carbon dioxide or hydrogen sulfide in the presence of methanol. *Fluid Phase Equilibria,* 21**,** 145-155.

NG, H. J. & ROBINSON, D. B. 1976. Measurement and Prediction of Hydrate Formation in Liquid Hydrocarbon-Water Systems. *Industrial & Engineering Chemistry Fundamentals,* 15**,** 293-298.

NG, H. J. & ROBINSON, D. B. 1985b. Hydrate Formation in Systems Containing Methane, Ethane, Propane, Carbon-Dioxide or Hydrogen-Sulfide in the Presence of Methanol. *Fluid Phase Equilibria,* 21**,** 145-155.

NG, H. J. & ROBINSON, D. B. 1994. New Developments in the Measurement and Prediction of Hydrate Formation for Processing Needs. *Annals of the New York Academy of Sciences,* 715**,** 450-462.

NGEMA, P. T., NELSON, W. M., NAIDOO, P., RAMJUGERNATH, D. & RICHON, D. 2014. Isothermal method for hydrate studies using a transparent variable volume cell. *Review of Scientific Instruments,* 85**,** 045123.

OGATA, K., HASHIMOTO, S., SUGAHARA, T., MORITOKI, M., SATO, H. & OHGAKI, K. 2008. Storage capacity of hydrogen in tetrahydrofuran hydrate. *Chemical Engineering Science,* 63**,** 5714-5718.

OHGAKI, K., MAKIHARA, Y. & TAKANO, K. 1993. Formation of CO_2 hydrate in pure and sea waters. *J. Chem. Eng. Jpn.,* 26 (5)**,** 558–564.

OHGAKI, K., TAKANO, K., SANGAWA, H., MATSUBARA, T. & NAKANO, S. 1996. Methane Exploitation by Carbon Dioxide from Gas Hydrates—Phase Equilibria for CO2-CH4 Mixed Hydrate System—. *JOURNAL OF CHEMICAL ENGINEERING OF JAPAN,* 29**,** 478-483.

OHMURA, R., KASHIWAZAKI, S., SHIOTA, S., TSUJI, H. & MORI, Y. H. 2002. Structure-I and Structure-H Hydrate Formation Using Water Spraying. *Energy & Fuels,* 16**,** 1141-1147.

OHMURA, R., MATSUDA, S., UCHIDA, T., EBINUMA, T. & NARITA, H. 2005. Phase equilibrium for structure-H hydrates at temperatures below the freezing point of water. *Journal of Chemical and Engineering Data,* 50**,** 993-996.

OKUTANI, K., KUWABARA, Y. & MORI, Y. H. 2008. Surfactant effects on hydrate formation in an unstirred gas/liquid system: An experimental study using methane and sodium alkyl sulfates. *Chemical Engineering Science,* 63**,** 183-194.

OLAJIRE, A. A. 2010. CO2 capture and separation technologies for end-of-pipe applications – A review. *Energy,* 35**,** 2610-2628.

ORR, J. F. M. 2009. CO2 capture and storage: are we ready? *Energy & Environmental Science,* 2**,** 449-458.

ØSTERGAARD, K. K., TOHIDI, B., BURGASS, R. W., DANESH, A. & TODD, A. C. 2001. Hydrate Equilibrium Data of Multicomponent Systems in the Presence of Structure-II and Structure-H Heavy Hydrate Formers. *Journal of Chemical & Engineering Data,* 46**,** 703-708.

PARK, J., SEO, Y.-T., LEE, J.-W. & LEE, H. 2006. Spectroscopic analysis of carbon dioxide and nitrogen mixed gas hydrates in silica gel for CO2 separation. *Catalysis Today,* 115**,** 279-282.

PARK, S.-S., AN, E.-J., LEE, S.-B., CHUN, W.-G. & KIM, N.-J. 2012. Characteristics of methane hydrate formation in carbon nanofluids. *Journal of Industrial and Engineering Chemistry,* 18**,** 443-448.

PARK, S.-S., LEE, S.-B. & KIM, N.-J. 2010. Effect of multi-walled carbon nanotubes on methane hydrate formation. *Journal of Industrial and Engineering Chemistry,* 16**,** 551-555.

PARK, S., LEE, S., LEE, Y., LEE, Y. & SEO, Y. 2013a. Hydrate-based pre-combustion capture of carbon dioxide in the presence of a thermodynamic promoter and porous silica gels. *International Journal of Greenhouse Gas Control,* 14**,** 193-199.

PARK, S., LEE, S., LEE, Y., LEE, Y. & SEO, Y. 2013b. Hydrate-based pre-combustion capture of carbon dioxide in the presence of a thermodynamic promoter and porous silica gels. *International Journal of Greenhouse Gas Control,* 14**,** 193-199.

PARK, S., LEE, S., LEE, Y. & SEO, Y. 2013c. CO2 Capture from Simulated Fuel Gas Mixtures Using Semiclathrate Hydrates Formed by Quaternary Ammonium Salts. *Environmental Science & Technology,* 47**,** 7571-7577.

PARRISH, W. R. & PRAUSNITZ, J. M. 1972. Dissociation Pressures of Gas Hydrates Formed by Gas Mixtures. *Industrial & Engineering Chemistry Process Design and Development,* 11**,** 26-35.

PARTOON, B. & JAVANMARDI, J. 2013. Effect of Mixed Thermodynamic and Kinetic Hydrate Promoters on Methane Hydrate Phase Boundary and Formation Kinetics. *Journal of Chemical & Engineering Data,* 58**,** 501-509.

PAULING, L. & MARSH, R. E. 1952. The Structure of Chlorine Hydrate. *Proceedings of the National Academy of Sciences,* 38**,** 112-118.

PELCKMANS, K., SUYKENS, J. A. K., VAN GESTEL, T., DE BRABANTER, D., LUKAS, L., HAMERS, B., DE MOOR, B. & VANDEWALLE, J. 2002. LS-SVMlab: A Matlab/C Toolbox for Least Squares Support Vector Machines. *LS-SVMlab: A Matlab/C Toolbox for Least Squares Support Vector Machines.*

PENG, D.-Y. & ROBINSON, D. B. 1976. A New Two-Constant Equation of State. *Industrial & Engineering Chemistry Fundamentals,* 15**,** 59-64.

POWELL, C. E. & QIAO, G. G. 2006. Polymeric CO2/N2 gas separation membranes for the capture of carbon dioxide from power plant flue gases. *Journal of Membrane Science,* 279**,** 1-49.

PRAUSNITZ, J. M. & CHUEH, P. L. 1968. *Computer calculations for high-pressure vapor-liquid equilibria*, Englewood Cliffs, N.J., Prentice-Hall.

RAMDIN, M., DE LOOS, T. W. & VLUGT, T. J. H. 2012. State-of-the-Art of CO2 Capture with Ionic Liquids. *Industrial & Engineering Chemistry Research,* 51**,** 8149-8177.

RAO, A. B. & RUBIN, E. S. 2002. A Technical, Economic, and Environmental Assessment of Amine-Based CO2 Capture Technology for Power Plant Greenhouse Gas Control. *Environmental Science & Technology,* 36**,** 4467-4475.

RENON, H. & PRAUSNITZ, J. M. 1968. Liquid-Liquid and Vapor-Liquid Equilibria for Binary and Ternary Systems with Dibutyl Ketone, Dimethyl Sulfoxide, n-Hexane, and 1-Hexene. *Industrial & Engineering Chemistry Process Design and Development,* 7**,** 220-225.

RICAURTE, M., DICHARRY, C., BROSETA, D., RENAUD, X. & TORRÉ, J.-P. 2013a. CO2 Removal from a CO2–CH4 Gas Mixture by Clathrate Hydrate Formation Using THF and SDS as Water-Soluble Hydrate Promoters. *Industrial & Engineering Chemistry Research,* 52**,** 899-910.

RICAURTE, M., DICHARRY, C., BROSETA, D., RENAUD, X. & TORRÉ, J. P. 2013b. CO2 removal from a CO2-CH4 gas mixture by clathrate hydrate formation using THF and SDS as water-soluble hydrate promoters. *Industrial and Engineering Chemistry Research,* 52**,** 899-910.

RICE, W. 2006. Hydrogen production from methane hydrate with sequestering of carbon dioxide. *International Journal of Hydrogen Energy,* 31**,** 1955-1963.

RIPMEESTER, J. A., TSE, J. S., RATCLIFFE, C. I. & POWELL, B. M. 1987. A new clathrate hydrate structure. *Nature,* 325**,** 135-136.

ROSSI, F., FILIPPONI, M. & CASTELLANI, B. 2012. Investigation on a novel reactor for gas hydrate production. *Applied Energy,* 99**,** 167-172.

ROUSSEEUW, P. J. & LEROY, A. M. 1987. *Robust Regression and Outlier Detection.*

ROVETTO, L. J., STROBEL, T. A., KOH, C. A. & SLOAN JR, E. D. 2006. Is gas hydrate formation thermodynamically promoted by hydrotrope molecules? *Fluid Phase Equilibria,* 247**,** 84-89.

ROWSELL, J. L. C. & YAGHI, O. M. 2004. Metal–organic frameworks: a new class of porous materials. *Microporous and Mesoporous Materials,* 73**,** 3-14.

SABIL, K. M., WITKAMP, G. J. & PETERS, C. J. 2010a. Estimations of enthalpies of dissociation of simple and mixed carbon dioxide hydrates from phase equilibrium data. *Fluid Phase Equilibria,* 290**,** 109-114.

SABIL, K. M., WITKAMP, G. J. & PETERS, C. J. 2010b. Phase equilibria in ternary (carbon dioxide + tetrahydrofuran + water) system in hydrate-forming region: Effects of carbon dioxide concentration and the occurrence of pseudo-retrograde hydrate phenomenon. *Journal of Chemical Thermodynamics,* 42**,** 8-16.

SAITO, S., KAWASAKI, T., OKUI, T., KONDO, T. & HIRAOKA, R. 1996a. *Proceedings of the 2nd International Conference On National Gas Hydrates*.

SAITO, Y., KAWASAKI, T., OKUI, T., KONDO, T. & HIRAOKA, R. 1996b. Methane storage in hydrate phase with soluble guests. *2nd International Conference on Nature Gas Hydrate.* Toulouse, 2–6 June.

SALEH, B. & WENDLAND, M. 2005. Measurement of Vapor Pressures and Saturated Liquid Densities of Pure Fluids with a New Apparatus. *Journal of Chemical & Engineering Data,* 50**,** 429-437.

SAMANTA, A., ZHAO, A., SHIMIZU, G. K. H., SARKAR, P. & GUPTA, R. 2011. Post-Combustion CO2 Capture Using Solid Sorbents: A Review. *Industrial & Engineering Chemistry Research,* 51**,** 1438-1463.

SATO, K., TOKUTOMI, H. & OHMURA, R. 2013. Phase equilibrium of ionic semiclathrate hydrates formed with tetrabutylammonium bromide and tetrabutylammonium chloride. *Fluid Phase Equilibria,* 337**,** 115-118.

SCHICKS, J. M. 2010. Gas hydrates. *Annual Reports Section "C" (Physical Chemistry),* 106**,** 101-117.

SCHICKS, J. M. & LUZI-HELBING, M. 2013. Cage occupancy and structural changes during hydrate formation from initial stages to resulting hydrate phase. *Spectrochimica Acta Part A: Molecular and Biomolecular Spectroscopy,* 115**,** 528-536.

SEO, Y.-T., KANG, S.-P., LEE, H., LEE, C.-S. & SUNG, W.-M. 2000. Hydrate phase equilibria for gas mixtures containing carbon dioxide: A proof-of-concept to carbon dioxide recovery from multicomponent gas stream. *Korean Journal of Chemical Engineering,* 17**,** 659-667.

SEO, Y.-T. & LEE, H. 2003. Structure and Guest Distribution of the Mixed Carbon Dioxide and Nitrogen Hydrates As Revealed by X-ray Diffraction and 13C NMR Spectroscopy. *The Journal of Physical Chemistry B,* 108**,** 530-534.

SEO, Y.-T. & LEE, H. 2004. Structure and Guest Distribution of the Mixed Carbon Dioxide and Nitrogen Hydrates As Revealed by X-ray Diffraction and 13C NMR Spectroscopy. *The Journal of Physical Chemistry B,* 108**,** 530-534.

SEO, Y.-T., MOUDRAKOVSKI, I. L., RIPMEESTER, J. A., LEE, J.-W. & LEE, H. 2005. Efficient Recovery of CO2 from Flue Gas by Clathrate Hydrate Formation in Porous Silica Gels. *Environmental Science & Technology,* 39**,** 2315-2319.

SEO, Y. & KANG, S.-P. 2010. Enhancing CO2 separation for pre-combustion capture with hydrate formation in silica gel pore structure. *Chemical Engineering Journal,* 161**,** 308-312.

SEO, Y., KANG, S.-P., LEE, S. & LEE, H. 2008a. Experimental Measurements of Hydrate Phase Equilibria for Carbon Dioxide in the Presence of THF, Propylene Oxide, and 1,4-Dioxane. *Journal of Chemical & Engineering Data,* 53**,** 2833-2837.

SEO, Y., KANG, S. P., LEE, S. & LEE, H. 2008b. Experimental Measurements of Hydrate Phase Equilibria for Carbon Dioxide in the Presence of THF, Propylene Oxide, and 1,4-Dioxane. *Journal of Chemical & Engineering Data,* 53**,** 2833-2837.

SEO, Y., LEE, H. & UCHIDA, T. 2002. Methane and Carbon Dioxide Hydrate Phase Behavior in Small Porous Silica Gels: Three-Phase Equilibrium Determination and Thermodynamic Modeling. *Langmuir,* 18**,** 9164-9170.

SEO, Y., LEE, S., CHA, I., LEE, J. D. & LEE, H. 2009. Phase Equilibria and Thermodynamic Modeling of Ethane and Propane Hydrates in Porous Silica Gels. *The Journal of Physical Chemistry B,* 113**,** 5487-5492.

SEO, Y. T., KANG, S. P. & LEE, H. 2001a. Experimental determination and thermodynamic modeling of methane and nitrogen hydrates in the presence of THF, propylene oxide, 1,4-dioxane and acetone. *Fluid Phase Equilibria,* 189**,** 99-110.

SEO, Y. T. & LEE, H. 2001. Multiple-phase hydrate equilibria of the ternary carbon dioxide, methane, and water mixtures. *Journal of Physical Chemistry B,* 105**,** 10084-10090.

SEO, Y. T., LEE, H. & YOON, J. H. 2001b. Hydrate phase equilibria of the carbon dioxide, methane, and water system. *Journal of Chemical and Engineering Data,* 46**,** 381-384.

SERVIO, P. & ENGLEZOS, P. 2001. Effect of temperature and pressure on the solubility of carbon dioxide in water in the presence of gas hydrate. *Fluid Phase Equilibria,* 190**,** 127-134.

SFAXI, I. B. A., DURAND, I., LUGO, R., MOHAMMADI, A. H. & RICHON, D. 2014. Hydrate phase equilibria of CO2 + N2 + aqueous solution of THF, TBAB or TBAF system. *International Journal of Greenhouse Gas Control,* 26**,** 185-192.

SHAH, K., MOGHTADERI, B. & WALL, T. 2012. Selection of Suitable Oxygen Carriers for Chemical Looping Air Separation: A Thermodynamic Approach. *Energy & Fuels,* 26**,** 2038-2045.

SHEN, L., WU, J., GAO, Z. & XIAO, J. 2010. Characterization of chemical looping combustion of coal in a 1 kWth reactor with a nickel-based oxygen carrier. *Combustion and Flame,* 157**,** 934-942.

SHI, L.-L., LIANG, D.-Q. & LI, D.-L. 2013. Phase Equilibrium Data of Tetrabutylphosphonium Bromide Plus Carbon Dioxide or Nitrogen Semiclathrate Hydrates. *Journal of Chemical & Engineering Data,* 58**,** 2125-2130.

SHI, L.-L., LIANG, D.-Q. & LI, D.-L. 2014. Phase equilibrium conditions for simulated landfill gas hydrate formation in aqueous solutions of tetrabutylammonium nitrate. *The Journal of Chemical Thermodynamics,* 68**,** 322-326.

SHIMADA, W., SHIRO, M., KONDO, H., TAKEYA, S., OYAMA, H., EBINUMA, T. & NARITA, H. 2005. Tetra-n-butylammonium bromide-water (1/38). *Acta Crystallographica Section C,* 61**,** o65-o66.

SHIN, K., CHA, J.-H., SEO, Y. & LEE, H. 2010. Physicochemical Properties of Ionic Clathrate Hydrates. *Chemistry – An Asian Journal,* 5**,** 22-34.

SHUKER, M. T. & ISMAIL, F. B. 2012. Predicting of Solid-Vapor-Liquid Equilibrium in Natural Gas Using ANNs. *International Petroleum Technology Conference.* Bankok, Thailand.

SLOAN, E. D. 2008a. *Clathrate hydrates of natural gases*, Marcel Dekker.

SLOAN, E. D. (ed.) 2008b. *Clathrate Hydrates of Natural Gases, Third Edition,* Golden, Colorado, U.S.A: CRC Press.

SLOAN, E. D. & KOH, C. A. 2008. *Clathrate hydrates of natural gases,* Boca Raton, FL, CRC Press.

SONG, C.-F., KITAMURA, Y., LI, S.-H. & JIANG, W.-Z. 2013a. Analysis of CO2 frost formation properties in cryogenic capture process. *International Journal of Greenhouse Gas Control,* 13**,** 26-33.

SONG, C.-F., KITAMURA, Y., LI, S.-H. & OGASAWARA, K. 2012. Design of a cryogenic CO2 capture system based on Stirling coolers. *International Journal of Greenhouse Gas Control,* 7**,** 107-114.

SONG, Q., LIU, W., BOHN, C. D., HARPER, R. N., SIVANIAH, E., SCOTT, S. A. & DENNIS, J. S. 2013b. A high performance oxygen storage material for chemical looping processes with CO2 capture. *Energy & Environmental Science,* 6**,** 288-298.

SONG, Y., WANG, X., YANG, M., JIANG, L., LIU, Y., DOU, B., ZHAO, J. & WANG, S. 2013c. Study of Selected Factors Affecting Hydrate-Based Carbon Dioxide Separation from Simulated Fuel Gas in Porous Media. *Energy & Fuels,* 27**,** 3341-3348.

STROBEL, T. A., HESTER, K. C., KOH, C. A., SUM, A. K. & SLOAN JR, E. D. 2009a. Properties of the clathrates of hydrogen and developments in their applicability for hydrogen storage. *Chemical Physics Letters,* 478**,** 97-109.

STROBEL, T. A., KOH, C. A. & SLOAN, E. D. 2009b. Thermodynamic predictions of various tetrahydrofuran and hydrogen clathrate hydrates. *Fluid Phase Equilibria,* 280**,** 61-67.

SU, F., LU, C., KUO, S.-C. & ZENG, W. 2010. Adsorption of CO2 on Amine-Functionalized Y-Type Zeolites. *Energy & Fuels,* 24**,** 1441-1448.

SUGAHARA, K., TANAKA, Y., SUGAHARA, T. & OHGAKI, K. 2002. Thermodynamic stability and structure of nitrogen hydrate crystal. *J. Supramol. Chem.,* 2**,** 365–368.

SUGAHARA, T., HAAG, J. C., PRASAD, P. S. R., WARNTJES, A. A., SLOAN, E. D., SUM, A. K. & KOH, C. A. 2009. Increasing Hydrogen Storage Capacity Using Tetrahydrofuran. *Journal of the American Chemical Society,* 131**,** 14616-14617.

SUGAHARA, T., MURAYAMA, S., HASHIMOTO, S. & OHGAKI, K. 2005. Phase equilibria for H2 + CO2 + H2O system containing gas hydrates. *Fluid Phase Equilibria,* 233**,** 190-193.

SUGINAKA, T., SAKAMOTO, H., IINO, K., SAKAKIBARA, Y. & OHMURA, R. 2013. Phase equilibrium for ionic semiclathrate hydrate formed with CO2, CH4, or N2 plus tetrabutylphosphonium bromide. *Fluid Phase Equilibria,* 344**,** 108-111.

SUGINAKA, T., SAKAMOTO, H., IINO, K., TAKEYA, S., NAKAJIMA, M. & OHMURA, R. 2012. Thermodynamic properties of ionic semiclathrate hydrate formed with tetrabutylphosphonium bromide. *Fluid Phase Equilibria,* 317**,** 25-28.

SUMIDA, K., ROGOW, D. L., MASON, J. A., MCDONALD, T. M., BLOCH, E. D., HERM, Z. R., BAE, T.-H. & LONG, J. R. 2011. Carbon Dioxide Capture in Metal–Organic Frameworks. *Chemical Reviews,* 112**,** 724-781.

SUN, C.-Y., CHEN, G.-J. & ZHANG, L.-W. 2010. Hydrate phase equilibrium and structure for (methane + ethane + tetrahydrofuran + water) system. *The Journal of Chemical Thermodynamics,* 42**,** 1173-1179.

SUN, Q., CHEN, G., GUO, X. & LIU, A. Experiments on the continuous separation of gas mixtures via dissolution and hydrate formation in the presence of THF. *Fluid Phase Equilibria*.

SUN, R. & DUAN, Z. H. 2005. Prediction of CH4 and CO2 hydrate phase equilibrium and cage occupancy from ab initio intermolecular potentials. *Geochimica Et Cosmochimica Acta,* 69**,** 4411-4424.

SUN, Z.-G., FAN, S.-S., GUO, K.-H., SHI, L., GUO, Y.-K. & WANG, R.-Z. 2002. Gas Hydrate Phase Equilibrium Data of Cyclohexane and Cyclopentane. *Journal of Chemical & Engineering Data,* 47**,** 313-315.

SUN, Z.-G. & LIU, C.-G. 2012. Equilibrium Conditions of Methane in Semiclathrate Hydrates of Tetra-n-butylammonium Chloride. *Journal of Chemical & Engineering Data,* 57**,** 978-981.

SUN, Z.-G., MA, R.-S., WANG, R.-Z., GUO, K.-H. & FA, S.-S. 2003a. Experimental Studying of Additives Effects on Gas Storage in Hydrates. *Energy & Fuels,* 17**,** 1180-1185.

SUN, Z.-G., WANG, R., MA, R., GUO, K. & FAN, S. 2003b. Natural gas storage in hydrates with the presence of promoters. *Energy Conversion and Management,* 44**,** 2733-2742.

SUN, Z. G., LIU, C. G., ZHOU, B. & XU, L. Z. 2011. Phase Equilibrium and Latent Heat of Tetra-n-butylammonium Chloride Semi-Clathrate Hydrate. *Journal of Chemical and Engineering Data,* 56**,** 3416-3418.

SUROVTSEVA, D., AMIN, R. & BARIFCANI, A. 2011. Design and operation of pilot plant for CO2 capture from IGCC flue gases by combined cryogenic and hydrate method. *Chemical Engineering Research and Design,* 89**,** 1752-1757.

SUYKENS, J. A. K. & VANDEWALLE, J. 1999. Least squares support vector machine classifiers. *Neural Processing Letters,* 9**,** 293-300.

TAKEYA, S., HONDOH, T. & UCHIDA, T. 2000. In Situ Observation of CO2 Hydrate by X-ray Diffraction. *Annals of the New York Academy of Sciences,* 912**,** 973-982.

TAKEYA, S., YONEYAMA, A., UEDA, K., MIMACHI, H., TAKAHASHI, M., SANO, K., HYODO, K., TAKEDA, T. & GOTOH, Y. 2012. Anomalously Preserved Clathrate Hydrate of Natural Gas in Pellet Form at 253 K. *The Journal of Physical Chemistry C,* 116**,** 13842-13848.

TAN, Q., QIN, W., CHEN, Q., DONG, C., LI, W. & YANG, Y. 2012. Synergetic effect of ZrO2 on the oxidation–reduction reaction of Fe2O3 during chemical looping combustion. *Applied Surface Science,* 258**,** 10022-10027.

TANG, J., ZENG, D., WANG, C., CHEN, Y., HE, L. & CAI, N. Study on the influence of SDS and THF on hydrate-based gas separation performance. *Chemical Engineering Research and Design*.

TANG, J., ZENG, D., WANG, C., CHEN, Y., HE, L. & CAI, N. 2013. Study on the influence of SDS and THF on hydrate-based gas separation performance. *Chemical Engineering Research and Design*.

TAYLOR, C. E. & KWAN, J. T. 2010. *Advances in the Studies of Gas Hydrates*, Springer.

THAKUR, N. K. & RAJPUT, S. 2011. *Exploration of gas hydrates : geophysical techniques*, Springer.

THIRUVENKATACHARI, R., SU, S., AN, H. & YU, X. X. 2009. Post combustion CO2 capture by carbon fibre monolithic adsorbents. *Progress in Energy and Combustion Science,* 35**,** 438-455.

THOMAS, M. & BEHAR, E. 1995. Structure H hydrate equilibria of methane and intermediate hydrocarbon molecules. *Proc. 73rd Gas Processors Association Convention*.

THOMSON, G. W. 1946. The Antoine Equation for Vapor-pressure Data. *Chemical Reviews,* 38**,** 1-39.

TOHIDI, B., BURGASS, R. W., DANESH, A., ØSTERGAARD, K. K. & TODD, A. C. 2000. Improving the Accuracy of Gas Hydrate Dissociation Point Measurements. *Annals of the New York Academy of Sciences,* 912**,** 924-931.

TOHIDI, B., DANESH, A., BURGASS, R. & TODD, A. 1996. Hydrate equilibrium data and thermodynamic modelling of methylcyclopentane and methylcyclohexane. *Proc. Second International Conference on Natural Gas Hydrates, Toulouse, 2-6 June*.

TOHIDI, B., DANESH, A., TABATABAEI, A. R. & TODD, A. C. 1997a. Vapor−Hydrate Equilibrium Ratio Charts for Heavy Hydrocarbon Compounds. 1. Structure-II Hydrates: Benzene, Cyclopentane, Cyclohexane, and Neopentane. *Industrial & Engineering Chemistry Research,* 36**,** 2871-2874.

TOHIDI, B., DANESH, A., TODD, A. C. & BURGASS, R. W. 1997b. Hydrate-free zone for synthetic and real reservoir fluids in the presence of saline water. *Chemical Engineering Science,* 52**,** 3257-3263.

TOHIDI, B., DANESH, A., TODD, A. C. & BURGASS, R. W. 2002. Application of quartz crystal microbalance to gas hydrate stability zone measurements. *4th International Conference on Gas Hydrates.*

TOHIDI, B., DANESH, A., TODD, A. C., BURGASS, R. W. & ØSTERGAARD, K. K. 1997c. Equilibrium data and thermodynamic modelling of cyclopentane and neopentane hydrates. *Fluid Phase Equilibria,* 138**,** 241-250.

TORRÉ, J. P., DICHARRY, C., RICAURTE, M., DANIEL-DAVID, D. & BROSETA, D. 2011. CO2 capture by hydrate formation in quiescent conditions: In search of efficient kinetic additives. *Energy Procedia,* 4**,** 621-628.

TORRE, J. P., RICAURTE, M., DICHARRY, C. & BROSETA, D. 2012. CO2 enclathration in the presence of water-soluble hydrate promoters: Hydrate phase equilibria and kinetic studies in quiescent conditions. *Chemical Engineering Science,* 82**,** 1-13.

TOWNSON, I., WALKER, V. K., RIPMEESTER, J. A. & ENGLEZOS, P. 2012. Bacterial Inhibition of Methane Clathrate Hydrates Formed in a Stirred Autoclave. *Energy & Fuels,* 26**,** 7170-7175.

TRUEBA, A. T., RADOVIC, I. R., ZEVENBERGEN, J. F., KROON, M. C. & PETERS, C. J. 2012. Kinetics measurements and in situ Raman spectroscopy of formation of hydrogen-tetrabutylammonium bromide semi-hydrates. *International Journal of Hydrogen Energy,* 37**,** 5790-5797.

TRUEBA, A. T., RADOVIĆ, I. R., ZEVENBERGEN, J. F., PETERS, C. J. & KROON, M. C. 2013. Kinetic measurements and in situ Raman spectroscopy study of the formation of TBAF semi-hydrates with hydrogen and carbon dioxide. *International Journal of Hydrogen Energy,* 38**,** 7326-7334.

TRUEBA, A. T., ROVETTO, L. J., FLORUSSE, L. J., KROON, M. C. & PETERS, C. J. 2011. Phase equilibrium measurements of structure II clathrate hydrates of hydrogen with various promoters. *Fluid Phase Equilibria,* 307**,** 6-10.

UCHIDA, T., EBINUMA, T. & ISHIZAKI, T. 1999. Dissociation Condition Measurements of Methane Hydrate in Confined Small Pores of Porous Glass. *The Journal of Physical Chemistry B,* 103**,** 3659-3662.

UCHIDA, T., IKEDA, I. Y., TAKEYA, S., KAMATA, Y., OHMURA, R., NAGAO, J., ZATSEPINA, O. Y. & BUFFETT, B. A. 2005. Kinetics and Stability of CH4–CO2 Mixed Gas Hydrates during Formation and Long-Term Storage. *ChemPhysChem,* 6**,** 646-654.

UCHIDA, T., TAKAGI, A., KAWABATA, J., MAE, S. & HONDOH, T. 1995. Raman spectroscopic analyses of the growth process of CO2 hydrates. *Energy Conversion and Management,* 36**,** 547-550.

UDACHIN, K. A., ENRIGHT, G. D., RATCLIFFE, C. I. & RIPMEESTER, J. A. 1997. Structure, Stoichiometry, and Morphology of Bromine Hydrate†. *Journal of the American Chemical Society,* 119**,** 11481-11486.

UDACHIN, K. A., RATCLIFFE, C. I. & RIPMEESTER, J. A. 2001. Structure, Composition, and Thermal Expansion of CO2 Hydrate from Single Crystal X-ray Diffraction Measurements†. *The Journal of Physical Chemistry B,* 105**,** 4200-4204.

UNRUH, C. H. & KATZ, D. L. 1949. GAS HYDRATES OF CARBON DIOXIDE METHANE MIXTURES. *Transactions of the American Institute of Mining and Metallurgical Engineers,* 186**,** 83-86.

VANDERWAALS, J. H. & PLATTEEUW, J. C. 1959. Clathrate Solutions. *Advances in Chemical Physics,* 2**,** 1-57.

VERRETT, J., POSTERARO, D. & SERVIO, P. 2012. Surfactant effects on methane solubility and mole fraction during hydrate growth. *Chemical Engineering Science,* 84**,** 80-84.

VON STACKELBERG, M. 1949. Solid gas hydrates. *Naturwissenschaften,* 11-12**,** 1–22

WAALS, J. H. V. D. & PLATTEEUW, J. C. 1959. Clathrate Solutions. *Advances in Chemical Physics.* John Wiley & Sons, Inc.

WALSH, M. R., KOH, C. A., SLOAN, E. D., SUM, A. K. & WU, D. T. 2009. Microsecond Simulations of Spontaneous Methane Hydrate Nucleation and Growth. *Science,* 326**,** 1095-1098.

WANG, B., CÔTÉ, A. P., FURUKAWA, H., O'KEEFFE, M. & YAGHI, O. M. 2008a. Colossal cages in zeolitic imidazolate frameworks as selective carbon dioxide reservoirs. *Nature,* 453**,** 207-211.

WANG, M., LAWAL, A., STEPHENSON, P., SIDDERS, J. & RAMSHAW, C. 2011. Post-combustion CO2 capture with chemical absorption: A state-of-the-art review. *Chemical Engineering Research and Design,* 89**,** 1609-1624.

WANG, X.-L., SUN, C.-Y., YANG, L.-Y., MA, Q.-L., TANG, X.-L., ZHAO, H.-W. & CHEN, G.-J. 2008b. Vapor−Hydrate Equilibria for the Methane + Hydrogen + Tetrahydrofuran + Water System†. *Journal of Chemical & Engineering Data,* 54**,** 310-313.

WILCOX, W. I., CARSON, D. B. & KATZ, D. L. 1941. Natural gas hydrates. *Industrial and Engineering Chemistry,* 33**,** 662-713.

WU, R., KOZIELSKI, K. A., HARTLEY, P. G., MAY, E. F., BOXALL, J. & MAEDA, N. 2013. Probability distributions of gas hydrate formation. *AIChE Journal,* 59**,** 2640-2646.

XU, C.-G., CHEN, Z.-Y., CAI, J. & LI, X.-S. 2013a. Study on Pilot-Scale CO2 Separation from Flue Gas by the Hydrate Method. *Energy & Fuels*.

XU, C.-G. & LI, X.-S. 2014. Research progress of hydrate-based CO2 separation and capture from gas mixtures. *RSC Advances,* 4**,** 18301-18316.

XU, C.-G., LI, X.-S., LV, Q.-N., CHEN, Z.-Y. & CAI, J. 2012. Hydrate-based CO2 (carbon dioxide) capture from IGCC (integrated gasification combined cycle) synthesis gas using bubble method with a set of visual equipment. *Energy,* 44**,** 358-366.

XU, C.-G., ZHANG, S.-H., CAI, J., CHEN, Z.-Y. & LI, X.-S. 2013b. CO2 (carbon dioxide) separation from CO2–H2 (hydrogen) gas mixtures by gas hydrates in TBAB (tetra-n-butyl ammonium bromide) solution and Raman spectroscopic analysis. *Energy,* 59**,** 719-725.

YANG, H., XU, Z., FAN, M., GUPTA, R., SLIMANE, R. B., BLAND, A. E. & WRIGHT, I. 2008. Progress in carbon dioxide separation and capture: A review. *Journal of Environmental Sciences,* 20**,** 14-27.

YANG, M., LIU, W., SONG, Y., RUAN, X., WANG, X., ZHAO, J., JIANG, L. & LI, Q. 2013a. Effects of Additive Mixture (THF/SDS) on the Thermodynamic and Kinetic Properties of CO2/H2 Hydrate in Porous Media. *Industrial & Engineering Chemistry Research,* 52**,** 4911-4918.

YANG, M., LIU, W., SONG, Y., RUAN, X., WANG, X., ZHAO, J., JIANG, L. & LI, Q. 2013b. Effects of additive mixture (THF/SDS) on the thermodynamic and kinetic properties of CO2/H2 hydrate in porous media. *Industrial and Engineering Chemistry Research,* 52**,** 4911-4918.

YANG, M., SONG, Y., ZHAO, Y., LIU, Y., JIANG, L. & LI, Q. 2011. MRI measurements of CO2 hydrate dissociation rate in a porous medium. *Magnetic Resonance Imaging,* 29**,** 1007-1013.

YANG, S. O. 2000. *Measurements and prediction of phase equilibria for water + natural gas components in hydrate-forming conditions.* Ph.D. thesis, Korea University.

YANG, S. O., YANG, I. M., KIM, Y. S. & LEE, C. S. 2000. Measurement and prediction of phase equilibria for water+CO2 in hydrate forming conditions. *Fluid Phase Equilibria,* 175**,** 75-89.

YAO, X., LIU, H., ZHANG, R., LIU, M., HU, Z., PANAYE, A., DOUCET, J. P. & FAN, B. 2005. QSAR and Classification Study of 1,4-Dihydropyridine Calcium Channel Antagonists Based on Least Squares Support Vector Machines. *Molecular Pharmaceutics,* 2**,** 348-356.

YE, N. & ZHANG, P. 2014a. Phase equilibrium and morphology characteristics of hydrates formed by tetra-n-butyl ammonium chloride and tetra-n-butyl phosphonium chloride with and without CO2. *Fluid Phase Equilibria,* 361**,** 208-214.

YE, N. & ZHANG, P. 2014b. Phase equilibrium and morphology characteristics of hydrates formed by tetra-n-butyl ammonium chloride and tetra-n-butyl phosphonium chloride with and without CO2. *Fluid Phase Equilibria,* 361**,** 208–214.

YE, N., ZHANG, P. & LIU, Q. S. 2014. Kinetics of Hydrate Formation in the CO2+TBAB+H2O System at Low Mass Fractions. *Industrial & Engineering Chemistry Research,* 53**,** 10249-10255.

YE, Y. & LIU, C. 2013. *Natural Gas Hydrates: Experimental Techniques and Their Applications,* Springer Berlin Heidelberg.

ZATSEPINA, O. Y. & BUFFETT, B. A. 2001. Experimental study of the stability of CO2-hydrate in a porous medium. *Fluid Phase Equilibria,* 192**,** 85-102.

ZATSEPINA, O. Y. & BUFFETT, B. A. 2002. Nucleation of CO2-hydrate in a porous medium. *Fluid Phase Equilibria,* 200**,** 263-275.

ZENG, Z. Y. & LI, X. S. 2011. Hydrate Formation Phase Equilibrium Model in the Porous Media Based on PC-SAFT Equation of State. *Chemical Journal of Chinese Universities-Chinese,* 32**,** 908-914.

ZHAI, H. & RUBIN, E. S. 2013. Techno-Economic Assessment of Polymer Membrane Systems for Postcombustion Carbon Capture at Coal-Fired Power Plants. *Environmental Science & Technology,* 47**,** 3006-3014.

ZHANG, J. & LEE, J. W. 2009a. Enhanced Kinetics of CO2 Hydrate Formation under Static Conditions. *Industrial & Engineering Chemistry Research,* 48**,** 5934-5942.

ZHANG, J., YEDLAPALLI, P. & LEE, J. W. 2009. Thermodynamic analysis of hydrate-based pre-combustion capture of. *Chemical Engineering Science,* 64**,** 4732-4736.

ZHANG, J. S. & LEE, J. W. 2009b. Equilibrium of Hydrogen + Cyclopentane and Carbon Dioxide + Cyclopentane Binary Hydrates†. *Journal of Chemical & Engineering Data,* 54**,** 659-661.

ZHANG, L.-W., HUANG, Q., SUN, C.-Y., MA, Q.-L. & CHEN, G.-J. 2005. Hydrate Formation Conditions of Methane + Ethylene + Tetrahydrofuran + Water Systems. *Journal of Chemical & Engineering Data,* 51**,** 419-422.

ZHANG, P., YE, N., ZHU, H. & XIAO, X. 2013. Hydrate Equilibrium Conditions of Tetra-n-butylphosphonium Bromide + Carbon Dioxide and the Crystal Morphologies. *Journal of Chemical & Engineering Data,* 58**,** 1781-1786.

ZHANG, Q., CHEN, G.-J., HUANG, Q., SUN, C.-Y., GUO, X.-Q. & MA, Q.-L. 2004. Hydrate Formation Conditions of a Hydrogen + Methane Gas Mixture in Tetrahydrofuran + Water. *Journal of Chemical & Engineering Data,* 50**,** 234-236.

ZHANG, W., WILDER, J. W. & SMITH, D. H. 2002. Interpretation of ethane hydrate equilibrium data for porous media involving hydrate-ice equilibria. *AIChE Journal,* 48**,** 2324-2331.

ZHANG, Y., YANG, M., SONG, Y., JIANG, L., LI, Y. & CHENG, C. 2014. Hydrate phase equilibrium measurements for (THF + SDS + CO2 + N2) aqueous solution systems in porous media. *Fluid Phase Equilibria,* 370**,** 12-18.

ZHONG, D.-L., DING, K., YANG, C., BIAN, Y. & JI, J. 2012. Phase Equilibria of Clathrate Hydrates Formed with CH4 + N2 + O2 in the Presence of Cyclopentane or Cyclohexane. *Journal of Chemical & Engineering Data,* 57**,** 3751-3755.

ZHONG, D.-L., LI, Z., LU, Y.-Y. & SUN, D.-J. 2014. Phase Equilibrium Data of Gas Hydrates Formed from a CO2 + CH4 Gas Mixture in the Presence of Tetrahydrofuran. *Journal of Chemical & Engineering Data,* 59**,** 4110-4117.

ZHONG, Y. & ROGERS, R. E. 2000. Surfactant effects on gas hydrate formation. *Chemical Engineering Science,* 55**,** 4175-4187.

ZHOU SHI-DONGAB, Y. Y.-S., ZHAO MIAO-MIAOA, WANG SHU-LIA, ZHANG GUO-ZHONGB 2014. Effect of graphite nanoparticles in promoting CO2 hydrate formation. *Energy & Fuels*.

Appendix A: CO_2 capture technologies

A.1 Absorption technology

Chemical absorption: A reaction between a flue gas and an aqueous solution of amines can be used to CO_2 removal. The most commonly used amines in this process is monoethanolamine (MEA). The reaction between CO_2 and MEA forms a weakly bonded intermediate compound (MEA carbamate) that can be regenerated by the application of heat energy to produce the chemical absorbent (MEA) and a CO_2 stream (Wang et al., 2011, Rao and Rubin, 2002, Olajire, 2010, Yang et al., 2008). The large equipment size and intensive energy input make it uneconomic and unprofitable process (Yang et al., 2008). Corrosion control is very important in amine systems. Corrosion control is very important in amine systems. For this aim, corrosion inhibitors and low concentrations of MEA are required. Chemical absorption has several advantages and drawbacks as shown in Table A. 1.

Table A. 1: Advantages and drawbacks of chemical absorption technology

Advantages	Drawbacks
- Solvent can be easily regenerated. - Purity of $CO_2 > 95\%$. - Non dependence on human operators.	- Degradation of solvents by SO_2, NO_2, HCl, HF, and oxygen in flue gas. - High regeneration costs. - High energy requirements for CO_2 release. - Large equipment size. - Low carbon dioxide loading capacity. - Use of inhibitors to control corrosion is necessary. - High equipment corrosion rate.

Physical absorption: CO_2 removal through physical absorption technologies are based on the solubility of CO_2 in the solvents. Henry's law is used to explain the solubility of gases in solvents. The solubility of a gas in a solvent may also strongly depend on the partial pressure and temperature of the gas. According to Henry's law, at high partial pressures and low temperatures, CO_2 is physically absorbed in a solvent (Olajire, 2010). The CO_2 is then regenerated using heat or pressure lessening. The CO_2 absorption capacity of solvents enhances with decreasing their temperatures and increasing their pressures. The physical absorption method may not be efficient due to the relatively high temperature of the flue gas and the low pressure of CO_2 in flue gas. Physical solvents must have several features including: low or moderate hygroscopicity, low vapour pressure at ambient temperature, low viscosity, non-corrosive to common metals, non-reactive with all components in the gas stream, and available commercially at a reasonable cost. General solvents are Selexol (dimethyl ethers of polyethylene glycol) and Rectisol (cold

methanol). Ionic liquids (ILs) are another class of absorbents (Hasib-ur-Rahman et al., 2010, Ramdin et al., 2012). They are regarded as a novel class of materials for CO_2 capture due to their unique characteristics, i.e. extremely low vapour pressures, wide liquid range, non-flammable, high CO_2 solubility, environmentally benign, thermal stability and excellent solvent power. Ionic liquids can absorb CO_2 at high temperatures. An important challenge for ionic liquids is their high viscosity and the high cost of ionic liquids. The advantages and drawbacks of physical absorption technique are summarized in Table A. 2.

Table A. 2: Advantages and drawbacks of physical absorption technique (Olajire, 2010, Belandria et al., 2012a)

Advantages	Drawbacks
- Low utility consumption - Requires less energy for regeneration than chemical absorption processes - Rectisol uses inexpensive, easily available methanol. - Selexol has a higher capacity to absorb gases than amines. - Selexol can remove H_2S and organic sulphur compounds. - Less expensive than chemical absorption	- More economical at high pressures. - Hydrocarbons are co-absorbed in Selexol, resulting in reduced product revenue and often requiring recycle compression. - Refrigeration is often required for the lean Selexol solution. - Requires a high partial pressure of CO_2 in the feed. - Capacity proportional to CO_2 partial pressure and temperature. - Low selectivity of solvent causes H_2 losses

A.2 Adsorption technology

Adsorption is considered as a separation technology that can be used for capturing CO_2 from flue gases (Samanta et al., 2011, Choi et al., 2009) such as activated carbons (AC) (Chen et al., 2013, Chen et al., 2010, Kumar et al., 2013a), zeolites (Wang et al., 2008a, Kim et al., 2012, Sun and Liu, 2012, Konduru et al., 2007, Su et al., 2010, Gao et al., 2004), metal organic frameworks (MOFs) (Rowsell and Yaghi, 2004, Li et al., 2011a, Sumida et al., 2011), carbon nanotubes (CNT) (Gui et al., 2013, Lu et al., 2008), metal-based adsorbents (such as CaO, Na_2O,…) (Figure A. 1). Numerous parameters determine the quality of CO_2 adsorbents consisting: adsorption/desorption kinetics, CO_2 capacity, regenerability and multicycle stability, and operating window, including adsorption and desorption temperatures.
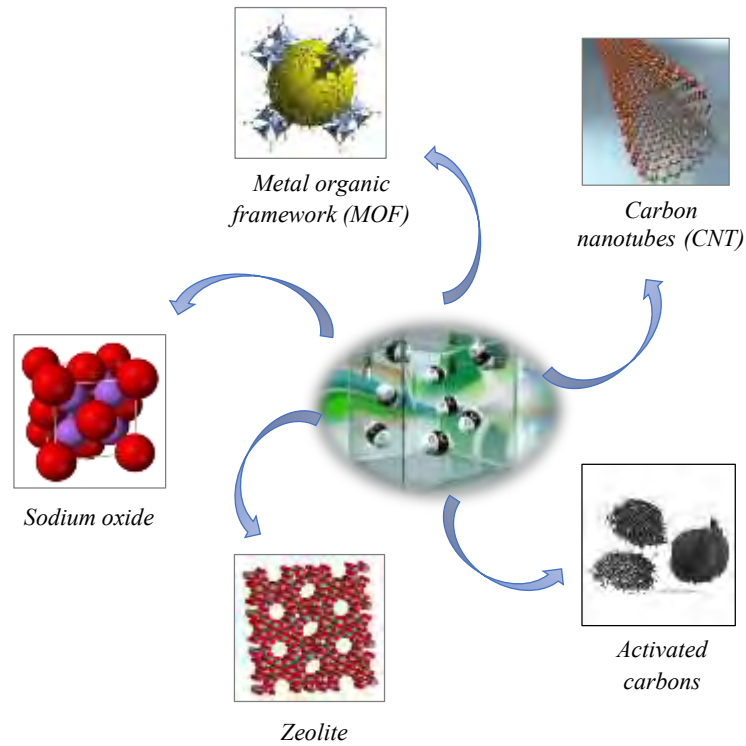
Figure A. 1: Solid adsorbent for separation process (Choi et al., 2009).

The most widely used methods for adsorption are pressure swing adsorption (PSA) and temperature swing adsorption (TSA). In pressure swing adsorption (PSA), the gas mixture flows through the adsorbent at pressures higher than atmosphere then the adsorbent is regenerated by decreasing the total or partial pressure. In TSA, the adsorbent is regenerated by increasing (Choi et al., 2009) temperature. The advantages and drawbacks of adsorption process are listed in Table A. 3.

Table A. 3: Advantages and drawbacks of adsorption technique.

Advantages	Drawbacks
• relatively simple • Commercially available. • Sorbent can be reused. • Low concentrations of CO_2 yield an optimum performance.	• Capacity and CO_2 selectivity of available adsorbents is low. • Sorbent susceptible to degradation. • Cannot handle easily large concentrations of CO_2. • Adsorption time is not practical. • Low degree of CO_2 separation. • Poor selectivity of sorbents to CO_2. • Operation costs higher than absorption processes.

A.3 Cryogenics

Cryogenic techniques is one of several technologies for capturing of CO_2 from gas mixtures by condensation and distillation at low temperatures. Hart and Gnanendran (Hart and Gnanendran, 2009) reported cryogenic CO_2 capture in natural gas using the CryoCell method.

Cryogenic separation is utilised for removing CO_2 from high pressure gases such as in pre-combustion capture processes or oxy-fuel combustion (input gas contains high concentration of CO_2) (Song et al., 2013a, Song et al., 2012, Hart and Gnanendran, 2009, Berstad et al.). The advantages and drawbacks of this capture approache is summarized in Table A. 4.

Table A. 4: Advantages and drawbacks of cryogenics technique

Advantages	Drawbacks
• No chemical absorbents are required. • The process can be operated at atmospheric pressures. • Smaller size of equipment since only O_2 is supplied for combustion.	• Some components, such as water, have to be removed before the gas stream is cooled. • Very expensive process. • Requires high energy consumption. • Corrosion might be caused by SO_2

A.4 Membranes

Membrane technology is an attractive technology to separate CO2 from hydrogen (pre-combustion systems), CO_2 from flue gases (post-combustion system) or oxygen from nitrogen (oxyfuel combustion system) (Zhai and Rubin, 2013, Brunetti et al., 2010). In other words, the membrane technologies are categorized into two main types:

- Gas separation membranes (separation of CO_2 from other gases)
- Gas absorption membrane (absorption of CO_2 from a gas stream into a solvent)

A.4.1 Gas separation membranes

In the membrane gas separation processes (Bernardo et al., 2009), membrane operates as a filter that CO_2 passes through this filter more easily than other gases as shown in Figure A. 2. In general, the operation of membranes is based on the concentration of gas, the size of the molecule, the tendency of the gas for the membrane material and difference in pressure across the membrane.

Membrane should have a number of properties to be porfitable for the capture of carbon dioxide (Powell and Qiao, 2006):

- high carbon dioxide permeability.
- high carbon dioxide/nitrogen selectivity.
- thermally and chemically robust,
- resistant to plasticisation,
- resistant to aging,
- cost effective,
- able to be cheaply manufactured into different membrane modules.

Different kind of gas separation membranes are available including: ceramic, polymeric and combination of both materials or mixed matrix membranes (Baker, 2002). Polymeric membranes are of particular interest for CO_2 separation due to their low cost, high performance separation, easy synthesis and mechanical stability.
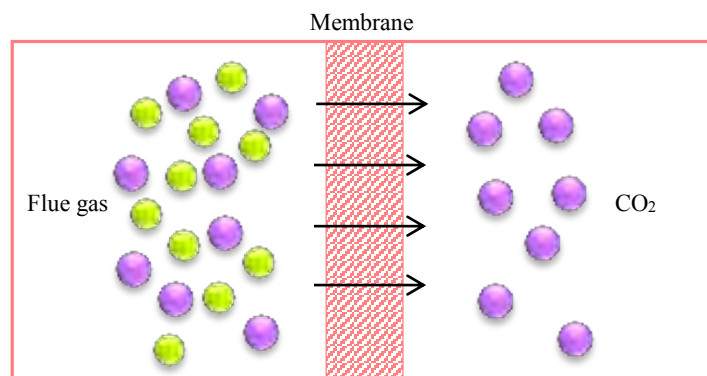

Membrane

Flue gas

CO_2

Figure A. 2: Membrane gas separation process

A.4.2 Gas absorption membrane

A membrane can be used with a solvent to CO_2 capture. As shown in Figure A. 3, the CO_2 diffuses through the pores in the membrane and gets absorbed by the solvent. This type of membrane is applied when the partial pressure of CO_2 is low because the driving force for gas separation is small. The advantages and drawbacks of membrane approache are listed in Table A. 5.
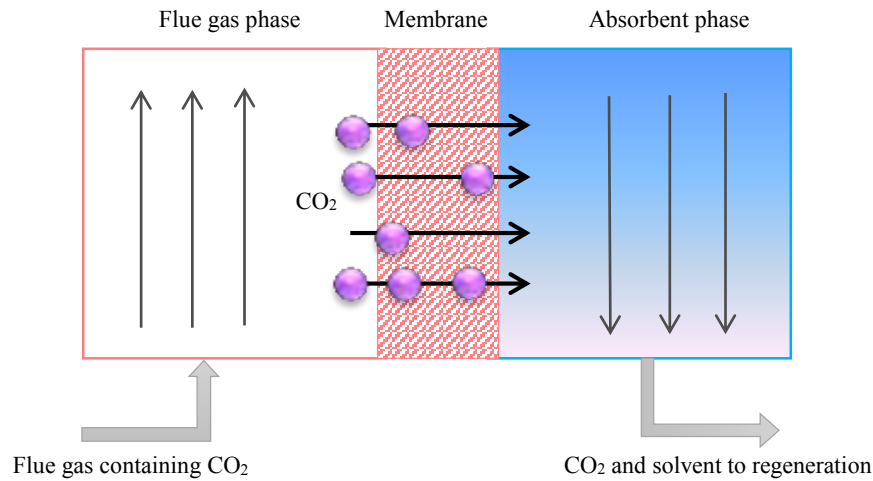
Figure A. 3: Principle of gas absorption membrane (Lv et al., 2012).

Table A. 5: Advantages and drawbacks of membrane technique.

Advantages	Drawbacks
• Relatively simple to operate • No regeneration energy is required • Simple modular system • No waste streams • Commercially available • Require low maintenance • Less energy intensive than PSA • No need to add chemicals or to regenerate an absorbent/adsorbent. • can be retrofitted easily	• Can be plugged by impurities in the gas stream. • low selectivity of membrane materials to CO_2 • Preventing membrane wetting is a major challenge. • Purity of the CO_2 in the permeate stream is low.

A.5 Chemical looping

Chemical looping combustion (CLC) has been presented as a capture technology for the separation of the CO_2 (Song et al., 2013b, Adanez et al., 2012, Hossain and de Lasa, 2008, Chiu and Ku, 2012). Instead of a single reaction stage, the CLC involves two reactions (oxidation and reduction reactions) to provide oxygen for the combustion of hydrocarbon-based fuels. The CLC process uses an oxygen carrier to provide oxygen and transfer it from the air to the fuel, avoiding the direct contact between them without significant energy penalty. The oxygen carrier is composed of a metal oxide such as CuO, CdO, NiO, CoO, Mn_2O_3, and Fe_2O_3 (Moldenhauer et al., 2012, Shah et al., 2012, Tan et al., 2012, Mattisson et al., 2004, García-Labiano et al., 2005, Shen et al., 2010, Dennis and Scott, 2010). The CLC is formed of two fluidized-bed reactors (air reactor and fuel reactor). The oxygen carrier circulates between the reactors. As shown in Figure

A. 4, oxygen is removed from air by reacting with metal particles in a fluidized bed to form metal oxides. The captured oxygen (in the form of metal oxide) is reduced by the fuel in a separate fluidized bed and oxidized to carbon dioxide and water. The abbreviation M_xO_y is used to describe the oxygen-carrier in its oxidized form, while M_xO_{y-1} is used for the reduced form.

A feasible oxygen-carrier material for CLC should (Hossain and de Lasa, 2008):

- Fast rate reactivity of fuel and oxygen in both reduction and oxidation cycles.
- Stability of reduction/oxidation cycles at high temperature.
- be environmentally benign.
- low tendency towards any kinds of mechanical or thermal degeneration.
- Capable to transform a large amount of the fuel to CO_2 and H_2O.
- Economically feasible.

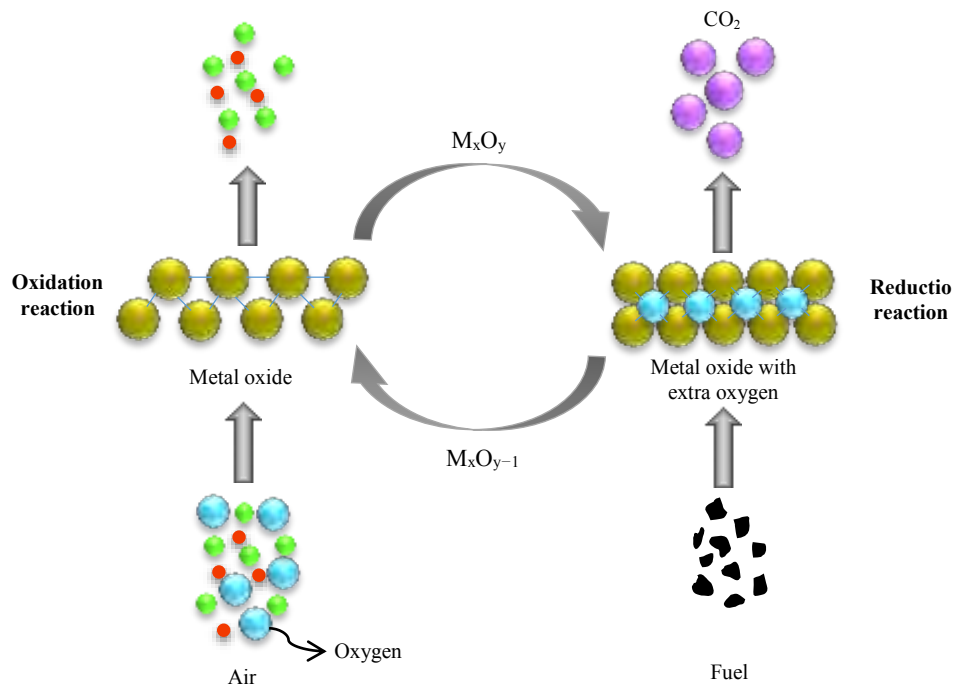The advantages and drawbacks of CLC are summarized in Table A. 6.

Figure A. 4: Chemical looping combustion (Mohammadi et al., 2014).

Table A. 6: Advantages and drawbacks of chemical looping combustion.

Advantages	Drawbacks
• CO_2 is inherently separated from the other flue gas components. • No extra energy is needed for CO_2 separation. • No need of special CO_2 separation equipment. • No thermal formation of NO_x. • Less operational cost.	• No large-scale demonstration has been performed. • Mn-based oxygen carriers have lower oxygen transfer capability and thermodynamic limitations of purifying the CO_2 stream. • Fe-based oxygen carriers have a larger endothermic reduction enthalpy and lower reactivity. • Ni- based oxygen carriers have thermodynamic limitation to convert the fuel to 100% CO_2 and H_2O.

A significant number of article have been published in absorption, adsorption, cryogenic, membrane and chemical looping for CO_2 capture and separation (Figure A. 5). A sharp increase in total number of publication in 2006–2013 shows capturing of CO_2 has attracted intense attention of scientist.
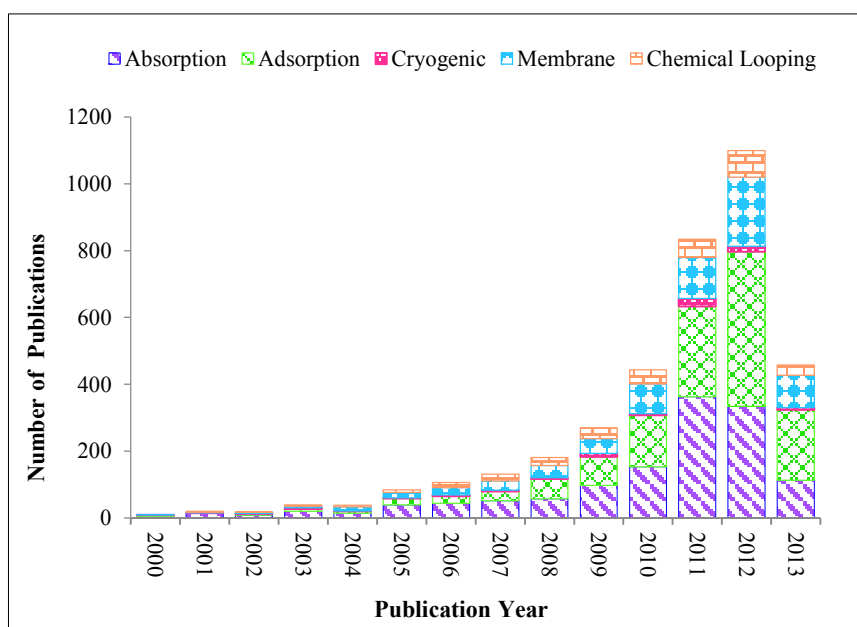

Figure A. 5: Number of publications on CO_2 capture by different thechniques.

Data from ISI Web of Knowledge, Thomson Reuters.

Appendix B: Estimation of uncertainty in measurements

The uncertainty of a measured variable is described as the interval between experimental quantities from the true value. Calculation of uncertainty in measurement adapted from NIST (National Institute of Standards and Technology).

The combined standard uncertainty (u_c) and the combined expanded uncertainty (U_c) are the most comprehensive descriptions for uncertainty. u_c demonstrates all the possible sources of uncertainties and can be represented as the mathematical expression:

$$u_c(x) = \pm \sqrt{\sum_i u_i(x)^2}$$
(B.1)

where the symbol u_i stands for various contributions to the uncertainty; Such as uncertainty from calibrations, uncertainty due to repeatability etc. $u_i(x)$ consists of several components which may be classified into two groups according to the method used to estimate their numerical values:

Type A: The estimation of uncertainty by the valid statistical method is termed a Type A evaluation of uncertainty. It may be evaluated from:

$$u_i(x) = \frac{\sigma}{\sqrt{N_{rp}}}$$
(B.2)

where σ stands for standard deviation of the data, and N_{rp} is the number of repeated data points.

Type B: The estimation of uncertainty by other means is termed a Type B evaluation of uncertainty. A Type B uncertainty of a variable is defined as a positive value which is defined as follows:

$$u_i(x) = \frac{b}{\sqrt{3}}$$
(B.3)

This value determines the upper and lower bounds of a distribution wherein the real value of the variable is located. Where quantity b is the half-width between the upper and lower limits.

when all sources of uncertainty are calculated for combined standard uncertainty, the combined expanded uncertainty determine from a combined standard uncertainty through the expression:

$$U_c(x) = k u_c(x)$$
(B.4)

Where k is coverage factor which is chosen on the basis of the level of confidence (usually 95%).

Temperature and pressure uncertainty

Uncertainty for temperature: the combined standard uncertainty for temperature is:

$$u_c(T) = \sqrt{u_{calibration}(T)^2 + u_{repeatability}(T)^2 + u_{instrument}(T)^2 + u_{procedure}(T)^2} \qquad \text{(B.5)}$$

$$u_{calibration}(T) = \sqrt{u_{correlation}(T)^2 + u_{Standard}(T)^2} \qquad \text{(B.6)}$$

Where:

- $u_{repeatability}$ (T) is the standard uncertainty due to measurement repeatability (Type A).
- $u_{instrument}$ (T) is the standard uncertainty of the measurement devices which is specified by supplier(Type B).
- $u_{procedure}$ *(T)* is the standard uncertainty of the graphical isochoric pressure-search method.
- $u_{correlation}$ (T) is the standard uncertainty due to the temperature calibration correlation (Type B).
- $u_{standard}$ (T) is the standard uncertainty of the standard temperature probe (Type B).

Subsequently, the combined expanded uncertainty is determined:

$$U_c(T) = 2u_c(T) \qquad \text{(B.7)}$$

The coverage factor (k_x) is 2 for confidence level of 95 %.

Uncertainty for temperature: Similarly, the combined standard uncertainty for pressure is:

$$u_c(P)$$
$$= \sqrt{u_{calibration}(P)^2 + u_{repeatability}(P)^2 + u_{instrument}(P)^2 + u_{procedure}(P)^2}$$
$$(B.8)$$

The combined expand uncertainty is achieved by multiplying coverage factor of 2 in the combined standard uncertainty.

Table B. 1: Summary of measurement uncertainties for the hydrate dissociation temperatures and pressures that measured with apparatus 1.

	T/ K	P/ KPa	P/ MPa
Calibration uncertainty	± 0.02	± 0.560	± 0.001
Repeatability uncertainty	± 0.00	± 0.259	± 0.000
Instrument uncertainty	± 0.02	± 0.003	± 0.000
Procedure uncertainty	± 0.03	± 15.000	± 0.015
Combined Standard Uncertainty	± 0.04	± 15.013	± 0.015
Combined expanded uncertainty	± 0.08	± 30.025	± 0.030

Table B. 2: Summary of measurement uncertainties for the hydrate dissociation temperatures and pressures that measured with apparatus 2.

	T/ K	P/ KPa	P/ MPa
Calibration uncertainty [1,2]	± 0.02	± 9.815	± 0.010
Repeatability uncertainty [1]	± 0.00	± 0.259	± 0.000
Instrument uncertainty [2]	± 0.02	± 0.003	± 0.000
Procedure uncertainty [1]	± 0.10	± 24.000	± 0.024
Combined Standard Uncertainty	± 0.10	± 25.931	± 0.026
Combined expanded uncertainty	± 0.21	± 51.861	± 0.052

Appendix C: Least squares support vector machine (LSSVM) algorithm

The least squares support vector machine (LSSVM) (Suykens and Vandewalle, 1999, Eslamimanesh et al., 2012a) algorithm is used to predict the hydrate dissociation pressures (Ilani-Kashkouli et al., 2013a, Ilani-Kashkouli et al., 2013b). For optimization using the LSSVM mathematical algorithm, it is required to minimize a cost function (Pelckmans et al., 2002):

$$Q_{LSSVM} = \frac{1}{2}w^T w + \gamma \sum_{k=1}^{N} e_k^2 \tag{C.1}$$

subject to:

$$y_k = w^T \varphi(x_k) + b + e_k \qquad k = 1,2,3, \dots, N \tag{C.2}$$

where w shows the slope of the linear regression (regression weight), γ indicates the relative weight of the summation of the regression errors and e_k is the regression error for N training objects. x_k is the input vector including the input elements and y_k is the output vector (gas hydrate dissociation pressure in this work). b indicates the linear regression intercept of the model, φ indicates the feature map, and finally superscript T indicates the transpose matrix.

Using the Lagrange function the regression weight (w) in Eqs (C.3) and (C.4) can be defined (Suykens and Vandewalle, 1999, Pelckmans et al., 2002, Yao et al., 2005):

$$w = \sum_{k=1}^{N} \alpha_k x_k \tag{C.3}$$

where

$$\alpha_k = 2\gamma e_k \tag{C.4}$$

As a result of linear regression between the independent and dependent variables of the LSSVM method, Eq (C.5) can be revised as (Suykens and Vandewalle, 1999, Pelckmans et al., 2002, Yao et al., 2005):

$$y_k = \sum_{k=1}^{N} \alpha_k x_k^T x + b \qquad\qquad (C.5)$$

Therefore, the value of the α_k (the Lagrange multipliers) can be calculated as:

$$\alpha_k = \frac{y_k - b}{x_k^T x + (2\gamma)^{-1}} \qquad\qquad (C.6)$$

The Kernel function can be well extended the linear regression to a non-linear form as shown below:

$$f(x) = \sum_{k=1}^{N} \alpha_k K(x, x_k) + b \qquad\qquad (C.7)$$

where K(x,x_k) is the Kernel function calculated from the inner product of the two vectors x and x_k in the feasible region built by the inner product of the vectors $\Phi(x)$ and $\Phi(x_k)$ as follows (Suykens and Vandewalle, 1999, Pelckmans et al., 2002, Yao et al., 2005):

$$K(x, x_k) = \Phi(x)^T . \Phi(x_k) \qquad\qquad (C.8)$$

The radial basis function (RBF) Kernel is commonly used for computing the Kernel function (Suykens and Vandewalle, 1999, Pelckmans et al., 2002):

$$K(x, x_k) = exp\left(\frac{-\|x_k - x\|^2}{\sigma^2}\right) \qquad\qquad (C.9)$$

where σ is the decision variable which deals with the external optimization algorithm during the calculations.

The mean square error (MSE) of the results of the LSSVM is used to evaluate the quality of the built model, which is defined as (Yao et al., 2005):

$$MSE = \frac{\sum_{i=1}^{n}\left(P_{Pred_i} - P_{exp_i}\right)^2}{n} \qquad\qquad (C.10)$$

where P is the hydrate dissociation pressure, subscripts rep./pred. and exp. denote the represented/predicted, and experimental dissociation pressure values respectively, n the number of samples.